



National Library  
of Canada

Acquisitions and  
Bibliographic Services Branch

395 Wellington Street  
Ottawa, Ontario  
K1A 0N4

Bibliothèque nationale  
du Canada

Direction des acquisitions et  
des services bibliographiques

395, rue Wellington  
Ottawa (Ontario)  
K1A 0N4

*Your file - Votre référence*

*Our file - Notre référence*

## NOTICE

The quality of this microform is heavily dependent upon the quality of the original thesis submitted for microfilming. Every effort has been made to ensure the highest quality of reproduction possible.

If pages are missing, contact the university which granted the degree.

Some pages may have indistinct print especially if the original pages were typed with a poor typewriter ribbon or if the university sent us an inferior photocopy.

Reproduction in full or in part of this microform is governed by the Canadian Copyright Act, R.S.C. 1970, c. C-30, and subsequent amendments.

## AVIS

La qualité de cette microforme dépend grandement de la qualité de la thèse soumise au microfilmage. Nous avons tout fait pour assurer une qualité supérieure de reproduction.

S'il manque des pages, veuillez communiquer avec l'université qui a conféré le grade.

La qualité d'impression de certaines pages peut laisser à désirer, surtout si les pages originales ont été dactylographiées à l'aide d'un ruban usé ou si l'université nous a fait parvenir une photocopie de qualité inférieure.

La reproduction, même partielle, de cette microforme est soumise à la Loi canadienne sur le droit d'auteur, SRC 1970, c. C-30, et ses amendements subséquents.

Canada

UNIVERSITY OF ALBERTA

APPLICATION OF SASW FOR EVALUATION OF PAVEMENT-LIKE  
STRUCTURES

BY  
DEBABRATA DAS



A THESIS

SUBMITTED TO THE FACULTY OF GRADUATE STUDIES AND RESEARCH  
IN PARTIAL FULFILMENT OF THE REQUIREMENTS FOR THE DEGREE OF  
DOCTOR OF PHILOSOPHY  
IN  
GEOTECHNICAL ENGINEERING

DEPARTMENT OF CIVIL ENGINEERING

EDMONTON, ALBERTA

FALL 1994



National Library  
of Canada

Acquisitions and  
Bibliographic Services Branch

395 Wellington Street  
Ottawa, Ontario  
K1A 0N4

Bibliothèque nationale  
du Canada

Direction des acquisitions et  
des services bibliographiques

395, rue Wellington  
Ottawa (Ontario)  
K1A 0N4

*Votre titre - Votre référence*

*Événement - Note de référence*

**The author has granted an irrevocable non-exclusive licence allowing the National Library of Canada to reproduce, loan, distribute or sell copies of his/her thesis by any means and in any form or format, making this thesis available to interested persons.**

**L'auteur a accordé une licence irrévocable et non exclusive permettant à la Bibliothèque nationale du Canada de reproduire, prêter, distribuer ou vendre des copies de sa thèse de quelque manière et sous quelque forme que ce soit pour mettre des exemplaires de cette thèse à la disposition des personnes intéressées.**

**The author retains ownership of the copyright in his/her thesis. Neither the thesis nor substantial extracts from it may be printed or otherwise reproduced without his/her permission.**

**L'auteur conserve la propriété du droit d'auteur qui protège sa thèse. Ni la thèse ni des extraits substantiels de celle-ci ne doivent être imprimés ou autrement reproduits sans son autorisation.**

ISBN 0-315-95169-9

**Canada**

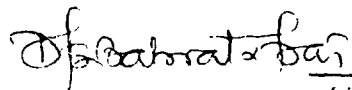
UNIVERSITY OF ALBERTA

RELEASE FORM

NAME OF AUTHOR	<i>Debabrata Das</i>
TITLE OF THESIS	<i>Application of SASW for evaluation of Pavement-like structures</i>
DEGREE	<i>Doctor of Philosophy</i>
YEAR DEGREE GRANTED	<i>1994</i>

Permission is hereby granted to the UNIVERSITY OF ALBERTA LIBRARY to reproduce single copies of this thesis and to lend or sell such copies for private, scholarly or scientific research purposes only.

The author reserves all other publication and other rights in association with the copyright in the thesis, and except as hereinbefore provided neither the thesis nor any substantial portion thereof may be printed or otherwise reproduced in any material form whatever without the author's prior written permission.



158/I/3, P.K. Guha Road  
Kumarpara  
Calcutta - 700 028  
INDIA

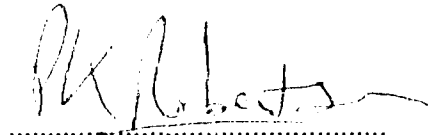
DATED      May, 1994



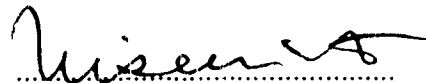
UNIVERSITY OF ALBERTA

FACULTY OF GRADUATE STUDIES AND RESEARCH

The undersigned certify that they have read, and recommend to the Faculty of Graduate Studies and Research for acceptance, a thesis entitled Application of SASW for Evaluation of Pavement - Like Structures submitted by Debabrata Das in partial fulfillment of the requirements for the degree of Doctor of Philosophy.



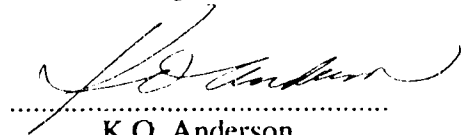
P.K. Robertson



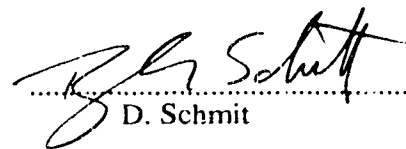
Z. Eisenstein



D. Sego



K.O. Anderson



D. Schmit



J. Hunter

Date: May 1994

## **ABSTRACT**

An improved version of the Spectral-Analysis-of-Surface-Waves (SASW) technique is presented for obtaining the stiffness profiles over shallow depths of ground structures having contrasting layer properties, such as, in pavements and basement concrete layers. Data-acquisition and field interpretation are automated using a Macintosh Computer, High-Speed Data-Acquisition Board, DMA Board with GPIB Interface, Interface-Control-Unit (ICU) and Power Amplifier. The calculation processes of transforming time-domain data to frequency-domain, calculation of auto-power spectra, cross-power spectra, phase of the cross-power spectra, coherence and phase velocities are done in real time in the field as the data are being collected. A software "SWAP" (Spectral Wave Analysis for Pavements) has been developed for this purpose using the LabVIEW programming technique. The results are obtained immediately in the field showing the variation of shear-wave velocity with depth. Shear wave velocity is directly related to the small strain stiffness of the material through which the wave propagates. The equipment set-up, data collection technique, data processing and test results are shown from various test sites of various subsurface conditions. A stand-alone Macintosh Application microcomputer program "MULTIMOD" was also developed for determining dispersion characteristics of multiple-mode Rayleigh waves.

## **ACKNOWLEDGEMENT**

The author wishes to express his gratitude to the following individuals who made this dissertation possible.

The author is particularly indebted to the Supervising Professor, Dr. P.K. Robertson, for his technical guidance, support and encouragement throughout the course of this study.

The author wishes to express his sincere thanks to Dr. N.R. Morgenstern for his valuable advice and directions in many difficult and complicated situations.

The author would like to thank the other members of his committee, Dr. Z. Eisenstein, Dr. D. Sego, Prof. K. Anderson and Prof. D. Schmitt for their invaluable comments and suggestions. The author would also like to extend his appreciation to Dr. D. Chan for his help during the authors first visit to Canada as a student.

The author owes a great deal to a special person, Ritika, for her encouragement and helping the author particularly for data collection when no one was available. She also helped in various stages for putting this dissertation together.

The author also thanks Roy Gitzel and Dale Lathe of Electronics Division of the Department of Civil Engineering for their technical help in the development of the data-acquisition equipment and computer programs. Appreciation is expressed to Gerry Cyre for his assistance during field work; Steve Gamble, Christine Hereygers and Jay Khajuria in the laboratory work; Sharon Dudas, Jo-Ann Latta, Eleanor Kangas and Joan Wigmore for different administrative tasks.

The author also owes a great deal to his friend and his wife Dr. David Y.F. Ho and Mrs. Georgina Ho for unselfishly passing much of their moral support during the last four years. The author also thanks Dr. P.K. Chatterjee for his advice on many occasions.

One of the most important accomplishments of being at the University of Alberta has been becoming associated with many other students. The author has particularly enjoyed his association with Dr. Aruna Ajjikuttira, Dr. Mrinal K. Das and Dr. (Mrs.) Saswati Das.

Various organizations and people made much of the work in this dissertation possible including Mr. Al Cepas of the City of Edmonton and the authors personal friends Dr. Arne Instanes of Norwegian Institute of Technology and Dr. Kofi Addo.

Finally, the authors parents, Hari Pada Das and Debi Rani Das, brother and sister, Debashis Das and Debarati Goswami, are the ones who have made this major task possible.

This research was funded from a grant by the National Science and Engineering Council of Canada.

## **TABLE OF CONTENTS**

**Release Form**

**Abstract**

**Acknowledgment**

**List of Tables**

**List of Figures**

### **CHAPTER 1**

<b>INTRODUCTION</b> .....	1
1.1 GENERAL/PROBLEM STATEMENT .....	1
1.2 OBJECTIVES .....	1
1.3 THESIS ORGANIZATION .....	2

### **CHAPTER 2**

<b>SEISMIC WAVES</b> .....	4
2.1 SEISMIC WAVES .....	4
2.2 BODY WAVE METHODS .....	8
2.3 SURFACE WAVE METHODS .....	11
2.4 STEADY STATE RAYLEIGH WAVE METHOD .....	12
2.5 SUMMARY .....	14

### **CHAPTER 3**

<b>SPECTRAL-ANALYSIS-OF-SURFACE-WAVES (SASW)</b> .....	25
3.1 INTRODUCTION .....	25
3.2 OVERVIEW OF SASW .....	26
3.2.1 DATA COLLECTION .....	26

3.2.2 EVALUATION OF THE RAYLEIGH WAVE DISPERSION CURVE .....	27
3.2.3 INVERSION OF THE DISPERSION CURVE.....	29
3.3 UNIVERSITY OF ALBERTA SASW SYSTEM .....	31
3.3.1 HARDWARE IMPLEMENTATION .....	31
3.3.2 SASW FIELD PROCEDURE .....	32
3.3.3 DATA ACQUISITION AND SIGNAL ANALYSIS .....	34
3.3.4 FORWARD MODELLING .....	39
3.4 SUMMARY .....	41

## **CHAPTER 4**

### **CURRENT METHODS FOR EVALUATING THE STRUCTURAL**

<b>INTEGRITY OF PAVEMENTS ....</b>	<b>48</b>
4.1 INTRODUCTION .....	48
4.2 STATIC DEFLECTION METHODS .....	48
4.3 DYNAMIC DEFLECTION METHODS.....	51
4.3.1 STEADY-STATE VIBRATORY LOADING.....	51
4.3.2 FALLING WEIGHT DEFLECTOMETER (FWD) .....	53
4.4 COMPARISON OF BENKELMAN BEAM, DYNAFLECT, FWD AND SASW. ....	55
4.5 PAVEMENT ANALYSIS .....	57
4.6 SUMMARY .....	59

## **CHAPTER 5**

<b>SASW - NEW DEVELOPMENTS .....</b>	<b>63</b>
5.1 INTRODUCTION .....	63
5.2 EQUIPMENT.....	63
5.2.1 DATA ACQUISITION .....	63
5.2.2 RECEIVERS .....	66

5.2.3 SOURCES .....	68
5.3 SOFTWARE .....	69
5.3.1 MICROCOMPUTER PROGRAM "SWAP" .....	69
5.4 FIELD PROCEDURE.....	74
5.5 MICROCOMPUTER PROGRAM "MULTIMOD".....	78
5.6 SUMMARY.....	80

## **CHAPTER 6**

<b>FIELD WORK AND LABORATORY WORK .....</b>	<b>94</b>
6.1 INTRODUCTION .....	94
6.2 SITE SELECTION .....	94
6.2.1 UNIVERSITY OF ALBERTA SASW TEST SECTION B-11, BASEMENT SLAB .....	95
6.2.2 UNIVERSITY OF ALBERTA LRT STATION SASW TEST SECTIONS, RIGID PAVEMENT .....	95
6.2.3 WHITEMUD DRIVE SASW TEST SECTION, FLEXIBLE PAVEMENT .....	96
6.2.4 KEILLOR ROAD SASW TEST SECTION, FLEXIBLE PAVEMENT .....	97
6.3 LABORATORY SEISMIC WAVE VELOCITY MEASUREMENTS.....	97
6.3.1 INTRODUCTION .....	97
6.3.2 PULSE TRANSMISSION METHOD.....	98
6.3.3 CALIBRATION FOR THE POLARISATION OF PIEZOELECTRIC TRANSDUCERS .....	100
6.3.4 CALIBRATION OF THE PIEZOELECTRIC CRYSTALS DUE TO THEIR EMBEDMENT IN THE TRANSDUCER .....	101
6.3.5 TEST PROCEDURE AND RESULTS .....	101
6.4 SUMMARY .....	102

## **CHAPTER 7**

<b>ANALYSIS AND PRESENTATION OF RESULTS .....</b>	<b>110</b>
7.1 INTRODUCTION .....	110
7.2 UNIVERSITY OF ALBERTA SASW TEST SECTION B-11, BASEMENT SLAB .....	111
7.3 UNIVERSITY OF ALBERTA LRT SASW TEST SECTION, RIGID PAVEMENT... ..	117
7.4 WHITEMUD DRIVE SASW TEST SECTION, FLEXIBLE PAVEMENT .....	120
7.5 KEILLOR ROAD SASW TEST SECTION, FLEXIBLE PAVEMENT. ....	124
7.6 SUMMARY. ....	129

## **CHAPTER 8**

<b>CONCLUSIONS AND RECOMMENDATIONS .....</b>	<b>174</b>
8.1 INTRODUCTION .....	174
8.2 CONCLUSIONS .....	174
8.3 RECOMMENDATIONS .....	176

<b>BIBLIOGRAPHY .....</b>	<b>179</b>
---------------------------	------------

## **APPENDICES**

I. "SWAP" PROGRAM SEQUENCE .....	190
II. TEST SITE FIGURES .....	196
III. EFFECT OF SASW-FM INPUT PARAMETERS ON SASW-FM OUTPUT RESULTS .....	229
IV. MODULUS PROFILES. ....	236
V. CALCULATION OF FROST THAW (KEILLOR ROAD).....	250



## **LIST OF TABLES**

Table 5.1	Specifications of PCB Model 482A16 Power Amplifier.....	81
Table 5.2	Characteristics of Model L-4 Geophones .....	82
Table 5.3	Specifications of PCB Model-309A accelerometers .....	82
Table 6.1	Travel times measured during Pulse Transmission testing .....	103
Table 7.1	Meteorological Summary of Test Dates on Flexible Pavements .....	132
Table 7.2	Ground Temperature Measurements at Keillor Road Site .....	133

## LIST OF FIGURES

Figure 2.1 Different components of seismic waves .....	15
Figure 2.2 Different types of elastic waves [after Borm, (1978)]. .....	16
Figure 2.3 Distribution of displacement waves from a circular footing on a homogenous, isotropic, elastic half-space [after Woods, (1968)].....	17
Figure 2.4 Variation of $V_p$ , $V_s$ & $V_r$ with $\nu$ (Poisson's ratio) [after Richart, (1962)] .....	17
Figure 2.5 Seismic methods .....	18
Figure 2.6 Principle of shear wave refraction survey [after Borm, (1978)].....	19
Figure 2.7 Principle of two-layer reflection [after Borm, (1978)] .....	20
Figure 2.8 Crosshole seismic method .....	20
Figure 2.9 Downhole seismic method.....	20
Figure 2.10 Schematic representation of up-hole, in-hole and bottom-hole methods .....	21
Figure 2.11 Horizontal and vertical components of P-wave, S-wave and R-wave in ideal medium [after Lamb, (1904)] .....	22
Figure 2.12 Surface wave propagation in elastic half-space [after Fung, (1965)].....	23
Figure 2.13 Amplitude ratio versus dimensionless depth for Rayleigh waves [after Richart et al., (1970)] .....	23
Figure 2.14 Surface wave dispersion in a uniform half space and a layered half space .....	24
Figure 2.15 Deformed shape of a half-space surface [after Richart et. al., (1970)] .....	24
Figure 3.1 General configuration of first generation of SASW tests .....	42
Figure 3.2 Common-Receiver-Midpoint (CRMP) Geometry .....	43
Figure 3.3 Common-Source (CS) Geometry .....	43
Figure 3.4 A typical coherence function diagram. ....	44
Figure 3.5 An idealized wrapped phase diagram. ....	45
Figure 3.6 University of Alberta SASW system [after Addo, (1992)] .....	46

Figure 3.7	A typical soil layer model for forward modelling [after Tokimatsu et. al. (1992)].	47
Figure 4.1	A schematic diagram of the Benkelman Beam [after O'Flaherty, (1988)].	60
Figure 4.2	Geometric configuration of loads and stations for Dynaflect [after Roeset et al., (1985)].	60
Figure 4.3	A schematic diagram of Dynatest 8000 model FWD test equipment [after Croney et al., (1991)]	61
Figure 4.4	A schematic diagram of the falling mass system of Dynatest 8000 model FWD device [after Croveti et al., (1989)]	61
Figure 4.5	Typical location of the loading plate and the deflection sensors of FWD [after Foxworthy et al., (1989)].	62
Figure 4.6	A typical deflection basin diagram [after Badu-Tweneboah et al. (1989)]	62
Figure 5.1	SASW equipment set-up as used in this research.	83
Figure 5.2	A schematic diagram of PCB Model 482A16 Power Amplifier	84
Figure 5.3	The circuit diagram of Interface Control Unit (ICU).	85
Figure 5.4	A schematic diagram of a typical geophone.	86
Figure 5.5	A schematic diagram of a typical ICP transducer	86
Figure 5.6	A schematic diagram of a typical ICP system	87
Figure 5.7	Front Panel Diagram of "SWAP".	87
Figure 5.8	A typical signal captured with a receiver	88
Figure 5.9	Conversion of phase from wrapped state to unwrapped state	89
Figure 5.10	First screen of "MULTIMOD" Software asking for layer parameters	90
Figure 5.11	Second screen of "MULTIMOD" Software asking for boundary conditions.	91
Figure 5.12	Third screen of "MULTIMOD" Software giving an idea of calculation time	92
Figure 5.13	Theoretical Dispersion Curve for first three Rayleigh Modes	93
Figure 6.1	Location of University of Alberta SASW Test Section B-11, Basement Slab	104
Figure 6.2	Location of University of Alberta LRT SASW Test Section, Rigid Pavement.	105

Figure 6.3	Location of Whitemud Drive SASW Test Section, Flexible Pavement .....	106
Figure 6.4	Location of Keillor Road SASW Test Section, Flexible Pavement .....	107
Figure 6.5	A schematic diagram of the Pulse Transmission Method. ....	108
Figure 6.6	Plot of travel times of wave signals .....	109
Figure 7.1	Dispersion Curve from Room CEB-B11 Basement Slab, November 1992 .....	134
Figure 7.2	Shear wave velocity profile from Room CEB-B11 Basement Slab, November 1992 .....	135
Figure 7.3	Dispersion curves (SASW-FM) from Room B-11 Basement Slab, November 1992 .....	136
Figure 7.4	Shear Wave Velocity Profile (SASW-FM output), Room CEB-B11, November 1992 .....	137
Figure 7.5	Comparison of Shear Wave Velocity Profile (Moving Point Average & SASW-FM), Room CEB-B11, Basement Slab, November 1992 .....	138
Figure 7.6	Comparison of Ccalc, Cfield and MULTIMOD output, Room CEB-B11, Basement Slab, November 1992 .....	139
Figure 7.7	Dispersion Curve from Room CEB-B11 Basement Slab, May 1993 .....	140
Figure 7.8	Shear wave velocity profile from CEB-B11 Basement Slab, May 1993 .....	141
Figure 7.9	Dispersion curves (SASW-FM) from Room B-11 Basement Slab, May 1993. ....	142
Figure 7.10	Shear Wave Velocity Profile (SASW-FM output), Room CEB-B11 May 1993 .....	143
Figure 7.11a	Comparison of Shear Wave Velocity Profile (Moving Point Average & SASW-FM) Room CEB-B11, Basement Slab, May 1993 .....	144
Figure 7.11b	Comparison of Shear wave Velocity Profile from Room CEB-B11 .....	145
Figure 7.12	Dispersion curve of Pavement Section CC .....	146
Figure 7.13	Shear wave velocity profile of Pavement Section CC .....	147
Figure 7.14	Dispersion curves (SASW-FM) from Pavement Section CC .....	148
Figure 7.15	Shear wave Velocity Profile (SASW-FM), Pavement Section CC .....	149
Figure 7.16	Comparison of Shear wave Velocity Profile (Moving Point Average & SASW-FM), Pavement Section CC .....	150

Figure 7.17	Comparison of Shear Wave Velocity profile (Moving Point Average & SASW-FM), Pavement Section EE .....	151
Figure 7.18	Comparison of Shear Wave Velocity Profile (Moving Point Average & SASW-FM), Pavement Section FF .....	152
Figure 7.19	Overlay plot of average shear wave velocity profile from Pavement Sections CC, EE & FF.....	153
Figure 7.20	Dispersion Curve from Whitemud Drive, April 9, 1993 .....	154
Figure 7.21	Shear wave velocity profile from Whitemud Drive, April 9, 1993 .....	155
Figure 7.22	Dispersion curves (SASW-FM) from W'Mud Drive, April 9, 1993 .....	156
Figure 7.23	Shear Wave Velocity Profile (SASW-FM output), Whitemud Drive, April 9, 1993 .....	157
Figure 7.24	Comparison of Shear Wave Velocity Profile (Moving Point Average & SASW-FM), Whitemud Drive, April 9, 1993 .....	158
Figure 7.25	Comparison of Shear Wave Velocity Profile (Moving Point Average & SASW-FM), Whitemud Drive, April 22, 1993 .....	159
Figure 7.26	Comparison of Shear Wave Velocity Profile (Moving Point Average & SASW-FM), Whitemud Drive, April 29, 1993 .....	160
Figure 7.27	Comparison of Shear Wave Velocity Profile (Moving Point Average & SASW-FM), Whitemud Drive, May 14, 1993 .....	161
Figure 7.28	Overlay Plot of average shear wave velocity profile at Whitemud Drive, all test dates.....	162
Figure 7.29	Ground temperature profile, Keillor Road .....	163
Figure 7.30	Dispersion curve from Keillor Road, April 14, 1993 .....	164
Figure 7.31	Shear wave velocity profile from Keillor Road, April 14, 1993. ....	165
Figure 7.32	Dispersion curves (SASW-FM) from Keillor Road, April 14, 1993.....	166
Figure 7.33	Shear Wave Velocity Profile (SASW-FM) from Keillor Road, April 14, 1993 .....	167
Figure 7.34	Comparison of Shear Wave Velocity Profile (Moving Point Average & SASW-FM), Keillor Road, April 14, 1993 .....	168
Figure 7.35	Comparison of Shear Wave Velocity Profile (Moving Point Average & SASW-FM), Keillor Road, April 22, 1993 .....	169
Figure 7.36	Comparison of Shear Wave Velocity Profile (Moving Point Average & SASW-FM), Keillor Road, April 29, 1993 .....	170
Figure 7.37	Comparison of Shear Wave Velocity Profile (Moving Point	

Average & SASW-FM), Keillor Road, May 14, 1993 .....	171
Figure 7.38 Overlay Plot of average shear wave velocity profile at Keillor Road, all test dates. ....	172
Figure 7.39 Comparison of Ccalc, Cfield and MULTIMOD output, Keillor Road, April 22, 1993 .....	173
Figure AI.1 Set up for creating a Site Folder and Data File .....	191
Figure AI.2 Set up for entering receiver spacing .....	192
Figure AI.3 Set up for capturing amplitude signals .....	193
Figure AI.4 Set up for plotting amplitude signals.....	194
Figure AI.5 Set up for dispersion calculation .....	195
Figure AII.1 Dispersion curve of Pavement Section EE .....	197
Figure AII.2 Shear wave velocity profile of Pavement Section EE.....	198
Figure AII.3 Dispersion curves (SASW-FM) from Pavement Section EE.....	199
Figure AII.4 Shear wave Velocity Profile (SASW-FM output), Pavement Section EE .....	200
Figure AII.5 Dispersion curve of Pavement Section FF .....	201
Figure AII.6 Shear wave velocity profile of Pavement Section FF. ....	202
Figure AII.7 Dispersion curves (SASW-FM) from Pavement Section FF .....	203
Figure AII.8 Shear wave Velocity Profile (SASW-FM output), Pavement Section FF .....	204
Figure AII.9 Dispersion curve from Whitemud Drive, April 22, 1993 .....	205
Figure AII.10 Shear wave velocity profile from Whitemud Drive, April 22, 1993. ....	206
Figure AII.11 Dispersion curves (SASW-FM) from Whitemud Drive, April 22, 1993 .....	207
Figure AII.12 Shear wave Velocity Profile (SASW-FM output), Whitemud Drive, April 22, 1993 .....	208
Figure AII.13 Dispersion curve from Whitemud Drive, April 29, 1993 .....	209
Figure AII.14 Shear wave velocity profile from Whitemud Drive, April 29, 1993. ....	210
Figure AII.15 Dispersion curves (SASW-FM) from Whitemud Drive, April 29, 1993 .....	211

Figure AII.16 Shear Wave Velocity Profile (SASW-FM output), Whitemud Drive, April 29, 1993 .....	212
Figure AII.17 Dispersion curve from Whitemud Drive, May 14, 1993 .....	213
Figure AII.18 Shear wave velocity profile from Whitemud Drive, May 14, 1993. ....	214
Figure AII.19 Dispersion curves (SASW-FM) from Whitemud Drive, May 14, 1993 .....	215
Figure AII.20 Shear wave Velocity Profile (SASW-FM output), Whitemud Drive, May 14, 1993 .....	216
Figure AII.21 Dispersion curve from Keillor Road, April 22, 1993 .....	217
Figure AII.22 Shear wave velocity profile from Keillor Road, April 22, 1993.....	218
Figure AII.23 Dispersion curves (SASW-FM) from Keillor Road, April 22, 1993 .....	219
Figure AII.24 Shear wave Velocity Profile (SASW-FM output), Keillor Road, April 22, 1993 .....	220
Figure AII.25 Dispersion curve from Keillor Road, April 29, 1993 .....	221
Figure AII.26 Shear wave velocity profile from Keillor Road, April 29, 1993.....	222
Figure AII.27 Dispersion curves (SASW-FM) from Keillor Road, April 29, 1993 .....	223
Figure AII.28 Shear Wave Velocity Profile (SASW-FM output) from Keillor Road, April 29, 1993 .....	224
Figure AII.29 Dispersion Curve from Keillor Road, May 14, 1993.....	225
Figure AII.30 Shear wave velocity profile from Keillor Road, May 14, 1993.....	226
Figure AII.31 Dispersion curves (SASW-FM) from Keillor Road, May 14, 1993 .....	227
Figure AII.32 Shear wave Velocity Profile (SASW-FM output), Keillor Road, May 14, 1993.....	228
Figure AIII.1 Effect of SASW-FM Input Parameters on SASW-FM Output Results (Set 1: Room CEB-B11, Basement Slab).....	230
Figure AIII.2 Effect of SASW-FM Input Parameters on SASW-FM Output Results (Set 2: Room CEB-B11, Basement Slab).....	231
Figure AIII.3 Effect of SASW-FM Input Parameters on SASW-FM Output Results (Set 3: Room CEB-B11, Basement Slab).....	232
Figure AIII.4 Effect of SASW-FM Input Parameters on SASW-FM Output Results (Set 4: Room CEB-B11, Basement Slab).....	233

Figure AIII.5 Effect of SASW-FM Input Parameters on SASW-FM Output Results (Set 5: Room CEB-B11, Basement Slab).....	234
Figure AIII.6 Effect of SASW-FM Input Parameters on SASW-FM Output Results (Set 6: Room CEB-B11, Basement Slab).....	235
Figure AIV.1 Modulus Profile, Room CEB-B11, November 1992.....	237
Figure AIV.2 Modulus Profile, Room CEB-B11, May 1993 .....	238
Figure AIV.3 Modulus Profile, Pavement Section CC .....	239
Figure AIV.4 Modulus Profile, Pavement Section EE .....	240
Figure AIV.5 Modulus Profile, Pavement Section FF .....	241
Figure AIV.6 Modulus Profile, Whitemud Drive, April 9, 1993.....	242
Figure AIV.7 Modulus Profile, Whitemud Drive, April 22, 1993.....	243
Figure AIV.8 Modulus Profile, Whitemud Drive, April 29, 1993.....	244
Figure AIV.9 Modulus Profile, Whitemud Drive, May 14, 1993.....	245
Figure AIV.10 Modulus Profile, Keillor Road, April 14, 1993 .....	246
Figure AIV.11 Modulus Profile, Keillor Road, April 22, 1993 .....	247
Figure AIV.12 Modulus Profile, Keillor Road, April 29, 1993 .....	248
Figure AIV.13 Modulus Profile, Keillor Road, May 14, 1993 .....	249



## **CHAPTER ONE**

### **INTRODUCTION**

#### **1.1 GENERAL/PROBLEM STATEMENT**

Seismologists were using surface wave techniques for profiling deep earth structures long before engineers started using them for profiling shallow 'near the surface' layers. The data analysis are very complex and the equipment necessary to perform surface wave testing were very expensive until the advent of state-of-the-art computer technology. Detailed descriptions of surface wave methods are given in chapters 2 and 3. The major advantage of surface wave methods is that all measurements can be performed from the ground surface without drilling any boreholes. The Spectral-Analysis-of-Surface-Waves (SASW) is a nondestructive testing method based on the dispersion characteristics of Rayleigh waves (Surface waves). SASW tests have been used for soil profiling over deeper layers. A detailed description of the SASW method is provide in Chapter 3. The present research has concentrated on using the SASW technique for obtaining the stiffness profiles over shallow depths of ground structures having contrasting layer properties, such as, pavements and concrete layers.

#### **1.2 OBJECTIVES**

The general purpose of this study has been to develop the SASW technique for pavement evaluation. Pavement evaluation means determining the structural integrity of the pavements. Existing methods for pavement evaluation are mostly deflection based. These techniques consist of measuring surface deflections under applied loads. Surface deflection measurement devices can be categorized as either static (e.g. Benkelman Beam) or dynamic

(e.g. Dynaflect, Falling Weight Deflectometer). SASW has the potential for pavement evaluation. The more detailed objectives of this dissertation are as follows:

1. Modify the existing University of Alberta SASW system to collect and interpret SASW data on pavements.
2. Develop SASW field procedures for evaluation of pavements using high frequency sources, and receivers.
3. Evaluate the modified SASW system at different pavement sites with varying stiffness profiles and layer thicknesses.

### 1.3 THESIS ORGANIZATION

This dissertation is divided into eight chapters.

Chapter one contains a general introduction to the topic as well as objectives and the work organization.

Chapter two gives background information on seismic waves.

Chapter three reviews the general SASW concept. It also includes a description of the existing University of Alberta SASW system.

Chapter four summarizes the current methods to evaluate the structural integrity of pavements.

Chapter five describes the new developments that have been implemented by this research.

Chapter six discusses different sites that have been selected for this research as well as describes the field and laboratory work that have been carried out for this study.

Chapter seven presents the analysis and discussion of results.

Chapter eight as the terminal section of the study providing a summary of the thesis, conclusions and major recommendations for further research.

## CHAPTER TWO

### SEISMIC WAVES

#### 2.1 SEISMIC WAVES

Before the SASW technique is discussed in detail, a brief background is given on seismic waves, their components and the corresponding evolution of the SASW technique. Figure 2.1 shows the different components of seismic waves and Figure 2.2 [after Borm, (1978)] illustrates the motion of the different types of waves.

When an impulsive vertical point load is applied on the surface of the ground, the energy which causes ground motion is transferred through the medium by elastic displacement waves (seismic waves). During seismic wave propagation analysis, the propagating medium is assumed to be homogenous, isotropic and an elastic half-space. Many authors [Lamb, H. (1904), Kolsky (1953), Ewing et. al (1957), Grant & West (1965)] have dealt with the propagation of seismic waves using the assumptions given above. The energy coupled into the soil by a vertical surface source is transmitted away from the source by a combination of compressional waves (P-), shear waves (S-), and Rayleigh (R-) waves. Based on Miller & Pursey's (1955) equation, for the case of an elastic half space with Poisson's ratio  $\nu = 0.25$  excited by a vertically oscillating circular disc, Woods (1968) showed the distribution of compressional waves (P-), shear waves (S-), and Rayleigh (R-) waves as shown in Figure 2.3.

Body waves propagate radially outwards from the source along hemispherical wave fronts, whereas Rayleigh waves propagate radially outward on a cylindrical wave front. The energy density of these waves decreases with distance from the source because the waves

encounter an increasingly larger volume of material as they travel outward. This phenomenon is called geometrical damping. For amplitudes the geometrical damping law governing body waves is expressed by  $1/r$  (except along the surface where it is  $1/r^2$ ) and the geometrical damping law for the Rayleigh wave is given by  $1/r^{0.5}$  where  $r$  = source-receiver distance. Miller and Pursey (1955) determined the distribution of total input energy among the three elastic waves to be 67% Rayleigh waves, 26% shear waves and 7% compression waves. Two-thirds of the total input energy is transmitted away from a vertical surface energy source by the Rayleigh wave, and Rayleigh waves decay much more slowly with distance than body waves.

In elastic materials the following relationships exist.

$$V_p = \left[ \frac{\lambda + 2G}{\rho} \right]^{\frac{1}{2}} = \left[ \frac{(1 - \nu)E}{(1 - \nu - 2\nu^2)\rho} \right]^{\frac{1}{2}} \quad [2.1]$$

$$V_s = \left[ \frac{G}{\rho} \right]^{\frac{1}{2}} \quad [2.2]$$

$$V_r = kV_s \quad [2.3]$$

where  $E$  = Young's Modulus of Elasticity

$$G = \frac{E}{2(1 + \nu)} = \text{Modulus of Rigidity or Shear Modulus}$$

$\rho$  = Mass Density

$\nu$  = Poisson's Ratio

$$\lambda = \frac{\nu E}{(1 + \nu)(1 - 2\nu)} = \text{Lamé's parameter}$$

$$k = \text{constant} = f(\nu) \quad 0.874 \leq k \leq 0.955$$

$V_p$  = P-wave velocity

$V_s$  = S-wave velocity

$V_r$  = Rayleigh wave velocity

In all materials  $V_r < V_s < V_p$  .

The shear wave velocity ( $V_s$ ) in soils is controlled primarily by

- void ratio ( $e$ )
- effective confining stress ( $\sigma'$ )
- stress history, and
- soil fabric.

The most important factor that influences the shear wave velocity is the effective stress state. The soil fabric relates to the cementation. High cemented materials experience high shear wave velocity and vice versa.

In elastic materials, velocities of P and S waves are frequency independent. In viscoelastic media, all waves are frequency dependent. It is possible to obtain solutions for viscoelastic media from those for elastic materials using the transformation described in Velostos and

Verbic, (1973). Solutions for deterministic problems concerning wave travel in non-linear materials are covered in Heierli, (1962) and Selig, (1964).

The ratio  $\frac{V_r}{V_s}$  depends on  $\nu$  and is frequency dependent except in an elastic halfspace [Bullen, (1953); Newmark & Rosenblueth, (1971)].  $\frac{V_p}{V_s}$  also depends on  $\nu$ . Variation of  $V_p$  and  $V_r$  with respect to  $V_s$  as a function of  $\nu$  is shown in Figure 2.4 [after Richart (1962)]. If  $\nu=0.5$ , there is no volume change and  $V_s=V_r$ .

In a layered medium, the velocity of the Rayleigh wave is a function of wavelength or frequency of the propagating wave, whereas in a homogenous, elastic half-space the velocity of the Rayleigh wave is constant. The dependency of the Rayleigh wave velocity on the wavelength indicates that Rayleigh waves are dispersive. High frequency waves, or those with short wavelengths, propagate in shallow layers, i.e. layers near the surface, while long wavelengths penetrate to deeper layers. The velocity of the Rayleigh waves is governed by the properties of the layer(s) through which the bulk of the wave propagates. Therefore, by applying Rayleigh waves over a wide range of frequencies, it is possible to evaluate velocities of different layers at a layered site.

Body wave methods and surface wave methods are the two main categories of seismic wave methods that are used to determine seismic velocity profiles. Both methods have their own advantages and limitations. Body wave methods are generally relatively simple in that there is less complex data acquisition and analysis procedures than surface wave methods. Both methods measure the travel time of the waves, but in body wave methods, the first arrival of compression or shear waves at a receiver are identified and the travel time is generally measured for the wave to propagate from the source to the receiver. The wave velocity is then calculated from the equation:

$$V_{ij} = \Delta_{ij}s / \Delta_{ij}t \quad [2.4]$$

where  $V_{ij}$  = Wave propagation velocity between receivers 'i' and 'j'

$\Delta_{ij}s$  = distance between two receivers

$\Delta_{ij}t$  = measured travel time between two receivers.

By measuring apparent velocities and then varying the receiver locations from the source, the velocity-depth function can be obtained. In surface wave methods, a more complex procedure is adopted to determine travel time. Body wave methods are often easy to interpret and therefore can be less prone to errors than the more complex surface wave methods. The advantages of the surface wave methods are that this type of wave can be generated by a vertically-acting source on the surface, and therefore, is the most easily measured type of wave in terms of signal-to-noise ratio [Rix, (1988)]. Seismic methods can be divided into different groups as shown in Figure 2.5. There are many advantages and disadvantages of each of the methods, which are briefly discussed in the following sections.

## 2.2 BODY WAVE METHODS

Details of the Refraction method can be found in Richart et. al, (1970) and Borm, (1978). The advantages of the refraction method lies in the ease of data acquisition and reduction, no requirement of boreholes (i.e. all measurements can be performed from the ground surface) and the determination of travel times is based on first arrivals at each sensor. The major disadvantage of this method is it's inability to resolve a low wave velocity layer under a high wave velocity layer, such as the case of pavements. As well this method cannot accurately recognize thin layers in a profile. When compression waves are used, this



method cannot resolve the velocity profile in soft, saturated soil conditions, because under fully saturated conditions the velocity of compression waves is approximately 1500 m/s irrespective of different soil skeleton stiffness (Biot, 1956; and Allen et. al 1980). The principles of shear wave refraction survey are shown in Figure 2.6 [after Borm, (1978)].

Details of the Reflection method can be found in Richart et. al, (1970); Borm, (1978) and Dobrin, (1976). The advantages of this method includes no requirement of boreholes, can identify low velocity layer below high velocity layer, can distinguish thin layers of profile. As most reflection surveys use compression waves, this method is problematic in saturated soil conditions. The absence of a strong reflecting boundary can also reduce it's effectiveness. Shear waves are presently being tried to overcome some of these difficulties. The principle of two-layer reflection is shown in Figure 2.7 [after Borm, (1978)].

Details of the Crosshole test method can be found in White, (1965); Stokoe and Woods, (1972); Schwarz and Musser, (1972); Woods, (1986); Ballard, (1976); Stokoe and Hoar, (1978); Hoar and Stokoe, (1978); ASTM (1988); Department of the Army, (1979). The advantages of this method includes increased control over the type of waves to be generated for specific purposes, determination of two-dimensional profile, wave travel path is almost constant with depth, lower velocity material overlain by higher velocity material may be detected. The disadvantages are that this method requires two or more boreholes, possibility of refraction of waves between boreholes, and possible inaccurate measurements due to vertical deviation of boreholes. The principle of the Crosshole test is shown in Figure 2.8.

Details of the Downhole test can be found in Stokoe and Hoar, (1978); Patel, (1981); Beeston et. al (1977). One important advantage of the Downhole test in comparison to the Crosshole test is that only one borehole is required. The Downhole test can detect lower

velocity layers overlain by higher velocity material. One of the disadvantages of this method lies in the lack of penetration of the waves due to the attenuation of high frequency waves with depth. When cased boreholes are used, the compression waves can travel through the casing faster than the waves travel through the soil skeleton potentially giving inaccurate results in these circumstances. A typical Downhole seismic method is shown in Figure 2.9. Robertson et al., (1986) described the development of seismic cone penetration test (SCPT), which is a "new" downhole test. Robertson et al (1986) also showed that the SCPT downhole method gives essentially the same results as the more costly cross-hole method, at sites where shear wave velocity anisotropy does not exist.

The principle of the Uphole method is similar to that of the Downhole test except that the source and receiver are reversed. In the Uphole method, measurement is made of the time a seismic signal takes to travel through the ground, between the source at a certain depth within a borehole and the detection points along a geophone spread at the surface [Lüdeling (1978)].

For the In-hole method, a source and one or more receivers are used in the same borehole to measure the time for body waves to travel vertically along the borehole wall from the source to the receivers. [Hoar, (1982)]

In the Bottom-hole method, a probe consisting of a source and one or more receivers is pushed into the natural soil beyond the bottom of a predrilled borehole and the time for body waves to travel vertically from the source to the receiver(s) is measured [Hoar, (1982)]. Schematic representation of Uphole, In-hole and Bottom-hole methods are shown in Figure 2.10.

### 2.3 SURFACE WAVE METHODS

Surface waves can be either Rayleigh waves or Love waves. The particle motion associated with Rayleigh waves is made up of a horizontal and vertical component and forms a retrograde ellipse on the surface. Rayleigh waves constitute 67% of the energy from a vertically oscillating surface source and the amplitude decreases at a ratio of  $1/r^{0.5}$ . Because of the high energy content and low ratio of geometrical damping, Rayleigh waves are well suited for surface seismic testing.

As mentioned earlier, surface waves travel in cylindrical wavefronts. In a homogenous half-space the surface wave is represented by the Rayleigh wave [Rayleigh, (1885)]. Rayleigh waves are only slightly influenced by a water table because the pore water cannot transmit shear. The insensitivity of the S-wave and R-wave to the water table represents a distinct advantage for techniques that use these waves. The only influences of the water table and pore fluids on the propagation of shear waves in the soil structure are through the buoyancy effects on unit weight of the soil and inertia forces [Richart et. al (1970)].

Most civil engineering applications consider only plane surface waves to avoid the complexities and inconvenience of dealing with complex forms of wave motion [Rix, (1988)]. The error due to this assumption is extremely low as pointed out by Aki and Richards, (1980); and Sánchez-Salinero et. al., (1987). If the input impulse is of a short duration, then the horizontal and vertical components of the P-wave, S-wave, and R-wave are shown in Figure 2.11(a,b) [after Lamb, (1904)]. It is seen that the R-wave is the most significant disturbance along the surface of a half-space and, at large distances from the source, may be the only clearly distinguishable wave. By combining the horizontal and vertical components of particle motion starting at point 1, the locus of surface-particle motion for the R-wave can be drawn as shown in Figure 2.11c. The path of the particle

motion describes a retrograde ellipse, in contrast to the prograde-ellipse motion associated with water waves. Surface wave propagation in an elastic half-space is shown in Figure 2.12 [after Fung, (1965)].

The amplitude ratio variation of the horizontal (i.e. radial) and vertical component of Rayleigh waves with dimensionless depth for different values of Poisson's ratio is shown in Figure 2.13 [after Richart et al., (1970)]. Surface waves are dispersive in nature i.e. the velocity of propagation of the wave varies with the frequency or wavelength. Surface wave dispersion in a uniform half space, in a layered half space in which velocity increases with depth, and in a layered half space in which velocity decreases with depth are illustrated in Figure 2.14.

The dispersive characteristics of surface waves are utilized in surface wave methods. In SASW, the velocity of propagation is termed as surface wave phase velocity (sometimes called apparent surface wave velocity). Phase velocity is defined as the velocity with which a seismic disturbance of a single frequency is propagated in the medium [Nazarian et. al, (1989)]. The phase velocity is a complex function of the shear and compression wave velocities of each of the layers in a layered half space [Rix, 1988]. The Spectral-Analysis-of-Surface-Waves (SASW) technique constitutes the measurement of surface wave dispersion, and the back calculation of shear wave velocities by means of a process called inversion.

## 2.4 STEADY STATE RAYLEIGH WAVE METHOD

The steady state Rayleigh Wave method is the predecessor of SASW testing method. In the steady state method, a vertically-acting vibrator is operated at a fixed frequency 'f'. The receivers are positioned on the ground by trial and error until the vertical motion is in phase

with the vibrator. The distance between two adjacent receivers is the wavelength  $L_R$  of the surface wave at that frequency. Therefore the phase velocity  $V_R$  of the surface wave at that frequency is:

$$V_R = f * L_R \quad [2.5]$$

The testing procedure is repeated for different frequencies until a complete dispersion curve has been drawn. This method is extremely time-consuming. The sinusoidal input source will displace the surface of the half-space in the form of a sine curve as shown in Figure 2.15 [after Richart et al., (1970)].

As shown on Figure 2.4,  $V_R$  is almost equal to  $V_S$ . Figure 2.13 shows that the bulk of R-waves travel through a zone of the halfspace about one wavelength deep. It can be further postulated that the average properties within this zone approximate the properties at a depth of one-half wavelength ( $L_R/2$ ) [Richart et. al, (1970)]. This assumption is reasonable for uniform- and layered-soil media [Heukelom and Foster (1960); Fry (1963); and Ballard (1964)]. By decreasing the frequency the wavelength increases and the sampled depth increases; conversely, by increasing the frequency the wavelength decreases and sampled depth decreases. For a homogenous, isotropic, elastic half-space, all frequencies will yield the same velocity, because the material properties are independent of depth in this case. For an elastic half space in which the elastic properties change gradually with depth, steady state vibration testing at the surface with different frequencies can determine the elastic properties of the half space [Richart et. al, (1970)]. However, this technique is very time-consuming and has not gained popularity.

## 2.5 SUMMARY

This chapter has provided a brief overview on seismic waves and has described the different methods available to measure seismic wave velocity profiles. Body wave methods such as refraction, reflection, crosshole, downhole, uphole, in-hole and bottom-hole have been explained in a concise format. Surface wave method such as steady state Rayleigh wave method was also discussed in this chapter. Details of the SASW technique will be given in the following chapter.

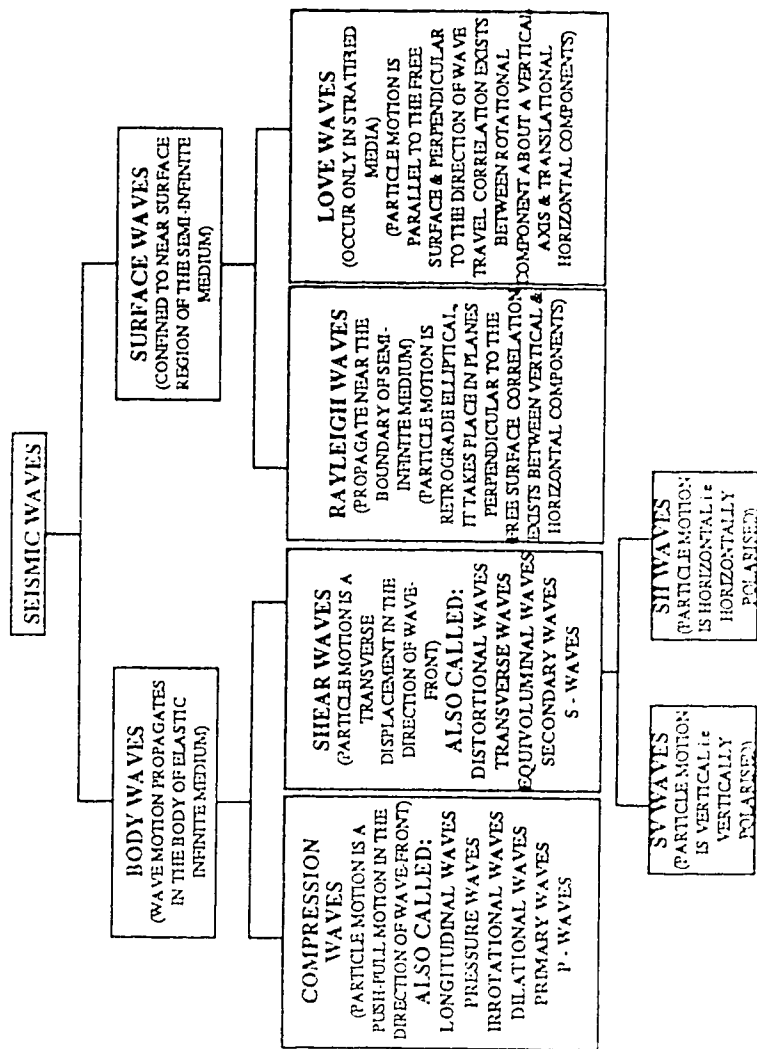
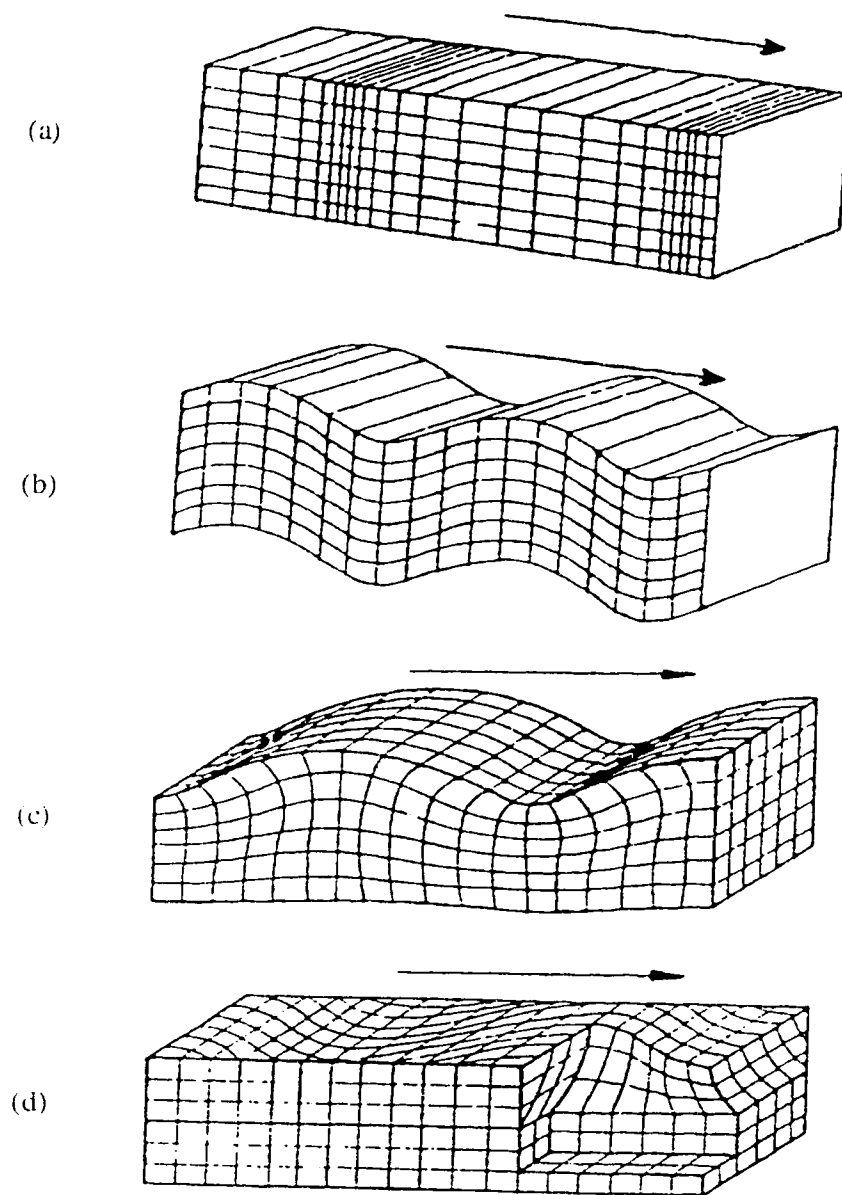


Figure 2.1 Different components of seismic waves



Body Waves: (a) Compressional wave, (b) Shear wave  
Surface Waves: (c) Rayleigh wave, (d) Love wave

Figure 2.2 Different types of elastic waves [after Borm, (1978)]



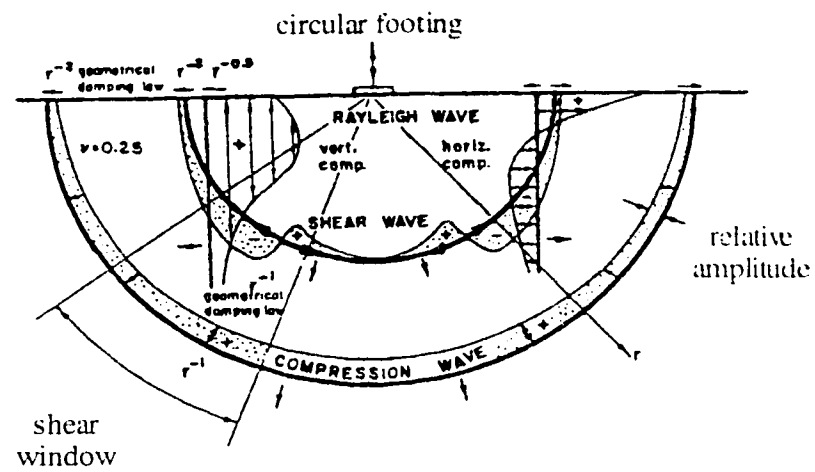


Figure 2.3 Distribution of displacement waves from a circular footing on a homogenous, isotropic, elastic half-space [after Woods, (1968)]

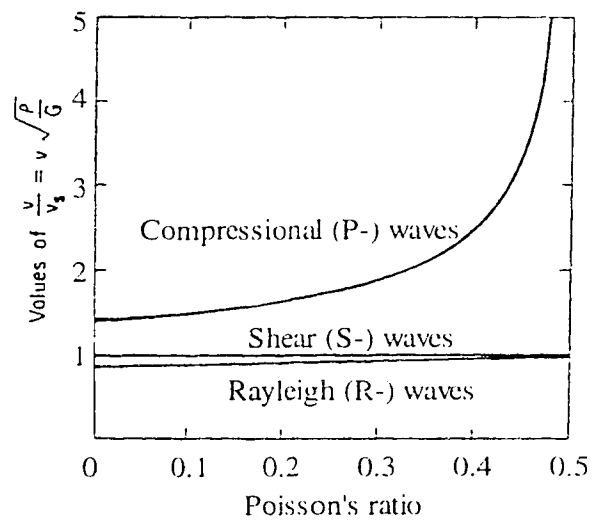


Figure 2.4 Variation of  $V_p$ ,  $V_s$  &  $V_r$  with Poisson's ratio [after Richart, (1962)]

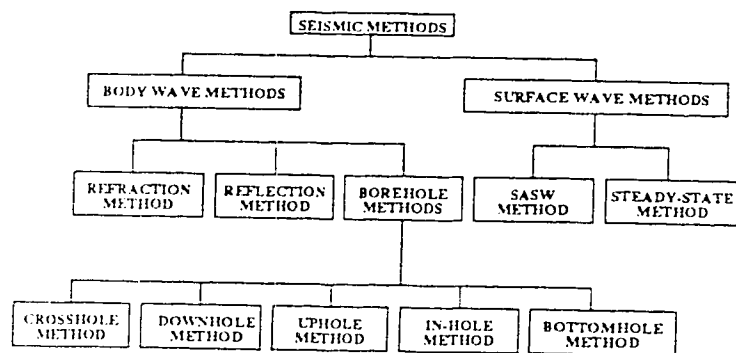


Figure 2.5 Seismic methods

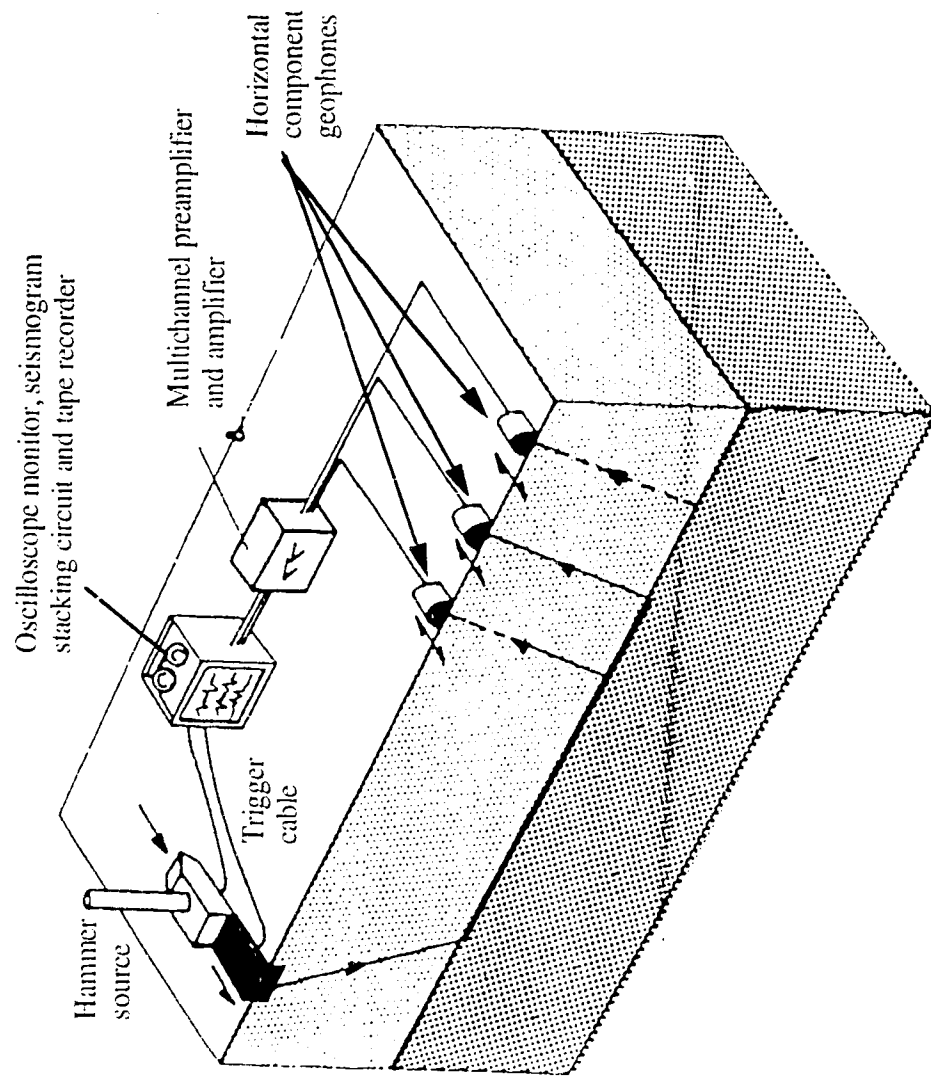


Figure 2.6 Principle of shear wave refraction survey [after Borm, (1978)]

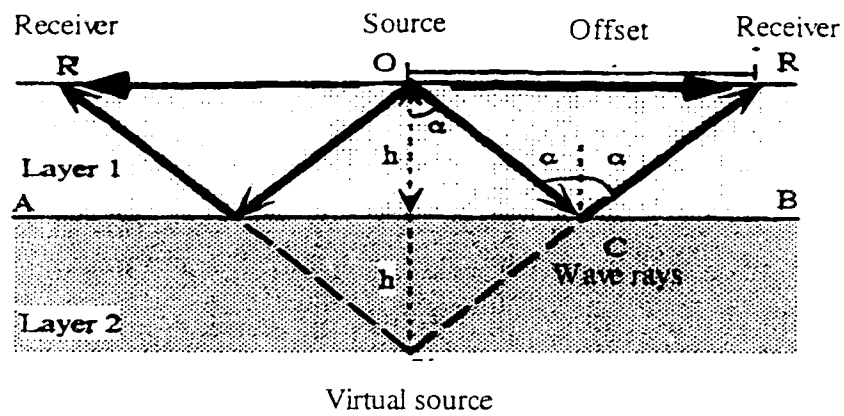


Figure 2.7 Principle of two-layer reflection [after Borm, (1978)]

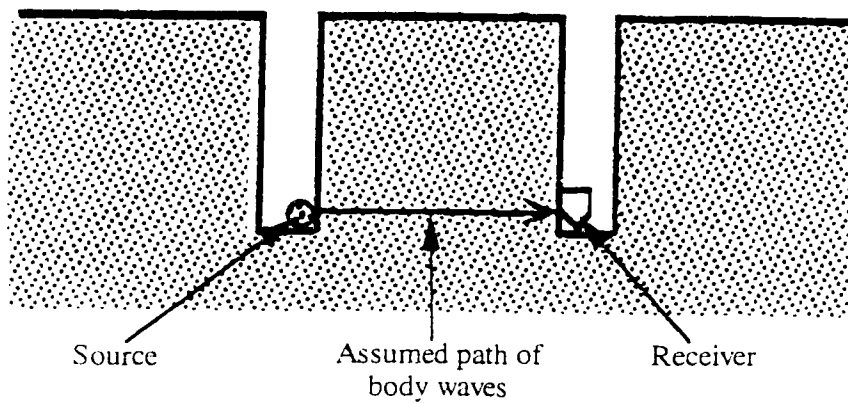


Figure 2.8 Crosshole seismic method

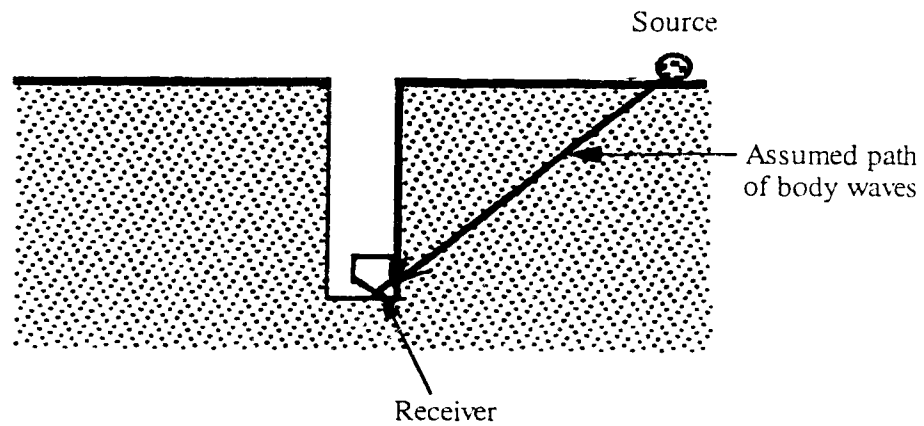


Figure 2.9 Downhole seismic method

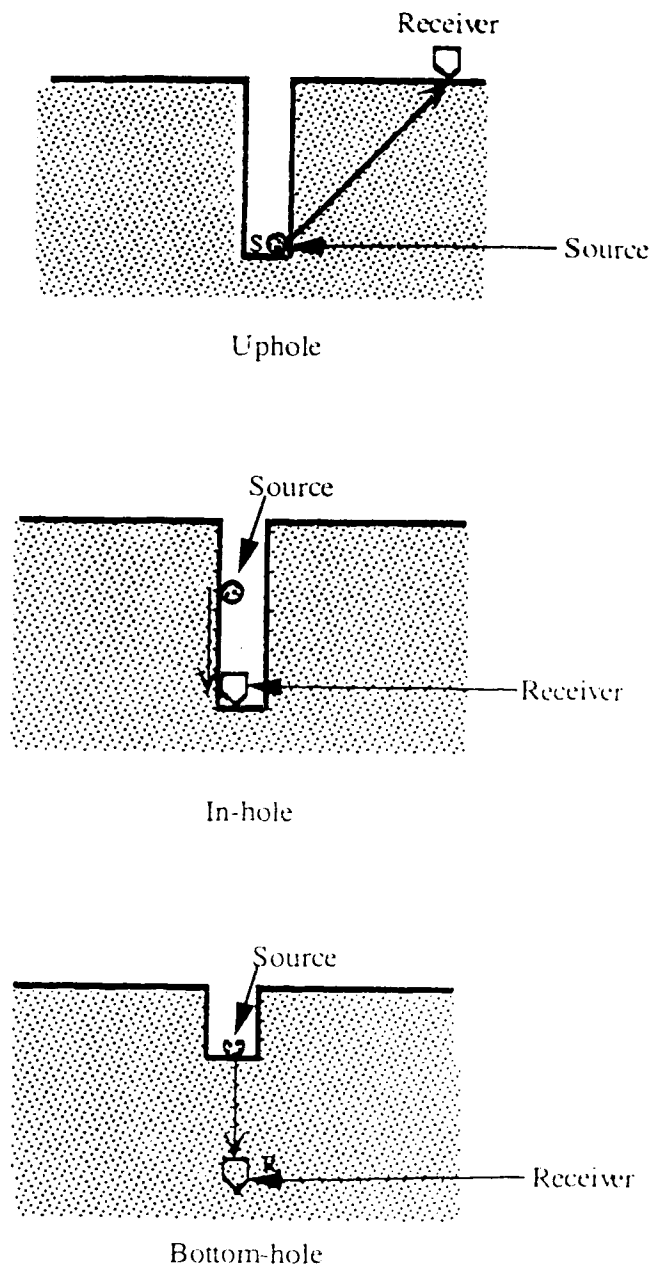


Figure 2.10 Schematic representation of up-hole, in-hole and bottom-hole methods

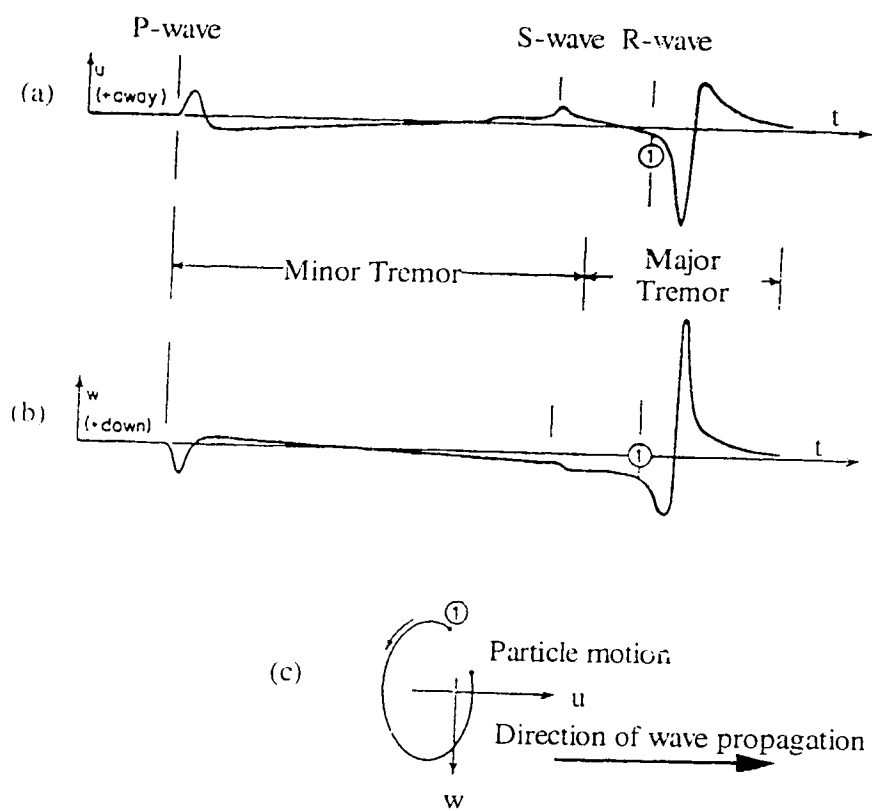


Figure 2.11 Horizontal and vertical components of P-wave, S-wave and R-wave in an ideal medium [after Lamb, (1904)]

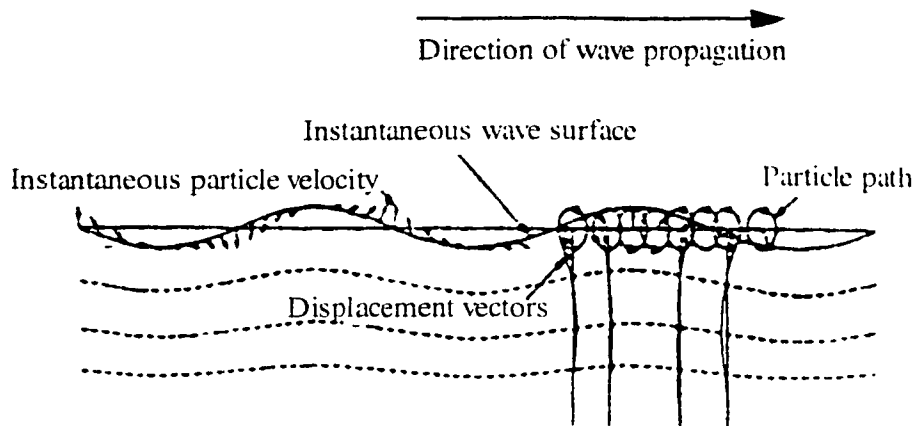


Figure 2.12 Surface wave propagation in elastic half-space [after Fung, (1965)]

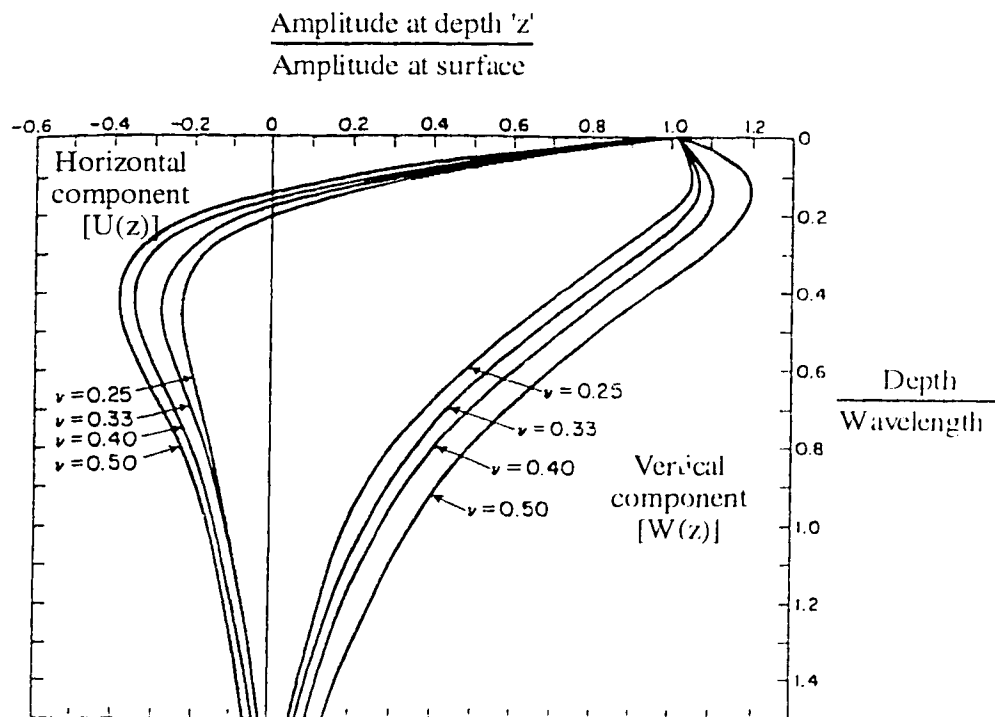


Figure 2.13 Amplitude ratio versus dimensionless depth for Rayleigh waves [after Richart et al., (1970)]

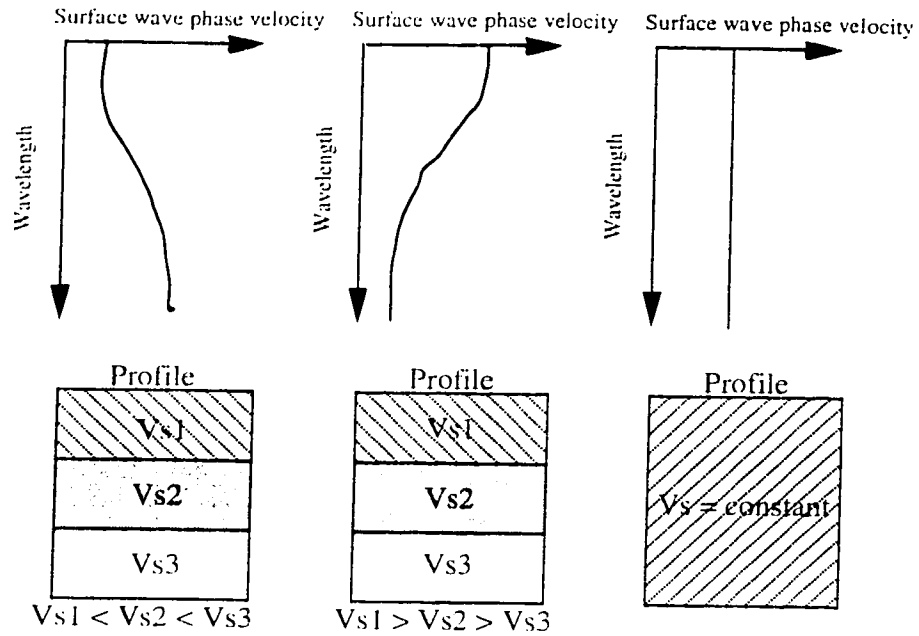


Figure 2.14 Surface wave dispersion in a uniform half-space and a layered half space

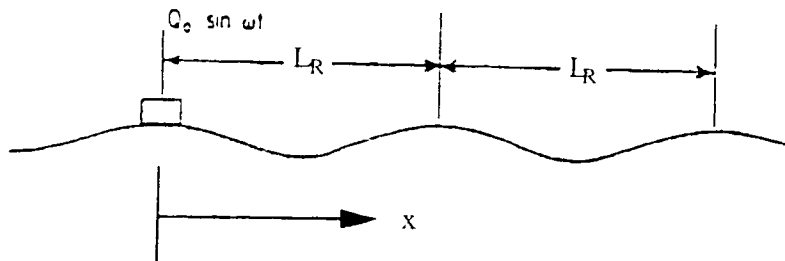


Figure 2.15 Deformed shape of a half-space surface [after Richart et al., (1970)]



## **CHAPTER THREE**

### **SPECTRAL-ANALYSIS-OF-SURFACE-WAVES (SASW)**

#### **3.1 INTRODUCTION**

Spectral-Analysis-of-Surface-Waves (SASW) is a small scale seismic method for in-situ evaluation of elastic moduli and layer thicknesses. This method is non-destructive, relatively simple and has the potential for full automation. The method is based on surface waves which was first discussed by Lord Rayleigh (1885).

SASW has numerous applications. Nazarian (1984) and Nazarian and Stokoe (1984) used SASW in the evaluation of profiles of soil sites and dams. Hiltunen and Woods (1988) achieved good correlations between cross-hole and SASW test results. Stokoe et. al. (1988) applied SASW for testing such hard-to-sample soils as gravelly materials, and slide debris. Stokoe and Nazarian (1983) have used SASW to measure the effectiveness of ground improvement at a site at which natural material was replaced by an engineered fill. All of these authors have used expensive spectrum-analyzers for data-acquisition.

A microcomputer based SASW system was developed at the University of Alberta (UA) by Addo(1992). The University of Alberta SASW system has the advantage of collecting and processing the SASW field data immediately in the field as the data is being collected.

This chapter will give an overview of the SASW technique followed by the details of the University of Alberta SASW system.

## 3.2 OVERVIEW OF SASW

The SASW testing procedure can be divided into three distinct phases: 1) data collection, 2) evaluation of the Rayleigh wave dispersion curve and 3) inversion of the dispersion curve to obtain the shear wave velocity profile.

### 3.2.1 DATA COLLECTION

A general configuration of the first generation of SASW equipment is shown in Figure 3.1. A surface wave is generated by an appropriate source (impulsive, monochromatic or random). The generated wave front is detected by two receivers as the wave propagates past them and is recorded on a spectrum analyzer.

The most common types of sources used have been simple hammers or dropped weights which impact the ground surface and create a transient wave containing a broad range of frequencies. Vibrators have also been employed to generate waves at a fixed frequency or at swept frequencies.

Receivers used for SASW testing depend on the range of frequencies used to profile the material. Vertically oriented transducers (velocity or acceleration) are generally used as receivers in the field. For profiling deeper layers, the receivers should be able to respond to low frequencies and therefore broad-band velocity transducers (geophones) are often used. For profiling shallow layers, the receivers should be capable of responding to high frequencies and therefore accelerometers are generally used.

The location of source and receivers are governed by the following five criteria:

- 1) velocity of the material to be tested,

- 2) desired depth of investigation,
- 3) range of frequencies,
- 4) attenuation properties of the medium,
- 5) amplification and noise level i.e. sensitivity of the instrumentation.

A detailed discussion regarding the location of source and receivers can be found elsewhere [Heisey, (1982)]. The general configuration of source-receiver geometry is shown in Figure 3.2 and 3.3. Figure 3.2 shows the Common-Receiver-Midpoint (CRMP) Geometry and Figure 3.3 shows Common-Source (CS) Geometry. The CRMP Geometry has the advantage of giving good quality dispersion curves because the heterogeneity of the subsurface layers in the longitudinal directions are taken into account. The main disadvantage of CRMP geometry is that it is very time-consuming for multiple-transducer array testing. The CS Geometry has the advantage of being less time-consuming for multiple array transducer testing because the source location is fixed. The disadvantage of CS Geometry is that there might be a possibility of introducing scattering of data due to lateral inhomogeneity of the subsurface layers. The time domain data collected from the field can be fed into a spectrum-analyzer which can operate either in a time-domain or a frequency-domain. The spectrum analyzer can be interfaced with a magnetic tape recorder or a disk drive for permanent storage and recall of data. However, spectrum analyzers are very expensive and generally record and analyze only two channels of data simultaneously.

### 3.2.2 EVALUATION OF THE RAYLEIGH WAVE DISPERSION CURVE

Variation of phase velocity with frequency (or wavelength) is known as dispersion and a plot of phase velocity versus wavelength is called a dispersion curve. The most important parameters required for the construction of a dispersion curve are the coherence function and the phase of the cross-power spectrum. The quality of a signal at a particular frequency

can be determined indirectly by calculating the coherence between the source and measured signals at that frequency. The coherence function is therefore a measure of signal to noise ratio. When there is no noise, the coherence function has a value of unity. The arithmetical proof that the phase of the cross-spectrum of two signals actually gives the phase lag between them is given in Addo (1992). A typical coherence function diagram is shown in Figure 3.4 and an idealized "wrapped-phase" diagram is shown in Figure 3.5. Nazarian and Stokoe (1986) have found that frequencies with a coherence value greater than 0.90 provide useful data. From inspection of the coherence function, the range of frequencies with a coherence value greater than 0.90 are selected and the phase velocity for those frequencies calculated.

The phase difference is 360 degrees for a travel time equal to the period of the wave. Therefore, for each frequency, the travel time between receivers can be calculated by:

$$t = T * \frac{\phi}{360} \quad [3.1]$$

where;       $t$  = travel time associated with the given frequency  
                   $T=1/f$  = period of the wave for the given frequency  
                   $f$  = given frequency  
                   $\phi$  = unwrapped phase

For a receiver spacing,  $s$ , the phase velocity  $V_{ph}$  at the given frequency is calculated from

$$V_{ph} = \frac{s}{t} \quad [3.2]$$

and the corresponding wavelength is equal to

$$L_R = V_{ph}/f \quad [3.3]$$

For each receiver spacing, this procedure is repeated for all frequencies satisfying the coherence criteria. Heisey et. al. (1982) suggested that an approximate range of wavelength ( $L_R$ ) for a given receiver spacing ( $s$ ) was found to be:

$$\frac{s}{2} \leq L_R \leq 3s \quad [3.4]$$

The attenuation of high frequency waves is more pronounced with distance than that of the low frequency waves. Waves with shorter wavelengths ( $L_R < 0.5s$ ), picked up by the receivers are eliminated because their amplitudes might be reduced drastically and consequently can be dominated by ambient noise. Long wavelengths ( $L_R > 3s$ ) are eliminated because they might not be fully developed when they arrive at the near receiver and also can be contaminated by body waves.

Equation 3.4 is used at each receiver spacing to eliminate those data points not satisfying the wavelength criteria. A final field dispersion curve is drawn by plotting the dispersion data for all receiver spacings satisfying both the coherence criteria and the wavelength criteria.

### 3.2.3 INVERSION OF THE DISPERSION CURVE

The velocities obtained from the dispersion curve are not shear wave velocities but are apparent or phase velocities. Inversion consists of determining the shear wave velocity profile from the phase velocity dispersion curve. The process developed by Nazarian

(1984) is based on forward modelling and involves the calculation of a theoretical dispersion curve that matches reasonably well with the measured dispersion curve. The theoretical dispersion curve can be constructed using a modified version of the Thomson (1950)-Haskell (1953) matrix formulation for multi-layered elastic media, as developed by Thrower (1965).

The "Axes Scaling" is a term used to define the transformation of 'Wavelength-Phase Velocity' relationship to 'Depth-Shear Wave Velocity' relationship. This axes scaling was carried out based on the following simple assumptions;

$$V_s = V_{ph} * 1.1$$

$$z = \lambda / 2$$

where  $V_{ph}$  = phase velocity,

$\lambda$  = wavelength,

$z$  = depth, and

$V_s$  = shear wave velocity.

The ratio of shear wave velocity and Rayleigh wave velocity varies between 0.87 and 0.95 for the range of Poisson's Ratio between 0.0 and 0.5 respectively. In other words, the ratio of shear wave velocity and Rayleigh-wave velocity varies between 1.05 and 1.15 for the same range of Poisson's Ratio. Therefore the Rayleigh-wave velocity in a layer is about 10% less than the shear wave velocity in the same layer, and hence the multiplier "1.1" appeared in the above equation. In the forward modelling process, the medium is divided into a number of layers and a shear wave velocity, compressional wave velocity, thickness and mass density for each layer is assumed. The theoretical dispersion curve is calculated and compared with the experimental (measured) dispersion curve. If these two curve match, the desired profile is obtained and if not, the assumed parameters are changed and

another theoretical curve constructed. Unless both the assumed shear wave velocities and the layer thicknesses correspond to the actual field conditions, the theoretical and the experimental dispersion curves will not match.

### 3.3 UNIVERSITY OF ALBERTA SASW SYSTEM

The University of Alberta SASW system uses a microcomputer to acquire and analyze surface wave data. The U of A SASW system can broadly be discussed in four different sections:

- 1) hardware implementation ,
- 2) SASW field procedure,
- 3) data acquisition and signal analysis, and
- 4) forward modelling.

#### 3.3.1 HARDWARE IMPLEMENTATION

The Apple Macintosh computer, Model IICx was selected because of its user-friendly interface and high graphics capabilities. LabVIEW (**L**aboratory **V**irtual **I**nstrument **E**ngineering **W**indow), an iconic programming environment, was used to develop the software for data acquisition and analysis. A direct memory access (DMA) card and a data-acquisition (A/D) card were installed in the computer. DMA assists the central processing unit (CPU) to handle the data as fast as the A/D card. The models of A/D and DMA cards were NB-MIO-16-9 and NB-DMA-8-G respectively, both of which are manufactured by National Instruments. Within the computer, the two cards were connected via a 50 pin RTSI cable. The A/D card had a maximum sampling rate of 100 kHz, a maximum of 8 channels for differential and 16 channels for single ended inputs. The interface between the

receivers and the microcomputer was provided by a locally made unit and was called "interface control unit" (ICU). It contained the circuits for external triggering, filtering and interface connections, directly or indirectly, from the receivers as well as a provision for remotely discriminating between waveform data by the push of a button. Two signals were fed into the ICU as input sources, inputs from receivers and from the instrumented hammer. The ICU was connected via a 50-pin ribbon cable to the A/D card. If a generated signal satisfies the minimum trigger conditions, data acquisition was initiated on the A/D card. The microcomputer was connected via the ICU to a filter, into which a maximum of four receivers can be connected. The NB-MIO-16 and DMA-8-G cards are installed in slots 2 and 3 of the microcomputer. Slot 1 contains the high resolution graphics card. A desk was modified for mounting and securing the computer, ICU and other related accessories. This desk was designed in such a way that it can be pushed into the back of a mid-sized van. For safety during transportation, the mounting desk is equipped with fasteners for securing the computer and its accessories. The computer may be powered by a portable generator or may run off an inverter attached to the battery of the transporting vehicle.

### 3.3.2 SASW FIELD PROCEDURE

The field procedure for SASW can be described as follows:

1. Two perpendicular lines are demarcated to guide the positioning of the receivers. The length of the lines are approximately twice as long as the maximum spacing anticipated at the site. The power to the computer is turned on and all the connections checked.
2. The location at one end of one of the lines is selected as the impact point. The geophone positions are marked along the line.



3. Receivers are coupled to the ground surface. Glue holders have been used for coupling accelerometers to pavement surfaces. It is the most stable and preferred method under normal conditions. During winter conditions, freezing mechanism can provide good contact between the receivers and the pavement. Receivers placed freely on the ground surface without any coupling mechanism tend to collect relatively low-quality data, and this method is not recommended.
4. The inputs data for the data acquisition software (SASW-DA) are then entered.
5. Trial tests are conducted to find the background noise of the signals and to ascertain how hard to hit the ground to obtain reasonable amplitudes. Trial tests are also useful to establish communication signs between the hammer and computer operators.
6. The actual test is then started by a hammer impact. The signals detected by the two receivers are displayed in real time in the time domain plot on the computer screen. The SASW-DA software then waits for the operator to accept or reject the signal. Criteria for acceptance of the signal include signal similarity with the trial signals, acquisition of the entire signal (i.e. the amplitude of the signal must start from zero and end at zero) and the amplitude at a later time should not exceed the highest initial amplitude (this occurs when the hammer operator is unable to control the rebound of the hammer after an impact). A better way to discriminate signals is to keep the averaged properties in memory before updating. The updated average may therefore be accepted if the coherence is improved and rejected if worsened. The SASW-DA software then waits for the next trigger.

7. The computer operator then signals the hammer operator for another impact which is subsequently processed. This step is repeated until the preset number of signals are acquired for averaging.
8. After the preset number of signals are acquired (usually five), the SASW-DA software displays the dispersion curve for that spacing and simultaneously saves it on disk. The procedure is repeated for all spacings.

After the SASW-DA software acquires the dispersion points for all spacings, the dispersion curve for the site is drawn based on a minimum coherence value. Such dispersion point observations for all spacings helps in identifying the spacings that yield the best data for a given impact source and receivers.

### 3.3.3 DATA ACQUISITION AND SIGNAL ANALYSIS

The University of Alberta SASW system as developed by Addo (1992) is shown in Figure 3.6.

The data acquisition and signal analysis consists of signal acquisition, frequency domain transformation and spectral analysis.

During data acquisition, it is important to ensure that the measured digital signal is a true representation of the original analog signal. If the time interval is  $\Delta t$  (and measured in seconds), then the sampling rate (or frequency)

$$f = \frac{1}{\Delta t} \text{ (in Hz).} \quad [3.5]$$

The upper limit of the range of the sampled process spectrum is called the Nyquist folding frequency. This is the maximum frequency that can be detected from data sampled at time spacing  $\Delta t$  (seconds). The phenomenon of aliasing is most important when analysing digital data. The sampling frequency must be high enough to cover the full frequency range of the continuous time series. Otherwise the spectrum from equally spaced samples will differ from the true spectrum because of aliasing.

In order to ensure that no information is lost in the measurement process, the sampling frequency should satisfy the following criteria:

$$f_{\min} \geq 2f_{\max} = \frac{1}{\Delta t} \quad [3.6]$$

where:  $f_{\min}$  = sampling frequency (Hz),  
 $f_{\max}$  = highest frequency content in the input signal (Hz),  
 $\Delta t$  = maximum sampling interval (sec).

This is called the Nyquist criterion. The other criterion that should be satisfied during data acquisition is called aliasing. Aliasing occurs due to inadequate discrete sampling at evenly-spaced intervals. Unequal-interval sampling complicates data-acquisition and frequency domain transformation [Addo, (1992)]. Therefore in actual data-acquisition, it is better to [Newland, (1975)]:

- 1) Estimate the frequency range of interest and the maximum frequency of significant spectral components in the signals to be analysed. If necessary filter the signals to remove excessive high frequency components.

- 2) Choose an appropriate sampling interval ( $\Delta t$ ) so that the Nyquist frequency ( $\frac{1}{2\Delta t}$ ) (Hz) exceeds the maximum frequency present and is at least (say) twice the frequency of interest.

During fast Fourier transformation, it is required to have the number of acquired samples to be a power of 2. If not, the sampled data should be padded with zeros up to the nearest power of two. The number of samples is also limited by hardware configuration such as the analog-to-digital converter.

Filtering is the process of removing unwanted frequencies and can be achieved in either analogue or digital mode. Analogue filtering is often used for anti-aliasing purposes.

The transformation of acquired time-domain signals to frequency domain is achieved by fast Fourier transformation (FFT). The FFT is a computer algorithm for calculating discrete Fourier transforms (DFT's). FFT offers an enormous reduction in computer processing time by reducing the number of operations from  $N^2$  for DFT to  $N \log_2 N$  for FFT.

Spectral analysis for SASW involves the study of the shape of each frequency content of the wave and the spectral analyses functions are used to compute phase lag and coherence values for each constituent frequency of the impact signal.

The phase velocity is the ratio of distance travelled by a monochromatic signal to the travel time taken i.e.

$$V_{ph} = \frac{\Delta x}{\Delta t} \quad [3.7]$$

where  $\Delta x = x_2 - x_1 = \text{receiver spacing} = s$

$\Delta t = \text{time lag.}$

The time lag  $\Delta t$  between the stations is given by:

$$\Delta t = \frac{\Delta \phi}{\omega} \quad [3.8]$$

where,  $\Delta \phi = \text{phase difference, and}$

$\omega = 2\pi f = \text{angular frequency.}$

After the signal has been dissociated into its frequency components, the phase difference of each frequency component between two receivers is calculated. This is achieved by calculating the cross-power-spectrum, which is the Fourier transform of the cross-correlation of the two signals and is defined as:

$$\bar{S}_{xy} = \overline{X(f)} * \overline{Y^*(f)} \quad [3.9]$$

where,  $\overline{X(f)} = \text{Fourier transform of the first signal } x(t),$

$\overline{Y^*(f)} = \text{Complex conjugate of the Fourier transform } Y(f) \text{ of the second}$   
 signal  $y(t).$

The phase of the cross-power-spectrum of two signals gives the phase lag between them. The phase obtained in this manner is folded and varies between  $-\pi$  to  $+\pi$ . This folded phase has to be unwrapped to obtain the true phase difference. This is known as the unwrapped phase. The unwrapped phase for each frequency component can be used to calculate the

time lag. And with a known receiver spacing and computed time lag, the velocity of each frequency component can be determined.

The signal quality at a particular frequency is indirectly obtained by determining the coherence between the source and measured signals at that frequency. The coherence function between any two time-domain signals represented by 'x' and 'y' is the ratio of their cross-power spectrum to the square root of the product of their auto-power-spectra and is defined as:

$$\overline{\gamma_{xy}(f)} = \frac{\overline{S_{xy}(f)}}{\sqrt{S_{xx}(f)} \cdot \sqrt{S_{yy}(f)}} \quad [3.10]$$

where,  $\overline{S_{xy}(f)}$  = cross-power spectrum of two acquired signals averaged over a number of data records, and  $S_{xx}(f), S_{yy}(f)$  = averaged auto-power spectra over the same number of records.

The coherence function is only applicable to averaged signals and a coherence value of unity indicates that there is no noise. Poor coherence can be encountered and may be attributed to leakage errors, poor signal-to-noise ratio, system non-linearity and/or extraneous noise.

The phase velocity of a monochromatic signal between two receivers at a known distance apart is given by:

$$V_{ph} = \frac{\omega}{\phi} * s \quad [3.11]$$

where,  $V_{ph}$  = phase velocity,  
 $\omega = 2\pi f$  = angular frequency,  
 $\phi$  = unwrapped phase,  
 $s$  = receiver spacing.

This equation is used to calculate the phase velocity of all frequencies at which the coherence value is greater than a predetermined minimum coherence.

A computer program SASW-DA (Spectral Analysis of Surface Wave - Data Acquisition) was written by Addo (1992) for acquiring and processing waveform data using a microcomputer. The computerized SASW system developed at the University of Alberta has reduced the cost of equipment set-up considerably by eliminating the expensive spectrum analyzer. Time for transferring the huge amount of data from the spectrum analyzer has been eliminated with the University of Alberta SASW system, since the raw data is collected and analyzed simultaneously in the microcomputer in the field. If a high-speed analogue-to-digital converter is used, more than two receivers can be used for data-acquisition using the micro-computer system for little or no extra cost, whereas a four-channel spectrum-analyzer can cost significantly more than a two-channel spectrum analyzer.

### 3.3.4 FORWARD MODELLING

The determination of elastic parameters, layer thicknesses and shear wave velocity profiles associated with a given experimental dispersion curve is referred to as inversion. The

inverse mapping from a dispersion curve to a structural model is non-linear and non-unique [Knopoff, (1961)], [Thrower, (1965)], [Mora, (1988)]. The process of inversion is difficult. Dorman and Ewing (1962) employed a technique of assuming an initial structure and iteratively updating previous guesses until computed and experimental dispersion curves match. This process is called forward modelling. For a stack of 'n' homogenous layers of infinite lateral extent including the half-space, calculating the dispersion curve involves the solution of a determinantal equation related to a set of ' $4n-2$ ' simultaneous homogenous equations for each wavelength in the dispersion curve. The procedure adopted for computing this determinantal equation is based on the fast form of the method originally proposed by Knopoff (1964) and considered only the fundamental Rayleigh mode. The boundary conditions for this eigenvalue problem are: continuity of two displacement components and two stress components at each interface, and vanishing of two stress components at the free surface. Using assumed layer thicknesses, mass densities, shear and compressional wave velocities, a theoretical dispersion curve is calculated based on elastodynamics [Haskell, (1953)]. A typical soil layer model for forward modelling is shown in Figure 3.7 [after Tokimatsu et. al. (1992)].

The layer parameters are then automatically perturbed for repeated dispersion calculations until the in-situ dispersion curve is satisfactorily matched. At this stage, the parameters of the layers are then assumed to be equal to the desired field properties. This process of matching theoretical and in-situ Rayleigh-wave dispersion curve is called optimization.

SASW-FM (Spectral Analysis of Surface Wave - Forward Modelling) is a computer program developed by Addo (1992) for calculating a theoretical dispersion curve that matches a given in-situ dispersion curve.



### 3.4 SUMMARY

This chapter has described the original SASW technique and the modified University of Alberta SASW system. The three phases of SASW testing, namely, collection of data, evaluation of the Rayleigh wave dispersion curve and the inversion of the dispersion curve have been described. The transition from the expensive spectrum analyzer to the microcomputer based SASW system has significantly improved the efficiency and cost-effectiveness of the technique.

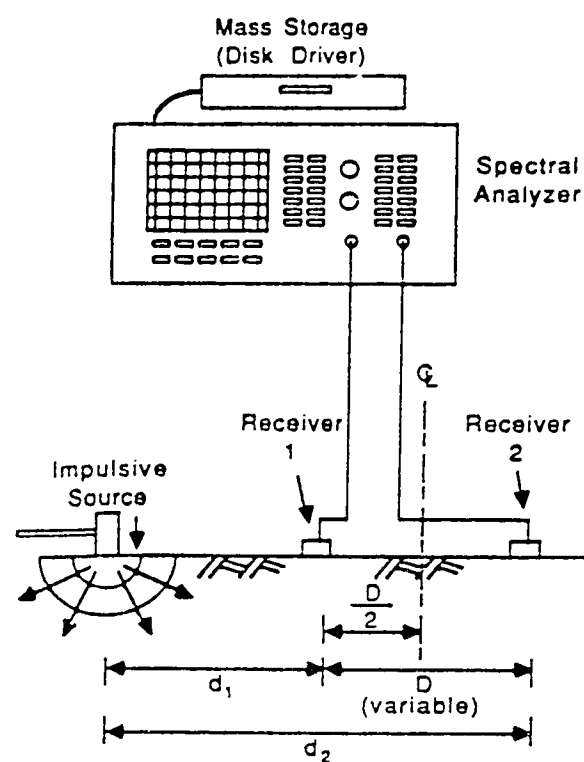


Figure 3.1 General configuration of first generation of SASW tests

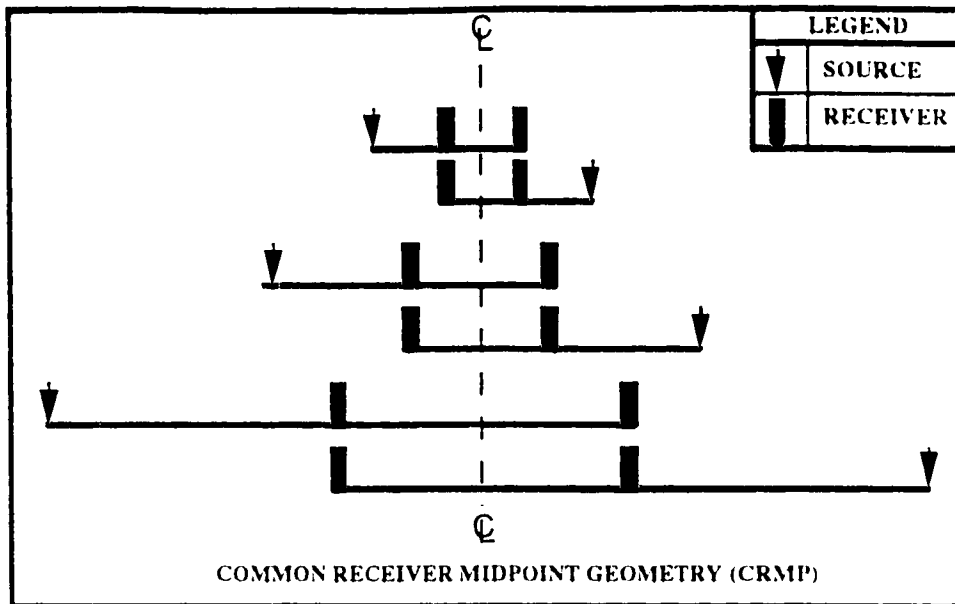


Figure 3.2 Common-Receiver-Midpoint (CRMP) Geometry

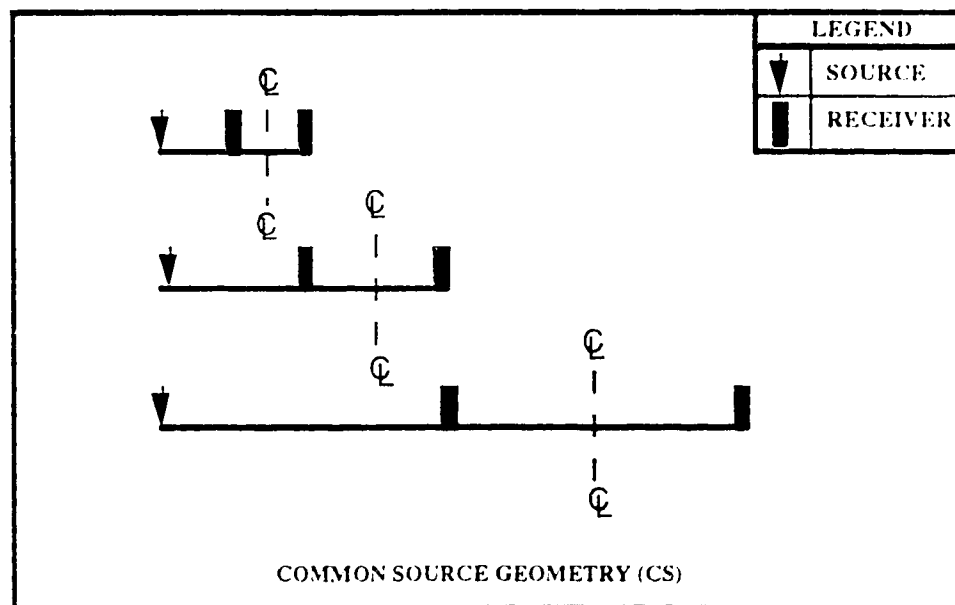


Figure 3.3 Common-Source (CS) Geometry

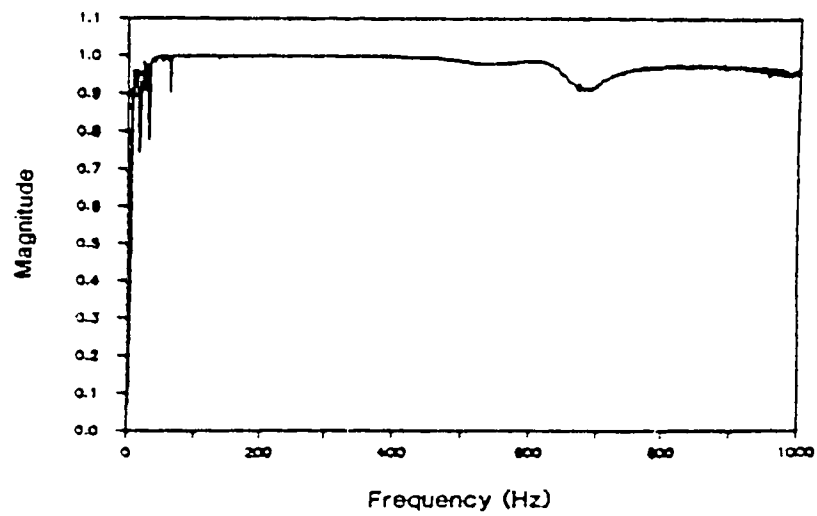


Figure 3.4 A typical coherence function diagram

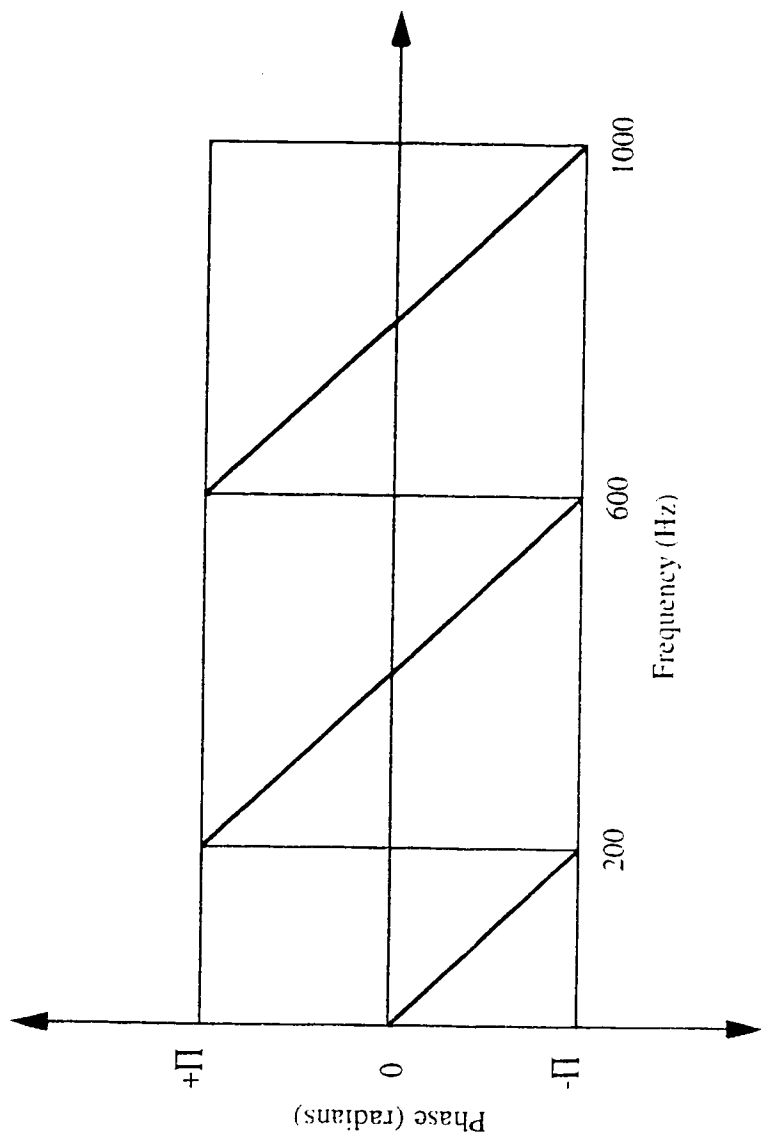


Figure 3.5 An idealized wrapped phase diagram

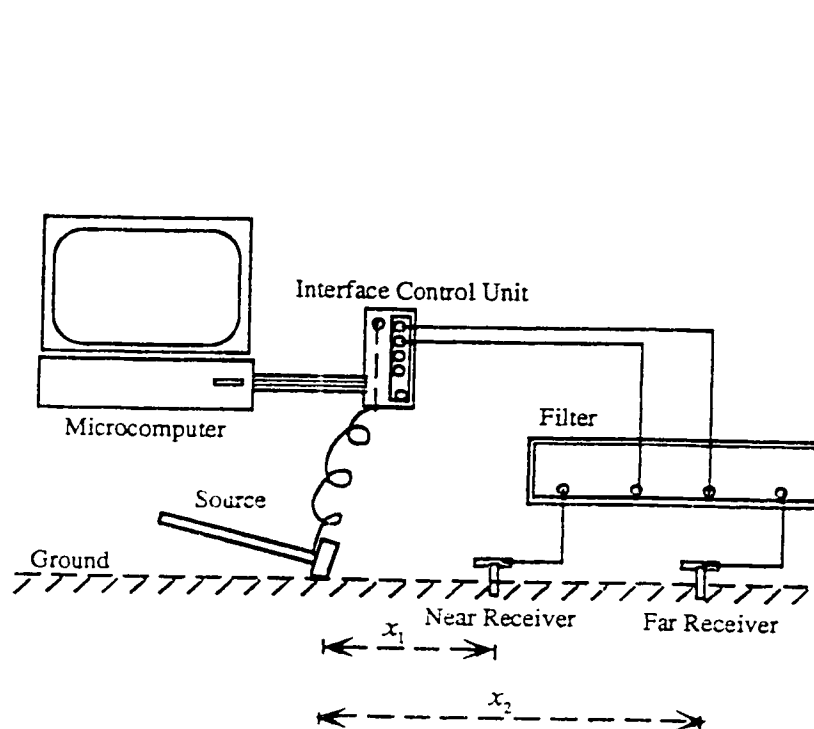


Figure 3.6 University of Alberta SASW System [after Addo (1992)]

Layer #	Thickness	Density	P-wave velocity	S-wave velocity
1	$H_1$	$\rho_1$	$V_{P1}$	$V_{S1}$
2	$H_2$	$\rho_2$	$V_{P2}$	$V_{S2}$
•	•	•	•	•
•	•	•	•	•
N-1	$H_{N-1}$	$\rho_{N-1}$	$V_{PN-1}$	$V_{SN-1}$
N	$\infty$	$\rho_N$	$V_{PN}$	$V_{SN}$

Figure 3.7 A typical soil layer model for forward modelling [after Tokimatsu et. al. (1992)]

## **CHAPTER FOUR**

### **CURRENT METHODS FOR EVALUATING THE STRUCTURAL INTEGRITY OF PAVEMENTS**

#### **4.1 INTRODUCTION**

Nondestructive testing has been used extensively in the last few decades for the evaluation of structural integrity of flexible and rigid pavements. In highway engineering, existing methods for pavement evaluation are mostly deflection based. These techniques consist of measurement of surface deflections under applied loads. Surface deflection measurement devices can be categorized as either static (e.g. Benkelman Beam) or dynamic (e.g. Dynaflect, falling weight deflectometer ).

#### **4.2 STATIC DEFLECTION METHODS**

Static deflection methods involve the measurement of the deflection response of a pavement to applied loads moving at a creep speed. The Benkelman (after its inventor's name) Beam is the most commonly used method in this category. It measures the response at the surface of a pavement that is subjected to a known load; it is then assumed that this response is elastic can be used to determine the overall condition, and the existing life of the pavement.

The original Benkelman beam was a 12 ft ( 3.65m) beam pivoted at the third point. This provides an 8-ft (2.44m) probe with the extreme tip resting on the pavement and supported at the near third point by a pivot point. The beam is pivoted at a point 8-ft (2.44 m) from the tip giving a 1:2 length ratio. The rear end is a 4-ft (1.22m) cantilever beam that moves upward when the pavement deflects downward. A dial indicator rests on the rear end and



measures this movement. This type of device requires a loaded truck to create the deflection to be measured. A schematic diagram of the Benkelman beam is shown in Figure 4.1 [after O'Flaherty, (1988)]. The Benkelman beam consists of an aluminum alloy beam that is sufficiently slender to fit within the space between the walls of the dual tyres (each inflated to 590 kN/m<sup>2</sup>) of either of the wheel assemblies on the rear axle of a special two-axle loading truck.

The Benkelman beam has been used for many years, and much of the early work in deflection-based overlay design for flexible pavements was based on this device. Only the maximum deflection is measured with the beam. The major technical problems associated with this method include, ensuring that the front supports are not in the deflection basin, and the difficulty or inability in determining the shape and size of the deflection basin. In Canada and the U.S., a rebound test procedure is adopted using the Benkelman Beam. In this method, additional thickness of granular material required to bring the existing pavement system up to the desired strength for the new pavement, is calculated based on maximum spring Benkelman Beam rebound value and expected number of cumulative 80 kN (18,000 lb) single axle loads. The total granular thickness can be converted into a practical design consisting of asphaltic concrete surfacing with a high quality crushed stone or gravel base and granular subbase (i.e. a "conventional" flexible pavement), or with an asphalt treated base and granular subbase (i.e. a "deep strength" flexible pavement), or with an asphalt treated base directly on subgrade (i.e. a "full depth" flexible pavement). The choice would normally be based on economics.

The general procedure [Asphalt Institute Method, (1983)] for using pavement deflections for structural evaluations is as follows:

1. Establish the length of pavement to be included in the structural evaluation.

2. Perform a deflection survey consisting of a minimum of 10 randomly selected points.
3. Calculate the representative rebound deflection (RRD). The RRD value is the mean of measured rebound deflections, which have been adjusted for temperature and the most critical period of the year (i.e. the spring time), plus two standard deviations. This value encompasses approximately 97% of all deflections measured.
4. Estimate the design Equivalent Axle Load (EAL<sub>d</sub>). The standard traffic analysis procedure for determining the design EAL required after an overlay requires that estimates be obtained of the number of vehicles of different types expected to use the proposed facility.
5. Determine the overlay thickness based on empirical relationships developed by using data from existing successful pavements.

The Roads and Transportation Association of Canada [RTAC (1976)] method was first presented in the Canadian Good Road Association (CGRA) Guide (1965). The present RTAC method, which is empirical, utilizes the results of deflection tests on different pavement structures, first to develop relationships between loads and structures, and second, to set criteria based on deflection values which apply to the experience-based method. Details of this method can be found in RTAC (1976).

Christison & Leung (1988) reported on large data base in Alberta, and suggested that deflections alone are not a measure of field serviceability and performance. Results have shown that when combined with continued and conscientious field performance observations, Benkelman Beam deflections can be a reliable indicator of potential pavement distress and the rate of change in serviceability with time.

## 4.3 DYNAMIC DEFLECTION METHODS

### 4.3.1 STEADY-STATE VIBRATORY LOADING

Vibratory equipment usually applies a sinusoidal force to the pavement structure. Deflections are measured with inertial motion sensors ( accelerometer or velocity sensors). Dynaflect is one of the methods that fall into the category of steady-state vibratory loading.

The Dynaflect is a dynamic force generator employing counter-rotating masses to apply a peak-to-peak force of 1,000 lb ( 4.4 kN ) at a fixed frequency of 8 Hz. Force is applied to the pavement through two 4-inch ( 100 mm) wide, 16-inch ( 400 mm ) diameter rubber-covered steel wheels spaced 20-inch ( 500 mm ) center-to-center. Deflections are measured with five geophones ( velocity sensors ) on the longitudinal axis through the loading wheels. Geometric configuration of loads and stations for Dynaflect are shown in Figure 4.2 [after Roesset et al. (1985)]. The equipment is simple and can be rapidly operated with a control unit and microcomputer. Because of the relatively light load applied, extrapolation of the results to heavier loads must be done with care, since many of the pavement components exhibit nonlinear stiffness characteristics [Epps et. al. (1986)].

In the case of the Dynaflect, the deflections measured at the various stations represent the amplitudes of the steady-state displacements at a given frequency ( 8 Hz ). It is a dynamic test but the interpretation of the results to estimate the moduli of the surface layer, base, and subgrade is based on a static analysis. These analyses assume that the soil in the subgrade is an elastic, uniform half-space or an elastic stratum of finite thickness. Realistically, the soil properties vary with depth, and in some cases, the soil is underlain at some depth by much stiffer, rock-like material which can cause reflections in the stress waves imparted

during the dynamic tests. Dynaflect is also very expensive compared with the whole SASW system.

Chang et. al. (1991) suggested that the main limitations of the Dynaflect is that the test is conducted at a single frequency and only the amplitudes of the steady-state vibrations are used. If one were to conduct the test at two different frequencies ( say 8 and 16 Hz ); it would at least allow a comparison of the measured deflection basins. If the results were almost identical for the two frequencies, one could conclude that dynamic effects are not important, that bedrock is located at a sufficient depth ( of the order of 70 ft or more ) and that a static analysis would be appropriate to backcalculate the elastic properties of the layers [Chang et. al. (1991)]. On the other hand, if the results showed clear differences at two frequencies, it would be apparent that dynamic effects are important. In this case, testing at other frequencies would be required.

The dynamic nature of the testing has an influence on the magnitude of the measured deflections as well as the shape of the deflection basin. For Dynaflect, these effects can lead to significant dynamic amplification when bedrock is at a depth ranging from about 6.5 m to 20 m, depending on the properties of the subgrade. The static analysis method will tend to underestimate the modulus of the subgrade and overestimate the moduli of the base and surface layer. It has also been found that the dynamic phenomena of resonance and inertial damping within the subgrade may result in significant differences in pavement response to static and dynamic loading. Because static analyses are currently used to analyze the Dynaflect data, significant errors may arise in back-calculating layer stiffnesses, particularly because the iterative schemes used in such analyses are ill-conditioned. SASW, on the other hand, is based on the propagation of surface waves, which is correlated with the shear wave velocity of the material through which the waves are propagating. The shear wave velocity is related with the subsurface material properties. SASW also has the

capability of profiling subsurface layers where the stiffness changes within a particular layer.

#### 4.3.2 FALLING WEIGHT DEFLECTOMETER (FWD)

The Falling Weight Deflectometer (FWD) measures a set of deflections of a deflection bowl under an impulse load of circular distribution, simulating the transient load of a passing vehicle. Variations in axle weight of actual vehicles can be simulated by choosing one of several levels of impulsive loads. Deflections are measured at various distances from the load, including at the load axis itself, using geophones.

The Falling Weight Deflectometer (FWD) is a trailer mounted device that can be towed by a light passenger vehicle. The device contains a drop weight (that can have different mass configurations) which is hydraulically lifted and dropped on a specially designed spring system or buffer. A schematic diagram of the Dynatest 8000 model FWD test equipment is shown in Figure 4.3 [after Croney et al. (1991)].

The impact is transmitted to the pavement through a rigid steel loading plate (standard 300mm diameter or 450mm diameter) which has a base of ribbed rubber to distribute the load uniformly over the whole loading base area. A schematic diagram of the falling mass system of Dynatest 8000 model FWD device is shown in Figure 4.5 [after Croveti et al. (1989)].

Both plates may tilt up to 6 degrees from the horizontal to conform to unleveled pavement surfaces [Croveti et al. (1989)]. The resulting load is a force impulse with peak magnitude ranging from about 7 kN to 125 kN depending on drop height, drop weight and pavement stiffness. The deflection created by the FWD load impulse is unidirectional and

approximately a half-sine wave shape with a total duration typically between 25 to 30 ms. This closely approximates the deflection impulse created by a moving truck wheel at a speed of 65 km/hr. The model 8000 of the Dynatest FWD has a dead weight of approximately 864 kg [Smith, (1985)].

Geophones are used to detect the signal impulse and measure surface deflections (up to 2 mm for Dynatest Model 8000 and up to 2.5 mm for other Dynatest Models) at the centre of the loading plate and at various other points ( 6 for Model 8000) along the surface. Typical location of the loading plate and the deflection sensors of the FWD are shown in Figure 4.5 [after Foxworthy et al. (1989)].

The velocity signal from the transducer is time integrated to convert the signal to a deflection signal. Closer spacing of geophones may be required for very thin flexible pavements; but for very thick pavements, the spacing of the outer three sensors should be increased [Ertman-Larsen and Stubstad, (1982), (1983)]. A typical deflection basin diagram is shown in Figure 4.6 [after Badu-Tweneboah et al. (1989)].

On-board microcomputers control and monitor the entire testing program for efficient operation by a one-person crew. An optional video camera and monitor are available to aid in the positioning of the FWD on joints in concrete pavements.

The state-of-the-art in data processing from FWD measurements is as follows. Asphalt concrete pavements with known layer thicknesses are analyzed using a set of deflections measured along the wheel path, typically in the center underneath the circular loading plate and at six adjacent locations outside the plate, spaced over 1.5 m to 2 m. These deflections together with known layer thicknesses are used to back-calculate the elastic stiffness (Young's modulus) of all pavement layers, including the subgrade, using available

computer programs for elastic layer analysis. Some of the computer programs are WESLEA, BISAR, WESDEF, BISDEF, PADAL, ELMOD, BISTRO, COMDEF, MODULUS, MODCOMP 2, CHEVDEF etc. Once the elastic stiffnesses are known, any stresses, strains and deflections for different loadings can be computed using the same or similar compatible programs.

The magnitude of the deflections and the shape of the deflection basin obtained from FWD tests are influenced by the dynamic effects of this test. Chang et. al. (1991) has shown that these effects are a function of the depth to bedrock when there is a sharp discontinuity in the values of the elastic modulus of the subgrade and that of the underlying rock.

The major limitations of FWD can be summarized as follows:

- 1) Thicknesses of pavement layers should be known or assumed.
- 2) FWD yields erroneous results if depth to bedrock is not known or if the depth to bedrock is very shallow (discussed in the next section).
- 3) Variation of moduli within different layers cannot be evaluated.
- 4) For thin ( $< 0.0762$  m) pavement layers, large variations in the stiffness of the subsurface layer will only slightly affect the shape or magnitude of the deflection basin.

#### 4.4 COMPARISON OF BENKELMAN BEAM, DYNAFLECT, FWD AND SASW

Benkelman beams have been in service the longest. Correlations between most other devices and the Benkelman Beam have been developed by various agencies. It has also been found that there is a large range of values for equivalent Benkelman Beam deflections

calculated from the same Dynaflect reading. The reason for this wide range of variability might be due to various factors, such as the load, rate of loading, time of loading, analysis procedure involving various assumptions, thickness and type of pavement structure, subgrade conditions, topographic position, traffic and other factors. Benkelman Beam measurements are made under an 18,000-pound single-axle load, whereas the magnitude of load placed on the pavement is quite small for Dynaflect. Therefore, highway engineers should be cautious and should not transfer data directly based on correlation developed by other agencies.

The Dynaflect imparts steady-state dynamic (harmonic) loading, whereas the FWD imparts an impulsive load developed by a weight falling on a spring-loaded single plate. Therefore, the Dynaflect operates on a single frequency whereas FWD is capable of generating a wide range of loading frequencies. If the subgrade soil extends to depths of 20 m or more, the static interpretation of the deflections measured in the Dynaflect tests might be reasonable [Roesset and Shao (1985)]. Substantial dynamic amplification can occur if much stiffer bedrock is encountered, leading to errors in the backcalculation of elastic properties for the pavement system. The situation is aggravated when the soil of the subgrade is not homogenous but has a stiffness increase with depth.

The data obtained from dynamic loading devices are analysed based on empirical correlations or on the basis of elastostatic and viscoelastic models. In static analysis, the inertia of the pavement is neglected. Therefore in the analysis, it is assumed that the dynamic response of the pavement structure is no different from the static response. Dynamic effects are less important for the FWD because a broad range of frequencies is excited. Even so there are still some ranges of depth to bedrock which might lead to erroneous estimates of the elastic moduli.



The SASW method has several potential advantages when compared with deflection-based methods, as follows:

1. No assumptions are needed regarding pavement layer thicknesses.
2. Once the shear wave velocity profile is known, the variation of moduli within different layers can be evaluated. The velocity of propagation of shear waves is related to the small-strain shear modulus of the material by the relationship:

$$G_0 = \rho * V_s^2 \quad [4.1]$$

where:  $G_0$  = small-strain shear modulus,  
 $\rho$  = mass density and  
 $V_s$  = shear wave velocity.

3. The SASW method can be used to predict the depth to bedrock as well as the moduli of the subgrade and bedrock.
4. Moduli of thin layers, especially thin surface layers in the pavement system can be measured.

It is these potential advantages of the SASW method that has resulted in this research. The strains associated with seismic testing are usually in the order of 0.001 percent or less. Moduli determined by seismic methods can be easily extrapolated to strain levels encountered in the field.

#### 4.5 PAVEMENT ANALYSIS

The major problem of correctly reproducing in situ conditions are overcome if the tests are carried out in situ. Over the years a number of different methods have been developed to

characterize the structural condition of pavement layers. Some of these methods are wave propagation methods and deflection methods as explained earlier.

The main difficulty in using wave propagation methods to determine the elastic parameters of pavement materials is that most pavement materials are non-linear elastic. The stresses induced by a light weight vibrator are very small, and in no way comparable to those induced by heavy traffic. The result of this is that moduli determined from wave velocities, in most cases, will be much larger than the moduli corresponding to heavy traffic loading. It is not surprising to find moduli obtained from wave propagation methods to be three times higher than the moduli found from FWD testing [Ullidtz, (1987)].

Heavy vibrators, truck wheel loads (Benkelman beam), and static plate loading tests have long been used to evaluate the structural condition of pavements. Often deflections are used directly as a measure of the structural condition but sometimes the structural condition is expressed as the "stiffness" of the pavement, i.e. the ratio of the maximum applied load to the maximum, or rebound, deflection. If the design procedure is based on critical stresses or strains in the different layers (which is the case for most of the versions of the analytical-empirical method) then the overall deflection, or stiffness, cannot be used directly to evaluate the structural condition [Ullidtz, (1987)]. To supplement the deflection the "radius of curvature" may be included. The proper "engineering" way of evaluating a pavement structure is to determine the modulus of each structural layer in the pavement, and then use the moduli to calculate the critical stresses or strains under different loading and climatic conditions. With the heavy vibrators the stress levels induced in the materials are very small compared to the stress levels induced by heavy traffic, resulting in significant deviation of the calculated moduli. Moreover, using a steady state vibration may cause problems with inertial effects, so that the response will depend on the frequency of the vibration. With a heavy wheel load, as used in the Benkelman beam test, the correct stress level can be

reproduced. In this case the problem is one of measuring the deflections with sufficient accuracy, particularly at some distance from the wheel load. This inaccuracy may cause very large errors in the derived layer moduli. Another, less important, difficulty is that the wheel velocity usually is much less than the velocity of the normal traffic loading. The difference in loading time influences the response of visco-elastic materials like asphalt. With static plate loading tests the same problem is encountered as with the heavy wheel load: deflections at some distance from the load cannot be measured accurately enough. In addition to this, the static plate load is, of course, even more distant from actual traffic loading than a slow moving wheel load. Most of the problems mentioned above can be overcome with the Falling Weight Deflectometer (FWD) tests. The FWD tests are described in details in the previous sections.

#### 4.6 SUMMARY

This chapter has briefly described some of the current methods for structural evaluation of pavements. The discussion covered three major methods: 1) Benkelman Beam method; 2) Dynaflect; 3) Falling Weight Deflectometer (FWD). Each method has its own advantages and limitations. Highway engineers should be cautious in correlating data obtained from the three different systems. The reader is directed to the references cited for a more thorough discussion of the non-destructive testing methods covered in this chapter.

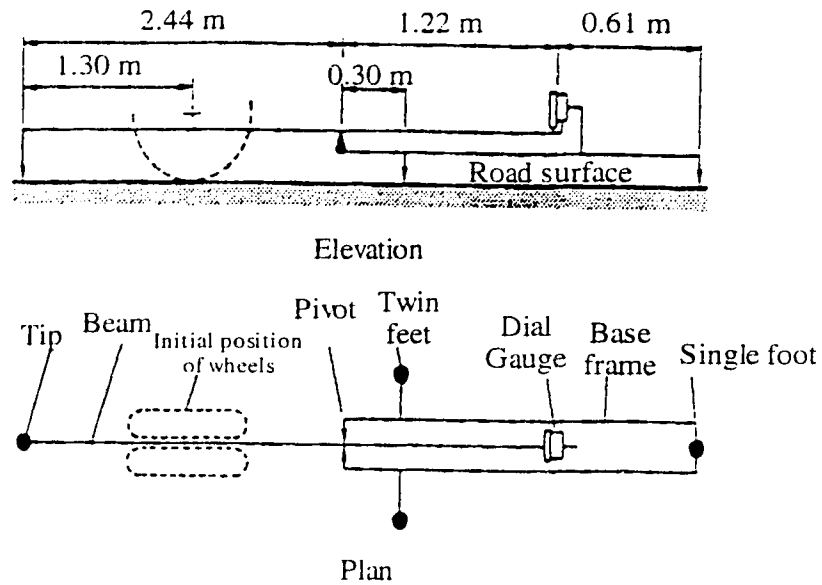
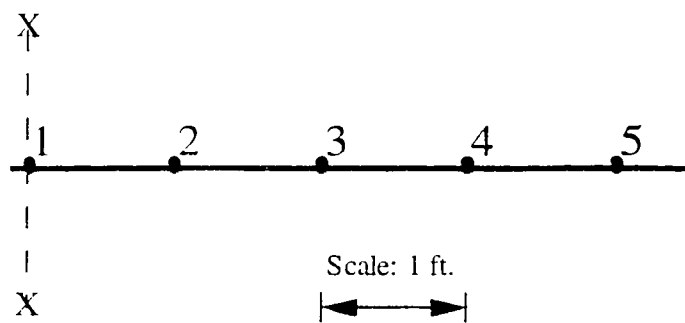


Figure 4.1 A schematic diagram of the Benkelman Beam [after O'Flaherty, (1988)]

## DYNAFLECT

$P = 500 \text{ lb.}$ ,  $F = 8 \text{ Hz.}$



$P = 500 \text{ lb.}$

Figure 4.2 Geometric configuration of loads and stations for Dynaflect [after Roesset et al., (1985)]

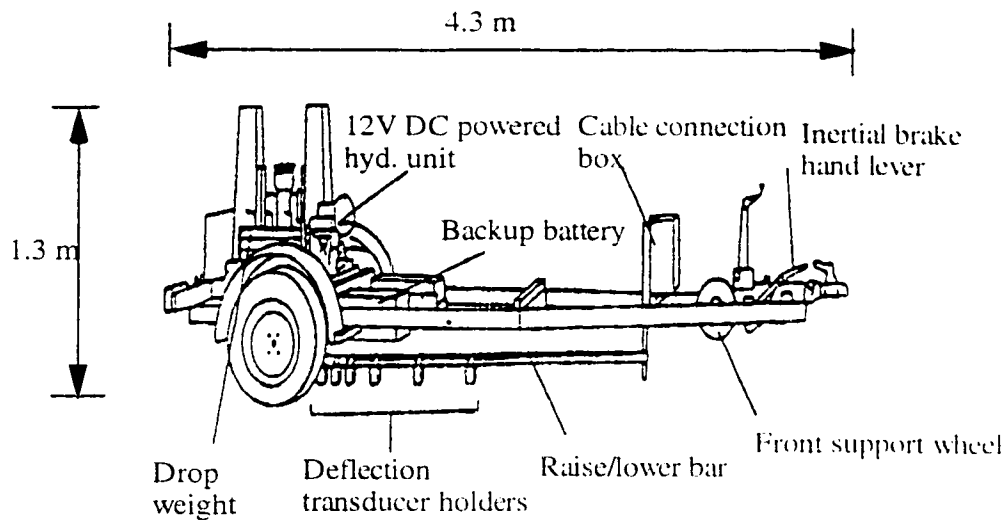


Figure 4.3 A schematic diagram of Dynatest 8000 model FWD test equipment [after Cronney et. al. (1991)]

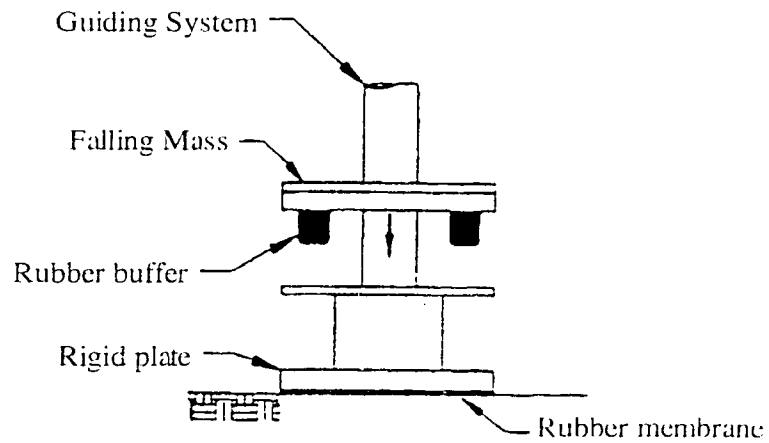


Figure 4.4 A schematic diagram of the falling mass system of Dynatest 8000 model FWD device [after Croveti et al., (1989)]

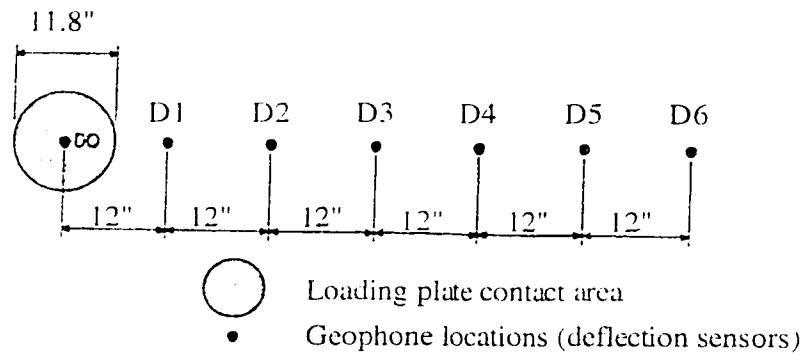


Figure 4.5 Typical location of the loading plate and the deflection sensors of FWD [after Foxworthy et al., (1989)]

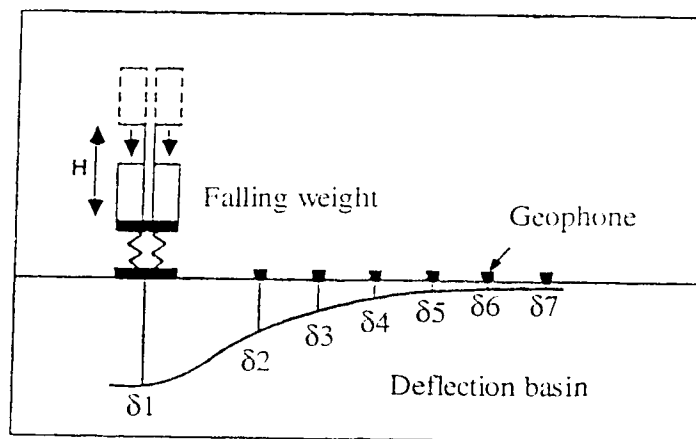


Figure 4.6 A typical deflection basin diagram [after Badu-Tweneboah et al., (1989)]

## **CHAPTER FIVE**

### **SASW - NEW DEVELOPMENTS**

#### **5.1 INTRODUCTION**

The recently developed computerized SASW technique [Addo, 1992] is an improvement over previous SASW techniques, where dynamic spectrum analyzers were used for data acquisition. However, one of the major drawbacks of the U of A SASW system has been its inability to profile shallow depths, particularly for pavement-like structures, where stiff layers overlie soft layers. This chapter describes the new developments that have been made to the U of A SASW system in terms of software and hardware as a result of this research to enable the system to measure the stiffness profile of pavement structures.

#### **5.2 EQUIPMENT**

The equipment used in this research can broadly be classified into three distinct categories: 1) Data-Acquisition (Computers, Data-acquisition cards, other hardware etc ); 2) Receivers and 3) Sources. The equipment set-up is shown in Figure 5.1.

##### **5.2.1 DATA ACQUISITION**

###### **Microcomputer**

All the data acquisition, data processing and data analysis for this research were done using a Macintosh Ilex computer with 8 MB Ram and 100 MB Hard Drive and a 13" monitor. The main reason for using this type of computer was access to a programming technique,

LabVIEW (Laboratory Virtual Instrument Engineering Window), which was only available for Macintosh computers when this research was initiated. LabVIEW, developed by National Instruments of Austin, Texas, USA, is an iconic programming environment for developing applications by creating on-screen control panels to emulate test instruments, data acquisition and analysis. The data-acquisition software "SWAP" developed for this research was created using LabVIEW. The Macintosh IIfx has 4 NuBus slots, which are useful for installing the relevant cards for successful operation and running of the "SWAP" program.

#### Data Acquisition Board

A NB-A2000 data acquisition board, manufactured by National Instruments was installed in the computer. The NB-A2000 is a 12 - bit resolution A/D plug-in board with a sampling rate of 1 MHz for the Macintosh NuBus computers. The board has four analog input channels. The board can sample one channel at 1 MHz, two channels simultaneously at 500 kHz, or four channels simultaneously at 250 kHz.

#### Direct Memory Access (DMA) Card

A NB-DMA2800 card, manufactured by National Instruments was installed in the computer so that the data acquired by the NB-A2000 data-acquisition board can be transferred to and from memory with DMA to increase the system throughput and free the Macintosh processor for other tasks. Therefore, the Macintosh processor can run an application while the NB-DMA2800 transfers data in the background. NB-DMA2800 is a 32 - bit DMA controller board which transfers data up to the rate of 3.1 Mbytes/sec to Macintosh NuBus memory and 32.0 Mbytes/sec to block-mode memory. Within the computer, the two cards are connected via a 50 pin RTSI cable.



## Power Amplifier

A PCB Model 482A16, 4 channel power supply with a variable gain was used for this research. The model 482A16 is a line powered four channel digitally controlled amplifier for ICP transducer systems. Each channel features independent gain select ( x1, x10, x100) and overload/fault display status. This unit also provides constant current excitation to the transducer over the signal line and decouples the signal from the DC bias voltage. The schematic diagram of the 482A16 Power Amplifier is shown in Figure 5.2 and the specifications are shown in Table 5.1.

## Interface Control Unit (ICU)

An Interface Control Unit (ICU) was made locally for the previous researcher [ Addo, 1992] for external triggering and interface connections. However, in this research, the ICU was used solely for external triggering purposes. Therefore, the input to the ICU were signals from an accelerometer attached to the hammer source. The actual interface between the data-acquisition board (installed in the computer) and the receivers and the energy sources was done using BNC Adaptor Cables which connects to the NB-A2000 board and is terminated with seven BNC connectors. The seven connectors of one end are marked as following: ACH0, ACH1, ACH2, ACH3, ATRIG, DTRIG and SAMPCLK\*. As only 2 channels were used for data collection in this research, the BNC connectors from the receivers were connected to ACH0 and ACH1 only. The ICU was powered by a 4.5 Volts battery adaptor and the ICU was connected to the DTRIG outlet of the BNC Adaptor Cable. All other outlets (ACH2, ACH3, ATRIG and SAMPCLK\*) were capped and insulated. A pair of Light Emitting Diodes (LED's) attached to the ICU indicate when the minimum trigger conditions were satisfied and the data acquisition initiated. The level and

slope of the trigger signal are adjustable depending on the requirements and field conditions. The circuit diagram of the ICU is shown in Figure 5.3.

### 5.2.2 RECEIVERS

#### Geophones

Geophones are basically velocity transducers. A schematic diagram of a typical geophone is shown in Figure 5.4. A mass is attached to a spring with a support to the earth. A wire or coil is attached to the mass and becomes a part of the total mass. When the earth moves, the magnet and support also move. The mass tends to remain stationary and lags behind the motion of the earth. Therefore, there is a relative motion between the coil and the magnetic field. Since the voltage induced in the coil is directly proportional to the relative velocity between the coil and the magnetic field, either the coil or the magnet is made part of the mass and the other component is attached to the frame. The resultant voltage output is directly proportional to the relative velocity of this motion ( between the mass and the frame), therefore the expression **VELOCITY TRANSDUCER**. The characteristics of the geophones ( Model L-4 Seismometer, manufactured by Mark Products) used in this research are shown in Table 5.2.

In order to cut down oscillations which lead to reduction in resolution, geophones are normally damped. Previously it was done by immersing the moving part in oil. These days, geophones are damped by use of eddy currents. The amount of damping is normally regulated by a suitable resistor which is shunted across the geophone terminal. Damping affects both the amplitude and phase responses. This is usually displayed in the response characteristic curves for the particular geophone type. Over-damping reduces detection sensitivity and too little damping leads to oscillation. Damping of 0.7 of the critical value

seems to be the practically accepted degree of damping for sensitivity with negligible oscillation.

### Accelerometers

The performance of conventional piezoelectric transducers ( i.e. those types utilizing piezoelectric ceramics and natural and synthetic crystals without built-in electronics) is highly dependent on the cable length and or type, as well as other factors, which prevent their use in moist or dirty environments, unless extensive measures are taken to seal cables and connectors. Hence these detectors were not considered for this work.

The design of Integrated Circuit Piezoelectric (ICP) Instrumentation, which combines a miniature IC voltage amplifier (Impedance converter) into the same package with the piezoelectric element, results in a very simple to operate 2-wire system with the following features, amongst others:

1. A fixed voltage sensitivity, independent of cable length or capacitance.
2. Low output impedance (100 ohms) allowing use in moist or dirty field environments (low noise).
3. A 2-wire system which allows the use of inexpensive co-axial cable or any conventional 2-conductor cable.

A schematic diagram of a typical basic ICP transducer and a typical ICP system is shown in Figure 5.5 and Figure 5.6 respectively. In this research, a pair of PCB Model-309A miniature 1 gram quartz accelerometers were used. The specifications of these accelerometers are given in Table 5.3. A built-in microelectronic amplifier converts the high impedance charge signal from the quartz crystal element into a high voltage, low impedance

output signal capable of transmission through long cables without degradation of the high quality signal. This overcomes the signal/noise problem common to most miniature accelerometers.

### 5.2.3 SOURCES

The primary type of source used in this research was an impact source. To generate sufficient surface wave energy over a wide range of frequencies, a number of impact sources have been used in the past such as : hand-held hammers, Standard Penetration Test (SPT) hammers, 50 to 200 lb ( 230 to 890 N) dropped weights, concrete blocks, a car, a 55 gallon (0.21 m<sup>3</sup>) drum filled with concrete, dynamic compaction weight etc.

Light hammers produce high frequencies, whereas heavy hammers produce low frequencies. Therefore, a combination of light and heavy hammers were utilised for this research. The weights of the hammers varied between 0.17 kg to 0.90 kg. If the direct impact of these hammers on the test surface did not produce sufficient high or low frequencies, steel plates or wooden blocks were placed on the test surface and the hammer impacts were done indirectly on these intermediate objects. A pretriggering feature of the NB-2000 data-acquisition board was built into the "SWAP" program to measure the entire signal. The hammer was instrumented using QMB-12D-90G (Silver color) or QMB-12-90C (Black color) miniature audio transducers. These miniature audio transducers were manufactured by Star Micronics. The output from these miniature audio transducers were connected to the ICU unit. As soon as the impact is made with the instrumented hammer on the test surface, and if the level of the trigger signal is more than the minimum set level, the computer will BEEP indicating to the operator that the signal is being generated and captured.

An alternate source is a vibrator, such as an electromechanical vibrator, which transmits continuous types of input motion to the ground. High frequency lightweight sources are necessary for profiling shallow depths and low frequency heavy sources are necessary for profiling deeper layers.

### 5.3 SOFTWARE

Two microcomputer programs have been developed for data-acquisition and analysis for this research. Microcomputer program **Spectral-Wave-Analysis-for-Pavements (SWAP)** is a data-acquisition program written in the LabVIEW programming environment. This program collects data and produces field dispersion curves immediately in the field as well as writes data to a file for future analysis. Another stand-alone application program "MULTIMOD" have been developed for determining dispersion characteristics of multiple-mode Rayleigh waves based on field data collected using "SWAP" program. These software procedures are described in detail in the following sections.

#### 5.3.1 MICROCOMPUTER PROGRAM "SWAP"

A software development environment called LabVIEW (**L**aboratory **V**irtual **I**nstruments **E**ngineering **W**orkbench) was used to develop the microcomputer program "SWAP" for data-acquisition in this research. LabVIEW, developed by National Instruments of Austin, Texas uses G programming environment. "SWAP" runs on Macintosh computers equipped with at least 5 MB RAM (Random Access Memory) and System 6.0.7 or later.

LabVIEW is a graphical programming system for data-acquisition and control, data analysis and data presentation. LabVIEW offers an innovative programming methodology in which software modules called Virtual Instruments (VIs) are graphically assembled. For

every computer program ( or VI ) developed using LabVIEW, there are two parts. One is the FRONT PANEL, which provides interactive control of the software system (simulating the front panel of a real instrument ) , and the other is the BLOCK DIAGRAM, which is the actual program and is hidden from the user. The FRONT PANEL developed for "SWAP" is shown in Figure 5.7.

Before collecting field data using "SWAP", the following controls should be adjusted in the FRONT PANEL:

1. BOARD NO. : The number of the NuBus slot, where the NB-A2000 data-acquisition board had been installed.
2. CHANNEL SELECTOR: This is the input channel to be sampled. It should be set to either CHAN 0 or CHAN 1 for 2 channel data acquisition. If receiver 1 (i.e. channel 1) is placed close to the impact source, then CHANNEL SELECTOR should be set to CHAN 0. If receiver 2 (i.e. channel 2) is placed close to the impact source, then CHANNEL SELECTOR should be set to CHAN 1. CHAN 2 and CHAN 3 are options provided in the program for data-acquisition with more than two transducers. These options are beyond the scope of this research.
3. A. TRIG: This is an automatic trigger control and should be enabled. If it is disabled, item nos. 4, 5, & 6 are ignored.
4. LEVEL: This is the signal voltage level for the trigger. It should be adjusted as per field conditions.

5. **TRIGGER POSITION:** This defines the number of samples to be taken before and after the trigger. If number of samples is 2048, and trigger position is 0.2, 410 samples are taken before the trigger and 1638 samples are taken after the trigger.
6. **SAMPLING RATE:** This controls the rate at which the data will be acquired.
7. **TOTAL SAMPLES:** This controls the number of samples to be recorded for all channels. Thus, if there are "X" channels and "Y" samples are required per channel, then  $\text{TOTAL SAMPLES} = X \cdot Y$ . The Fast-Fourier Transformation (FFT) criteria requires TOTAL SAMPLES to be a power of 2.
8. **SET COUNT:** This indicates the number of signals to be averaged for plotting the dispersion curve.

The general SASW and the University of Alberta SASW field procedures were described in Sections 3.2 and 3.3, respectively. Upon execution of the newly developed "SWAP", a folder is created for each site and all data files corresponding to that particular site is stored in that folder. "SWAP" then prompts the user to enter the following information:

1. Site folder name,
2. Data file name, and
3. Receiver spacing in metres.

For the "SWAP" data acquisition software, the name of the site is entered in the first prompt. For the second prompt, usually the data file name is entered with a suffix "for" or "rev" as for example: "1.0mfor" or "1.0mrev". 1.0m indicates the receiver spacing whereas "for" or "rev" indicate whether the data is taken in the forward or reverse mode. Other information like hammer size, receiver type etc. can also be entered in the file name to let the user get a brief idea about the content of the file. Receiver spacings are entered in the third prompt.

After this information has been entered; the Site Name, Date of Testing, Time of Testing, Receiver Spacing will be displayed on the FRONT PANEL and the program will wait for the first impact to be made on the test surface.

After the impact, the amplitudes, unwrapped phase and the coherence will be displayed on the FRONT PANEL. The user then has to decide whether to accept or reject this signal based on the requirements of the site or project. If the user decides to accept this signal, the knob of the button should be moved to the ACCEPT position and then the program will allow the user to make the second impact. COUNT DONE as displayed on the FRONT PANEL will be increased by 1 each time a signal is accepted, until COUNT DONE equals SET COUNT. When these values are equal, a dispersion curve is plotted for this receiver spacing, including all data points. At that stage, the button NEXT SPACING should be clicked to continue the data collection for the next spacing. If not, clicking STOP button will terminate the program.

The data file will contain the following information:

1. Site Name,
2. Date of Testing,



3. Time of Testing,

4. Receiver Spacing (m).

After recording the above information, the data file will create nine columns with the following headings:

1. Serial No.: This is the number of samples
2. Time: This is the time elapsed corresponding to each sample since triggering
3. Amp 1: This is the amplitude time signal from Channel 1.
4. Amp 2: This is the amplitude time signal from Channel 2.
5. Frequency: This is the frequency associated with each sample
6. Phase: This is the unwrapped phase associated with each sample.
7. W. Length: This is the wavelength of each sample. Small wavelength is associated with high frequencies and shallow depths whereas large wavelengths are associated with low frequencies and deeper layers.
8. Ph. Velocity: This is the phase velocity associated with each frequency.
9. Coherence: This is the signal-to-noise ratio and it varies between 0 and 1. A Coherence of 1 indicates a good signal.

Some of the the segments of "SWAP" to perform the above mentioned tasks are shown in Appendix A.

#### 5.4 FIELD PROCEDURE

In this research, the common-receiver-midpoint (CRMP) geometry was chosen for field testing at all sites. Although one receiver spacing should be sufficient to perform testing on one site, several receiver spacings were used to compensate for more attenuation during propagation. The individual dispersion curves from each source-receiver spacing were combined to form the composite dispersion curve for the site.

For each site, an imaginary centerline was established, which would remain constant throughout the test. This centerline is often perpendicular to the traffic flow direction. A line along the direction of flow and perpendicular to the centerline was drawn or marked so that the source and the receivers could be moved along that line. The source was placed in such a way that the distance between the source and the near-receiver was equal to the receiver spacings. Sanchez-Salinero et. al. (1987) found that this configuration was a good compromise between theoretical considerations, such as the reduction of near-field effects and wave attenuation, etc. Impact type sources (hammers) were used to generate the surface waves and accelerometers or geophones were used to capture the waves as they propagated through the medium. Accelerometers were used for high frequency sources (smaller hammers) with small receiver spacings for profiling shallow depths, whereas geophones were used for low frequency sources (big hammers) with large receiver spacings for profiling deeper layers.

After obtaining an experimental dispersion curve with this configuration, the location of the source was reversed with respect to the receivers keeping the receivers fixed at the previous

location. The experimental dispersion curve was subsequently obtained with this reversed source-receiver configuration but keeping the spacing between receivers and the source and the near receiver constant. Common-receiver-midpoint geometry was employed in this study because there were no space-limitations and to reduce the effect of heterogeneity, if at all present. In order to have a good contact between the test surface and the accelerometers, "LOCTITE" Super Bonder 430 manufactured by Loctite Corporation was used. It would take only a few minutes for the Super Bonder to fix properly. The geophones were large and weighed about 2.15 kg each and the self-weight was often sufficient for good contact with the ground.

Once a pair of dispersion data were collected with a single spacing, the source and the receivers were moved to the next receiver spacing keeping the imaginary centerline midway between the receivers. The source was subsequently reversed with respect to the receivers and the procedure was continued until the final receiver spacing was completed.

Typical signals captured with the receivers are shown in Figure 5.8. The pre-trigger delay provides the initial quiet period. After the waves pass the receivers, the ground returns to its original rest position. The total power contained in the impulsive time signal is distributed over the entire range of frequencies and according to Parseval's theorem, the power of a signal in the time-domain is equal to the power of the same signal in the frequency domain. After the amplitude signals are displayed on the computer screen using the computer program "SWAP", a decision is made whether to accept or reject the captured signals. This decision is generally made based on the quality of amplitude signals and the coherence function. The minimum acceptable coherence limit considered for this research was 0.98. The other factor which helps in judging the quality of the amplitude signal is the possible "double-hit" on the test surface, which can be identified by the presence of two peaks in the amplitude signal with a quiet period between.

Once good quality signals are established, they are accepted and the operator instructs the "SWAP" program to continue. This results in performing linear spectra  $H_1(f)$  and  $H_2(f)$  on the amplitude signals  $Y_1(t)$  and  $Y_2(t)$  respectively. Both  $H_1(f)$  and  $H_2(f)$  have real and complex components. These linear spectra are used to compute auto-power spectra, cross-power spectrum and the coherence function. Each impact on the ground generates a pair of amplitude signals and a set of calculations, mentioned above. Generally five impacts were done and the results of the above calculations were averaged for a single source-receiver configuration.

The phase of the cross-power spectrum plays an important role in the calculation of phase velocity. With the receiver spacing known, this phase is utilised in calculating the field dispersion curve. The cross-power,  $S_{XY}(f)$ , of the signals  $x(t)$  and  $y(t)$  is a complex number and is defined as:

$$S_{XY}(f) = X^*(f) \times Y(f) \quad [5.1]$$

where  $X^*(f)$  = complex conjugate of  $X(f)$

$$X(f) = \mathbf{F}\{x(t)\}, \text{ and} \quad [5.2]$$

$$Y(f) = \mathbf{F}\{y(t)\}. \quad [5.3]$$

Because  $S_{XY}(f)$  is an array of complex numbers,  $S_{XY}(f)$  can be separated into an array of Real part,  $\text{Re}\{S_{XY}\}$  and an Imaginary part,  $\text{Im}\{S_{XY}\}$ .  $S_{XY}$  can graphically be represented on a complex plane where real axis is the x-axis and the imaginary axis is the y-axis. Therefore, it is possible to calculate the magnitude and phase of the Cross-Power Spectrum,  $S_{XY}(f)$  using the following:

$$\text{Magnitude} = \sqrt{\left[\text{Re}\{S_{xy}\}\right]^2 + \left[\text{Im}\{S_{xy}\}\right]^2} \quad [5.4]$$

$$\text{Phase} = \tan^{-1} \left[ \frac{\text{Im}\{S_{xy}\}}{\text{Re}\{S_{xy}\}} \right] \quad [5.5]$$

The phase is computed in radians and varies between  $+\pi$  radians and  $-\pi$  radians. Thus the phase obtained from Cross Power Spectrum is termed as "folded phase" or "wrapped phase". It is necessary to unwrap the phase by eliminating discontinuities when absolute values exceed  $\pi$ . Each segment of the phase jump  $-\pi$  radians to  $+\pi$  radians ( or vice versa) is patched back to its proper location by placing it end-to-end. Figure 5.9 illustrates the conversion of phase from its wrapped state to unwrapped state. The wrapped phases of points 'D', 'G' and 'J' are all zero radians whereas the unwrapped phases of points 'D', 'G' and 'J' are  $-2\pi$ ,  $-4\pi$  and  $-6\pi$  respectively. This phenomenon is called "Unwrapping". This unwrapped phase is used to calculate the phase velocity with the following equations:

$$\text{Phase Velocity} \quad V = \frac{X}{t} \quad [5.6]$$

$$\text{where} \quad t = \left( \frac{\phi}{2\pi} \right) \left( \frac{1}{f} \right) = \text{time lag}$$

$X$  = distance between two receivers

$\phi$  = unwrapped phase in radians

$f$  = frequency

Finally, the individual dispersion curves from each source-receiver spacing are combined to form the composite dispersion curve for each site.

### 5.5 MICROCOMPUTER PROGRAM "MULTIMOD"

A stand-alone Macintosh Application microcomputer program "MULTIMOD" has been developed for determining dispersion characteristics of multiple-mode Rayleigh waves based on some prior knowledge of subsurface layers. The development of this software was necessary to evaluate possible higher modes. The software SASW-FM (Addo, 1992) is based on fundamental mode and there was a need to evaluate whether higher modes are recorded at some of the pavement sites.

The relationship between phase velocity  $c_m$ , and wave number  $k_m$ , for the fundamental (  $m = 1$  ) and higher (  $m > 1$  ) Rayleigh modes at a given frequency 'f' is implicitly defined by:

$$\left( \frac{\dot{u}}{\dot{w}} \right)_m = \frac{J_{22} - J_{12}}{J_{11} - J_{21}} = \frac{J_{42} - J_{32}}{J_{31} - J_{41}} \quad [5.7]$$

in which  $J_{ij}$  = element of the matrix  $\mathbf{J}$  defined by Haskell (1953) and a function of  $H$ ,  $\rho$ ,  $V_p$ ,  $V_s$ ,  $c_m$ ,  $k_m$ ; and  $\left( \frac{\dot{u}}{\dot{w}} \right)_m$  = an imaginary number of the m-th mode defining the amplitude ratio between the horizontal and vertical particle velocities on the ground surface. The correlations among  $c_m$ ,  $k_m$ ,  $f$ , and wavelength  $\lambda_m$  are defined by:

$$c_m = f\lambda_m \quad [5.8]$$

$$c_m = \frac{2\pi f}{k_m} \quad [5.9]$$

The "MULTIMOD" Software is based on the dispersion equation as given in Equation 5.7. When the "MULTIMOD" Software is initiated, a front panel will be displayed on the

computer screen as shown in Figure 5.10, prompting for input of assumed layer parameters. Once the layer parameters are entered, pressing the OK button will lead to the next screen as shown in Figure 5.11. This screen is basically asking for the boundary conditions between which the calculation process will take place. The objective of this program is to find a wavenumber between the assigned Phase Velocities where the determinant is zero. Each root will correspond to each mode of vibration. Pressing the OK button will lead to the third screen as shown in Figure 5.12. This window gives the user an estimate of the approximate time the calculation process might take. If the user wishes to continue, the software will ask for the filename where the results are to be stored.

A synthetic profile has been considered for a trial run with the "MULTIMOD". The output of this run has been shown in Figure 5.13. This trial was done in order to compare the output results with Gucunski et. al. (1991) and also to check whether the "MULTIMOD" is functioning properly. The output results from Gucunski et. al. (1991) are also shown in Figure 5.13. The results are quite comparable. Another synthetic profile has been considered later in Chapter 7 to compare the output from "MULTIMOD" with the measured profile for basement slab in Room CEB-B11.

A dynamic system with multiple degrees of freedom can be used as an analogy to describe the transition from the first to higher Rayleigh modes [Lysmer (1965)]. The dynamic system consists of two masses and two sets of springs, representing layers, and a damper representing a half-space. The top spring is stiffer than the spring at the bottom, which is quite similar in having a stiff top soil layer and a soft bottom soil layer. For low frequencies, as long as the excitation frequency is close to the first natural frequency of the system, the force at the top is well transmitted to the lower mass, representing a softer layer, and to the dampers, representing a half-space. As frequency increases and the second mode becomes dominant, only the top mass exhibits significant displacements. The lower

mass acts as an isolator, preventing transmission of forces to the dampers below. A similar process occurs in layered soil system where the phenomena of oscillations are replaced by the phenomena of wave propagation. At higher frequencies, a softer layer does not allow a transmission towards lower layers so that wave propagation is governed by the material properties of the surface layer, represented by higher Rayleigh modes.

The above analogy can be compared with a typical pavement structure. The top stiff pavement layer is analogous to the top mass and the top stiffer spring of the dynamic system. The intermediate soft layer of a typical pavement system is analogous to the bottom mass and the less stiff spring of the dynamic system. The half space corresponds to the damper. In practice, high frequencies are required for profiling shallow layers and low frequencies are required for deeper layers as described in the analogy of the dynamic system.

## 5.6 SUMMARY

This chapter has described the new developments that have been accomplished as part of this research. This includes modified hardware and newly developed software. High frequency accelerometers, extremely fast data-acquisition boards, and an energy source capable of generating a wide range of frequencies, including high frequencies, were the major focus of attention in this research. New data-acquisition software "SWAP" and an analytical program "MULTIMOD" have also been developed as a part of this research. The data-acquisition program was developed with the assistance of the Electronics Division of the Civil Engineering Department.



Channels		4
Transducer excitation	volt	+ 24
Excitation Current	mA	2 - 20
Voltage Gain ( Selectable)		x1, x10, x100
Frequency Response( $\pm 5\%$ )	Hz	0.225 to 100 kHz
Maximum output signal	volt	$\pm 10$
Output Impedance	ohms	< 50
Overload Detection	volt	$\pm 10$
Signal to Noise	x1	> 120
	x 10	> 90
	x 100	> 72
Cross Talk	x 1	> 130
	x 10	> 120
	x 100	> 100
DC offset (all gains)	mV	$\pm 50$
Power Required ( 50 to 400 Hz)	VAC	110 or 220
Connectors: INPUT	JACK	BNC
	JACK	BNC
Size (L x W x H)	inch	9.7 x 2.9 x 6.3
Weight	lbs	2

Table 5.1 Specifications of PCB Model 482A16 Power Amplifier

Serial #	8625	8626	8627	8628
U of A Serial #	0188104	0188106	0188107	0188105
Coil Resistance (ohms)	5500	5500	5500	5500
Frequency (Hz)	1.0	1.0	1.0	1.0
Force Constant Calibration (k Dynes Amp)	39.2	40.9	41.1	42.3
Mass (gm)	972.8	966.6	979.8	968.2
Weight (kg)	2.1	2.1	2.1	2.1

Table 5.2 Characteristics of Model L-4 Geophones

Serial #	4306	4307
Voltage Sensitivity (mV/g)	5.44	5.63
Transverse Sensitivity (%)	2.2	1.3
Resonant Frequency (kHz)	120	120
Time Constant (s)	0.1	0.1
Output Bias Level (V)	8.8	9.0
Range ( $\pm$ g)	1000	1000
Resolution (g)	0.02	0.02
Temp. Range (deg. F)	-40/+150	-40/+150

Table 5.3 Specifications of PCB Model-309A accelerometers

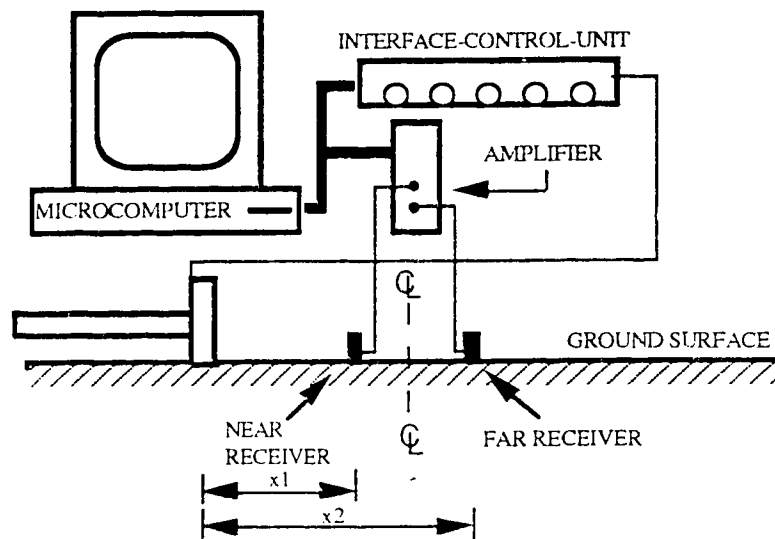


Figure 5.1 SASW equipment set-up as used in this research

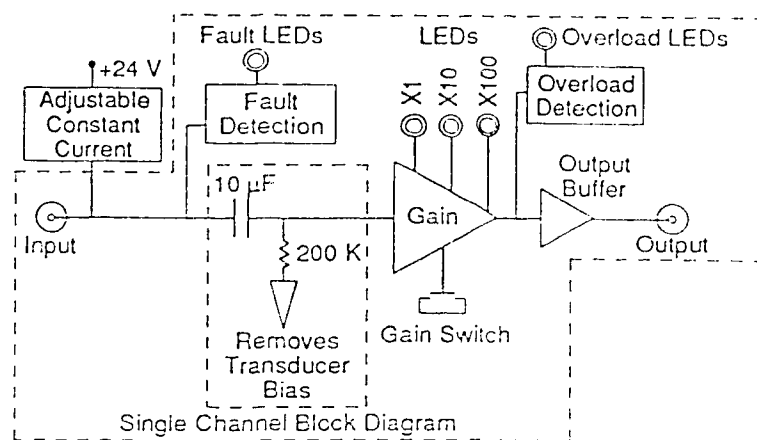


Figure 5.2 A schematic diagram of PCB Model 482A16 Power Amplifier



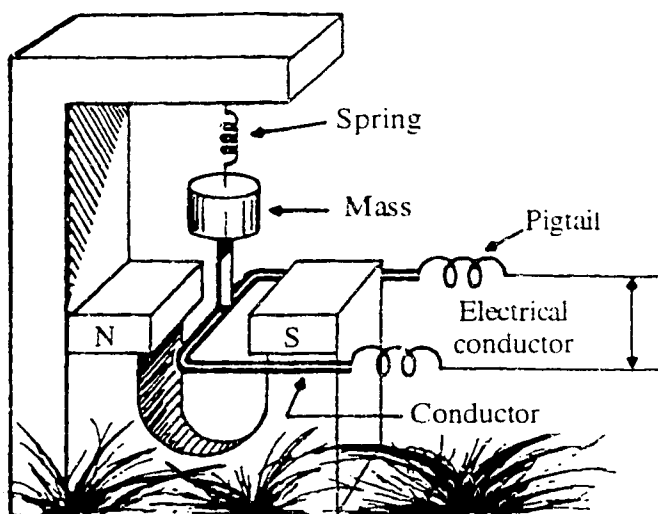


Figure 5.4 A schematic diagram of a typical geophone

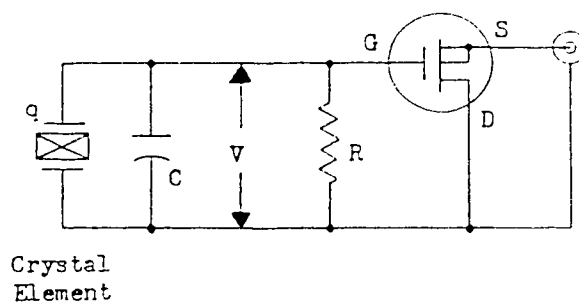


Figure 5.5 A schematic diagram of a typical ICP transducer

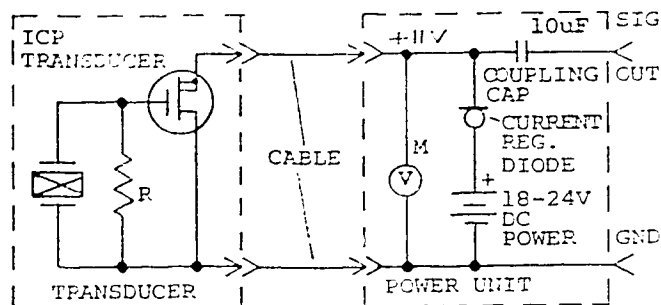


Figure 5.6 A schematic diagram of a typical ICP system

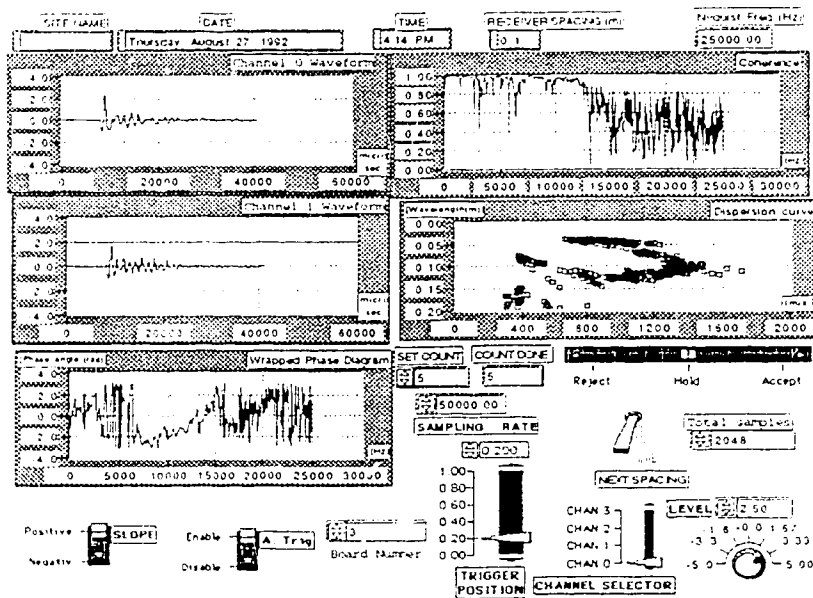


Figure 5.7 Front Panel Diagram of "SWAP"

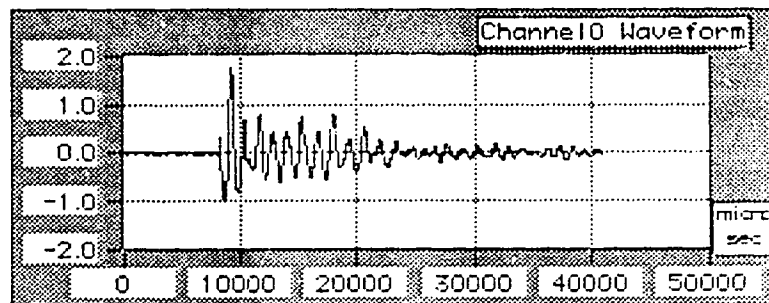


Figure 5.8 A typical signal captured with a receiver



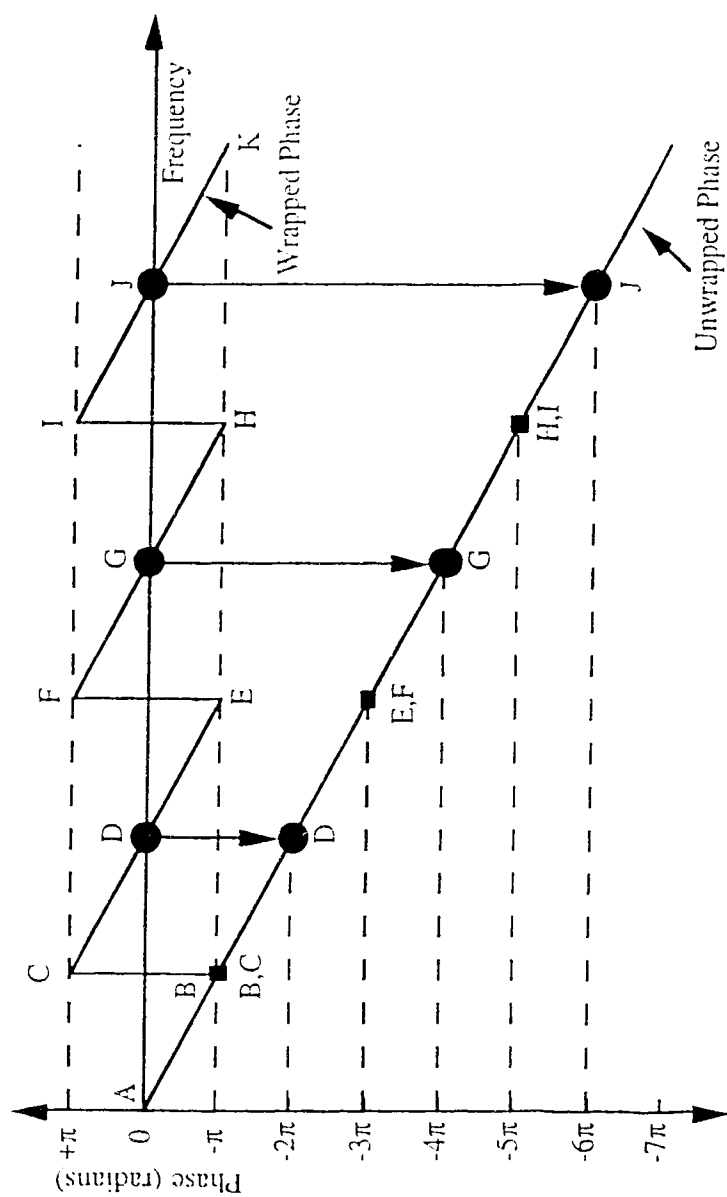


Figure 5.9 Conversion of phase from wrapped state to unwrapped state

# MULTIMOD Software

by Debabrata (David) Das, under supervision of  
 PROF. P. K. ROBERTSON  
 Department of Civil Engineering  
 UNIVERSITY OF ALBERTA  
 Edmonton, Alberta  
 CANADA T6G 2G7

\*\*\*\*\*


This Software will work for 4 layers including Half-Space.

\*\*\*\*\*

LAYER NO.	THICKNESS(m)	UNIT WEIGHT (kg/m <sup>3</sup> )	Vp(m/s)	Vs(m/s)
1	<input type="text" value="0.15"/>	<input type="text" value="2400"/>	<input type="text" value="4700"/>	<input type="text" value="3000"/>
2	<input type="text" value="0.10"/>	<input type="text" value="2000"/>	<input type="text" value="5000"/>	<input type="text" value="2500"/>
3	<input type="text" value="0.05"/>	<input type="text" value="2000"/>	<input type="text" value="5000"/>	<input type="text" value="2500"/>
Half Space	<input type="text" value="INF"/>	<input type="text" value="1800"/>	<input type="text" value="1470"/>	<input type="text" value="600"/>

Click OK to continue

Figure 5.10 First screen of "MULTIMOD" Software asking for layer parameters


MULTIMOD Software

# MULTIMOD Software

by Debabrata (David) Das, under supervision of  
PROF. P. K. ROBERTSON  
Department of Civil Engineering  
UNIVERSITY OF ALBERTA  
Edmonton, Alberta  
CANADA T6G 2G7

\*\*\*\*\*  
This Software will work for 4 layers including Half-Space.  
\*\*\*\*\*

MIN Wavenumber	MAX Wavenumber	STEP Wavenumber
<input type="text" value="100"/>	<input type="text" value="200"/>	<input type="text" value="1"/>

MIN Phase Vel. (m/s)	MAX Phase Vel. (m/s)	STEP Phase Vel. (m/s)
<input type="text" value="500"/>	<input type="text" value="3500"/>	<input type="text" value="100"/>

Click OK to continue

Figure 5.11 Second screen of "MULTIMOD" Software asking for boundary conditions

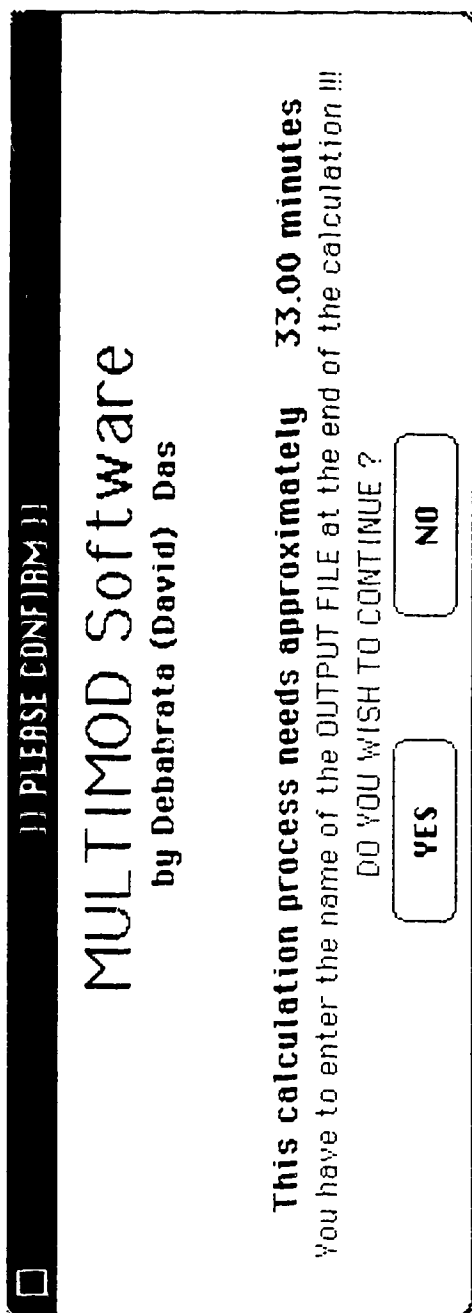


Figure 5.12 Third screen of "MULTIMOD" Software giving an idea of calculation time

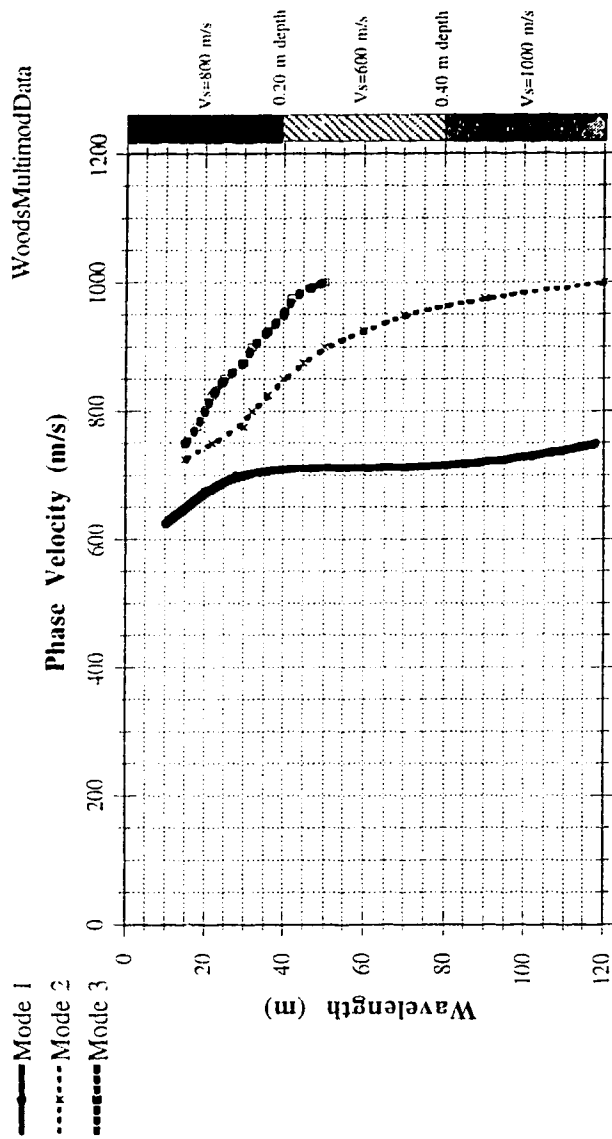


Figure 5.13 Theoretical Dispersion curve for first three Rayleigh Modes

## **CHAPTER SIX**

### **FIELD WORK AND LABORATORY WORK**

#### **6.1 INTRODUCTION**

Six sites were selected in the City of Edmonton, Alberta, Canada to perform the field work for this research based on the following criteria:

- proximity to the Civil Engineering Building to reduce travelling time,
- variety of roads ranging from 'stiff' to 'soft' pavements,
- availability of existing data related to the preselected roads or basement layer.

Core samples were also obtained from one of the sites in order to perform laboratory seismic wave velocity measurements. This chapter describes the selected sites in detail. A description of the laboratory seismic wave velocity measurement and results obtained from laboratory testing are also included in this chapter.

#### **6.2 SITE SELECTION**

The selection of the test sites were based mainly on the criteria mentioned above. The intention of this research was to study the effectiveness of the SASW technique on various types of structural layers ranging from stiff, thick Portland Cement Concrete (PCC) pavement sections to relatively soft, thin Asphalt Concrete (AC) pavement sections. The details of the sites selected to perform the field work for this research are described in the following sections.

### 6.2.1 UNIVERSITY OF ALBERTA SASW TEST SECTION B-11, BASEMENT SLAB

This test section is located on the basement floor of Room CEB-B11 in the Department of Civil Engineering, University of Alberta. Because the design drawing of the cross-section of this basement slab was not available, a core was obtained to determine the thickness of the concrete slab directly by measurement and to measure the velocity of the core. The site location plan for this test location is shown in Figure 6.1. This site was selected to allow testing under controlled temperature conditions to evaluate the repeatability of the SASW technique.

### 6.2.2 UNIVERSITY OF ALBERTA LRT STATION SASW TEST SECTIONS, RIGID PAVEMENT

These pavement sections are located on the campus of the University of Alberta. The test sections were located on the 89 Avenue between 112 Street and 114 Street and on 112 Street. Until the summer of 1992, these pavement sections were part of a flexible pavement system. During the summer of 1992, the flexible pavement was removed and replaced with a new rigid concrete pavement consisting of 250 mm of portland cement concrete overlying 150 mm of soil cement. Three different locations were selected for field testing purposes. One of the test sections was located on the west side of 89 Avenue between 112 Street and 114 Street (SASW Test Section CC). The Civil Engineering building is to the north of the test section and Saint Joseph's College is to the south of this test section. The second test section (SASW Test Section EE) was located on the east side of 89 Avenue between 112 Street and 114 Street. One of the entrances to the University LRT station is to the north of this section and HUB Mall, a student residence lies is to the northeast of this test section. The third test section (SASW Test Section FF) is located on the north side of 112 Street between 87 Avenue and 89 Avenue. All the tests at these sites were conducted between

1:30 A.M. and 5:30 A.M. when the transit buses were not in operation. The site plan for these test-locations are shown in Figure 6.2.

### 6.2.3 WHITEMUD DRIVE SASW TEST SECTION, FLEXIBLE PAVEMENT

This test section is located on Whitemud Drive Eastbound on 178 Street offramp ( under the bridge ) in the City of Edmonton. Whitemud Drive is one of the most important freeways in the City of Edmonton linking the east and the west ends of the city. Although the test section is part of the fully-constructed highway system, the test section was surrounded by concrete barriers and had not been opened for traffic. Therefore, no special arrangements were needed with the City of Edmonton for diversion of traffic during testing. However, when the impact was made on the road surface during SASW data-acquisition, care was taken to ensure that no traffic was passing-by causing extra vibration. The field testing at this location was done for a period of one month ( April 09/93, April 22/93, April 29/93 and May 14/93) to study the effectiveness of the SASW technique during the spring-thaw period. Although it was not intended to select the test location immediately under the bridge ( 178 Street ), bad weather on the first day controlled the selection of the test location. Therefore, there was little direct sunlight falling on the test section even on the brightest day. Normally the lowest point of the ground is under the bridge to allow for a surface water catch basin. Therefore, extra caution had been taken not to perform SASW testing directly on the catch basin. Records from the City of Edmonton showed that this pavement section had been constructed in 1989 and that the road structure consists of 250 mm of Asphalt Concrete overlying 150 mm of soil cement. In discussions with the City officials, it was revealed that an insulation ( Dow HI 40) of about 200 mm thickness was placed below the soil cement, but no accurate records were available pertaining to the thickness of this insulation. The site plan for this test section is shown in Figure 6.3.



#### 6.2.4 KEILLOR ROAD SASW TEST SECTION, FLEXIBLE PAVEMENT

Keillor Road is a part of the flexible pavement system in the City of Edmonton. This road served as a short cut route to downtown Edmonton from the south west side of the city until it was closed in the Fall of 1992. Since then, this road has been intended for bicycles only. This road is old and rather poorly constructed and has been overlaid several times to reach the present condition. City officials could not provide any recorded documents pertaining to the structural formation of this pavement. Information gathered through conversation with some old people revealed that Keillor Road is actually an old oily road and does not have a real pavement structure. Drilling was carried out to collect samples and measure the thickness of the road structure. The field testing at this location was done for a period of one month ( April 14/93, April 22/93, April 29/93 and May 14/93). On April 20/93, drilling was performed and temperature sensors (thermistors) were installed in the ground to monitor the change in ground temperature with time. The site plan for this test section is shown in Figure 6.4.

### 6.3 LABORATORY SEISMIC WAVE VELOCITY MEASUREMENTS

#### 6.3.1 INTRODUCTION

Three different basic laboratory techniques can be used for transmitting and measuring compressional (p-) and shear (s-) wave velocities in soil and rock. These methods are resonance, bender element and pulse transmission. The pulse transmission method was adopted for the seismic wave velocity measurements in the concrete core samples obtained from B-11 because the test specimens were very stiff.

Simple low-cost sonic velocity equipment was used to measure compressional and shear wave velocities in this case. The equipment consisted of a high-powered pulse generator and sets of pulsing and sensing heads.

### 6.3.2 PULSE TRANSMISSION METHOD

In the pulse transmission method, two piezoelectric transducers are attached to the ends of the test specimen. The top piezoelectric transducer was selected as the trigger transducer and the bottom piezoelectric transducer was selected as the receiving transducer. The signal received at the receiving transducer was amplified and fed to a digital oscilloscope. The trigger signal was also fed to the oscilloscope, so that the time of trigger and the exact time of arrival of the received signal could be assessed.

A pulse from the waveform generator provides the electric pulse to the transmitting piezoelectric crystal and triggers the oscilloscope trace. The transmitter vibrates according to the change of voltage with time, generating a mechanical pulse in the specimen. The mechanical pulse is attenuated as the seismic wave travels through the specimen. The receiving piezoelectric crystal converts this attenuated wave into an electric pulse that is displayed on the oscilloscope screen. The travel time of the mechanical pulse through the specimen is determined from the oscilloscope, and the velocity is calculated from:

$$V = \frac{L}{t} \quad [6.1]$$

where:

V = seismic velocity

L = length of the test specimen, and

t = first arrival time.

Once the compressional wave velocity and the shear wave velocities had been computed, the Poisson's Ratio of the test specimen was calculated using the following equation:

$$\nu = \frac{\left[ 0.5 \left( \frac{V_p}{V_s} \right)^2 - 1 \right]}{\left[ \left( \frac{V_p}{V_s} \right)^2 - 1 \right]} \quad [6.2]$$

where:

$\nu$  = Poisson's ratio

$V_p$  = compressional wave velocity

$V_s$  = shear wave velocity

By using a set of either p- or s-wave transducers, both the compressional wave velocity,  $V_p$  and shear wave velocity,  $V_s$  were measured. A schematic diagram of the pulse transmission method is given in Figure 6.5.

The pulsing and sensing heads ( diameter: 53 mm and height: 53 mm) used for this laboratory experimentation were identical and interchangeable. They were attached to the flat ends of the specimen by means of Dow Corning high vacuum grease - a silicone lubricant. BNC connectors were used to connect these heads to the pulse generator and to a PHILIPS PM-3365A oscilloscope. Hewlett Packard Color Pro Digital Plotter was also linked to the oscilloscope to obtain hard copies of the wave signals.

The pulse generator used for this purpose was manufactured by the Slope Indicator Company. It develops a 1000 volt pulse in the form of a rapid rise with exponential decay. This pulse was fed into the top of the specimen. Although the pulse repetition rate can be

adjustable between 20 to 150 repetitions per second, the rate was kept constant for the whole testing program to preserve the consistency of the input pulse. The pulse generator also generates a trigger pulse which was used to trigger the oscilloscope. The trigger pulse on the pulse generator was connected to Channel B of the oscilloscope through a BNC connector. Due to the fact that the output voltage of the pulse generator was extremely high, there was no need for amplifying either the input pulse or output pulses.

The pulsing and sensing heads contain piezoelectric crystals to generate either compressional or shear waves. The transducers are housed in magnesium, which protects them from stray electromagnetic pick-up, and mechanical damage. The use of magnesium shielding also improves the energy transmission across the face plate. The energy is further enhanced by the application of a bonding agent between the heads and the surfaces of the test specimens.

### 6.3.3 CALIBRATION FOR THE POLARISATION OF PIEZOELECTRIC TRANSDUCERS

Before the piezoelectric transducers were used for seismic velocity measurements, calibration for the polarisation of the pulsing head and the sensing head was performed. Polarisation is important for the performance of the transducers. The polarisation was performed by fixing the sensing head on one end of the cylindrical concrete sample and placing the pulsing head on the other end of the sample. Seismic wave signals were then recorded for every 15 degree rotation of one head. The pulsing head and the sensing head were considered polarised when the recorded signal was the strongest. The orientation of both the heads were then determined and marked.

#### 6.3.4 CALIBRATION OF THE PIEZOELECTRIC CRYSTALS DUE TO THEIR EMBEDMENT IN THE TRANSDUCER

This calibration was carried out to determine the correction factors for the travel times due to the embedment of the piezoelectric crystals in the transducers. The piezoelectric crystals are embedded within the transducer chambers and are not in direct contact with the concrete core samples. This results in longer travel times of the wave signals through the test specimen because the wave signals have to travel that extra distance between the location of piezoelectric crystals and the ends of the test specimen. The calibration was carried out, in part, by placing the pulsing head and the sensing head in direct contact and then by placing the heads at the ends of concrete core samples with lengths varying from 2 cm. to 11.5 cm. The travel times of the wave signals were recorded for all of the combinations and results are shown in Figure 6.6. In the determination of the first arrival signals for the p- and s-waves, the amplitude of the wave signals were enlarged so that the selection of the first arrival could be performed more accurately. The calibration showed that the piezoelectric transducers performed as designed and that the measurements were repeatable and consistent. The correction factors for the piezoelectric crystals due to their embedment in the transducer were 3.25  $\mu\text{s}$  and 5.46  $\mu\text{s}$  for the p- and s- wave, respectively.

#### 6.3.5 TEST PROCEDURE AND RESULTS

The concrete core obtained from the basement floor slab of Room # CEB-B11 of Civil Engineering Building was approximately 8.7 cm. in diameter and approximately 14.50 cm. in length. The bottom end of the concrete core sample was not flat as it was in direct contact with gravels under the basement slab. There was also a thin layer of cement on top of the sample. Therefore, before performing the Pulse Transmission tests on this specimen, the ends of the specimen were trimmed and made flat using a diamond saw so that the actual

wave velocity measurements were done on the actual concrete and the error in velocity measurements minimized by the elimination of inconsistent layers and boundary conditions.

After the top and bottom layers were trimmed, the length of the specimen was 115 mm. The diameter remained the same. Close examination of the specimen revealed that there was a major crack in the sample extending from top to bottom. The test specimen was then cut into three pieces having lengths of 20 mm, 40 mm and 50 mm. The specimen of 20 mm length was broken into two pieces during cutting because of the presence of the crack. Seismic tests were then conducted on each of the samples. Three measurements were done for each sample. Travel-times measured for the samples as well as for the calibration are presented in Table 6.1 and the results are plotted in Figure 6.6. The shear wave and compressional wave velocities were then computed based on Figure 6.6 and the values were  $V_p = 4400$  m/s and  $V_s = 3400$  m/s. As can be observed from Figure 6.6, the test data was consistent throughout the testing, except for the case of shear wave velocity measurements in the sample of length 115 mm.

#### 6.4 SUMMARY

This chapter described the different sites that were selected as a part of this research to perform the required field work. The primary reason for field testing was to evaluate the developed SASW system and the associated computer programs. The different sites were selected based on the criteria as mentioned in section 6.1. A description of the laboratory seismic wave velocity measurement and results obtained from laboratory testing on pieces of the concrete slab from basement floor were also included in this chapter. In the next chapter the results obtained from field testing will be presented and discussed.

B11 Concrete Core sample  
 Initial length of the concrete core before trimming: 14.0-14.5 cm  
 Diameter of the concrete core before trimming: 8.7 cm  
 Test Date: JANUARY 19/93  
 PULSE TRANSMISSION METHOD

Experiment #	Bonding Agent	Concrete thickness (cm)	Observed ts ( $\mu$ s)	Observed tp ( $\mu$ s)
1	Nothing, except pressure from top	0	5.96	3.67
2	-do-	0	5.99	3.70
3	-do-	0	6.06	3.69
4	Dow Corning Grease	0	6.50	3.87
5	-do-	0	6.53	3.70
6	-do-	0	6.55	3.88
7	Honey	0	6.22	3.72
8	-do-	0	6.24	3.68
9	-do-	0	6.21	3.67
10	Dow Corning Grease	11.5	37.5	30.7
11	-do-	11.5	37.1	29.8
12	-do-	11.5	35.7	27.5
13	Dow Corning Grease	4.0	19.6	11.7
14	-do-	4.0	19.8	11.5
15	-do-	4.0	20.0	11.3
16	Dow Corning Grease	5.0	21.9	14.8
17	-do-	5.0	22.4	15.2
18	-do-	5.0	21.9	15.5
19	Dow Corning Grease	2.0	13.1	8.8
20	-do-	2.0	12.9	8.6
21	-do-	2.0	13.1	8.7
22	Nothing, except pressure from top	0	5.42	3.23
23	-do-	0	5.48	3.23
24	-do-	0	5.50	3.32

Table 6.1 Travel times measured during Pulse Transmission testing

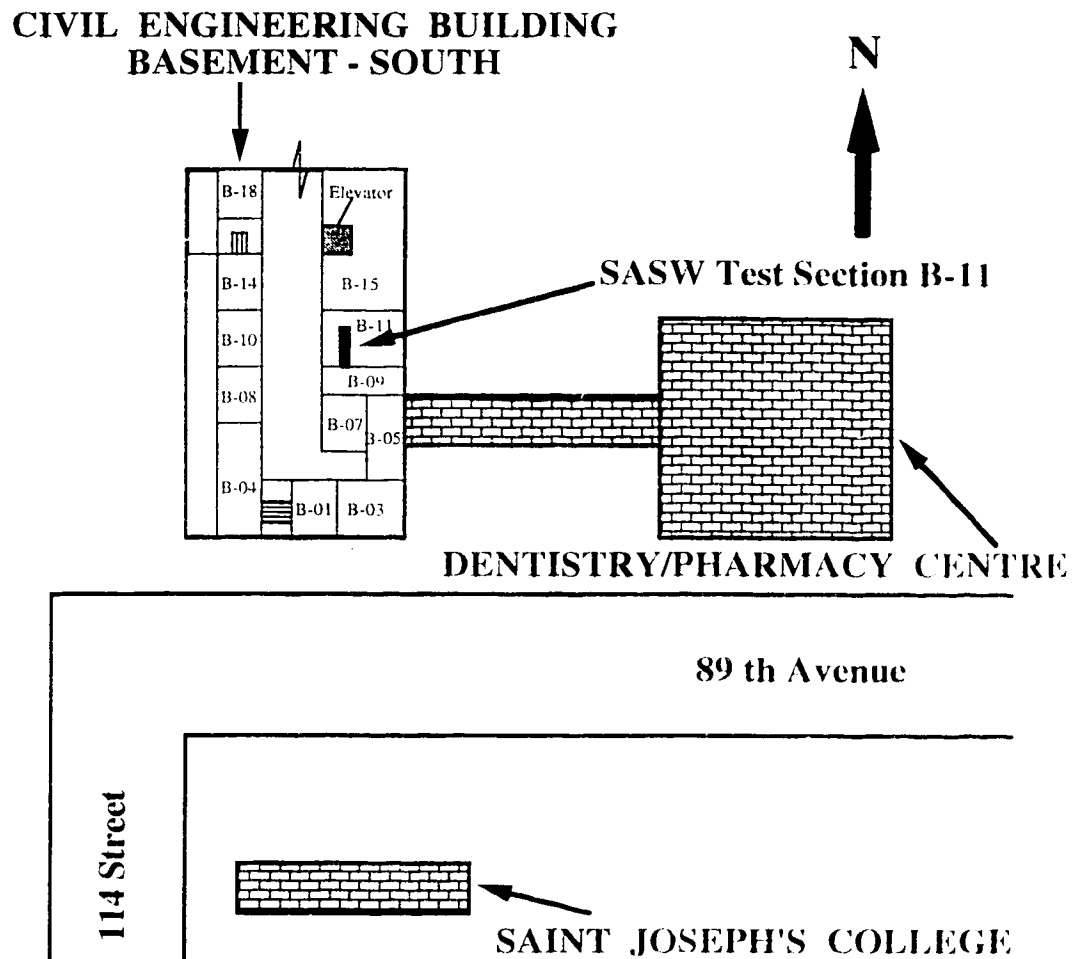


Figure 6.1 Location of University of Alberta SASW Test Section B-11, Basement Slab



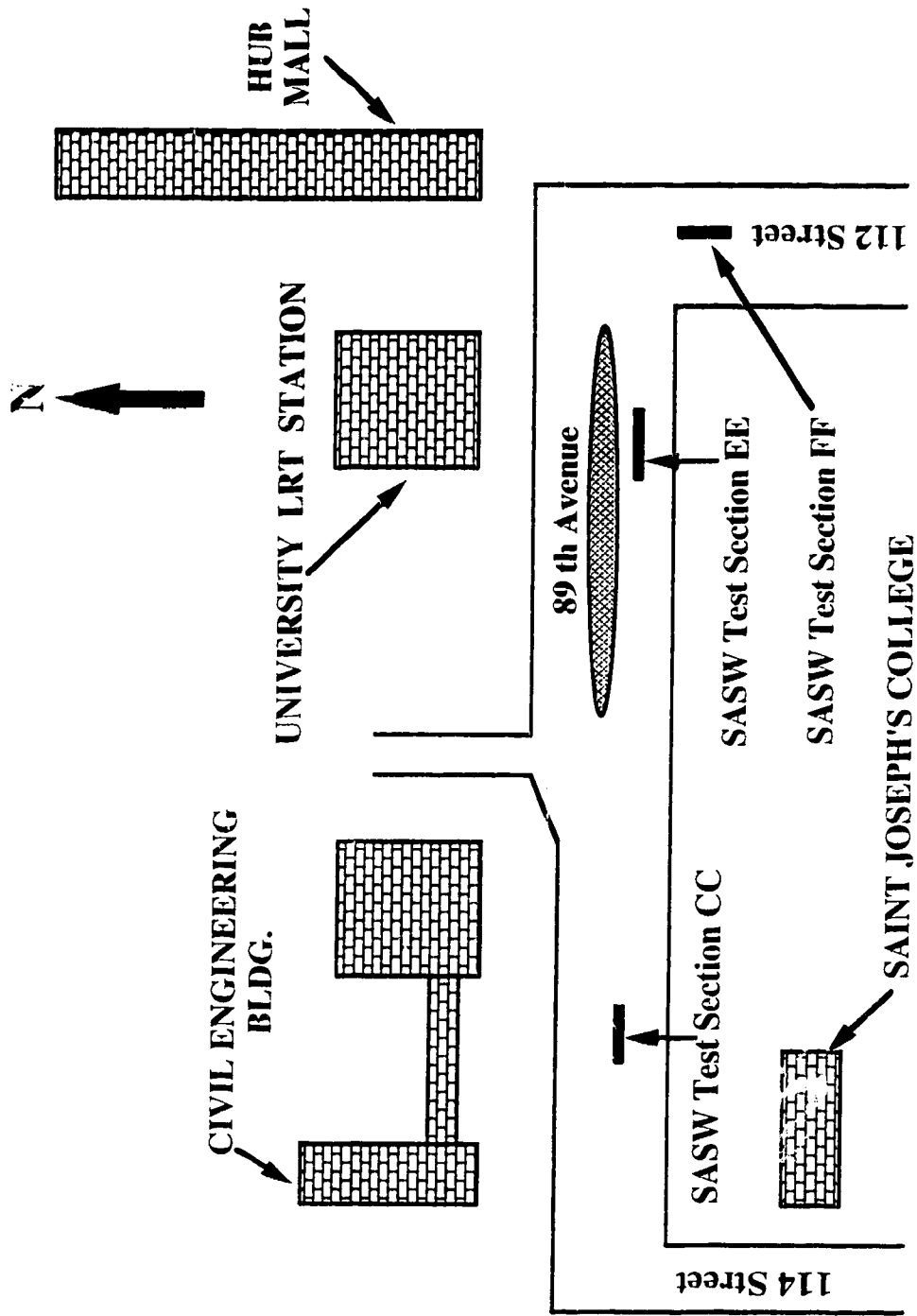


Figure 6.2 Location of University of Alberta LRT SASW Test Section, Rigid Pavement

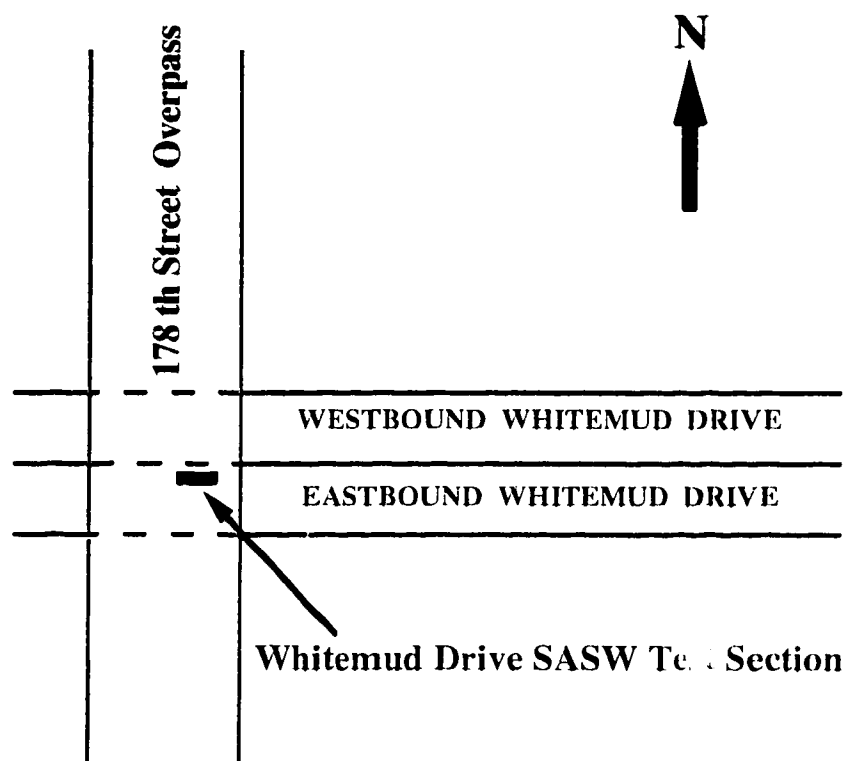


Figure 6.3 Location of Whitemud Drive SASW Test Section, Flexible Pavement

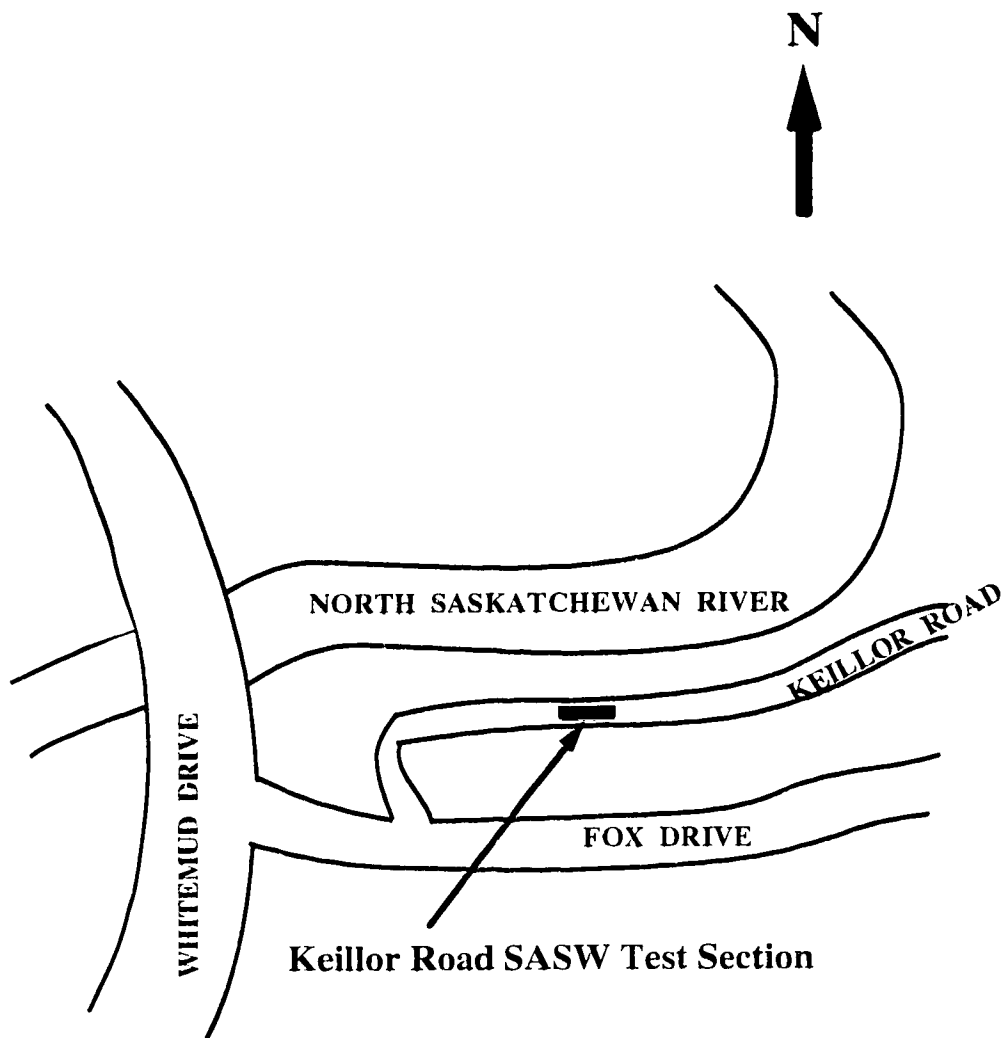


Figure 6.4 Location of Keillor Road SASW Test Section, Flexible Pavement

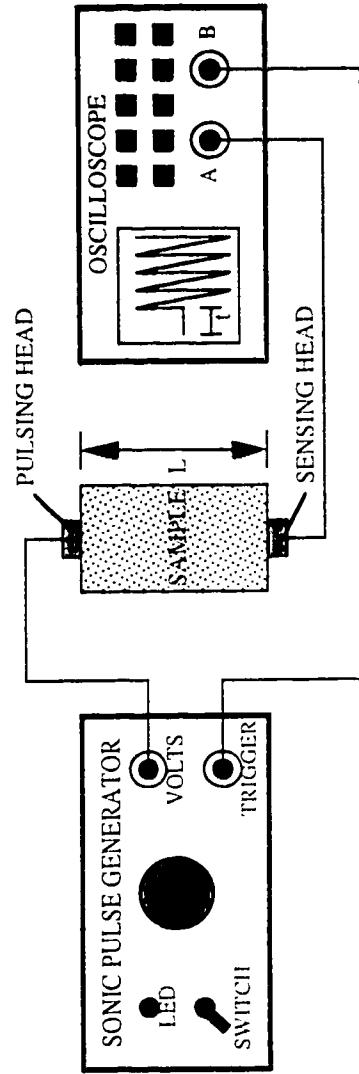


Figure 6.5 A schematic diagram of the Pulse Transmission Method

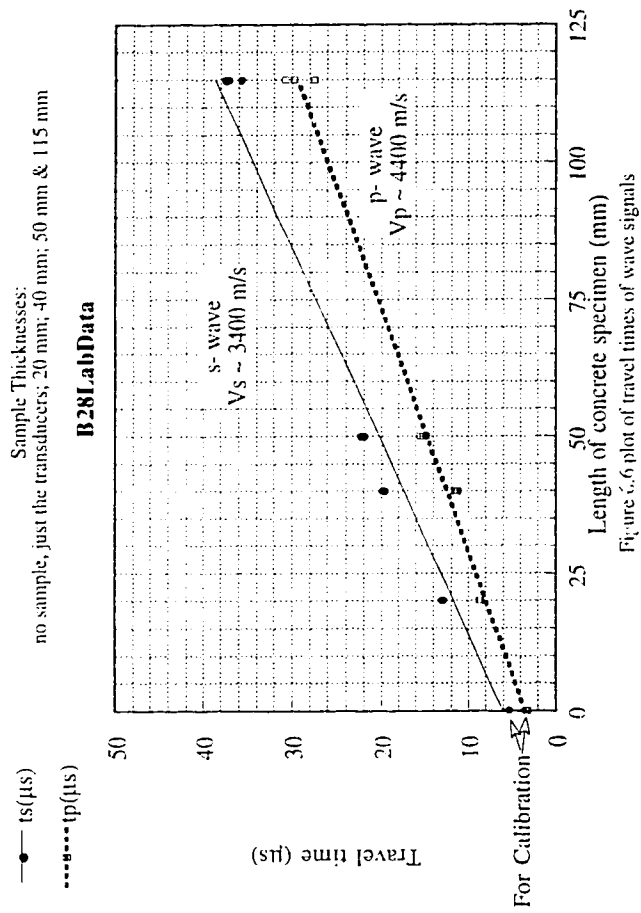


Figure 6.6 plot of travel times of wave signals

## **CHAPTER SEVEN**

### **ANALYSIS AND PRESENTATION OF RESULTS**

#### **7.1 INTRODUCTION**

This chapter analyses and discusses the test results obtained from SASW testing at the sites mentioned in the previous chapter. The Microcomputer program "SWAP" was used for data-acquisition purposes. Details of "SWAP" were provided in Chapter 5. Attempts were also made to use forward modelling software SASW-FM developed by Addo (1992) for comparison purposes.

The Test Section B-11, Basement Slab was selected to check the effectiveness of the newly developed SASW system on a stiff surface and where the subsurface soil might not be frozen during the winter months. This site was also selected to evaluate the repeatability of the SASW tests. An attempt was also made to perform multimodal analysis using "MULTIMOD" software on the test results obtained from this site to evaluate the effect of higher Rayleigh Modes. Another important aspect of this site was the possibility of obtaining an actual core sample for comparison purposes in terms of thickness and velocity.

The University of Alberta LRT Rigid Pavement sites were selected to perform the next series of SASW tests. SASW tests were performed on these sections to check the repeatability and the effectiveness of SASW system on an extremely stiff rigid pavement. These pavement sections were newly built; therefore, there was very little chance of any cracks or other weak areas in the pavement structure. Design drawings were also readily available for these test sections.

The Whitemud Drive pavement site was selected to see how the SASW performs on a flexible pavement designed for heavy traffic. The site was selected in such a way that the traffic flow would not be disturbed and that there was no need for extra precautions to avoid traffic injuries. Pavement structure information except the insulation layer thickness was readily available from the City of Edmonton. Also, the efficiency of the SASW system to identify any possible frozen layer, and the effect of spring-thaw on the SASW results were studied. The SASW tests were carried out over a period of six weeks to achieve these objectives.

Keillor Road was a part of a flexible pavement system used for low traffic volume. SASW tests were performed at this site to study the effect of spring-thaw on the SASW results. Drilling was performed and thermistors installed to monitor the ground temperature over a one month period and to compare the SASW results with these variables.

## 7.2 UNIVERSITY OF ALBERTA SASW TEST SECTION B-11, BASEMENT SLAB

This test section is located on the basement floor of Room CEB-B11 in the Department of Civil Engineering, University of Alberta. Two sets of data were collected from this test section, once during the winter months of November, 1992 and once during the spring-thaw period of May, 1993.

Because the design drawing of the cross-section of this basement slab were not available, a core was obtained to get a cylindrical concrete sample to determine the thickness of the concrete slab. The concrete slab thickness was measured to be 0.145 m. Below the concrete slab, a gravel layer was found for an additional depth of about 0.150 m.

The dispersion points, as determined from the SASW test on November, 1992 are shown in Figure 7.1. Also shown, is the average dispersion curve obtained by performing moving point average of the data points. This was achieved using a commercially available software package. These computer plots are obtained by fitting a smoothed curve based on Stineman Function to the data. Based on the above dispersion curve, the shear wave velocity profile is shown in Figure 7.2 using the simple axes scaling technique. The axes scaling was carried out based on the following simple assumptions;

$$V_s = V_{ph} * 1.1$$

$$z = \lambda / 2$$

where  $V_{ph}$  = phase velocity

$\lambda$  = wave length

$z$  = depth

$V_s$  = shear wave velocity.

Also shown in Figure 7.2, is the subsurface soil profile as obtained from coring at the site. Figure 7.1 and Figure 7.2 shows the approximately 2400 data points from the SASW test. The total time for testing was approximately 4 hours. However, this was the first test section, and many aspects of the test procedure were tried before the actual data-acquisition, consuming more time than for later tests. Results show that the shear wave velocity is about 2900 m/s to a depth of 0.20 m. There is a transition zone with shear wave velocity decreasing to about 700 m/s at a depth of 1.5 m into the subgrade.

The shear wave velocity from laboratory seismic velocity measurement tests using the Pulse Transmission method was found to be 3400 m/s. Details of the laboratory seismic velocity measurement tests were discussed in Section 6.3.



Data from the averaged dispersion curve as shown in Figure 7.1 was used as an input for the forward modelling program SASW-FM, developed by Addo (1992). The output from SASW-FM gives a comparison of the measured field phase velocity profile ( $C_{field}$ ) with the theoretical calculated phase velocity ( $C_{calc}$ ). Figure 7.3 shows the comparison between the measured field dispersion profile and the SASW-FM calculated match. SASW-FM performs an optimization of layer thicknesses and velocity parameters in an effort to match the measured field dispersion profile. Figure 7.4 shows the resulting shear wave velocity - depth profile based on the match shown in Figure 7.3. Figure 7.3 shows the initial and optimized dispersion curves obtained from forward modelling. The analysis was based on an assumed layered soil model from the steady vibration processing of Rayleigh wave data. The number of layers and the magnitude of the layer parameters were based on the shape, curvature and position of the dispersion curve in the phase velocity - wavelength space. The calculations of the initial dispersion curve and the iteration of the assumed model parameters until a matching dispersion curve was found, were all done by the computer program SASW-FM, which was described in Addo (1992). The forward modelling produces a profile made up of 10 layers with a shear wave velocity ranging from about 3000 m/s at the surface to about 700 m/s at a depth of 1.5 m. In a homogenous, isotropic, elastic, half-space, the velocity of surface waves does not vary with frequency (or wavelength). However, since the properties of pavement layers vary with depth, surface wave velocity varies with wavelength. This frequency dependency of surface waves in a vertically heterogenous medium is termed dispersion, and surface waves are said to be dispersive waves. A plot of wave velocity versus wavelength is called a dispersion curve. The velocity of propagation of interest in SASW testing is called the surface wave phase velocity (sometimes called apparent surface wave velocity). Phase velocity is defined as the velocity with which a seismic disturbance of a single frequency is propagated in the medium. SASW-FM matches the experimental and theoretical dispersion curves only when the input layer parameters match with the soil profile where the tests were conducted.

Figure 7.4 shows the layer parameters which best matched the experimental and theoretical dispersion curves as shown in Figure 7.3. Figure 7.5 compares the shear wave velocity profiles from the forward modelling and the simple empirical axes scaling based on the moving point average of measured dispersion points. The forward modelling appears to give a much better shear wave velocity profile when compared to the soil profile obtained from the core.

The scatter in the data points can be due to various reasons. The sharp contrast in layer stiffnesses as well as very thin upper layers might be the most likely contributor for the scatter. Moreover, there is a likely possibility that for shorter spacings, used for profiling near-surface layers, the signals might have been contaminated by body waves. Impact sources have been used in this research for generating surface waves. Therefore, there was little control of the required frequencies for profiling each discrete depth. The experimental dispersion curves obtained for each of the test sites represent test data obtained from different receiver spacings and receiver types. Geophones were used for large receiver spacings, whereas accelerometers were used for small receiver spacings.

An attempt was made to enter different input layer parameters, such as thicknesses and shear wave velocities, into the SASW-FM, keeping the field dispersion curve constant. This site was selected for performing this comparative study. The results of this investigation are attached in Appendix III. It was observed that SASW-FM gives almost identical layer parameters when compared to the input values. But the interesting thing that was observed was that, until the input parameters are within reasonable values of the actual field conditions, the theoretical dispersion curve doesn't match the field dispersion curve. Therefore, once a shear wave velocity profile is obtained using a simple empirical axes scaling technique, a reasonable assumption can be made for the input values for SASW-FM. If the input layer parameters are close to the actual field conditions, less iterations are

required saving lots of computer time. There also seems to be a problem of uniqueness with the SASW-FM output results. This might be due to the solution of dispersion equation for a possible 'local' minima and not 'global' minima. The shear wave velocity profile using the simple empirical axes scaling technique is obtained directly from the experimental dispersion curve. Therefore it lacks the capability of producing distinct changes in sub-surface profile.

The "MULTIMOD" software for multimodal analysis was also used for this site. This was done to check if any higher Rayleigh modes were dominant over the fundamental mode for any depth. The assumed soil model for input to "MULTIMOD" as well as the results obtained from the multimode analysis are presented in Figure 7.6. Figure 7.6 shows that for the soil profile where the stiffness is gradually decreasing with depth, the dispersion curve obtained by performing the moving point average matches reasonably well with the fundamental mode from theoretical calculations based on the assumed profile. Therefore, it appears that for soil conditions with soil stiffness gradually decreasing with depth, the moving point averaging of data points obtained from "SWAP" data-acquisition software provides reasonable results, thus avoiding the need for the time-consuming multimodal analysis.

The next series of SASW tests at this site were conducted on May 14, 1993. The field dispersion points and the moving point averaged dispersion curve is shown in Figure 7.7. The shear wave velocity profile is shown in Figure 7.8. The comparison of the field dispersion curve (phase velocity versus wavelength) with the theoretical dispersion curve as obtained from SASW-FM is shown in Figure 7.9. The theoretical shear wave velocity profile as obtained from SASW-FM is shown in Figure 7.10. Finally, the comparison of the moving point averaged shear wave velocity profile and the theoretical shear wave velocity profile as obtained from SASW-FM is shown in Figure 7.11a.

The comparison of shear wave velocity profile obtained from November 1992 and May 1993 test dates are shown in Figure 7.11b. The results are almost identical. The shear wave velocity is about 2900 m/s to a depth of 0.20 m. The shear wave velocity decreased to about 700 m/s into the subgrade at a depth of 1.5 m. Since, this site is located in the basement of the Civil Engineering Building, there is no chance of the ground becoming frozen during the winter months. Since ground conditions do not change significantly during the winter and the spring time at this location, the almost identical sets of results indicate the repeatability of the SASW system.

The shear wave velocity ( $V_s$ ) in sub soils is controlled primarily by the following,

- void ratio ( $e$ ),
- effective confining stress ( $\sigma'$ ),
- stress history,
- soil fabric.

The very high stiffness values recorded immediately beneath the concrete may be due to the high effective confining stresses due to the weight of the building and / or possible compaction carried out during construction. The  $V_s$  values of about 700 m/s are somewhat high for very stiff natural soils down to a depth of about 5 m. This high value of 700 m/s may be due to the increased stress due to the building. The SASW tests were conducted within 2m relative to the walls of the basement room. The foundation system for the Civil Engineering building consists of the basement slab supported on the footing underneath the walls. That results in the stress bulb underneath the footing. There is also a possibility of increasing the stiffness of the subsoil due to drying underneath the basement slab.

The modulus profiles for this test section are shown in Appendix IV.

### 7.3 UNIVERSITY OF ALBERTA LRT SASW TEST SECTION, RIGID PAVEMENT

SASW tests were conducted at three different locations at the University of Alberta campus. Three different test locations were selected based on available cross-sectional information of the pavement structure. These test sections were Section CC, Section EE and Section FF as shown in Figure 6.2. The three different locations have the same pavement structure, consisting of a rigid pavement structure with 0.25 m of Portland Cement (PC) Concrete and 0.15 m of Soil Cement over the compacted clay subsoil. The field tests took place between the months of September and November, 1992.

Five figures are shown for each test section:

- a) the measured data points and the resulting moving point averaged dispersion curve (wavelength versus phase velocity);
- b) the moving point averaged shear wave velocity profile with depth based on axes scaling and the cross-section of the pavement from the design drawings;
- c) the forward modeling output (using SASW-FM of Addo, 1992) showing the comparison of measured and theoretical dispersion curve;
- d) the theoretical shear wave velocity profile as obtained from SASW-FM output;
- e) comparison of moving point averaged shear wave velocity (based on axes scaling) and the theoretical shear wave velocity obtained from SASW-FM.

All the graphs are plotted on a semi-logarithmic wavelength or depth scale to allow a better view of the pavement section at shallow depths.

The plots from Pavement Section CC are shown in Figures 7.12, 7.13, 7.14, 7.15 and 7.16 respectively. The field dispersion points and the moving point averaged dispersion curve are shown in Figure 7.12. There are approximately 3400 dispersion points in this figure. The shear wave velocity profile is shown in Figure 7.13. Also shown in this figure is the pavement cross-section obtained from the design drawings. The shear wave velocity is approximately 5100 m/s to a depth of about 0.15 m; at that point there is a transition zone with the shear wave velocity decreasing to about 550 m/s into the subgrade soil. The layer of soil cement is not clearly identified from the dispersion data. The transition zone might be due to gradual stiffening of the upper layers as the temperature dropped during November, 1992. The comparison of the field dispersion curve (phase velocity versus wavelength) with the theoretical dispersion curve as obtained from SASW-FM is shown in Figure 7.14. There is a good agreement between the field and theoretical dispersion curve. The theoretical shear wave velocity profile as obtained from SASW-FM is shown in Figure 7.15. Finally, the comparison of the moving point averaged shear wave velocity profile and the theoretical shear wave velocity profile as obtained from SASW-FM is shown in Figure 7.16. The forward modelling again gives a clearer picture of the ground profile.

The field dispersion points and the moving point averaged dispersion curve, the shear wave velocity profile, the comparison of the field dispersion curve (phase velocity versus wavelength) with the theoretical dispersion curve as obtained from SASW-FM, and the theoretical shear wave velocity profile as obtained from SASW-FM for Pavement Sections EE and FF are all presented in Appendix II. The comparison of the moving point averaged shear wave velocity profile and the theoretical shear wave velocity profile as obtained from SASW-FM for sections EE and FF are shown in Figures 7.17 and 7.18, respectively. As

can be seen from these figures, the shear wave velocities in the PC Concrete layer and the Soil Cement layers are approximately 4700 m/s and 3800 m/s respectively. Below the soil cement, the shear wave velocity decreased to about 500 m/s into the subgrade soil.

For these three pavement sections, the shear wave velocity of the top PC Concrete layered varied between 4700 m/s to 5100 m/s, which is a difference of approximately 8%; whereas for the subgrade soil, the shear wave velocities varied between 500 m/s to 550 m/s. The interesting feature of the newly developed SASW technique is that it can give an overall picture of the subsoil stiffness profile. The comparison of shear wave velocity profile as obtained from SASW-FM for three pavement sections CC, EE and FF are shown in Figure 7.19. Although the shear wave velocities are almost identical below 0.4 m depth, there is a slight variation in shear wave velocities in the upper layers. The variation is within  $\pm 10\%$ . This variation of shear wave velocity in the upper layers is quite consistent with the variation of phase velocities for shorter wavelengths. The other factors that can contribute to the variability in the upper layers might be, placement of concrete and soil cement in different layers, quality of concrete mix and others.

The measured  $V_s$  values of between 4400 m/s and 5000 m/s are reasonable for high quality PC concrete. The measured  $V_s$  values of between 3500 m/s to 4000 m/s also appear to be reasonable for high quality recently-placed soil cement. Average PCC moduli has been found as high as 58 GPa by Anderson (1989). For shear wave velocity of 5000 m/s, the Young's moduli can be calculated as 130 GPa. This shear wave velocity is obtained from SASW testing, which is a small strain test. Therefore the moduli obtained from SASW testing will be on the higher side. A study has been done where for the same experimental dispersion curve, different layer parameters have been tried. Result shows that the experimental and theoretical dispersion curves match only when the input layer parameters are close to the actual soil conditions. The plots are shown in Appendix III. Because this

pavement was new, it was not possible to obtain cores and carry out measurements in lab on concrete and soil cement. The ultimate value of  $V_s$  of about 500 m/s for the natural soil at a depth of 5 m is reasonable for the stiff surface soils encountered in Edmonton. The shear wave velocity of 500 m/s in this case is higher than that obtained by Addo (1992) at a nearby location with the SCPT. The reason for the difference might be attributed to the fact that the present site has been compacted recently in order to accommodate heavy traffic such as transit buses. Moreover, a high quality PC concrete pavement has been built in the present location and the present field testing was done almost in the winter months. Addo (1992) performed his field tests in summer months.

The modulus profiles for these test sections are shown in Appendix IV.

#### 7.4 WHITEMUD DRIVE SASW TEST SECTION, FLEXIBLE PAVEMENT

As mentioned earlier, this test site was located on a portion of the eastbound lane under the 178 Street overpass. This lane was not opened for traffic. This test site was selected to check the effectiveness of the newly developed SASW system on a flexible pavement system designed for heavy traffic. This particular site was also unique in the sense that an insulated layer existed under the pavement which might have prevented the formation of a frozen layer underneath the pavement.

An attempt was made to drill a borehole at this test section of the pavement to check the subsurface soil conditions. However, because of insufficient height under the overpass and the presence of an insulation layer underneath the pavement, the drilling program was cancelled for this site. The pavement layer structure and associated information was obtained from the City of Edmonton. This site consists of a 0.25 m thick asphalt concrete over a 0.15 m thick soil cement. However, the insulation thickness could not be obtained



from any sources, but in discussion with the City officials, it was revealed that an insulation (Dow HI 40) of about 200 mm thickness was placed below the soil cement.

Air Temperature Data of the test dates for the City of Edmonton are presented in Table 7.1. The first set of SASW tests at this site were performed on April 9, 1993. It was a cloudy day and there was a lot of snowfall. Since the test section was located under the 178 Street Overpass, the pavement surface was clear of snow. The dispersion points, as determined from the SASW test on April 9, 1993, are shown in Figure 7.20. Also shown, is the average dispersion curve obtained by performing moving point average of the data points. Based on the above dispersion curve and using axes scaling, the shear wave velocity profile is shown in Figure 7.21. Also shown in Figure 7.21, is the subsurface soil profile. When the subgrade layer begin to thaw, the shear wave velocity of that layer will decrease.

Data from the averaged dispersion curve, as shown in Figure 7.20, was used as input for the forward modelling program SASW-FM. The comparison between the field phase velocity ( $C_{field}$ ) and the theoretical phase velocity ( $C_{calc}$ ) is shown in Figure 7.22. The field and theoretical phase velocities match reasonably well. The resulting shear wave velocity profile from SASW-FM, is shown in Figure 7.23. The comparison of shear wave velocity profile based on the moving point averaged axes scaling and from theoretical calculations are shown in Figure 7.24. The shear wave velocity of the asphalt concrete and soil cement layers are approximately 3600 m/s and 2800 m/s respectively. The measured shear wave velocity in the insulation layer is approximately 2600 m/s. The shear wave velocity decreased to 800 m/s into the subgrade soil layer. This freeway is meant for heavier traffic. Therefore the compaction of the subsoil might be quite higher than normal, giving high shear wave velocity of about 800 m/s in the subsoil.

The second testing program at this site was undertaken on April 22, 1993 with the same testing procedure. The maximum and minimum temperatures of this day were 18.6°C and 7.0°C, respectively and the mean temperature of the day was 12.8°C. The field dispersion points and the moving point averaged dispersion curve, the shear wave velocity profile, comparison of the field dispersion curve (phase velocity versus wavelength) with the theoretical dispersion curve as obtained from SASW-FM, and the theoretical shear wave velocity profile as obtained from SASW-FM are presented in Appendix II. The comparison of the moving point averaged shear wave velocity profile and the theoretical shear wave velocity profile as obtained from SASW-FM is shown in Figure 7.25. The theoretical results show slightly higher shear wave velocity values for the top 1 m than the shear wave velocity values based on axes scaling. The shear wave velocity based on SASW-FM is about 2900 m/s for the top asphalt concrete layer. The soil cement has an average shear wave velocity of about 2400 m/s. The shear wave velocity in the insulation layer is approximately 2100 m/s and the shear wave velocity decreased to about 700 m/s into the subgrade.

The third set of SASW tests at this site were conducted on April 29, 1993. The maximum, minimum and the mean temperatures for this day were recorded to be 16.5°C, 5.0°C and 10.8°C, respectively. The field dispersion points and the moving point averaged dispersion curve, the shear wave velocity profile, comparison of the field dispersion curve (phase velocity versus wavelength) with the theoretical dispersion curve as obtained from SASW-FM, and the theoretical shear wave velocity profile as obtained from SASW-FM are presented in Appendix II. The comparison of the moving point averaged shear wave velocity profile and the theoretical shear wave velocity profile as obtained from SASW-FM is shown in Figure 7.26. The shear wave velocity is approximately 2900 m/s for the top asphalt concrete and 2200 m/s for the soil cement layer. The shear wave velocity decreased

to about 1100 m/s at the insulation layer. The shear wave velocity further decreased to 700 m/s in the subgrade soil.

The fourth and the final SASW testing program at this site was conducted on May 14, 1993. The maximum, minimum and the average air temperatures of the day were 18.2°C, 7.9°C and 13.1°C, respectively. The field dispersion points and the moving point averaged dispersion curve, the shear wave velocity profile, the comparison of the field dispersion curve (phase velocity versus wavelength) with the theoretical dispersion curve as obtained from SASW-FM, and the theoretical shear wave velocity profile as obtained from SASW-FM, are presented in Appendix II. The comparison of the moving point averaged shear wave velocity profile and the theoretical shear wave velocity profile as obtained from SASW-FM is shown in Figure 7.27. As can be seen from these figures, the approximate shear wave velocity in the top asphalt concrete layer is about 3000 m/s. The soil cement has a shear wave velocity of 2200 m/s. The shear wave velocity decreased to about 1550 m/s in the insulated layer. Below the insulation layer, the subgrade soil has a shear wave velocity of about 600 m/s.

An overlay plot for all the test dates obtained from this site is presented in Figure 7.28 for comparison purposes. The interesting feature of this figure is that below the insulation layer, the shear wave velocity change was very small. Therefore, it appears that the presence of the insulation layer has reduced the effect on the stiffness of the ground conditions in the subgrade soil due to seasonal temperature changes. The shear wave velocity of the upper part of the profile decreased with the increased temperature. On April 9/1993, the maximum air temperature was the lowest, followed by April 29/1993, May 14/1993 and April 22/1993.

The air temperatures for the April 22, 29 and May 14 tests were similar ( $13^{\circ}\text{C}$ ,  $11^{\circ}\text{C}$ ,  $14^{\circ}\text{C}$ , respectively). The air temperature for the April 9 test was considerably lower at  $2^{\circ}\text{C}$ . Hence, the decrease in stiffness profile within the top asphalt layer and the soil cement seems reasonable. Table 8.3 in Yoder & Witczak (1975) presented typical asphalt concrete modulus values as a function of test temperatures. At  $4.4^{\circ}\text{C}$ , the average Young's modulus of asphalt concrete is approximately 11,034 MPa and at  $37.8^{\circ}\text{C}$ , the average Young's modulus is 690 MPa. These modulus values are obtained from high strain level tests, whereas SASW tests are conducted at very low strain levels. The modulus obtained from SASW tests can be as high as five times than that obtained from high strain level tests. On April 9, 1993, when the temperature was  $2^{\circ}\text{C}$ , the shear wave velocity obtained from SASW tests for the asphalt concrete was 3600 m/s. If unit weight of asphalt concrete is assumed to be  $1800 \text{ kg/m}^3$  and Poisson's ratio as 0.3, then the shear wave velocity of 3600 m/s translates into Young's modulus of 60,700 MPa. This is about five times higher than the Young's modulus measured at  $4.4^{\circ}\text{C}$  from high strain level tests. Insulating layers are generally made of foam plastic, which have low coefficients of thermal conductivity. Therefore the stiffness of the insulation layer is less sensitive to temperature changes. The measured profiles are remarkably repeatable below the insulation layer for all profiles.

The modulus profiles for this test section are shown in Appendix IV.

## 7.5 KEILLOR ROAD SASW TEST SECTION, FLEXIBLE PAVEMENT

The description of Keillor Road Test Section was provided in Section 6.2. The first SASW test at this site was performed on April 14, 1993. The test lasted approximately two hours during the day.

Drilling was done at the same site on April 20, 1993 and samples were collected. It was found out that the ground was frozen from a depth of 0.61 m to a depth of 1.22 m. Twelve thermistors were installed into the borehole from a depth of 0.25 m below ground surface to a depth of 1.35 m. After the thermistors were installed, the hole was filled with sand to allow the thermistors to stabilize to the actual ground temperature conditions before any temperature measurements were taken. The hole was covered to stop infiltration of water or moisture into the hole that might affect the actual readings.

The first set of temperature readings were taken on April 22, 1993. Two more sets of temperature readings were taken on April 30, 1993 and May 14, 1993, respectively. The air temperature data for the City of Edmonton were obtained from the weather office and are presented in Table 7.1. The ground temperature measurements are presented in Table 7.2. The thermistor readings are plotted in Figure 7.29. It is seen that the frost zone extended from 0.7 m below ground surface to about 1.4 m depth based on April 22, 1993 data. The ground temperature subsequently increased with the advance of spring.

The second, third and fourth set of SASW tests were performed at the same location on April 22, April 29 and May 14, 1993 respectively. These tests were performed over this one month period to evaluate the ability of the newly developed SASW system to delineate the frost zone.

The stratigraphy at this site, shown adjoint to the shear wave velocity plots, is based on data obtained from drilling and soil sample examination. It was extremely difficult to obtain an intact sample from the black top layer. The black top could be explained as a cold mix on gravel base. The site is overlain with 0.20 m of black top (asphalt) which is underlain by 0.70 m of compacted clay with gravels overlying a stiff lacustrine clay deposit.

The SASW dispersion points for the April 14 test is shown in Figure 7.30. Also shown, is the average dispersion curve obtained by performing moving point average of the data points. Based on the above dispersion curve, the moving-point-averaged shear wave velocity profile using axes scaling is shown in Figure 7.31. Also shown in Figure 7.31, is the subsurface soil profile as obtained by drilling. The depth of the frozen zone was established based on the April 22 measurements. Figure 7.31 shows that the shear wave velocity in the black top is about 1800 m/s. The shear wave velocity increased at the level of the frozen layer to a value of about 1000 to 1200 m/s. Within the upper unfrozen clay layer with gravels, there is a transition of shear wave velocity from 1800 m/s below the black top to 600 m/s near the top of the frozen layer. Below the frozen layer, the shear wave velocity dropped to 400 m/s in the subgrade soil. Data from the averaged dispersion curve was used as an input to the forward modelling program SASW-FM. The comparison of the field phase velocity ( $C_{field}$ ) and the theoretical phase velocity ( $C_{calc}$ ) is shown in Figure 7.32. The field and theoretical phase velocities match reasonably well. The calculated shear wave velocity profile based on SASW-FM is shown in Figure 7.33. The comparison of shear wave velocity profile as obtained by performing a moving point average and axes scaling and from theoretical calculations (SASW-FM), are shown in Figure 7.34. As mentioned earlier, the shear wave velocity is about 1800 m/s to a depth of 0.20 m, which is the thickness of the black top. The shear wave velocity in the frozen layer section is about 1000 m/s and in the subgrade soil below the frozen layer is about 400 m/s. The shear wave velocity of the unfrozen clay below the black top is about 700 m/s.

The field dispersion points and the moving point averaged dispersion curve, the shear wave velocity profile, the comparison of the field dispersion curve (phase velocity versus wavelength) with the theoretical dispersion curve as obtained from SASW-FM, and the theoretical shear wave velocity profile as obtained from SASW-FM for the April 22 test, are presented in Appendix II. The comparison of the moving point averaged shear wave

velocity profile and the theoretical shear wave velocity profile for the April 22 test is shown in Figure 7.35. The shear wave velocity, as obtained from SASW-FM, is about 1800 m/s for the black top. The shear wave velocity dropped to 700 m/s in the unfrozen clay with gravels layer and then increased to 1000 m/s in the frozen layer. The shear wave velocity further dropped to 400 m/s in the subgrade soil layer. The frozen layer has been clearly identified in this profile.

The third set of SASW tests at this site were conducted on April 29, 1993. The field dispersion points and the moving point averaged dispersion curve, the shear wave velocity profile, comparison of the field dispersion curve (phase velocity versus wavelength) with the theoretical dispersion curve as obtained from SASW-FM, and the theoretical shear wave velocity profile as obtained from SASW-FM are presented in Appendix II. The comparison of the moving point averaged shear wave velocity profile and the theoretical shear wave velocity profile as obtained from SASW-FM is shown in Figure 7.36. The SASW-FM shows that the shear wave velocity is approximately 1200 m/s for the black top. Then the shear wave velocity decreased to about 700 m/s just above the frozen layer. There is a very slight increase in the shear wave velocity to about 1000 m/s in the frozen layer. The shear wave velocity of the subgrade soil is about 400 m/s.

The fourth and the final SASW testing program at this site was conducted on May 14, 1993. The frozen layer had thawed by this time. The field dispersion points and the moving point averaged dispersion curve, the shear wave velocity profile, the comparison of the field dispersion curve (phase velocity versus wavelength) with the theoretical dispersion curve as obtained from SASW-FM, and the theoretical shear wave velocity profile as obtained from SASW-FM, are presented in Appendix II. The comparison of the moving point averaged shear wave velocity profile and the theoretical shear wave velocity profile as obtained from SASW-FM is shown in Figure 7.37. As can be seen from SASW-FM

figure, the approximate shear wave velocity in the black top is about 1000 m/s. Then the shear wave velocity dropped to 700 m/s in the unfrozen clay layer with gravels and the shear wave velocity further dropping to about 400 m/s in the subsoil layer.

An overlay plot showing the shear wave velocity profiles for different test dates at this site is presented in Figure 7.38 for comparison purposes. The shear wave velocity of the black top clearly decreased as the air temperature increased, indicating that the black top became softer. The actual temperatures in the black top could not be directly measured, but it can be reasonably assumed that the The frozen layer was clearly identified on three occasions. The overlay plot shows the disappearance of frozen layer as the temperature increased. The exact temperatures of the black top during testing were not taken. But it can be reasonably assumed that the pavement temperature was greater than the air temperature due to absorption of heat on the black surface. The variation of pavement temperatures with time can be assumed to follow the same trend as the variation of air temperatures with time. The dispersion curve shows steady decrease in stiffness.

The modulus profiles for this test section are shown in Appendix IV. The calculation of frost penetration is shown in Appendix V.

A multimode analysis, using 'MULTIMOD" was performed on the dispersion curve obtained from April 22/1993 test date. This was done to study the influence of higher Rayleigh modes in Rayleigh wave dispersion curves for irregular soil profiles. The resulting output is shown in Figure 7.39. The figure indicates that the average dispersion curve obtained from axes scaling falls between the Mode 1 and Mode 2. Although Modes 2 and 3 did not develop for the whole range of wavelength, it seems Mode 2 had the highest medium response at the level of frozen layer followed by the dominance of fundamental mode in the half-space. The phenomenon of dominance of higher modes at any particular



level (here, the level of frozen layer) produces an inversely dispersive trend in that region. Further studies are required to understand and implement the role of higher modes on the analysis of complicated sites. The measurement and application of modal displacements in the analysis are one of the most effective ways to visualize the influence of higher Rayleigh modes.

The Mode 1 from the "MULTIMOD" output doesn't seem to match with the output of SASW-FM. SASW-FM is a computer program for calculating a theoretical dispersion curve that matches a given experimental dispersion curve. Initial guess as of shear-wave velocity and thickness for each layer, as well as the experimental dispersion points, are made as input parameters. The parameters of the model are adjusted until a set of best-fit parameters are found for which wavelengths and phase velocities match the experimental relationship to a predetermined accuracy. Therefore the issue of matching the experimental and theoretical dispersion curves based on best-fit layer parameters, controls the output of SASW-FM. On the other hand, "MULTIMOD" operates only on the layer parameters and no matching technique is necessary.

The shear wave velocity of the black top gradually decreased as the pavement temperature increased. Scattering of the data can further be minimized and interpreted successfully with further research as well as development of more sophisticated software, as discussed in the next section.

## 7.6 SUMMARY

The results obtained using the microcomputer program "SWAP" compare well with the available data for four test sites. However, there is some complication in the interpretation of results, for sites where the stiffness of the subsurface layers do not gradually decrease

with depth, such as at the Keillor Road site. Further improvements are needed in the experimental and analytical process to improve the quality of in-situ dispersion curve, with less scattering of the dispersion points. Signals of desired frequencies might not have been generated with the simple sources used in this study. The large stiffness contrast in the adjacent layers and the presence of thin layers might have some effect on the in-situ dispersion curve, a point which should be addressed in future research. Although body waves attenuate more rapidly with distance than surface waves, further research is needed to properly detect and eliminate the presence of body waves recorded by the receivers, particularly for small receiver spacings when profiling shallow layers. The Whitemud Drive site has an insulation layer underneath the soil cement, limiting the changes in soil conditions during winter months. The Keillor Road site had a frozen layer, which gradually thawed as the temperature increased. An interesting feature with the Keillor Road site is that, when the frozen layer ceased to exist, the scatter of measured SASW data was reduced.

The interesting features observed from this study have been;

- The "SWAP" software appears to have adequately captured the relevant surface wave data.
- Although there is considerable scatter in the data, the SASW technique appears to provide reasonably consistent stiffness profiles in a wide range of shallow pavement structures. It seems that SASW gives better results when there is sharp change in layer stiffnesses, compared to subsoil profiles where the stiffness changes gradually with depth.
- The simple moving point averaging technique combined with the simple empirical axes scaling technique appears to produce reasonable average stiffness profiles. Some of the stiffness profiles are shown in Appendix IV.

The forward modelling, using SASW-FM, appears to give better stiffness profiles and better layer definition than the simple empirical axes-scaling technique. Although the difficulties of uniqueness and operator sensitivity still exists with SASW-FM, it would be wise to use other more effective forward-modelling programs for defining layer boundaries and subsurface shear wave velocity profile.

Location: Edmonton Municipal Airport; Latitude: 53°34'N; Longitude: 113°31'W; Elevation: 671 metres (ASL)

Date	Temperature (°C)			Degree - Days			Relative Humidity		Precipitation (mm)			Snow on Ground (cm)	Bright Sunshine (Hours)
	Maximum	Minimum	Mean	Heating	Growing (Base 5°C)	Cooling (Base 5°C)	Maximum	Minimum	Rainfall	Snowfall	Total Precipitation		
April 9, 1993	4.8	-0.5	2.2	15.8			100	65	1.6	7.8	9.4	TR	0.0
April 14, 1993	12.5	-0.9	5.8	12.2	0.8		93	38					12.4
April 22, 1993	18.6	7.0	12.8	5.2	7.8		57	26	TR		TR		6.0
April 29, 1993	16.5	5.0	10.8	7.2	5.8		81	36	0.2		0.2		5.6
May 14, 1993	18.2	7.9	13.1	4.9	8.1		58	23					14.6

Table 7.1 Meteorological Summary of Test Dates on Flexible Pavements

Source:  
 "Monthly Meteorological Summary", obtained from:  
 Climatology Services Unit  
 Atmospheric Science and Issues Branch  
 2nd Floor, Twin Atria Bldg.  
 4998 - 98 Avenue  
 Edmonton, Alberta  
 CANADA T6B 2X3  
 Tel. (403) 468-7957; Fax. (403) 495-3529

No.	Thermistor Identification No.	Depth below ground surface (cm)	Ground Temperature (°C)		
			April 22, 1993	April 30, 1993	May 14, 1993
1	C5	25.3	7.32	10.13	17.32
2	C4	35.3	6.83	8.10	17.04
3	C3	45.3	5.79	7.35	16.73
4	C2	55.3	3.87	6.13	15.35
5	C1	65.3	1.43	4.31	13.09
6	A7	75.3	- 0.05	2.86	11.22
7	A6	85.3	- 0.44	1.32	9.14
8	A5	95.3	- 0.96	- 0.23	17.43
9	A4	105.3	- 0.88	- 0.44	5.19
10	A3	115.3	- 1.09	- 0.73	3.25
11	A2	125.3	- 0.78	- 0.55	1.69
12	A1	135.3	- 0.47	- 0.31	0.62

Table 7.2 Ground Temperature Measurements at Keilior Road Site

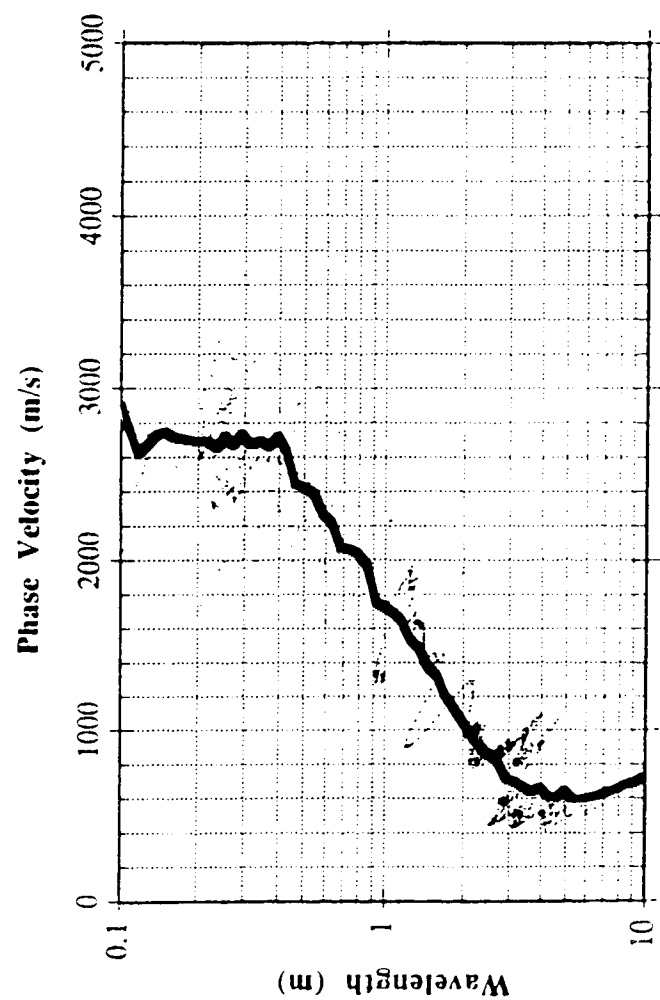


Figure 7.1 Dispersion Curve from Room CEB-B11 Basement Slab, November 1992

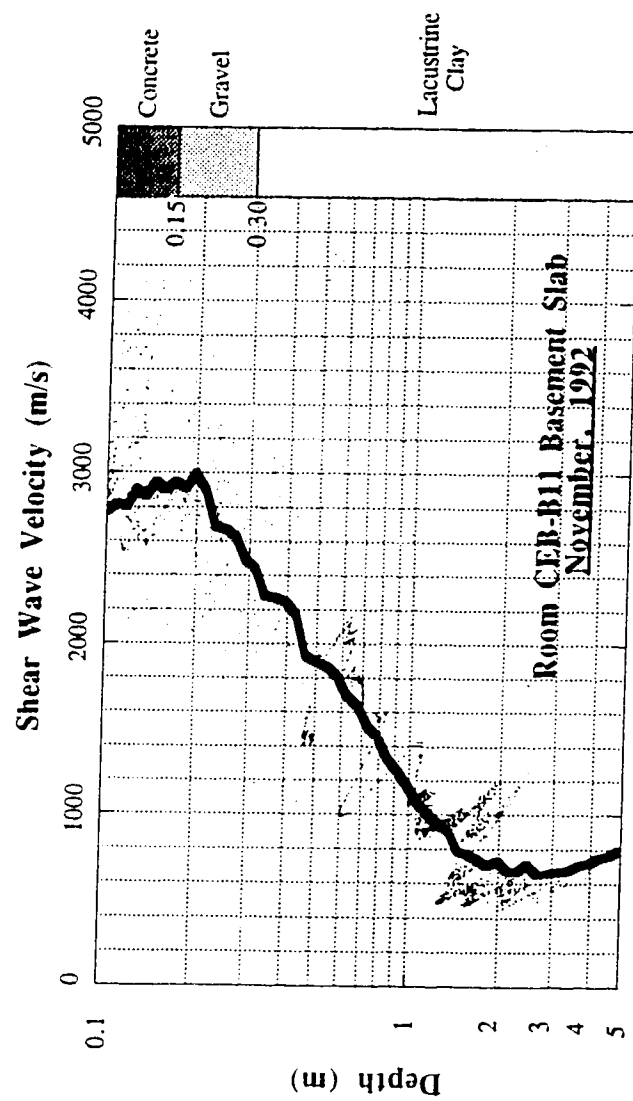


Figure 7.2 Shear wave velocity profile from Room CEB-B11 Basement Slab, November 1992

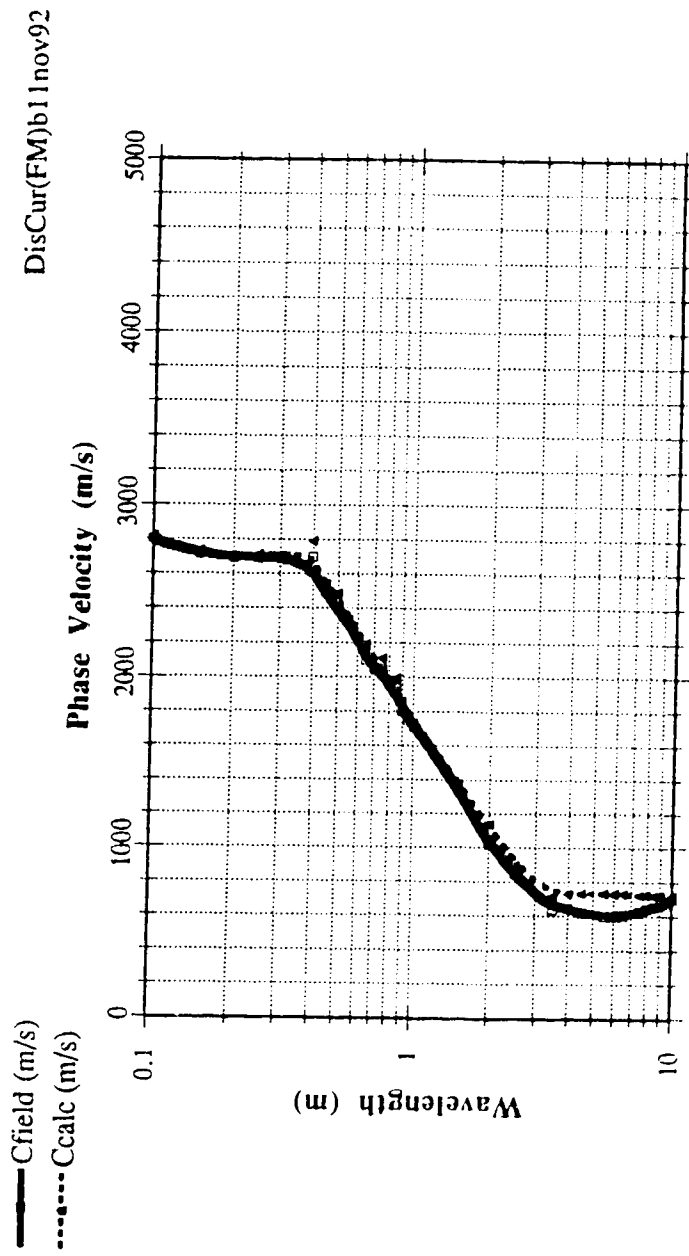


Figure 7.3 Dispersion curves (SASW-FM) from Room B-11 Basement Slab, November 1992



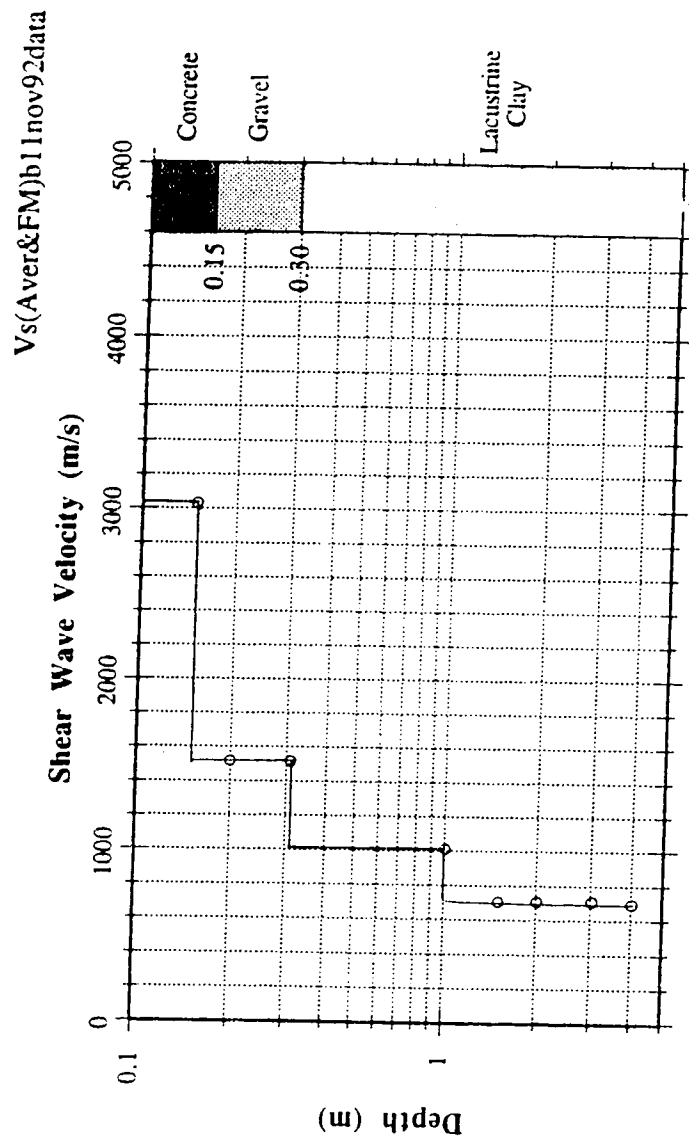


Figure 7.4 Shear Wave Velocity Profile (SASW-FM output), Room CEB-B11, November 1992

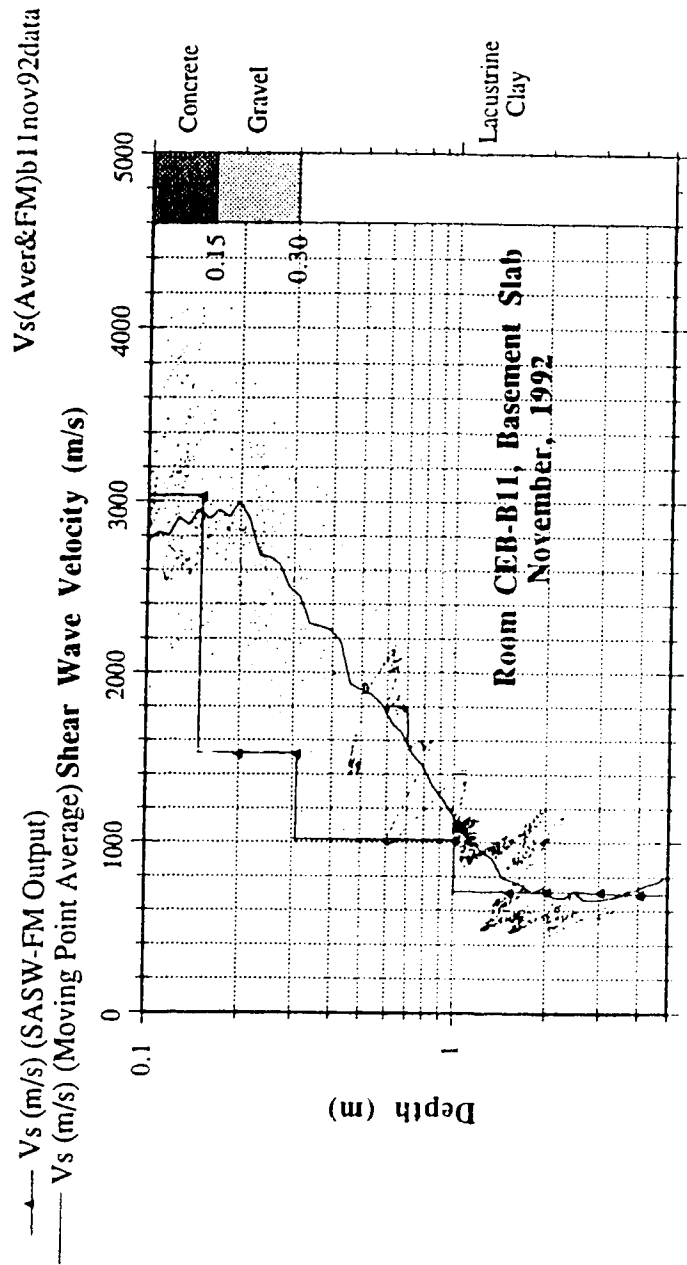


Figure 7.5 Comparison of Shear Wave Velocity Profile (Moving Point Average & SASW-FM)  
 Room CEB-B11, Basement Slab, November 1992

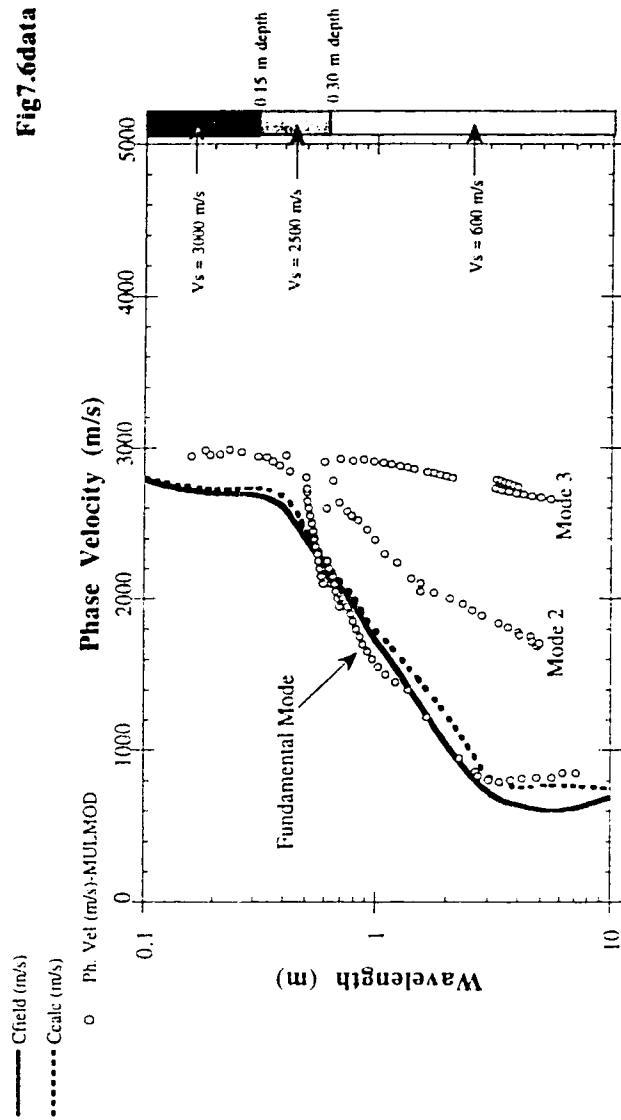


Figure 7.6 Comparison of Ccalc, Cfield and MULTIMOD output, Room CEB-B11, Basement Slab, November 1992

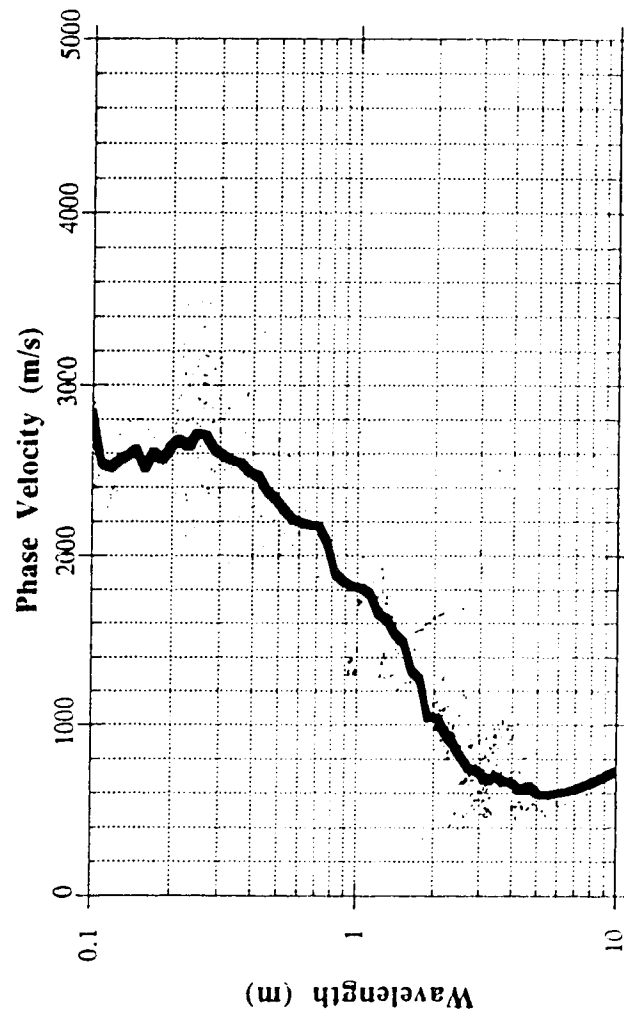


Figure 7.7 Dispersion Curve from Room CEB-B11 Basement Slab, May 1993

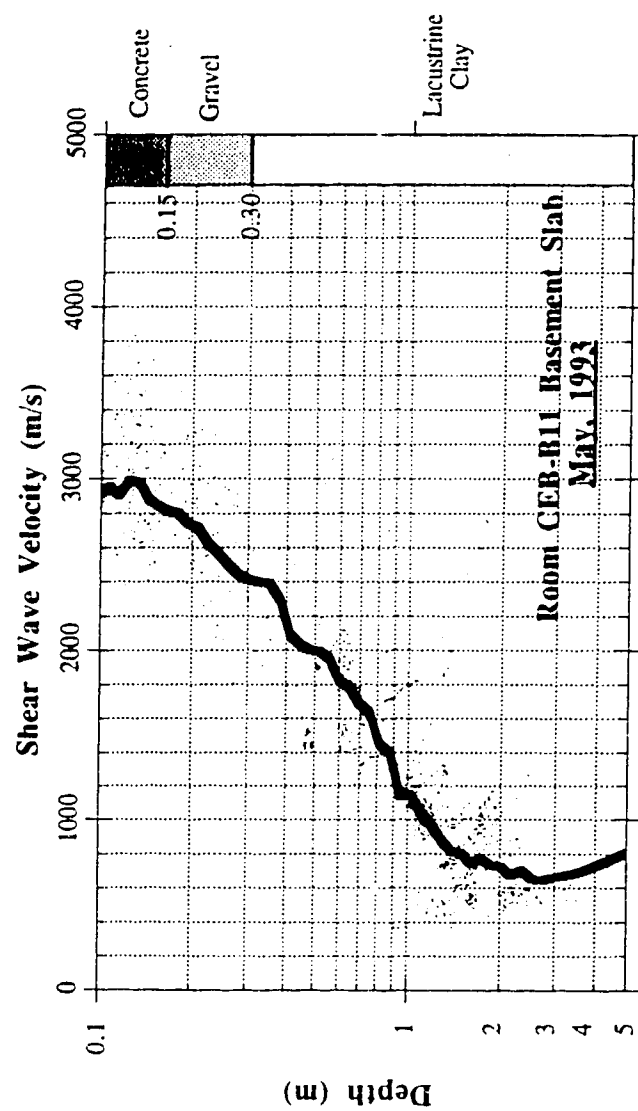


Figure 7.8 Shear wave velocity profile from Room CEB-B11 Basement Slab, May 1993

DisCur(FM)b11may93

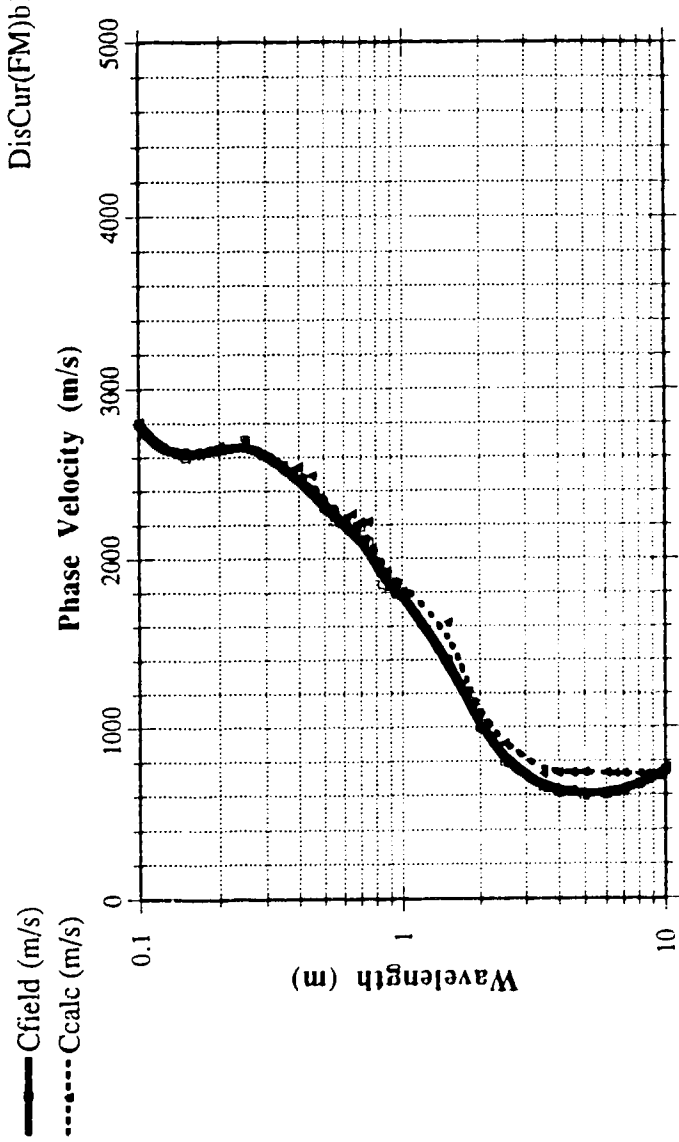


Figure 7.9 Dispersion curves (SASW-FM) from Room B-11 Basement Slab, May 1993

Vs(Aver&FM)b11may93data

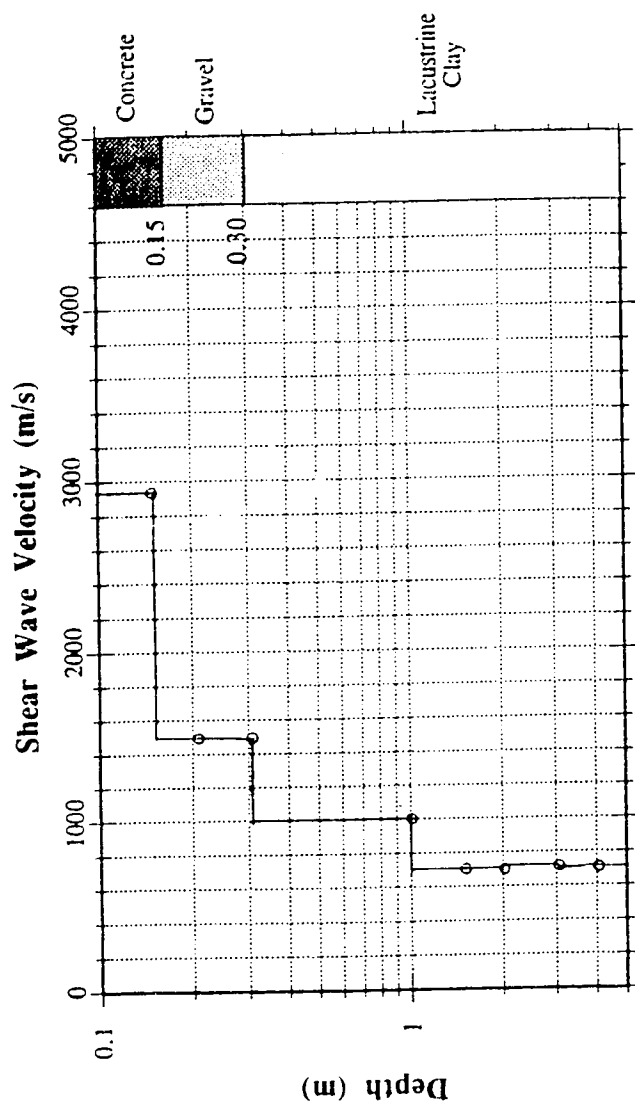


Figure 7.10 Shear Wave Velocity Profile (SASW-FM output), Room CEB-B11, May 1993

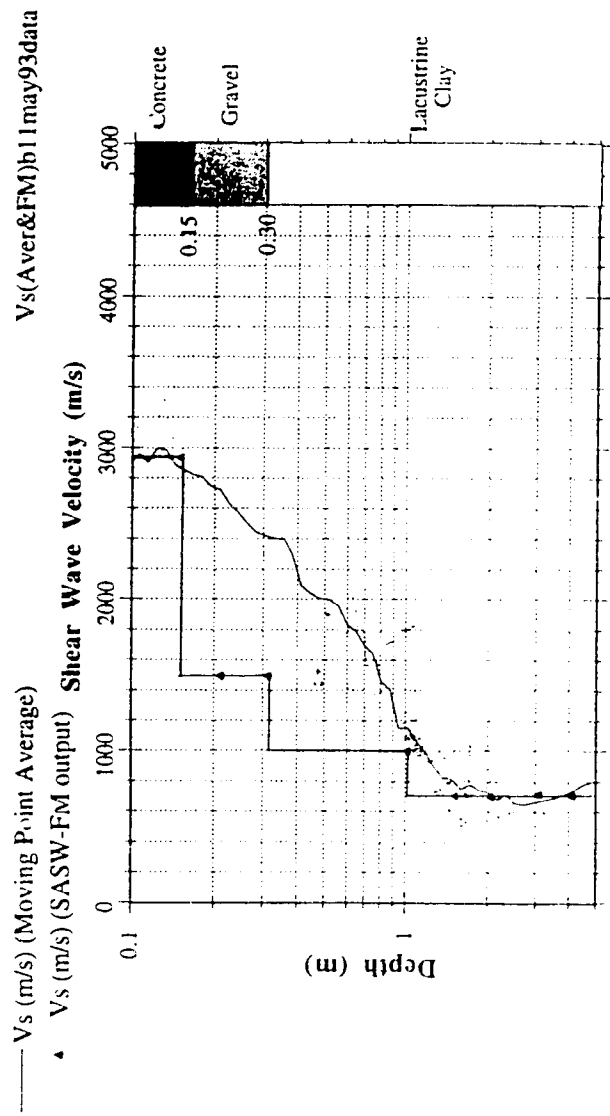


Figure 7.11a Comparison of Shear Wave Velocity Profile (moving Point Average & SASW-FM)  
Room CEB-B11, Basement Slab, May 1993



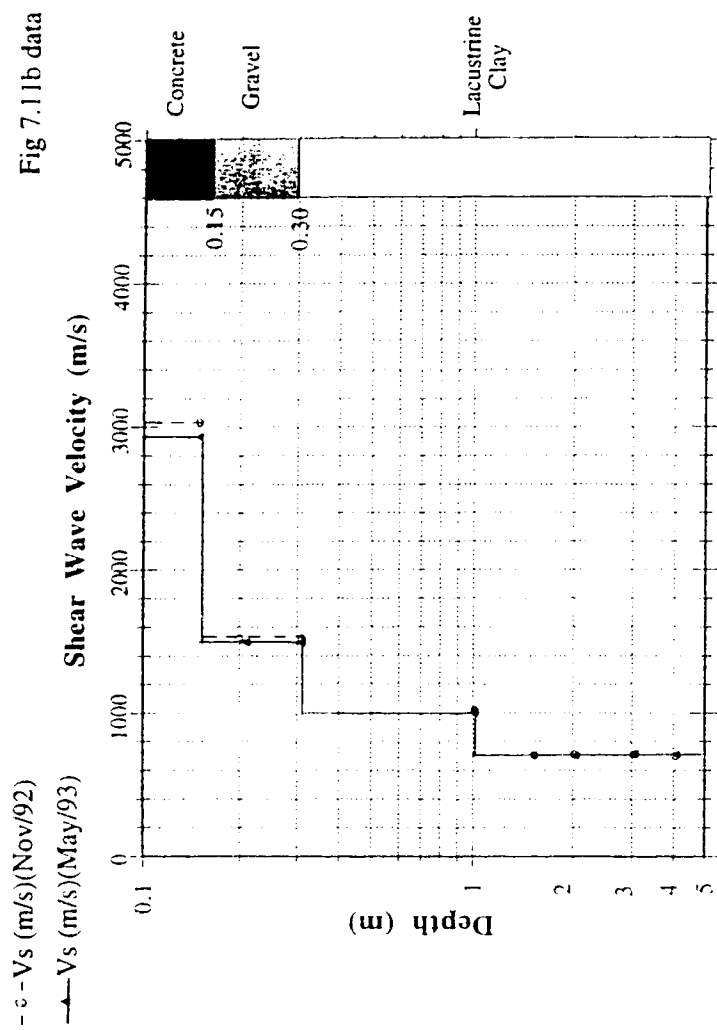


Figure 7.11b Comparison of Shear Wave Velocity Profile from Room CEB-B11

Fig7.12data

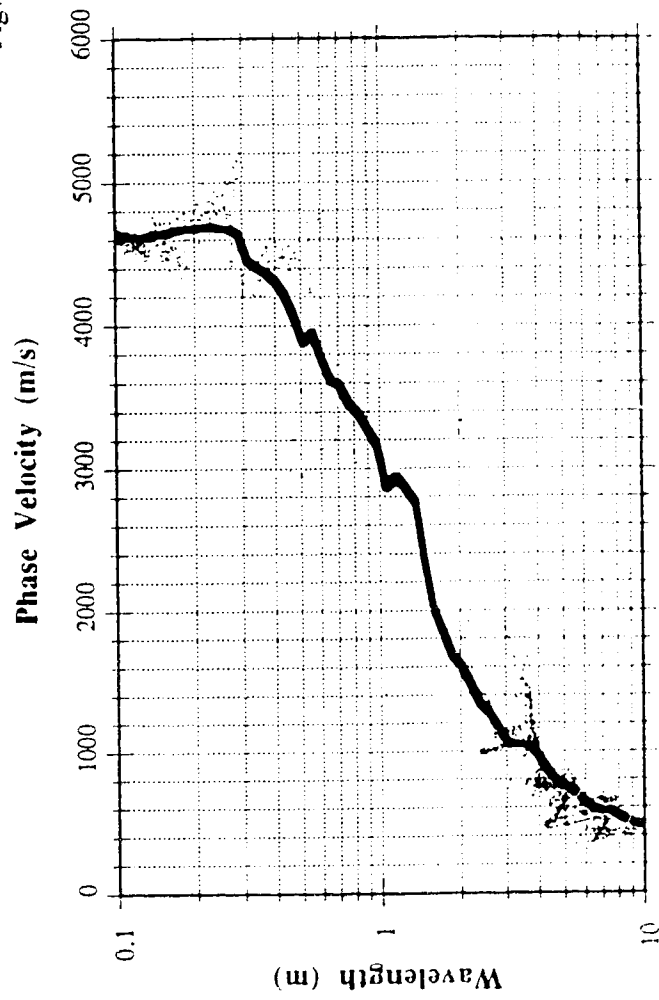


Figure 7.12 Dispersion curve of Pavement Section CC

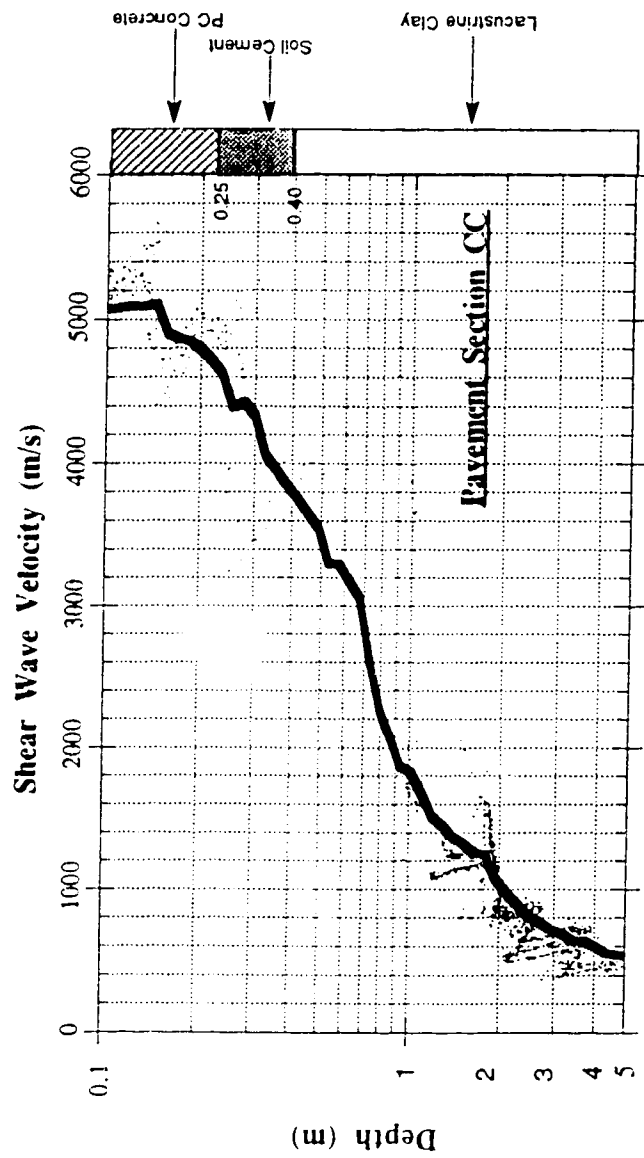


Figure 7.13 Shear wave velocity profile of Pavement Section CC

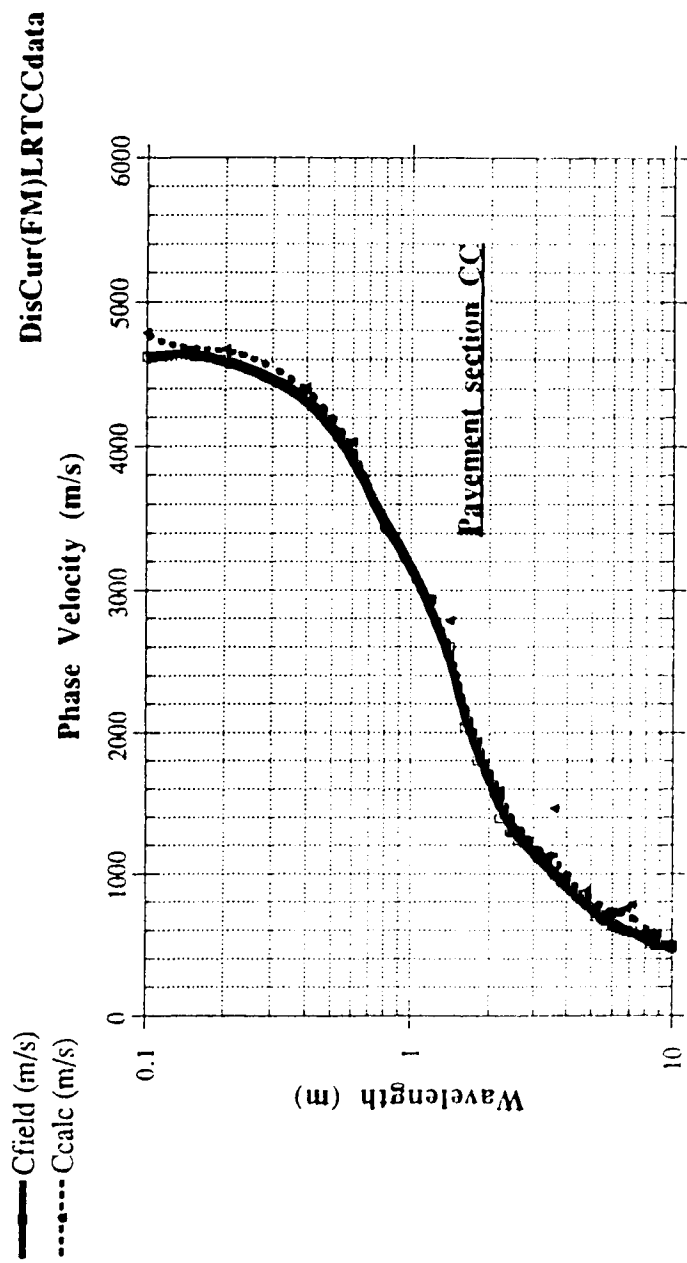


Figure 7.14 Dispersion curves (SASW-FM) from Pavement Section CC

Fig7.13&7.15&7.16

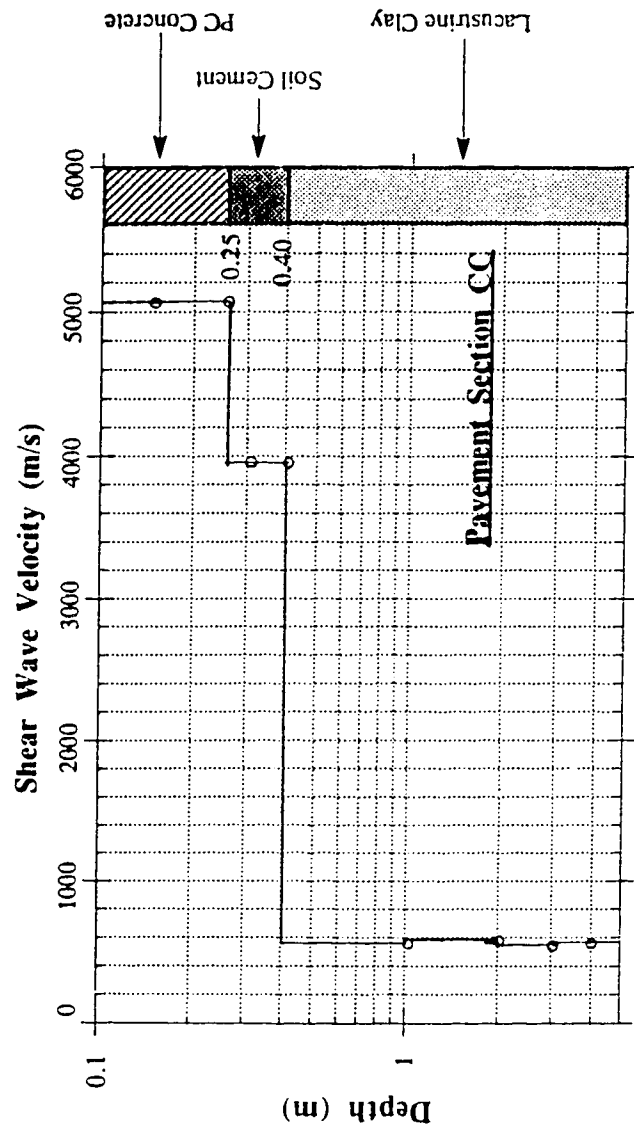


Figure 7.15 Shear wave Velocity Profile (SASW-FM), Pavement Section CC

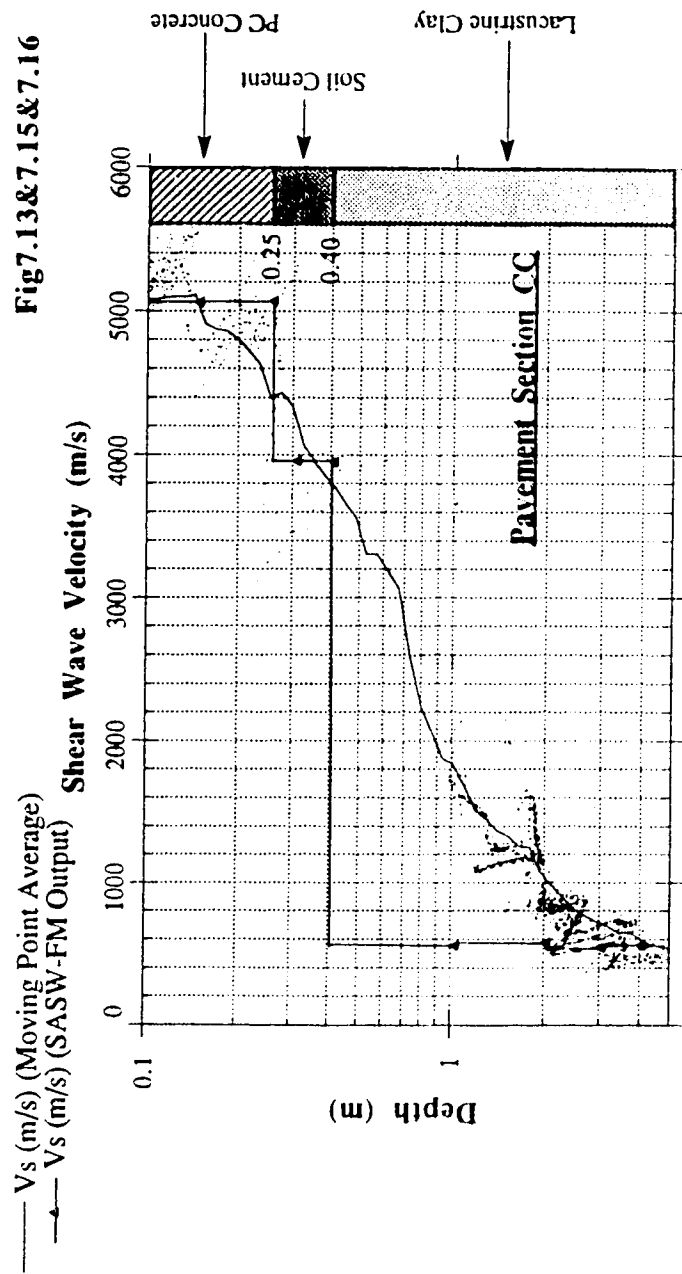


Figure 7.16 Comparison of Shear Wave Velocity Profile (Moving Point Average & SASW-FM)  
 Pavement Section CC

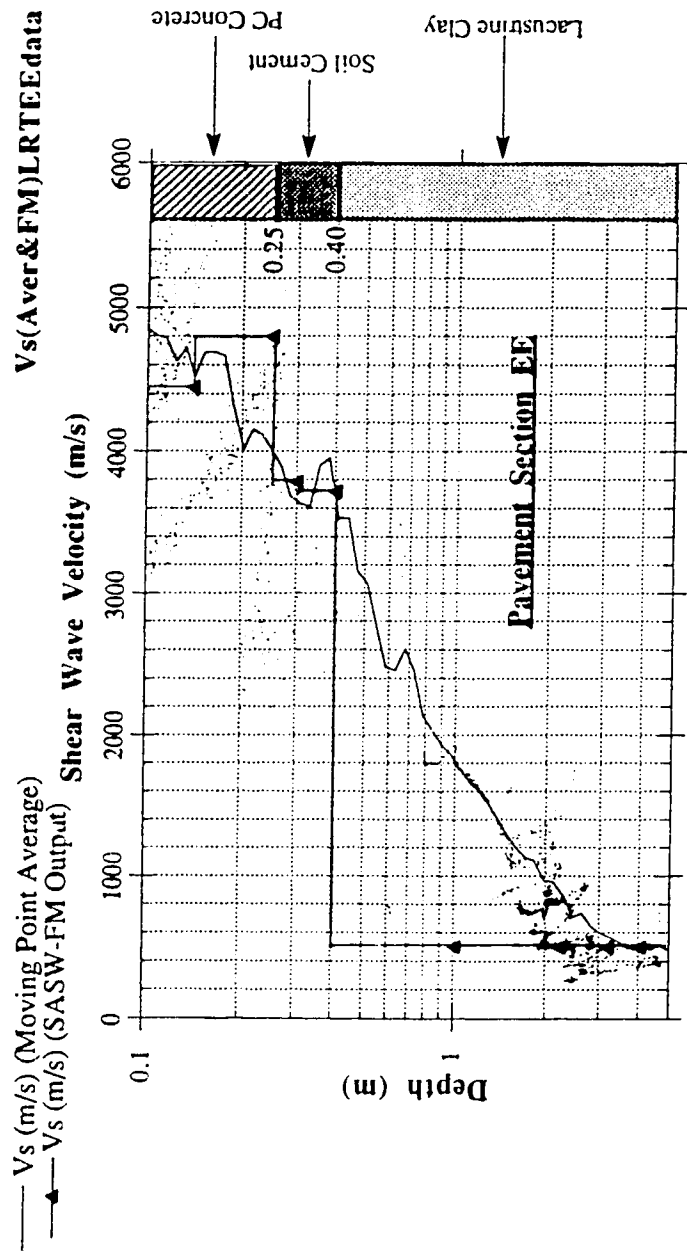


Figure 7.17 Comparison of Shear Wave Velocity profile (Moving Point Average & SASW-FM)  
Pavement Section EE

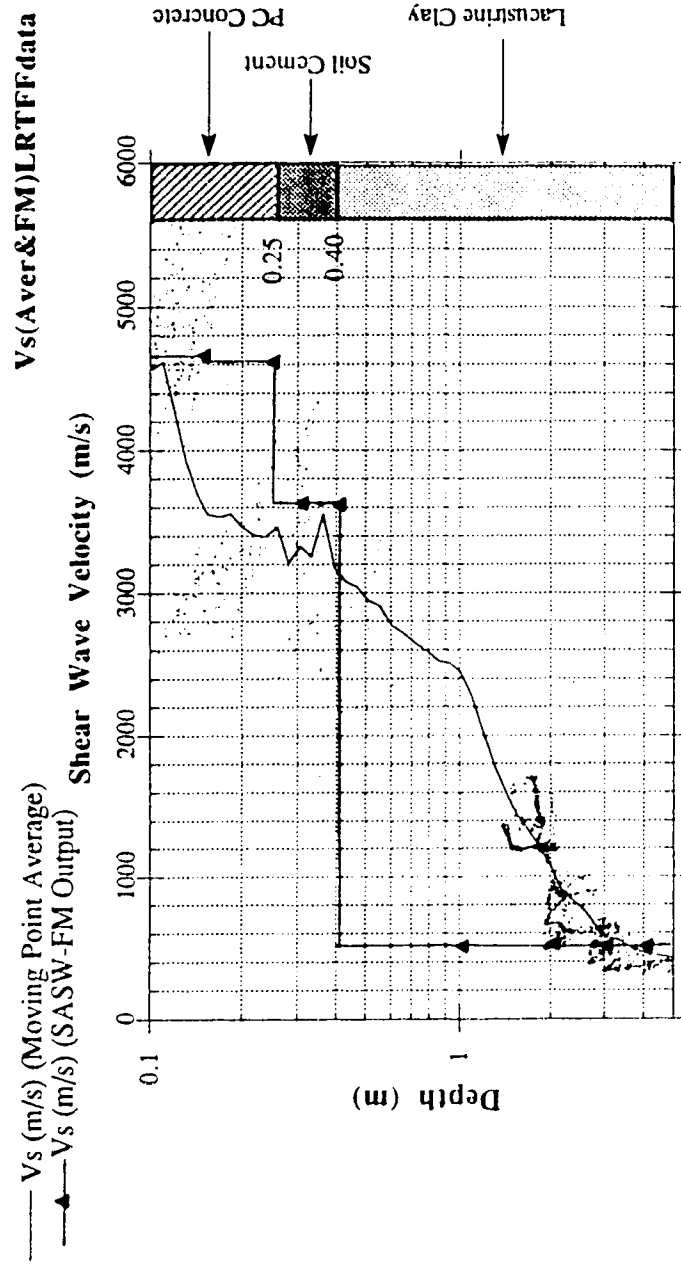


Figure 7.18 Comparison of Shear Wave Velocity Profile (Moving Point Average & SASW-FM) Pavement Section FF



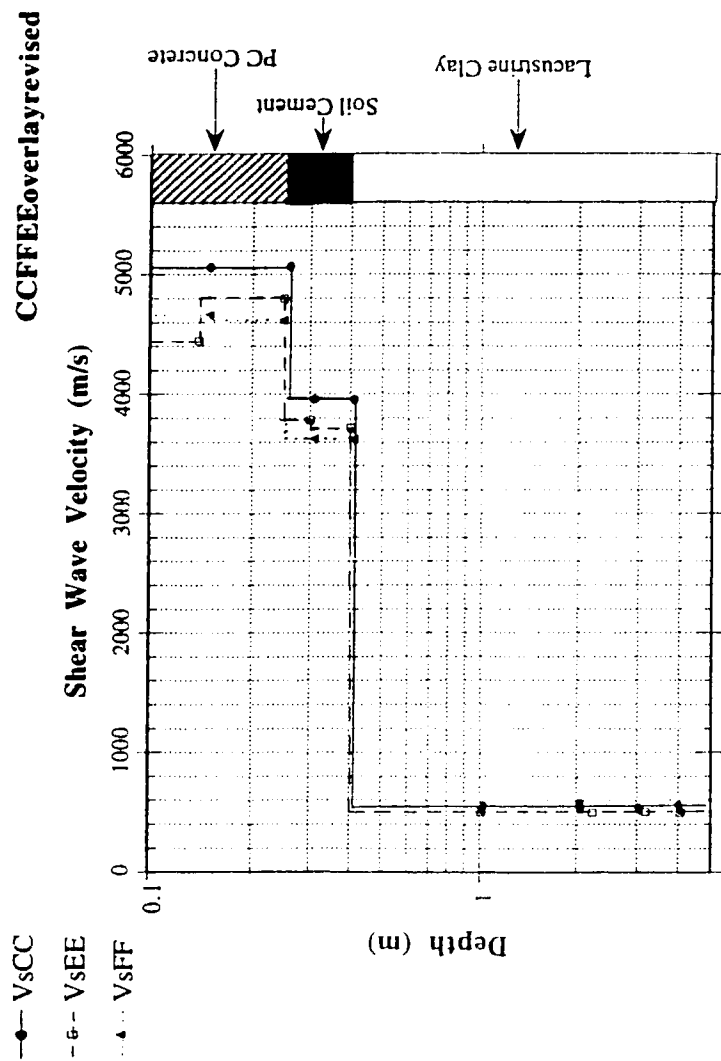


Figure 7.19 Overlay plot of average shear wave velocity profile from Pavement Sections CC, EE & FF

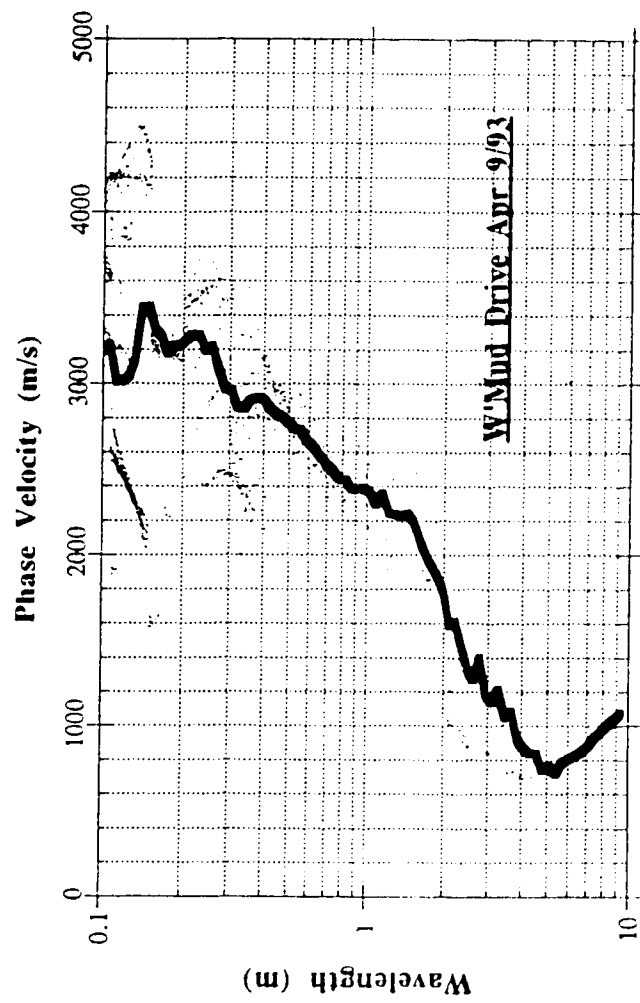


Figure 7.20 Dispersion Curve from Whitmud Drive, April 9, 1993

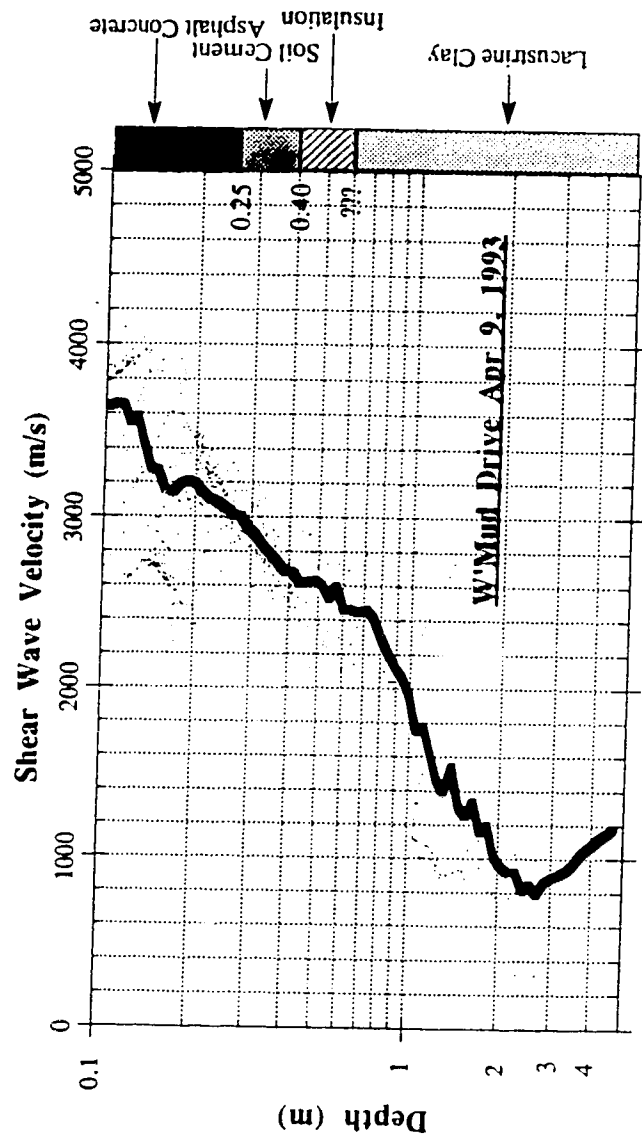


Figure 7.21 Shear wave velocity profile from Whitemud Drive, April 9, 1993

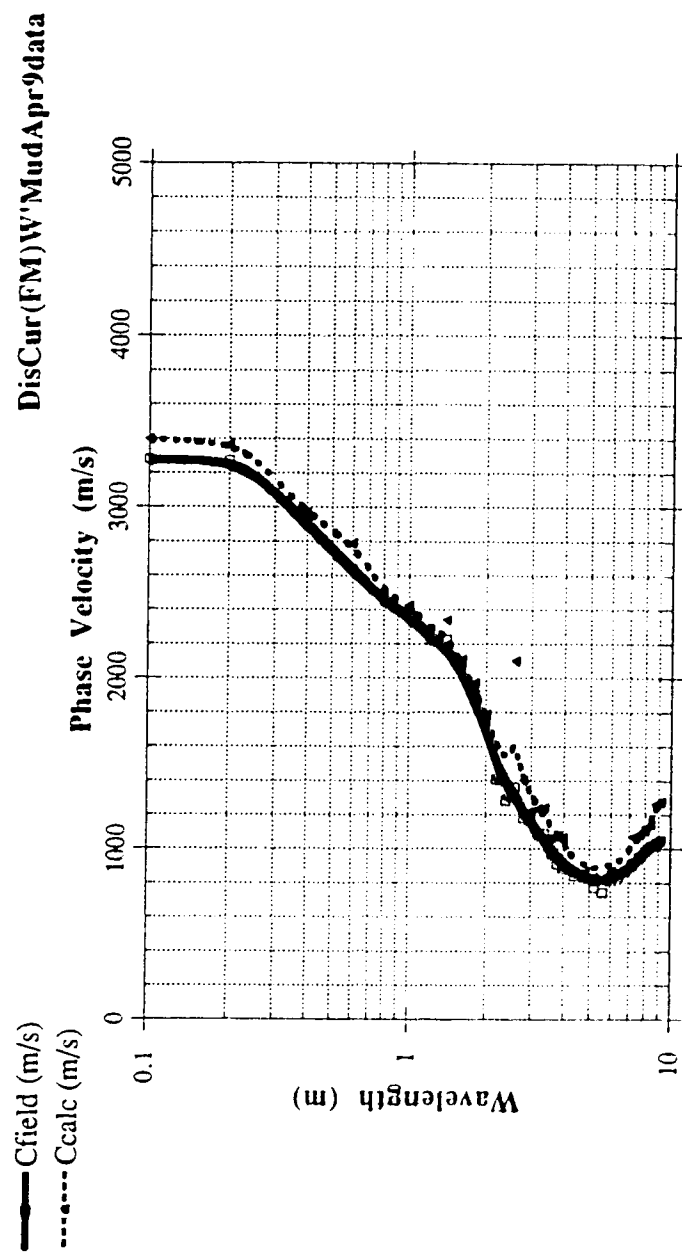


Figure 7.22 Dispersin curves (SASW-FM) from W'Mud Drive, April 9, 1993

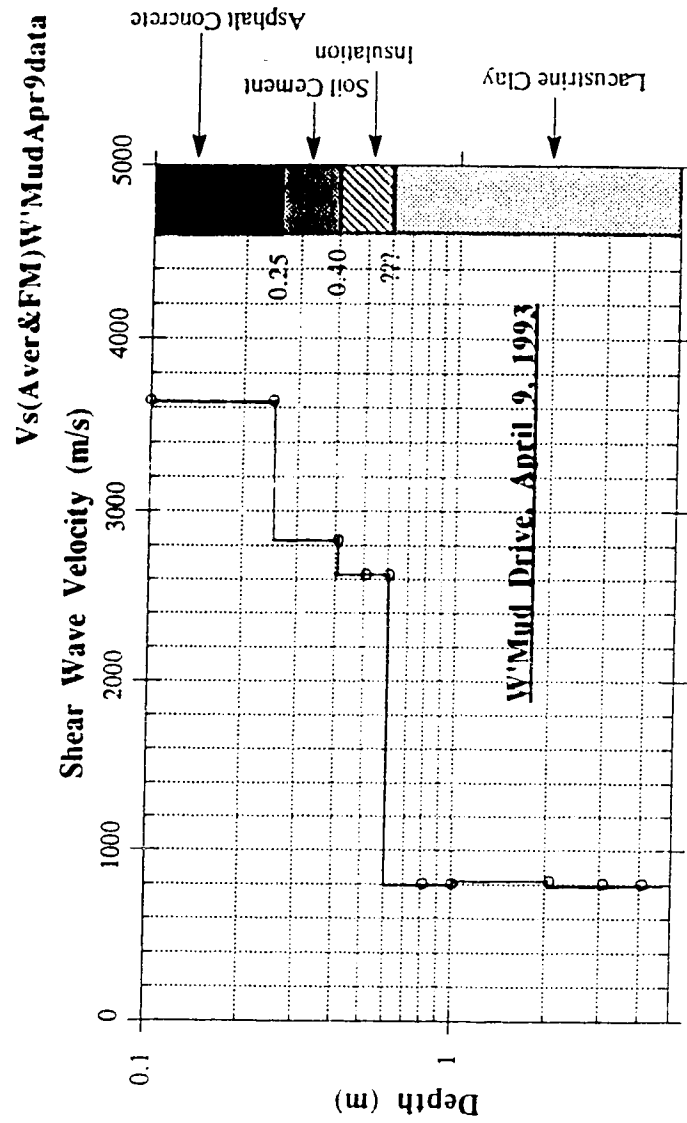


Figure 7.23 Shear Wave Velocity Profile (SASW-FM) output, Whitemud Drive, April 9, 1993.

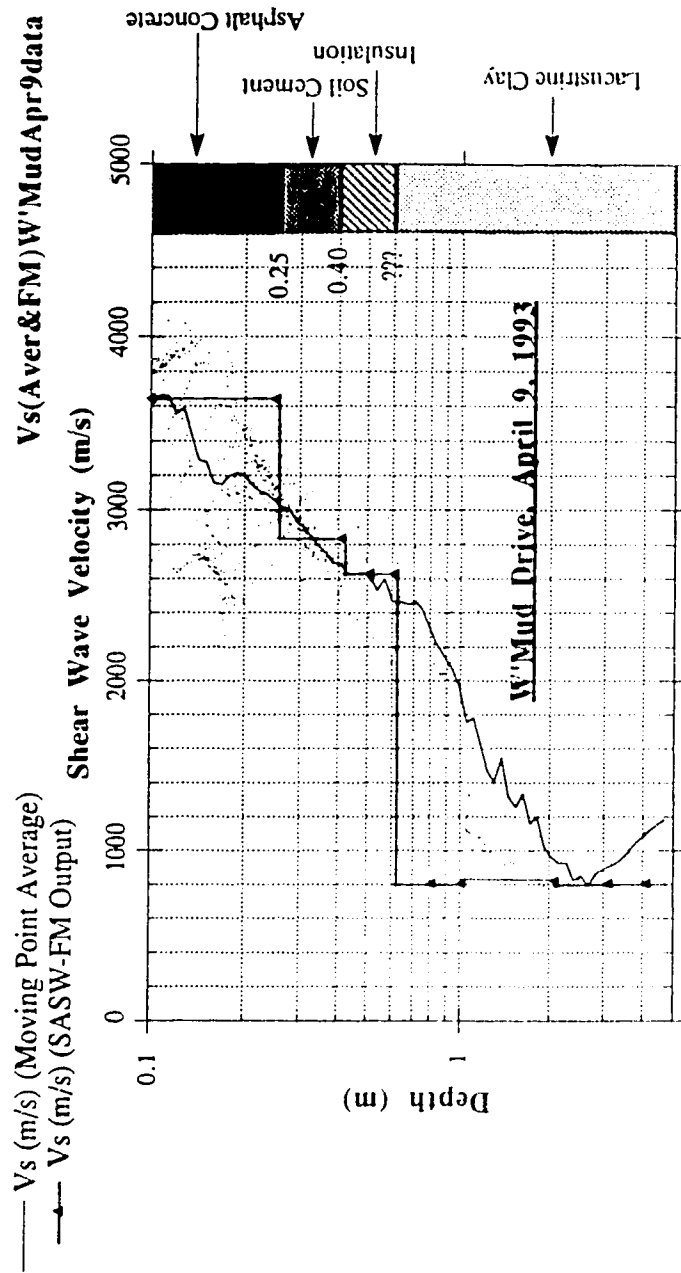


Figure 7.24 Comparison of Shear Wave Velocity Profile (Moving Point Average & SASW-FM) Whittemud Drive, April 9, 1993

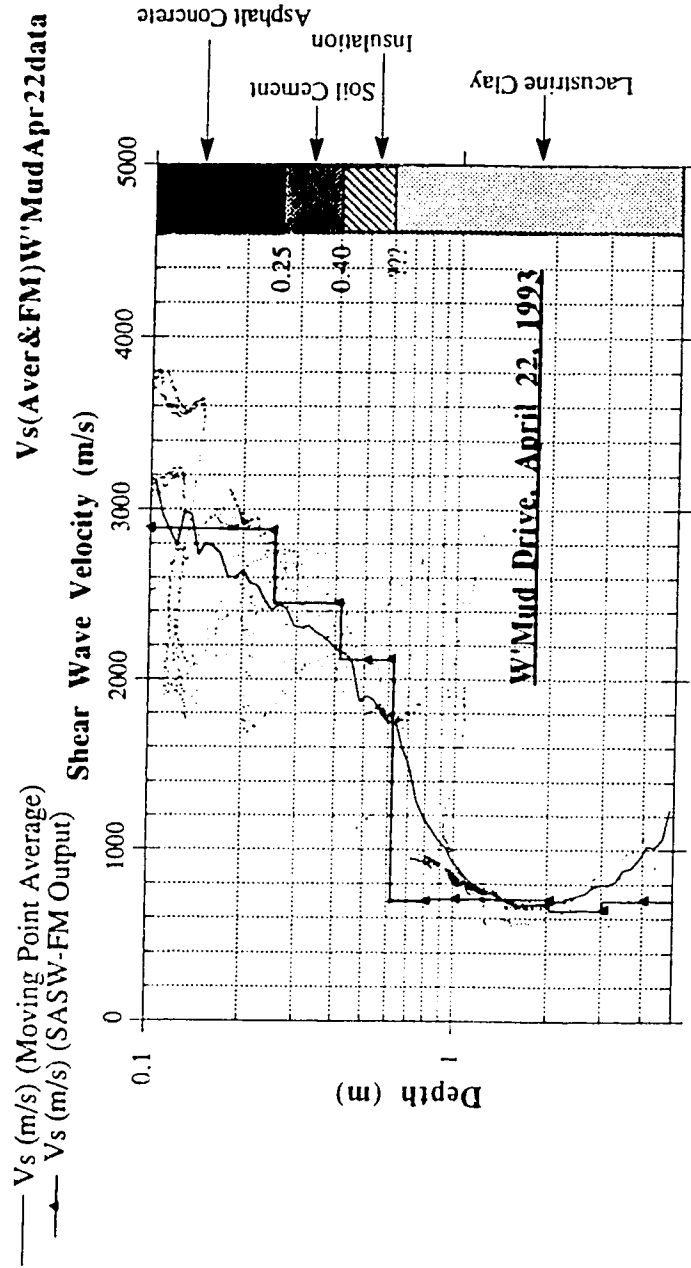


Figure 7.25 Comparison of Shear Wave Velocity Profile (Moving Point Average & SASW-FM) Whitemud Drive, April 22, 1993

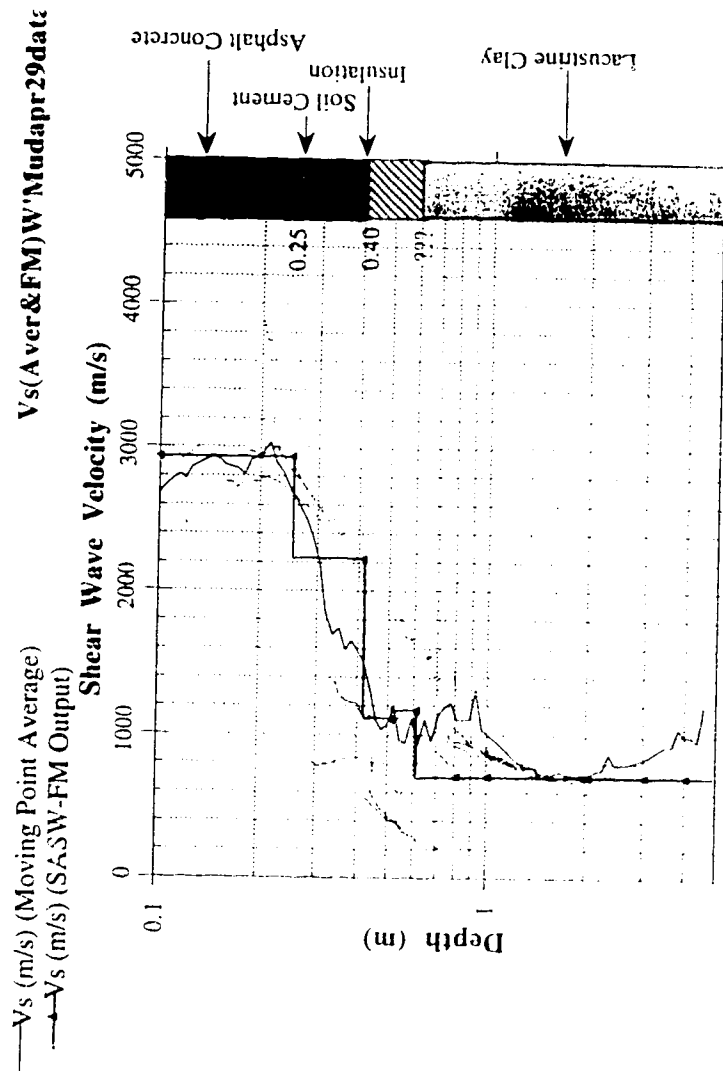


Figure 7.26 Comparison of Shear Wave Velocity Profile (Moving Point Average & SASW-FM)  
Whitemud Drive, April 29, 1993



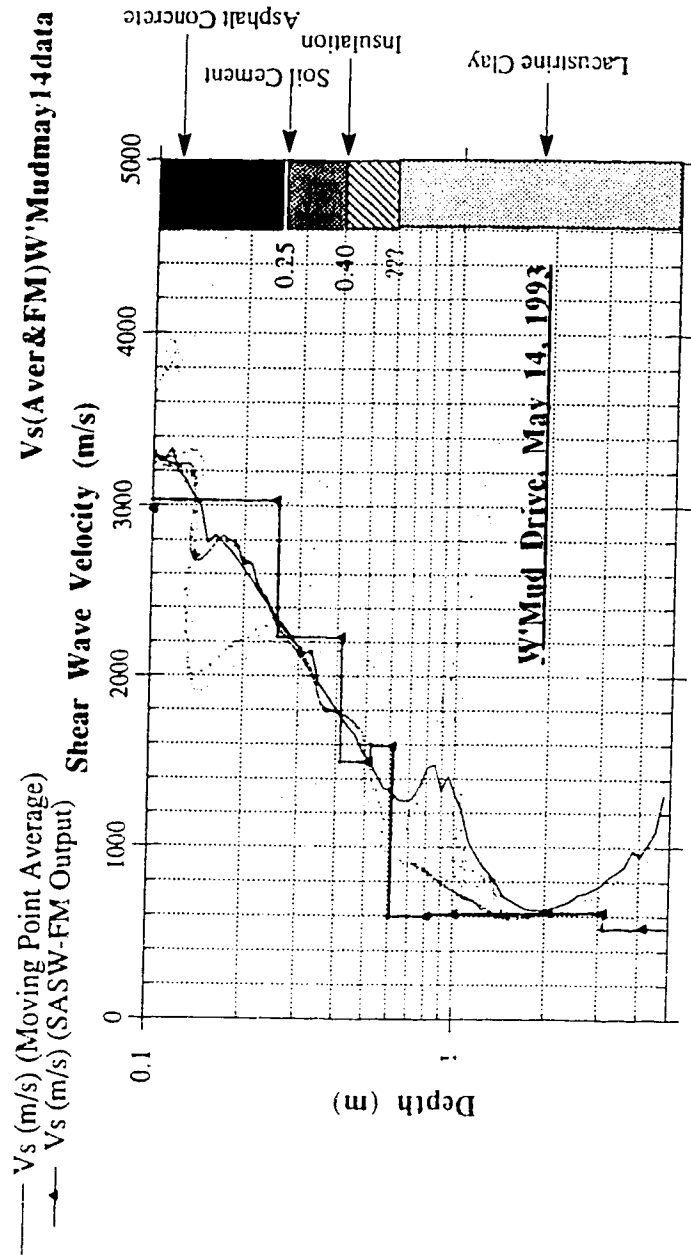


Figure 7.27 Comparison of Shear Wave Velocity Profile (Moving Point Average & SASW-FM),  
Whitemud Drive, May 14, 1993

# W'MudOverlayreviseddata

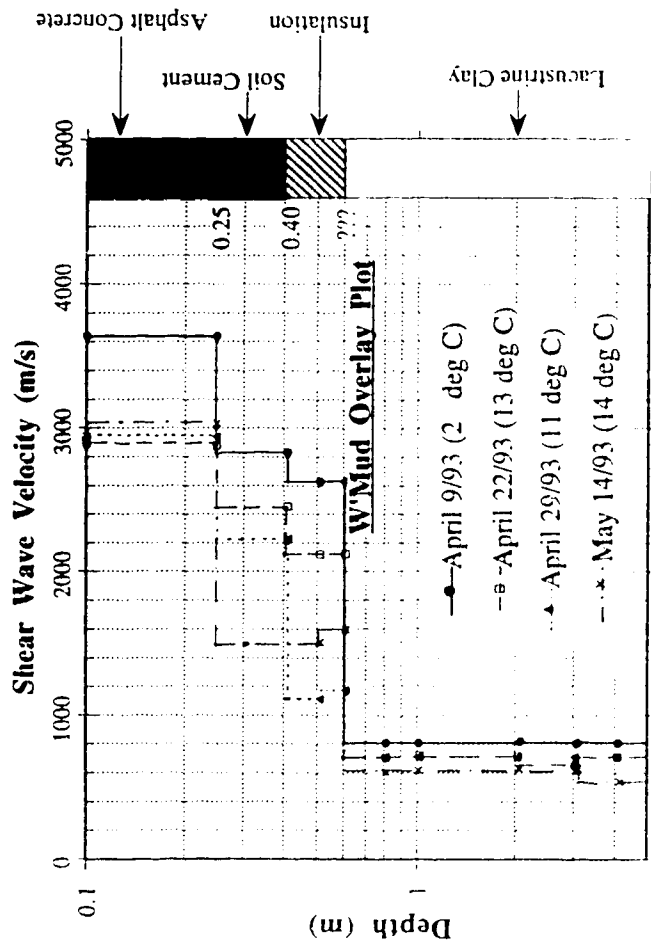


Figure 7.28 Overlay Plot of average shear wave velocity profile at Whitemud drive, all test dates

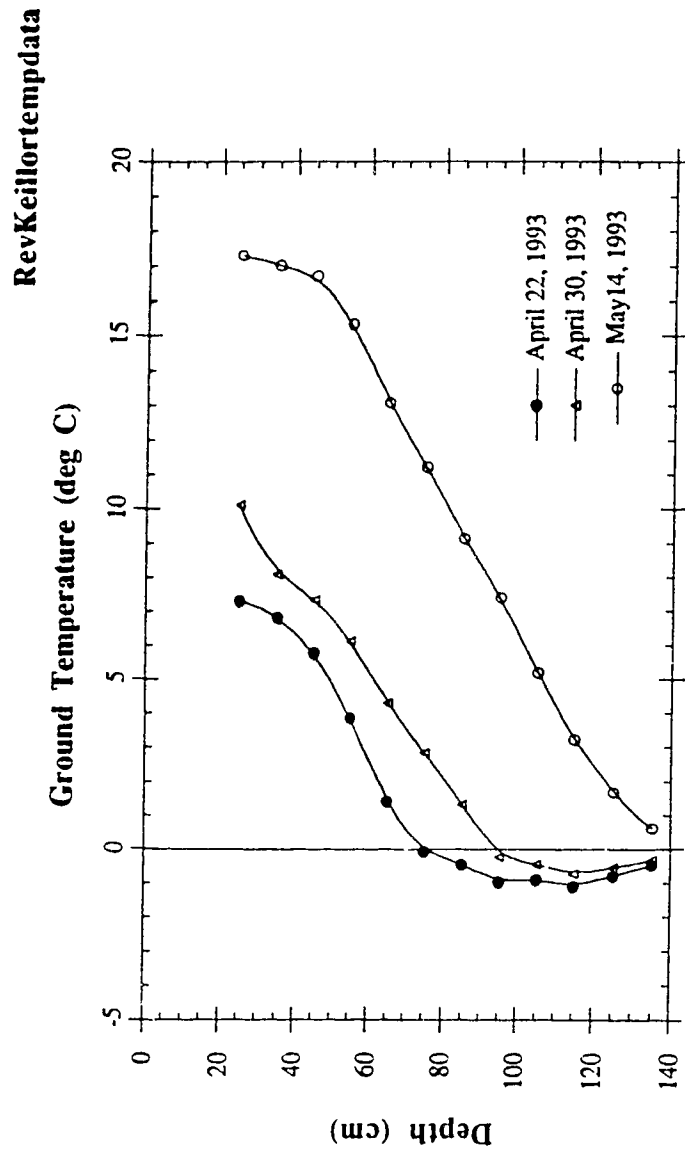


Figure 7.29 Ground temperature profile, Keillor Road

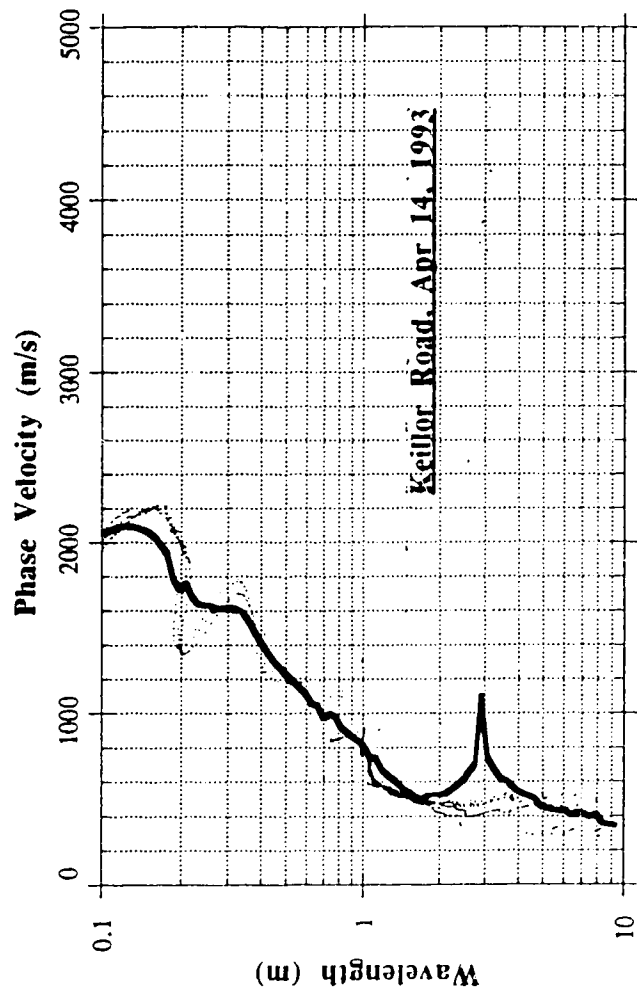


Figure 7.30 Dispersion curve from Keillor Road, April 14, 1993

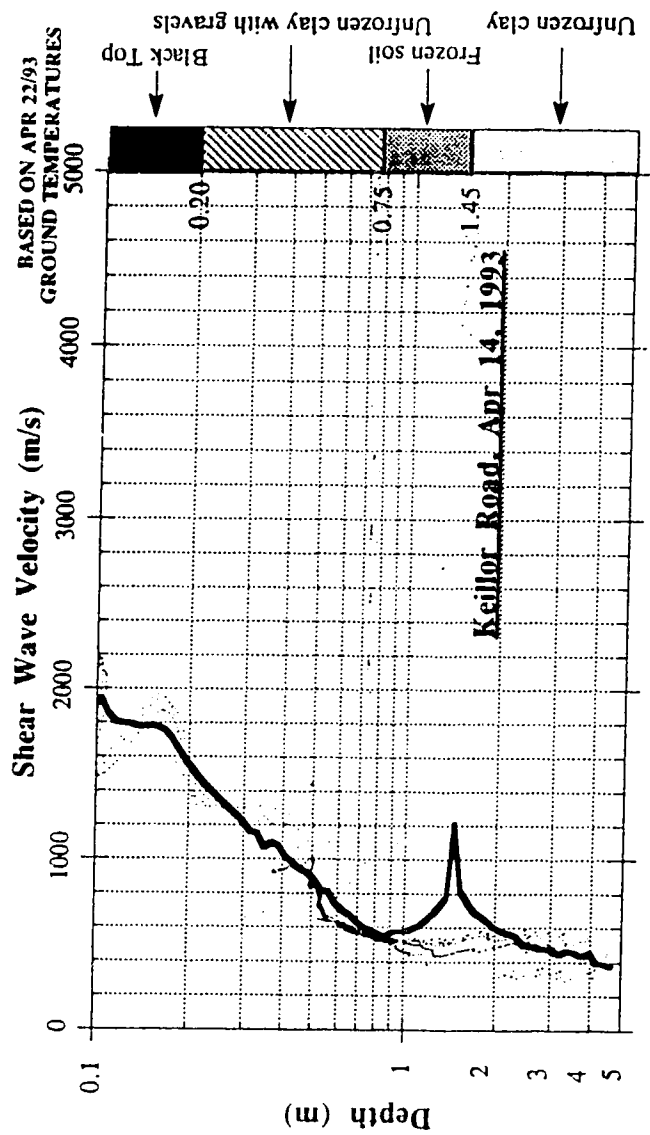


Figure 7.31 Shear wave velocity profile from Keillor Road, April 14, 1993

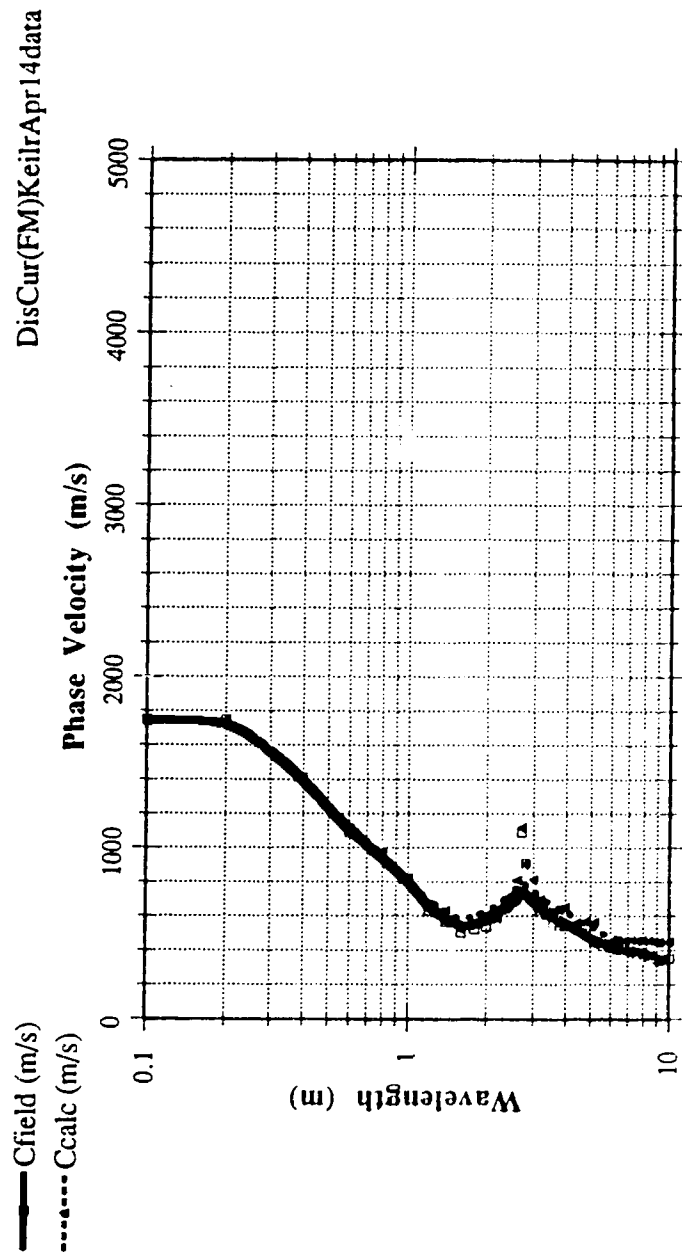


Figure 7.32 Dispersion curves (SASW-FM) from Keillor Road, April 14, 1993

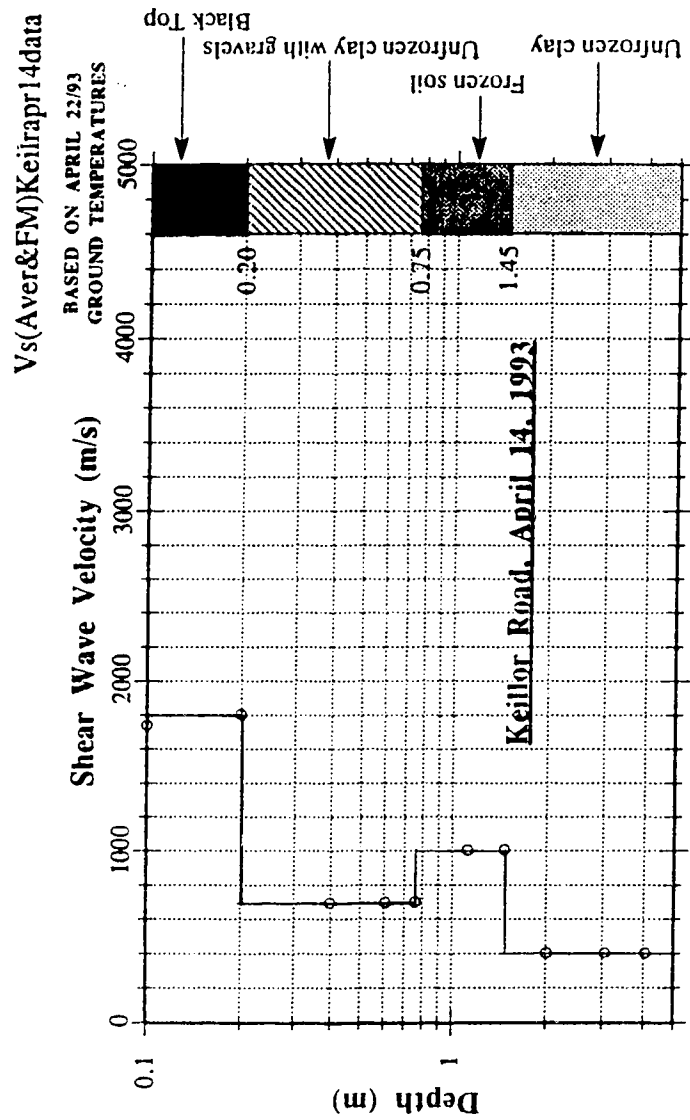


Figure 7.33 Shear Wave Velocity Profile (SASW-FM) from Keillor Road, April 14, 1993

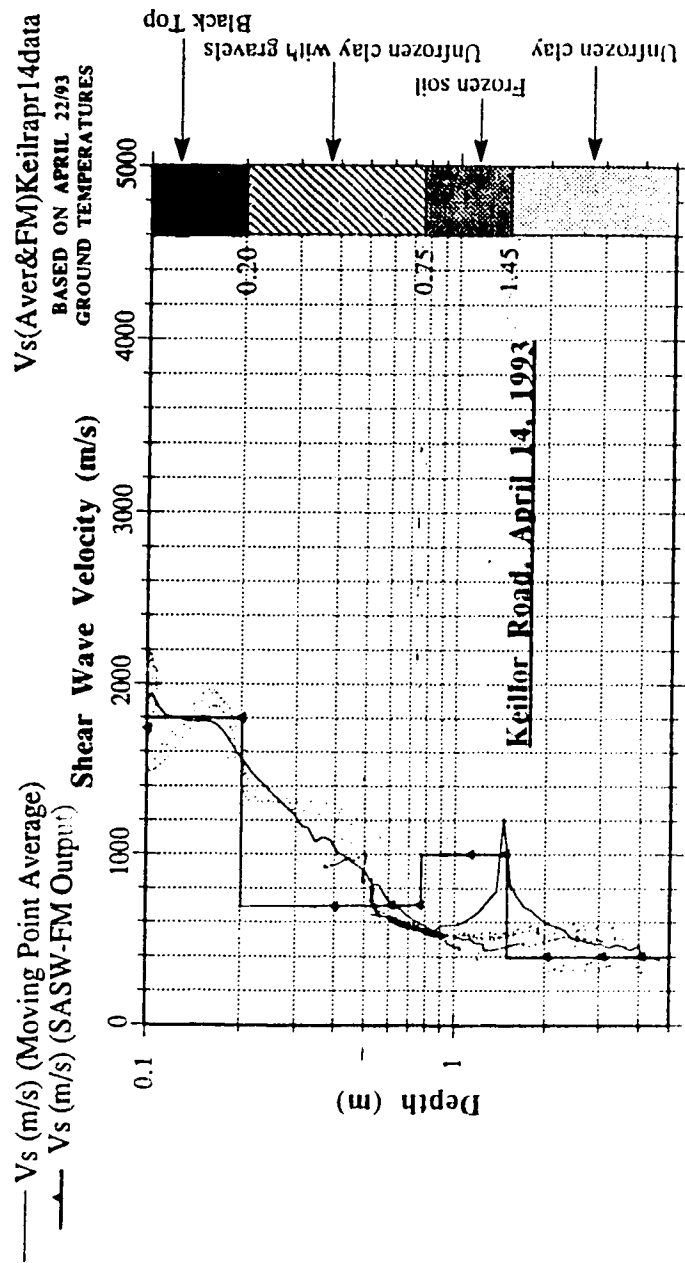


Figure 7.34 Comparison of Shear Wave Velocity Profile (Moving Point Average & SASW-FM), Keillor Road, April 14, 1993



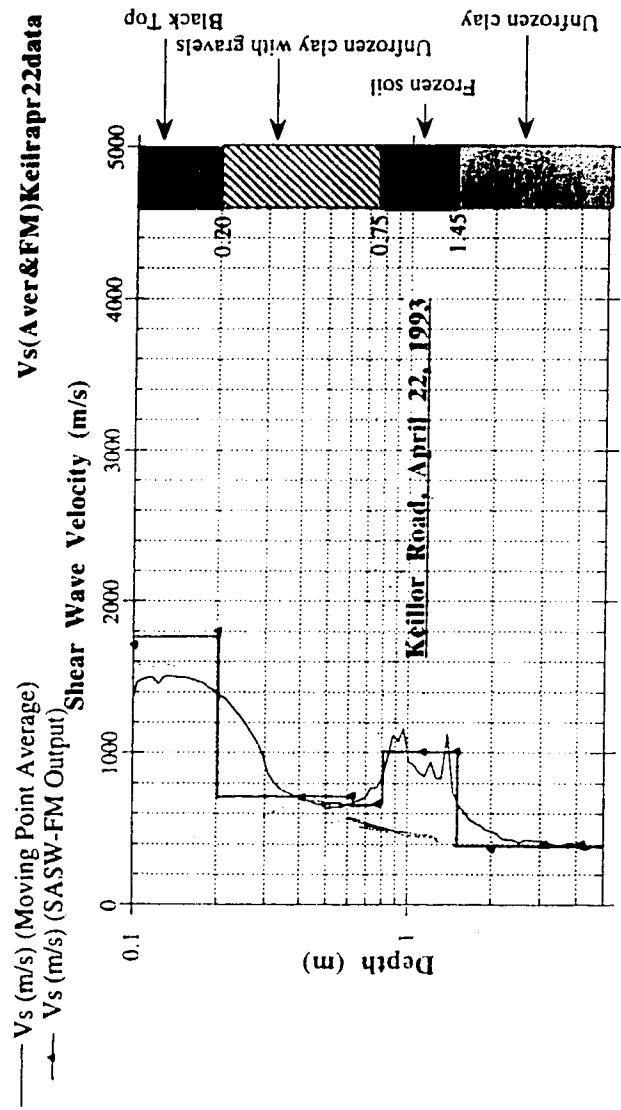


Figure 7.35 Comparison of Shear wave Velocity Profile (Moving Point Average & SASW-FM), Keillor Road, April 22, 1993

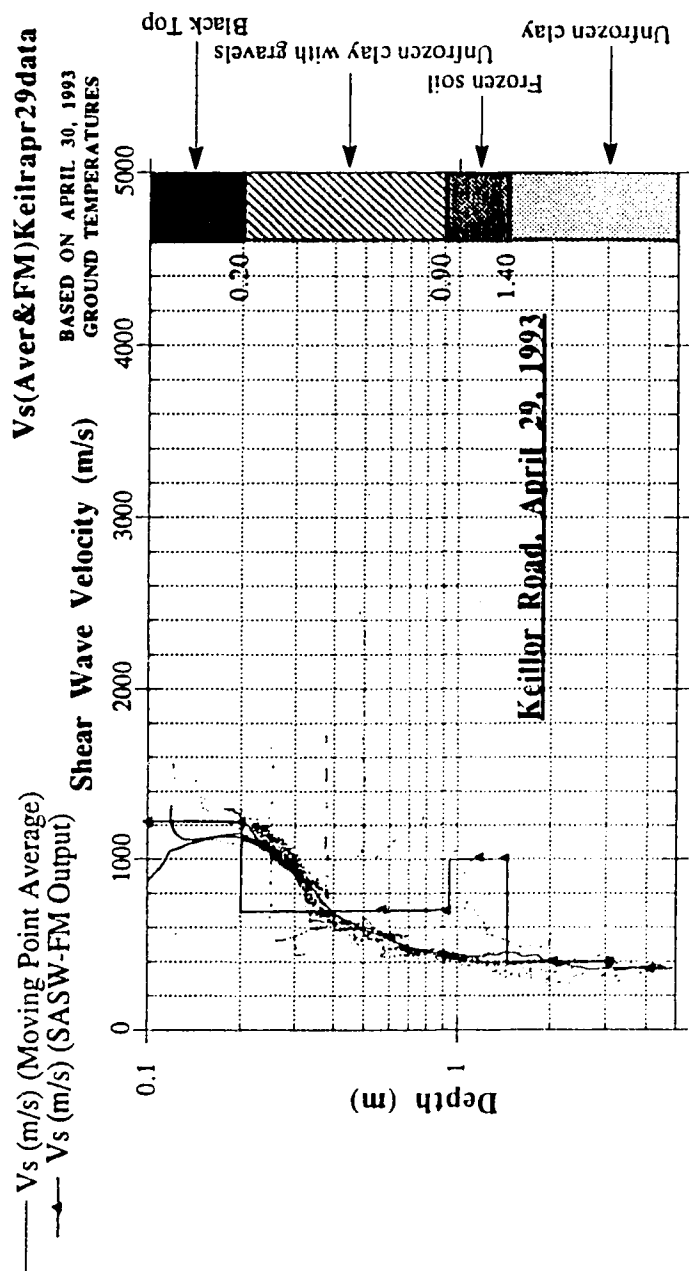


Figure 7.36 Comparison of Shear Wave Velocity Profile (Moving Point Average & SASW-FM), Keillor Road, April 29, 1993

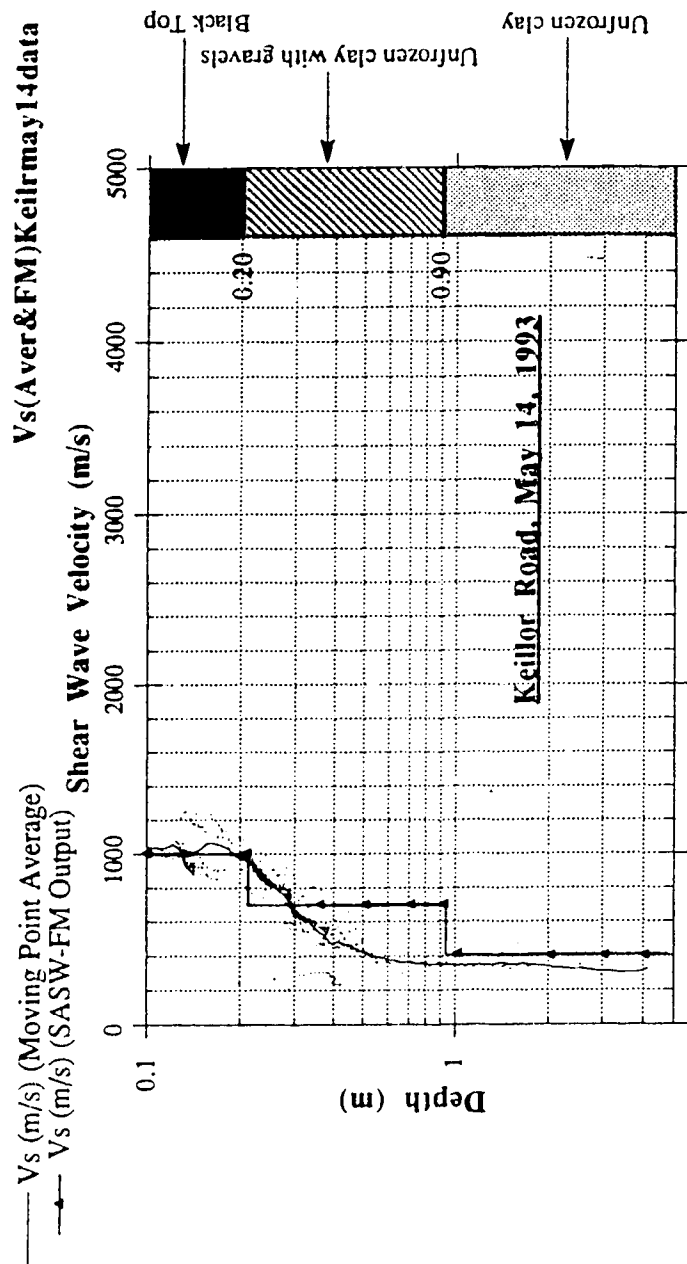


Figure 7.37 Comparison of Shear Wave Velocity Profile (Moving Point Average & SASW-FM), Keillor Road, May 14, 1993

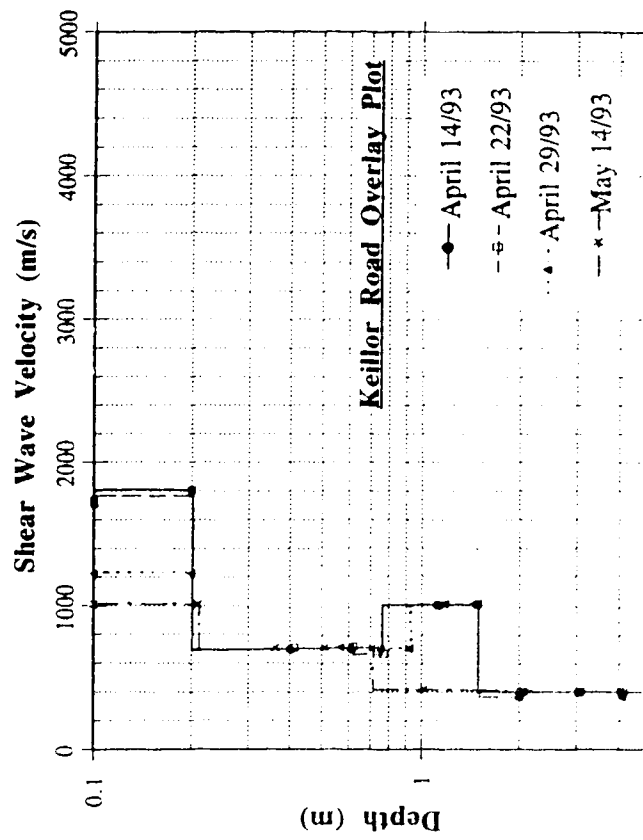


Figure 7.38 Overlay Plot of average shear wave velocity profile at Keillor Road, all test dates

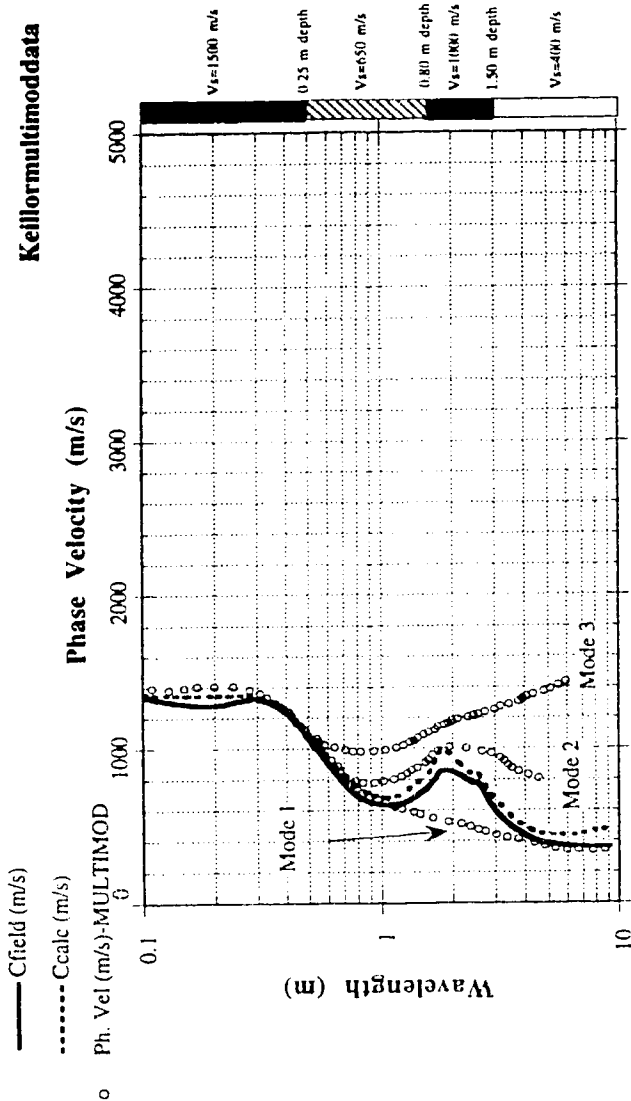


Figure 7.39 Comparison of Ccalc, Cfield and MULTIMOD output,  
Keillor Road, April 22, 1993

## **CHAPTER EIGHT**

### **CONCLUSIONS AND RECOMMENDATIONS**

#### **8.1 INTRODUCTION**

An improved version of the Spectral-Analysis-of-Surface-Waves (SASW) technique has been developed for obtaining the stiffness profiles over shallow depths of ground structures having contrasting layer properties, such as, pavements and concrete layers.

Data-acquisition and field interpretation are fully automated using a Macintosh Computer, High-Speed Data -Acquisition Board, DMA Board with GPIB Interface, Interface-Control-Unit (ICU) and Power Amplifier. The calculation process for transforming time-domain data to frequency-domain, calculation of auto-power spectra, cross-power spectra, phase of the cross-power spectra, coherence and phase velocities are done in real time in the field as the data is being collected. The software "SWAP" (Spectral Wave Analysis for Pavements) has been developed for this purpose using the LabVIEW programming technique. The results are obtained immediately in the field showing the variation of phase velocity with wavelength. The equipment set-up, data-collection technique, data processing and test results from different sites having different stratigraphy and environmental conditions were evaluated in this research.

#### **8.2 CONCLUSIONS**

The conclusions that can be drawn from this research may be outlined as follows:

1. A low-cost portable micro-computer system has been configured to perform SASW testing for obtaining the stiffness profiles over shallow depths of ground structures having contrasting layer properties, such as, pavements and concrete layers overlying a subgrade.
2. The simple moving point averaging and axes scaling techniques appear to produce reasonable average stiffness profiles.
3. Forward modelling, using SASW-FM, appears to give better stiffness profiles and better layer definitions than the simple empirical axes-scaling technique.
4. Without resorting to expensive and complicated multimodal analysis, the SASW is capable of producing a global view of the subsurface stiffness profiles, including approximate layer boundaries.
5. Results indicate that the change in ground conditions during freeze-thaw cycle can be adequately identified using SASW testing methods.
6. The softening of the surface layer for flexible asphaltic pavements due to the increase in air temperature can be detected using SASW.
7. The combination of low frequency geophones and high frequency accelerometers together with small, medium and large hammers can provide the required data for profiling shallow depths, including the top few centimetres of pavement and concrete layers.

8. The SASW technique appears to be remarkably robust in producing reasonable stiffness profiles for pavement structures. With continued improvements, the technique can be expected to produce significantly better stiffness profiles than that obtained in this study.

### 8.3 RECOMMENDATIONS

Although the improved micro-computer based SASW system has replaced expensive spectrum analyzers and proved to be more portable, cost-effective and less time consuming, there are many areas of research which can be explored to make the present SASW system more effective. Some of the areas where future research can be directed may be outlined as follows:

1. Receiver arrays containing more than two receivers can be used during data-acquisition. This could reduce the testing time considerably, because one receiver array could provide many combinations of receiver spacings. Therefore, a modified data-acquisition program is needed which can handle receiver arrays containing four or more receivers. This would also require a faster computer or additional data-acquisition boards.
2. Small hand-held vibrators, capable of vibrating the ground surface at very high frequencies, as well as sweeping frequencies should be considered. This would provide more energy to the ground at the required frequencies which would be an improvement over the problem of inadequate energy at larger spacings with small-hammer impacts. Small subroutine programs can also be implemented on the main data-acquisition program to control and change the frequency of the vibrator directly from the computer



without other manual operations. Frequencies could be adjusted to focus the surface wave to a particular depth.

3. With the present SASW system, at least two persons are required during field testing: an operator, who operates the computer and instructs an assistant, who provides the impact on the ground. The van housing the computer is generally parked a few metres away from the test section. Therefore, a constant communication should be maintained between the operator and the assistant and both should be familiar with each others' signals for an effective testing program. Future SASW systems can eliminate the assistant by developing an instrumented system containing all the sensors, geophones and a vibrator source which can be lowered mechanically from a vehicle and placed on the test section while the operator controls the whole procedure through his computer.
4. The measured scatter in dispersion data can be reduced by studying the effect of the three-dimensional nature of the ground and the effect of higher modes on the propagation of surface waves. More studies should also be undertaken to correlate the phase and coherence data on the reduction of scattering of the dispersion points.
5. The vertical and horizontal particle displacements can also be measured simultaneously during data-acquisition and should be implemented in the main data-acquisition program to consider the effects of higher modes and reduction of scattering on the dispersion curves.
6. Care should also be taken to ensure that body waves are not picked up by the receivers and should be totally eliminated before processing the data.

7. More emphasis should be placed on the multimodal analysis using a much faster computer and advanced programming techniques.

## BIBLIOGRAPHY

1. Addo , Kofi. (1992). **Development of a Computerized SASW Technique**; Ph.D. Dissertation; University of Alberta, Edmonton, Canada
2. Addo , Kofi & P. K. Robertson. (1991). **Shear Wave Velocity Measurements Using Rayleigh Surface Waves**; Proc. 44th Canadian Geotechnical Conference 1, Paper No. 11:11-1 to 11-10
3. Aki , K. & P. G. Richards. (1980). **Quantitative Seismology: Theory and methods**; W. H. Freeman and Company. 932 pp
4. Aldrich, Harl P. (1956). **Frost Penetration Below Highway and Airfield Pavements**; Highway Research Board Bulletin, No. 135
5. Allen , N. F. ; F.E. Richart, Jr. & R.D. Woods. (1980). **Fluid Wave Propagation in Saturated and Nearly Saturated Sand**; Journal of the Geotechnical Engineering Division ASCE. 106, No. GT3:235-254
6. American Society for Testing and Materials. (1988). **Standard Test Methods for Crosshole Seismic Testing**; Annual Book of ASTM Standards American Society for Testing and Materials. D4428 M-84:14 pp14 pp
7. Anderson, M. (1989). **A Data Base Method for Backcalculation of Composite Pavement Layer Moduli**; Non-destructive Testing of Pavements and Backcalculation of Moduli, ASTM STP 1026, A.J. Bush III and G.Y. Baladi, Eds., American Society for Testing and Materials, Philadelphia, 1989, pp. 201-216

8. Asphalt Institute. (1983). **Asphalt Overlays for Highway and Street Rehabilitation**; Manual Series 17. The Asphalt Institute, College Park, Md.
  
9. Badu-Tweneboah, K., Manzione, C.W., Ruth, B.E. and Miley, W.G. (1989). **Prediction of Flexible Pavement Layer Moduli from Dynaflect and FWD Deflections**; Non-destructive Testing of Pavements and Backcalculation of Moduli, ASTM STP 1026, A.J. Bush III and G.Y. Baladi, Eds., American Society for Testing and Materials, Philadelphia, 1989, pp. 245-277
  
10. Ballard, R. F. (1976). **Method for Crosshole Seismic Testing**; Journal of Geotechnical Engineering, Proc. ASCE ASCE. GT 12:1261-1273
  
11. Ballard, Jr., R. F. (1964). **Determination of Soil Shear Moduli at Depth by In-situ Vibratory Techniques**; WES, Misc. Paper 4-691
  
12. Beeston , H. E. & T. V. McEvilly. (1977). **Shear Wave Velocities from Down-Hole Measurements**; Int. J. Earthquake Engineering Struc. Dyn. 5 181-190
  
13. Biot , M. A. (March 1956). **Theory of Propagation of Elastic Waves in a Fluid-Saturated Porous Solid**; J. Acoustical Society of America 28:168-191
  
14. Born , Günter W. (1978). **Methods from Exploration Seismology: reflection, Refraction and Borehole Prospecting**; Rock Dynamics and Geophysical Aspects A. A. Balkema. 3:87-114
  
15. Bullen , K. E. (1953). **An Introduction to the Theory of Seismicity**;

Cambridge University Press.

16. Canadian Good Roads Association (CGRA) Guide, 1965.
  
17. Chang, D.W., Kang, Y.V., Roesset, J.M. and Stokoe, K.H. III.(1991). **Effect of depth to bedrock on deflection basins obtained with Dynaflect and FWD tests**; A paper presented at 1991 Annual General Meeting of the Transportation Research Record.
  
18. Christison, J.T., and Leung, P.S. (1988). **Temperature Adjustment factors for Benkelman Beam Rebound Deflections and seasonal variations in pavement strength**. Report No. HTE 88/07
  
19. Croney, D. and Croney, P. (1991). **The Design and Performance of Road Pavements**, Second edition, McGraw Hill Book Comapny, 592 pp
  
20. Crovetti, J.A., Shahin, M.Y. and Touma, B.E. (1989). **Comparison of two Falling Weight Deflectometer devices, Dynatest 8000 and KUAB 2M-FWD., ASTM STP-1026**, pp 59-69
  
21. Department of Army. **Geophysical Exploration; Engineering Manual** Corps of Engineers. 1110-1-1802
  
22. Dobrin , M. B. (1976). **Introduction to Geophysical Prospecting**; McGraw-Hill. 3rd Edition:630 pp
  
23. Dorman , J. & M. Ewing. (1962). **Numerical Inversion of Seismic Surface**

**Wave Dispersion Data and Crust-Mantle Structure in the New York-Pennsylvania Area; Journal of Geophysical Research 67 :5227-5241**

24. Epps, J.A., and Monismith, C.L.(1986). **Equipment for obtaining pavement condition and traffic loading data; NCHRP-126**; Transportation Research Board, National Research Council, Washington D.C.
  
25. Ertman-Larsen, H.J. and Stubstad, R.N. (1982). **The use of non-destructive testing in flexible pavement rehabilitation design; Proc. Int. Symp. on Bearing Capacity of Roads and Airfields, 1, pp. 31-41.**
  
26. Ertman-Larsen, H.J. and Stubstad, R.N. (1983). **The use of non-destructive testing in flexible pavement thickness design; Interne Notater 143**; Statens Vejlaboratorium Vejdirektoratet, Denmark.
  
27. Ewing , W. M. ; W. S. Jardetzky & F. Press. (1957). **Elastic Waves in Layered Media**; McGraw-Hill Book Company, Inc..
  
28. Foxworthy, P.T. and Darter, M.I. (1989). **ILLI-SLAB and FWD Deflection basins for characterization of rigid pavements; ASTM STP 1026**; pp. 368-386
  
29. Fry , Z. B. (1963). **Development and Evaluation of Soil Bearing Capacity, foundations of Structures; WES, Tech. Rep. 3-632, Report No. 1**
  
30. Fung , Y. C. (1965). **Foundations of Solid Mechanics**; Prentice-Hall, Inc.. 525 pp

31. Grant , F. S. & G. F. West. (1965). **Interpretation Theory in Applied Geophysics**; McGraw-Hill Book Company Inc..
  
32. Gucunski , N. & R.D. Woods (1991). **Use of Rayleigh Modes in Interpretation of SASW Test**; Proc. Second International Conference on Recent Advances in Geotechnical Earthquake Engineering and Soil Dynamics, St. Louis, Missouri, Paper No. 10.10, pp 1399 - 1408.
  
33. Haskell , N. A. (1953). **The Dispersion of Surface Waves on Multilayered Media**; Bulletin of the Seismological Society of America 43, No.1:17-34
  
34. Heirli , W. (1962). **Inelastic Wave Propagation in Soil Columns**; Journal of the Soil Mechanics and Foundations Division Proc. ASCE. 88/SM6:33-63
  
35. Heisey, J.S. (1982), **Determination of in-situ shear wave velocity from Spectral Analysis of Surface Waves**; M.Sc. thesis, Department of Civil Engineering, University of Texas at Austin, Texas, 300 pp
  
36. Heisey, J.S., Stokoe, K.H. II, and Meyer, A.H. 91982). **Moduli of Pavement Systems from Spectral Analysis of Surface Waves**; Research Record No. 852, Transportation Research Board, pp. 22-31
  
37. Heukelom , W. & C. R. Foster. (Feb 1960). **Dynamic testing of Pavements**; Journal of the Soil Mechanics and Foundations Division, Proc. ASCE ASCE. 86, No. SM1, part 1:1-28

38. Hiltunen, D.R. and Woods, R.D. (1988). **SASW and Crosshole Test Results Compared; Earthquake Engineering and Soil Dynamics II - Recent Advances in Ground-Motion Evaluation**, Proceedings of the Specialty Conference of Geotechnical Engineering Division at Park City, Utah, ASCE, New York, NY, 279-289 pp
  
39. Hoar , R. J. (1982). **Field Measurement of Seismic Wave Velocity and Attenuation for Dynamic Analyses; Ph.D. Dissertation** The University of Texas at Austin. 478 pp
  
40. Hoar , R. J. & K. H. Stokoe, II. (1978). **Generation and Measurement of Shear Waves In Situ; Dynamic Geotechnical Testing** American Society for Testing and Materials. ASTM STP 654:3-29
  
41. Knopoff , L. (1961). **Green's Function for Eigenvalue Problem and the Inversion of Love Wave Dispersion Data; Journal of Geophysics** 4:161-173
  
42. Knopoff , L. (1964). **A Matrix Method for Elastic Wave Problems; Bulletin of the Seismological Society of America** 54 :431-438
  
43. Kolsky , H. (1953). **Stress Waves in Solids**; Clarendon Press.
  
44. Lamb , H. (1904). **On the Propagation of Tremors Over the Surface of an Elastic Solid; Philosophical Transactions, Series A** Royal Society. 203:1-42
  
45. Lüdelling , Rolf. (1978). **Shear Wave Measurements Using the Seismic Up-Hole Method; Rock Dynamics and Geophysical Aspects** A. A. Balkema. 139-148



46. Lysmer , J. (1965). **Vertical Motion of Rigid Footings**; U.S. Army Engineer Waterways Experiment Station , Report No. 3-115, Vicksburg, Mississippi. 137 pp.
  
47. Miller , G. F. & H. Pursey. (1955). **On the Partition of Energy Between Elastic Waves in a Semi-Infinite Solid**; Proceedings, Series A Royal Society. 233:55-59
  
48. Mora , P. (1988). **Elastic Wavefield Inversion and the Adjoint Operator For the Elastic Wave Equation**; Mathematical Geophysics D. Reidel Publishing Co.. 117-137
  
49. Nazarian , S. (1984). **In situ Determination of Elastic Moduli of Soil Deposits and Pavement Systems by Spectral-Analysis-of-Surface-Waves-Method**; Ph. D. Dissertation University of Texas at Austin, Texas. 453 pp
  
50. Nazarian , S. & K. H. Stokoe, II. (1984). **In-situ Shear Wave Velocities from Spectral-Analysis-of-Surface-Waves**; Proc. Eighth World Conference on Earthquake Engineering 3:31-38
  
51. Nazarian, S. and Stokoe, K.H. II, (1986). **Use of surface waves in Pavement Evaluation**; Research Record No. 1070, Transportation Research Board, washington, D.C., pp. 132-144
  
52. Nazarian , Scheil & Kenneth H. Stokoe, II. (1989). **Nondestructive Evaluation of Pavements by Surface Wave Method**; Nondestructive Testing of Pavements and Backcalculation of Moduli, ASTM STP 1026 American Society for Testing and materials. 119-137

53. Newland, D.E., (1975). **An introduction to Random vibrations and spectral analysis**; Longman, New York, pp. 285
  
54. Newmark , N. M. & E. Rosenblueth. (1971). **Fundamentals of Earthquake Engineering**; Prentice-Hall Inc..
  
55. O'Flaherty, C.A. (1988). **Highways**, Volume 2, Highway Engineering, Third edition, Edward Arnold, 684 pp
  
56. Patel , N. S. (May 1981). **Generation and Attenuation of Seismic Waves in Downhole Testing**; Masters Thesis The University of Texas at Austin. 411 pp
  
57. Rayleigh , Lord J. W. S. (1885). **On Waves Propagated Along the Plane Surface of an Elastic Solid**; Proc., London Math Society ,Vol. 17 (Series 1), pp 4-11
  
58. Richart, Jr. , F. E. (1962). **Foundation Vibrations**; Trans. ASCE 127, Part 1:863-898
  
59. Richart, Jr. , F. E. ; J.R. Hall, Jr. & R. D. Woods. (1970). **Vibrations of Soils and Foundations**; Prentice-Hall, Inc.. 414 pp
  
60. Rix , Glenn Jay. (1988). **Experimental Study of Factors Affecting the Spectral-Analysis-Of-Surface-Waves Method**; Ph.D Thesis The University of Texas at Austin.

61. Roads and Transportation Association of Canada (RTAC) (1976). **Pavement Management Guide**, Ottawa, Ontario.
  
62. Robertson, P.K., Campanella, R.G., Gillespie, D., and Rice, A. (1986). **Seismic CPT to Measure In-Situ Shear Wave Velocity**; J. Geotech Eng. Div. ASCE., Vol. 112, No.8, pp. 791-804.
  
63. Robertson, P.K. and Addo, K.O. (1991). **Recent In-Situ Methods to Determine Seismic Velocity profiles**; Geotechnical News, September 1991, pp 26-30
  
64. Roesset , J. M. & K. Y. Shao. (1985). **Dynamic Interpretation of Dynaflect and Falling Weight Deflectometer Tests**; Transportation Research Record 1022:7-16
  
65. Sanchez-Salinero, I.; J.M. Roesset; K.Y. Shao; K.H. Stokoe, II & G.J. Rix. (1987). **Analytic Evaluation of Variables Affecting Surface Wave Testing of Pavements**; Transportation Research Record 1138:86-95
  
66. Schwarz , S. D. & J. M. Musser, Jr. (1972). **Various Techniques for Making In-Situ Shear Wave Velocity Measurements**; Proc. Int. Conf. Microzonation II:593-608
  
67. Selig , E. T. (1964). **Characteristics of Stress Wave Propagation in Soil**; Proc. Symp. Soil-Structure Interaction 27-61
  
68. Smith, R.B. (1985). **Preliminary Evaluation of the Dynatest 8000 Falling Weight Deflectometer**; Australian Road Research, 15(4), Dec'85, pp. 229-238.

69. Stokoe, II , K. H. & R. J. Hoar. (1978). **Field Measurement of Shear Wave Velocity by Crosshole and Downhole Seismic Methods;** Rock Dynamics and Geophysical Aspects Balkema. 3:115-137
  
70. Stokoe, K.H. II and Nazarian, S. (1983). **Effectiveness of Ground Improvement from Spectral Analysis of Surface Waves;** Proceedings of the Eighth European Conference of Soil Mechanics and Foundation Engineering, Helsinki, Finland
  
71. Stokoe, K.H. II, Nazarian, S., Rix, G.J., Sanchez-Salinero, I., Sheu, J.C., and Mok, Y.J., (1988). **In-Situ Seismic Testing of Hard-To-Sample Soils by Surface Waves Method;** Earthquake Engineering and Soil Dynamics II - Recent Advances in Ground-Motion Evaluation; Proceedings of the Specialty Conference of Geotechnical Engineering Division at Park City, Utah, ASCE, New York, NY, 264-278 pp
  
72. Stokoe, II , K. H. & R. D. Woods. (1972). **In Situ Shear Wave Velocity by Cross-Hole Method;** Journal of the Soil Mechanics and Foundations Division Proc. ASCE. 98, No. SM5:443-460
  
73. Thomson, W.T. (1950). **Transmission of Elastic Waves Through a Stratified Soil Medium;** Journal of Applied Physics, Vol. 21, No. 2, February, pp. 89-93
  
74. Thrower, E.N. (1965). **The Computation of the Dispersion of Elastic Waves in Layered Media;** Journal of Sound and Vibration, Academic Press, London,

England, Vol. 2, No. 3, July, pp. 210-226

75. Tokimatsu, K., Shinzawa, K. and Kuwayama, S. (1992). **Use of Short-Period Microtremors for  $V_s$  profiling**; Journal of Geotechnical Engineering, Vol. 118, No. 10, October 1992, pp. 1544-1558
  
76. Ullidtz, P. (1987). **Pavement Analysis**; Elsevier
  
77. Veletsos , A. S. & B. Verbic. (1973). **Vibration of Viscoelastic Foundations**; Earthquake Engineering and Structural Dynamics 2:87-102
  
78. White, J. E. (1965). **Seismic Waves: Radiation, Transmission, and Attenuation**; McGraw-Hill Book Company Inc.. 302 pp
  
79. Woods , R. D. (1968). **Screening of Surface Waves in Soils**; Journal of the Soil Mechanics and Foundations Division ASCE. 94 : 951-979
  
80. Woods , R. D. (1986). **In Situ Tests for Foundation Vibrations**; Use of In Situ Tests in Geotechnical Engineering ASCE. 336-375
  
81. Yoder, E.J. and Witczak, M.W. (1975). **Principles of Pavement Design**, Second edition, John Wiley and Sons, Inc., New York, 711 pp

# **APPENDIX I**

## **"SWAP" Program Sequence**

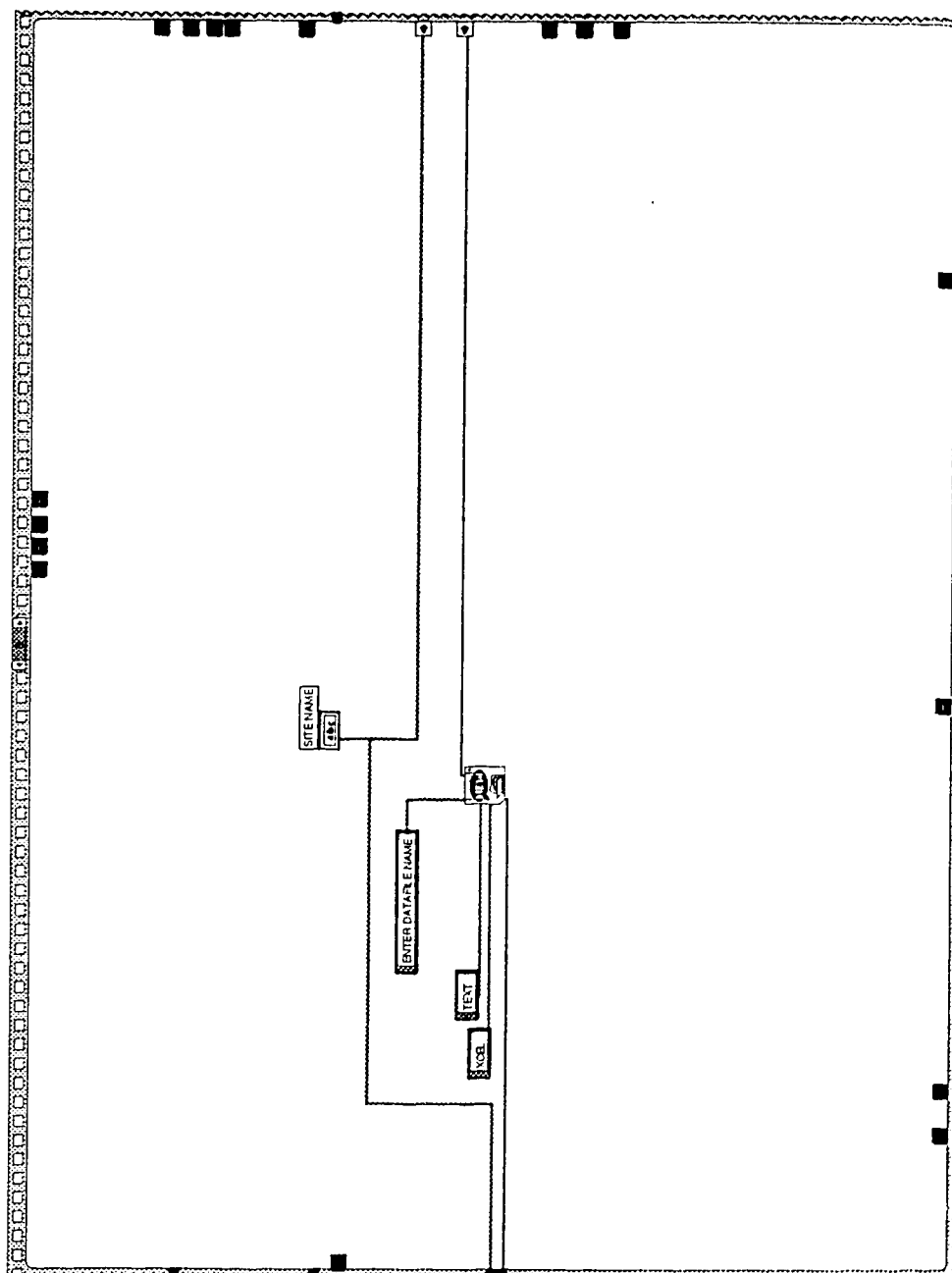


Figure AI.1 Set up for creating a Site Folder and Data File

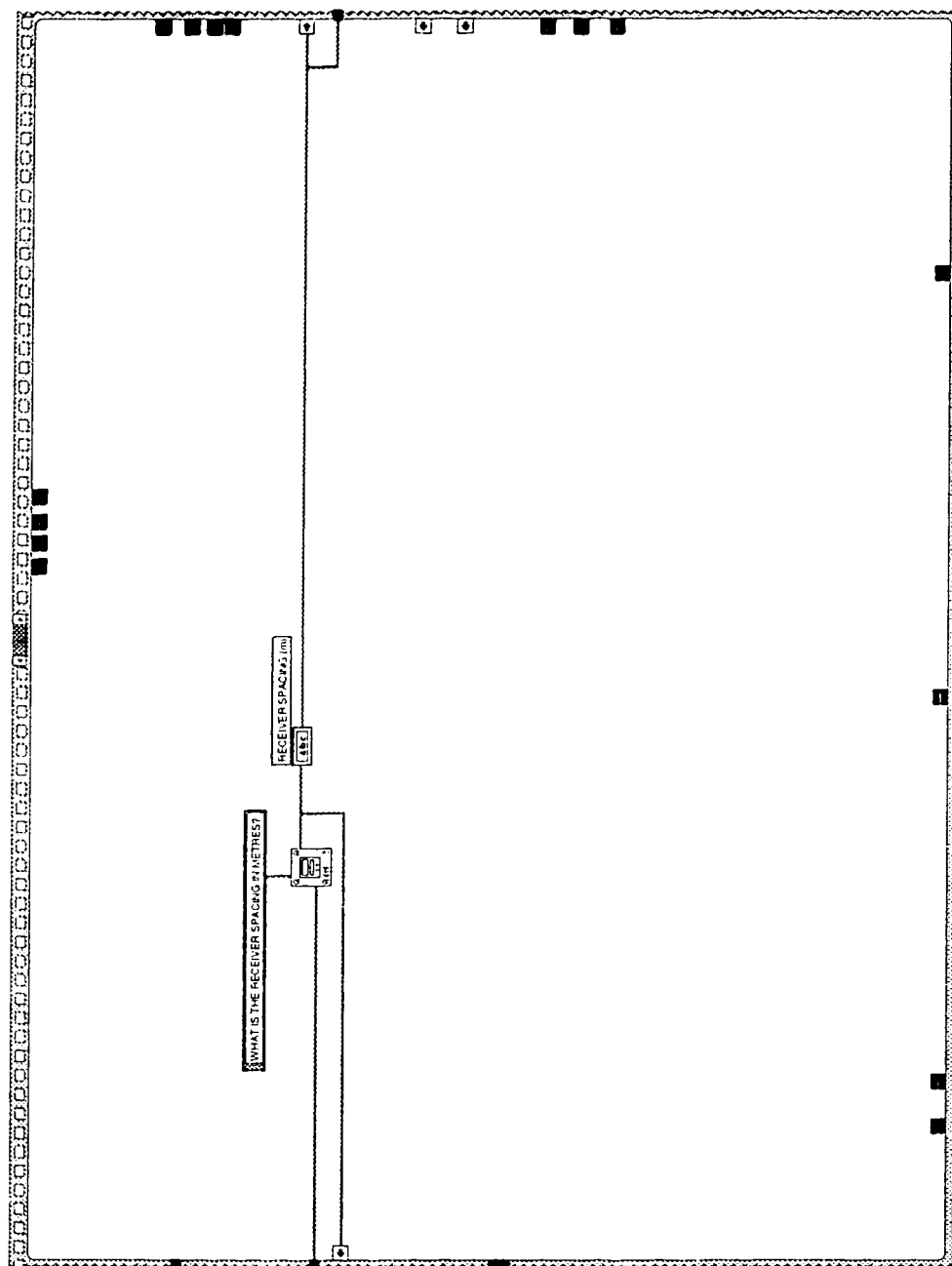


Figure AI.2 Set up for entering receiver spacing



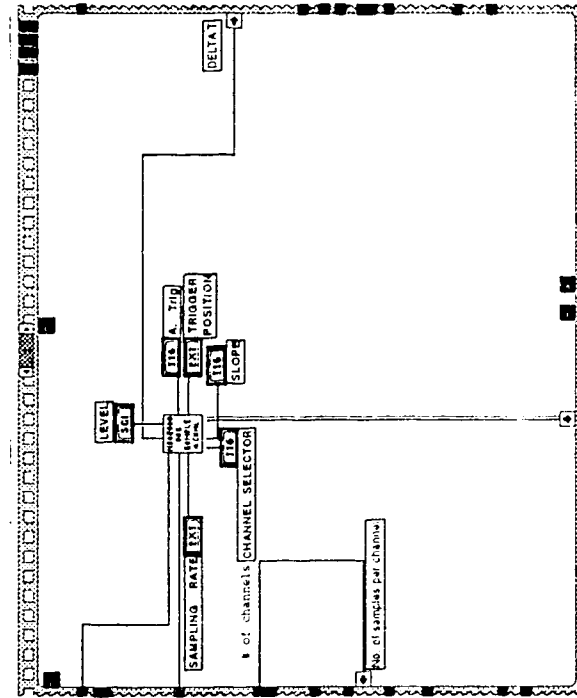


Figure A1.3 Set up for capturing amplitude signals

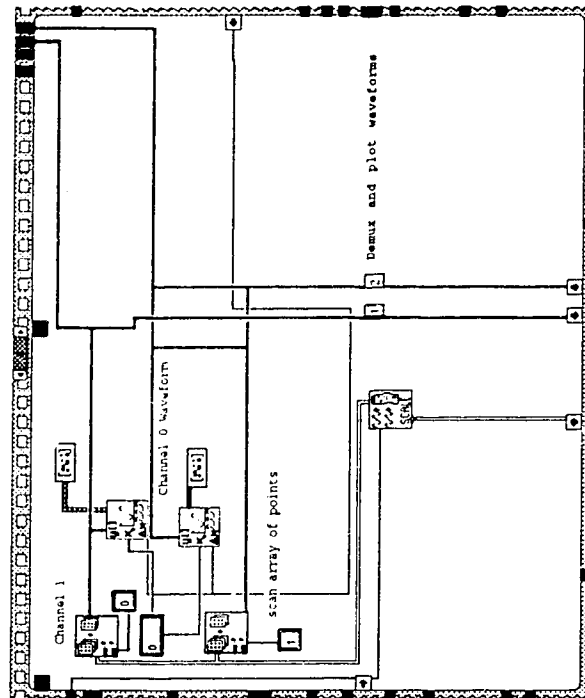


Figure AI.4 Set up for plotting amplitude signals

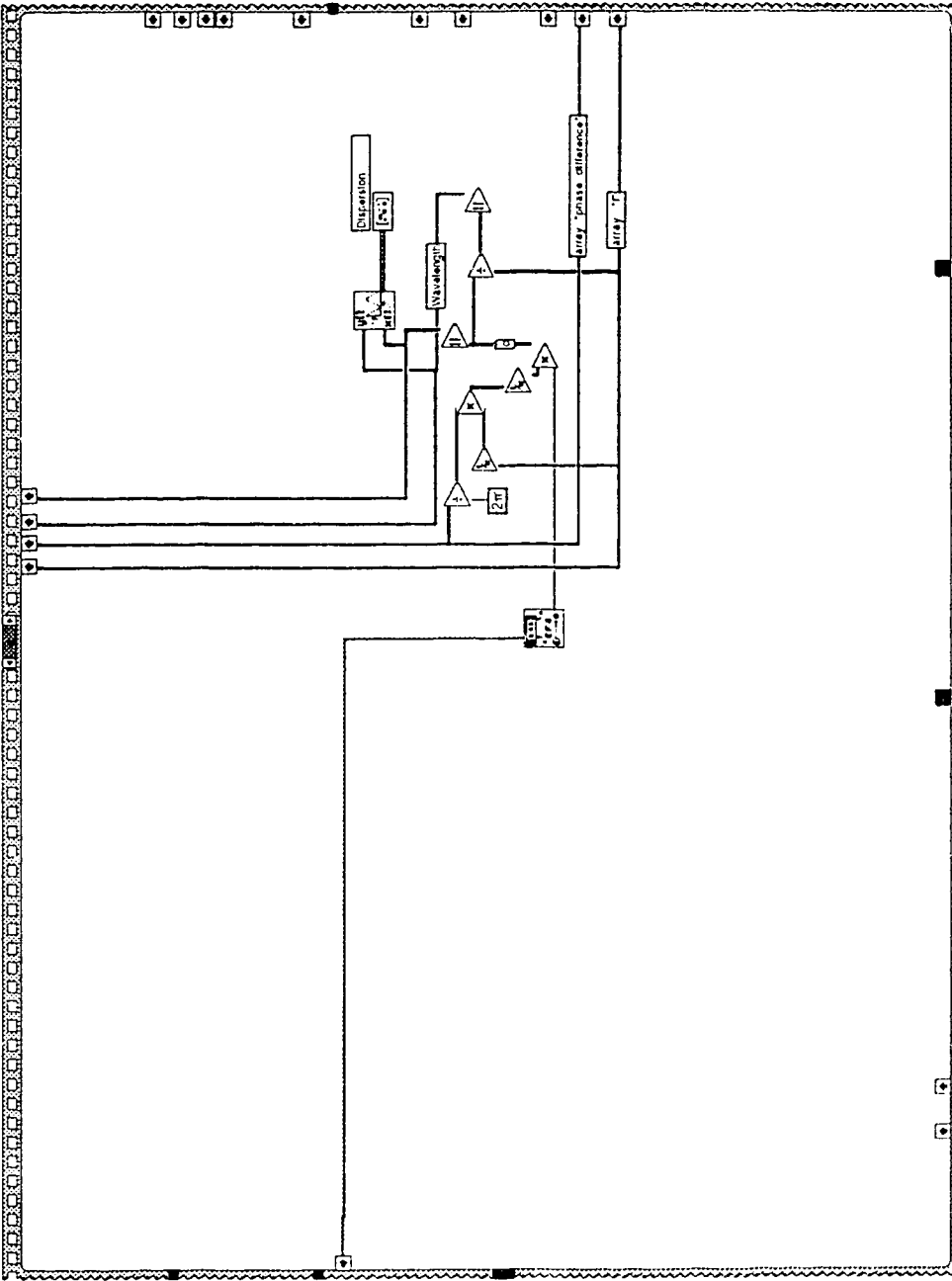


Figure A1.5 Set up for dispersion calculation

# **APPENDIX II**

## **Test Site Figures**

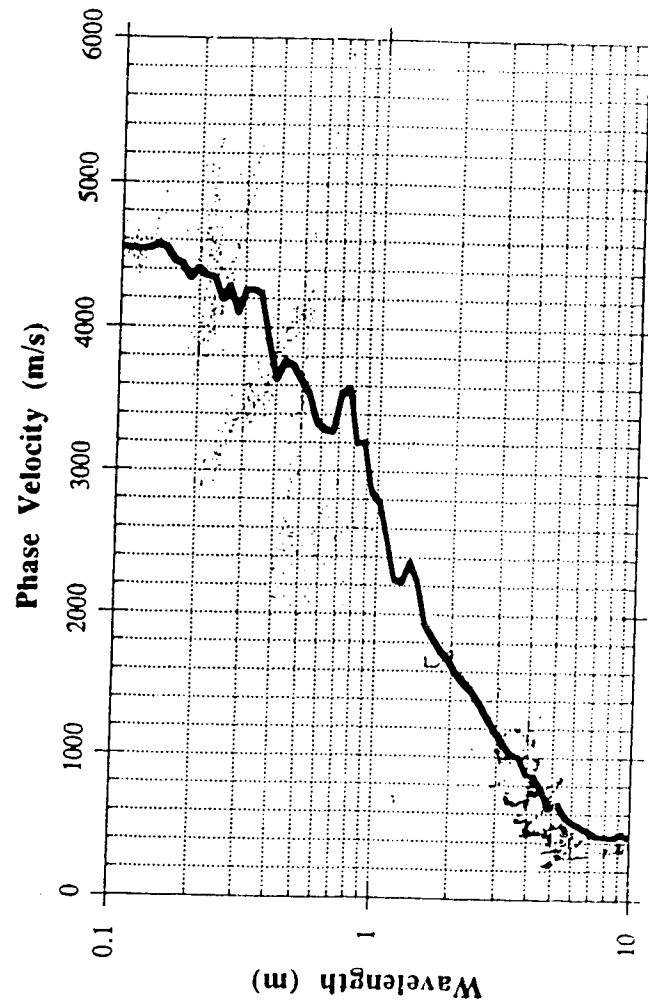


Figure A II.1 Dispersion curve of Pavement Section EE

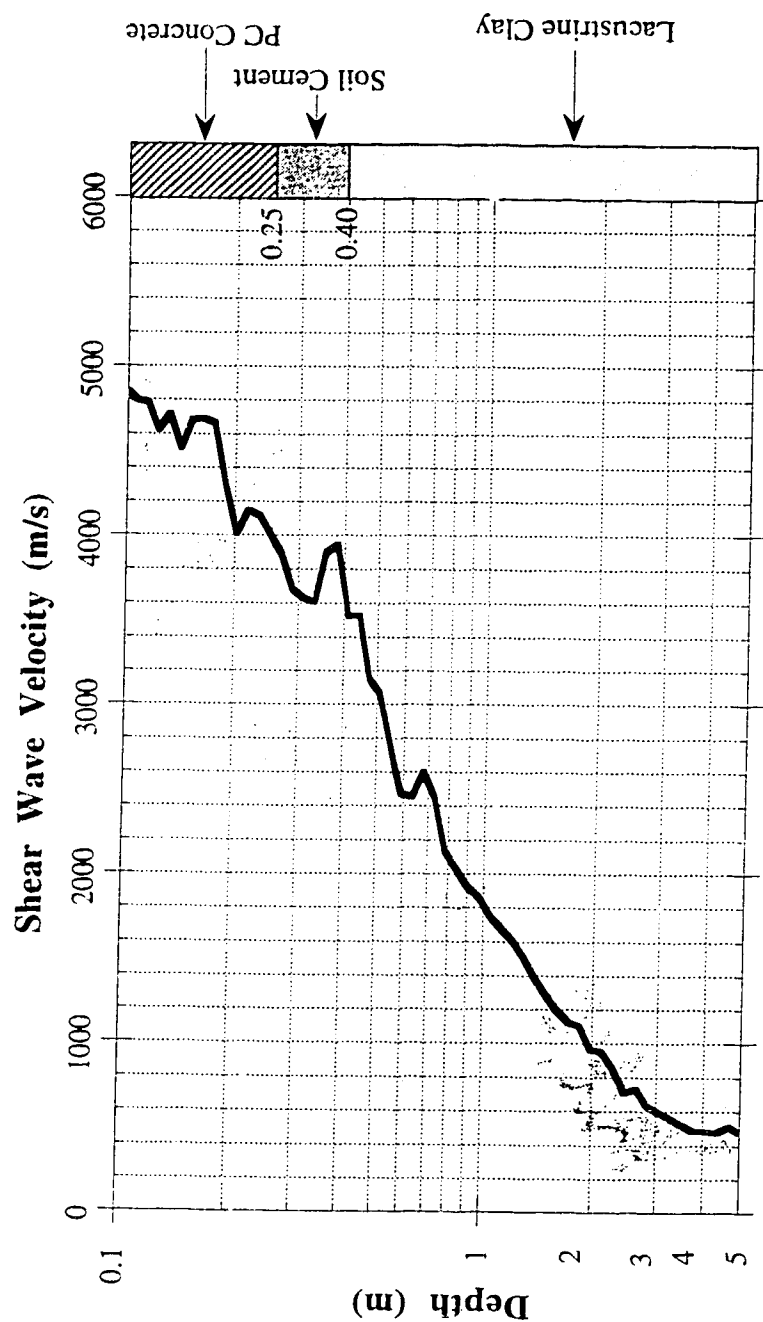


Figure A II.2 Shear wave velocity profile of Pavement Section EE

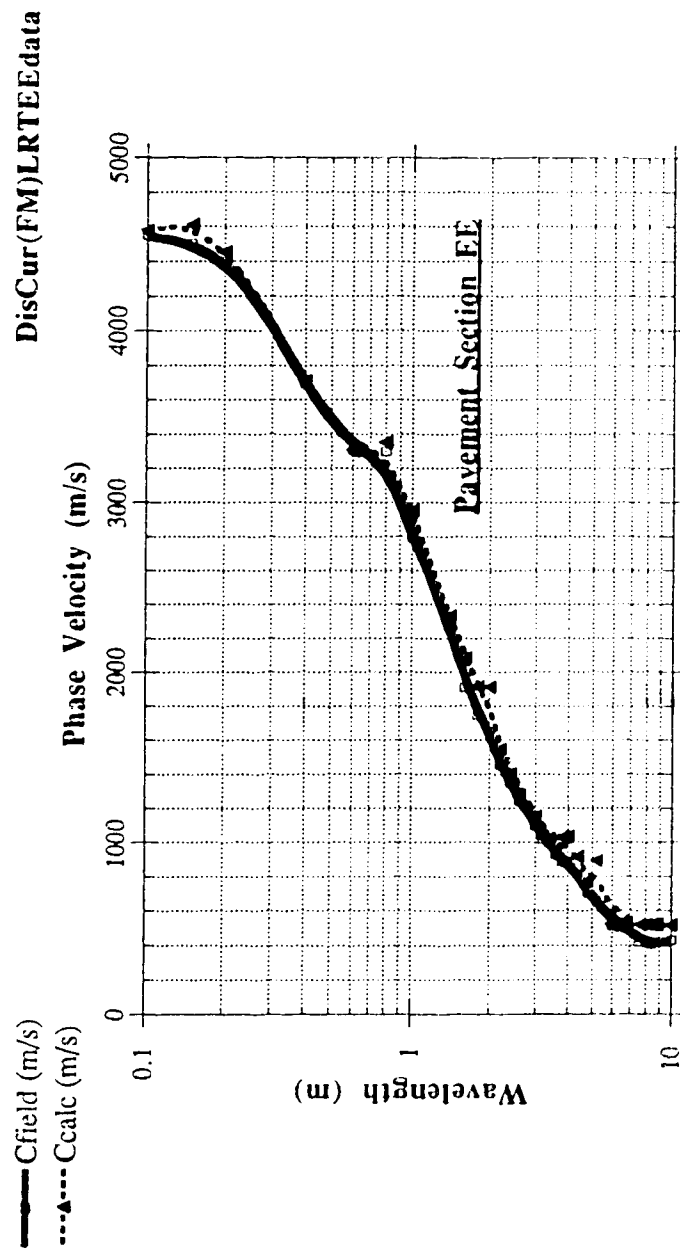


Figure A 11.3 Dispersion curves (SASW-FM) from Pavement Section EE

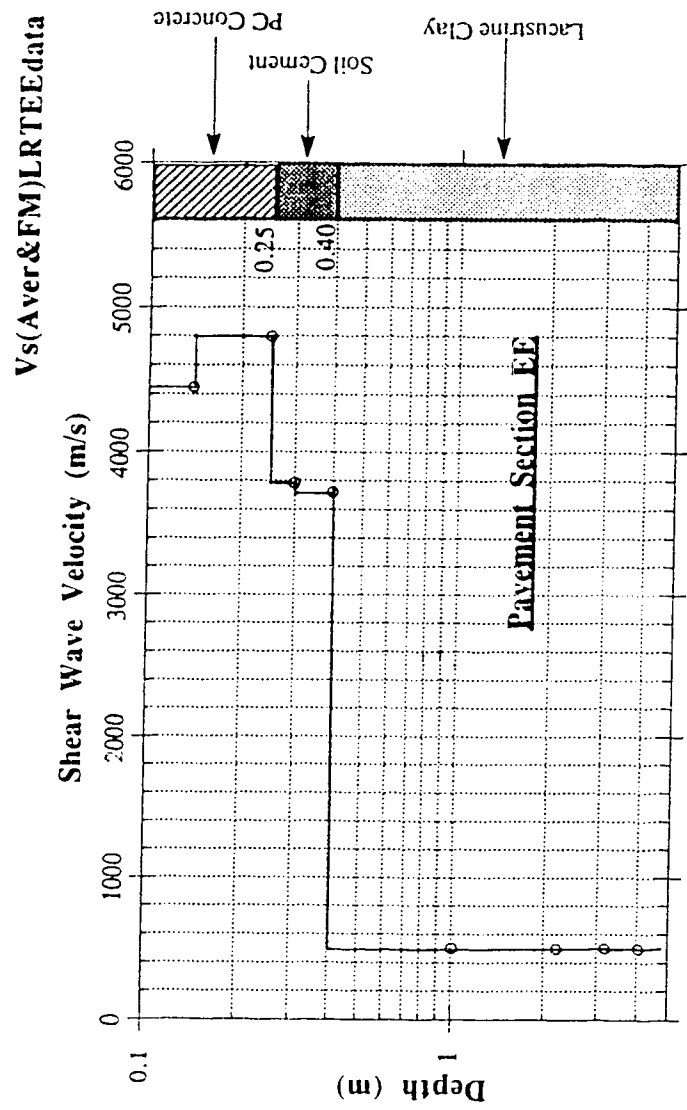


Figure A II.4 Shear Wave Velocity Profile (SASW-FM output) Pavement Section EE



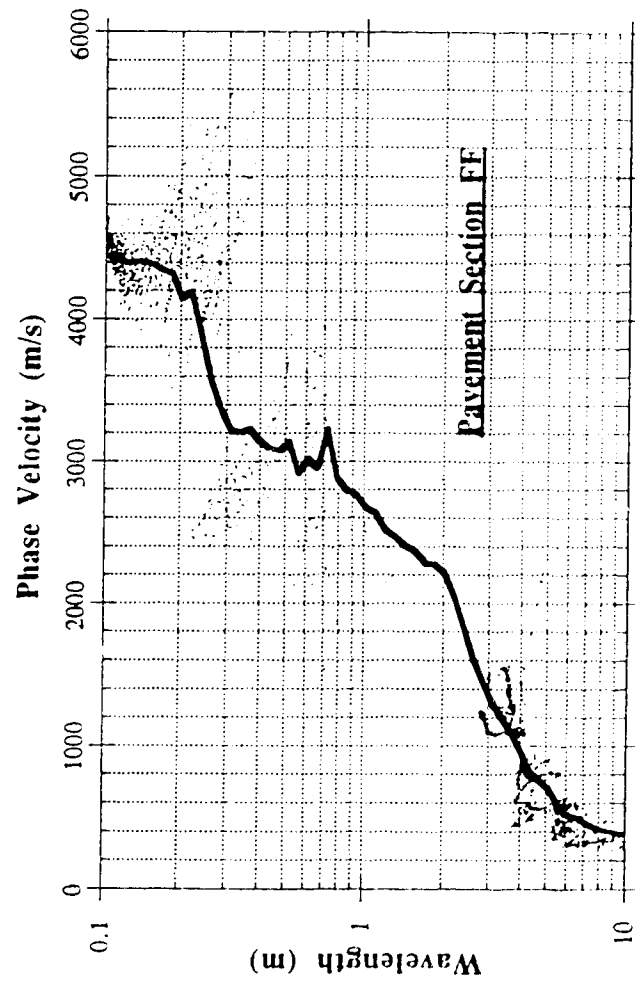


Figure A II.5 Dispersion curve of Pavement Section FF

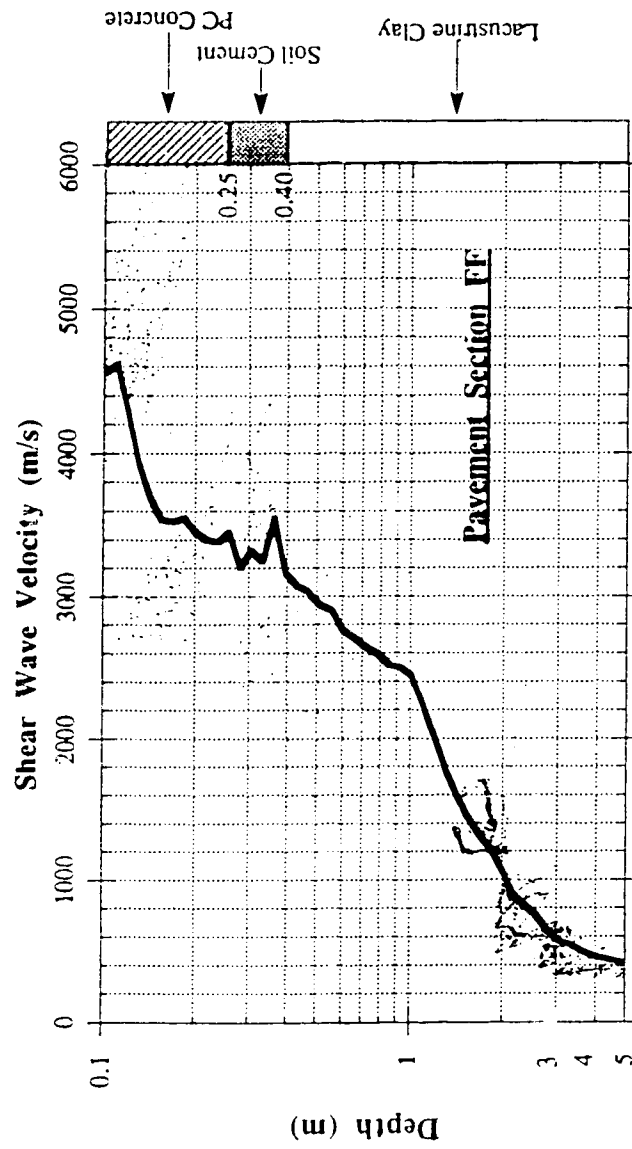


Figure A II.6 Shear wave velocity profile of Pavement Section FF

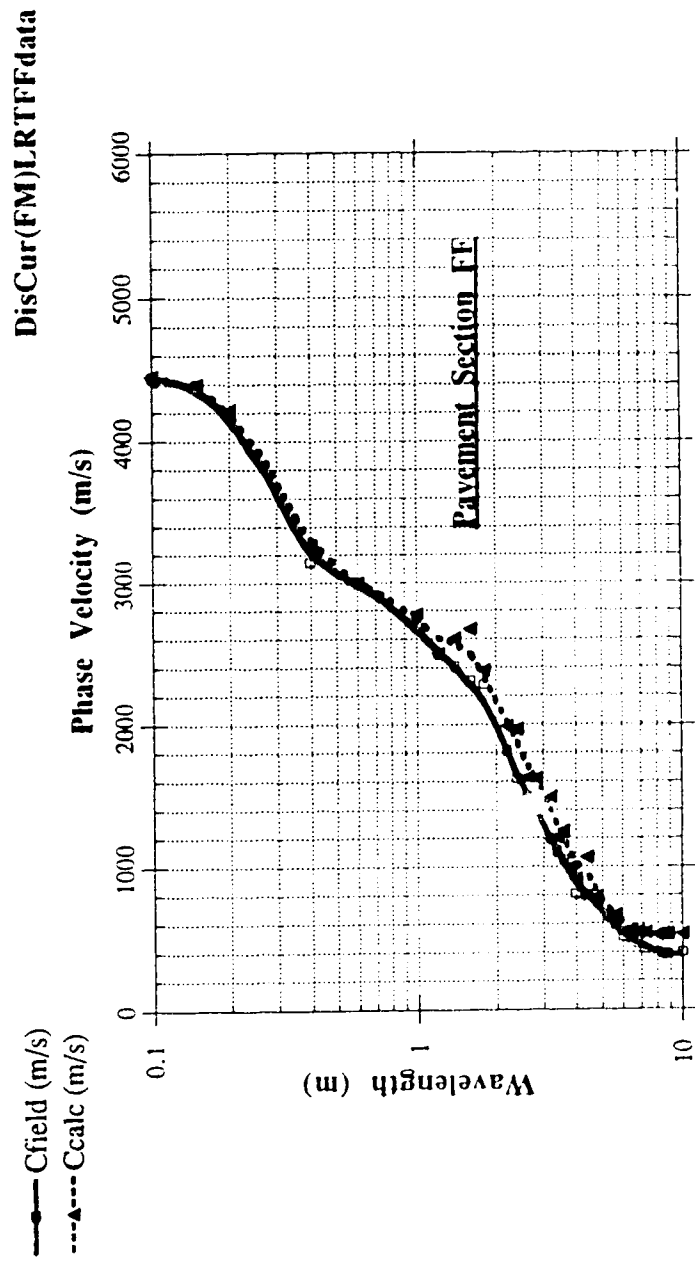


Figure A II.7 Dispersion curves (SASW-F1,f) from Pavement Section FF

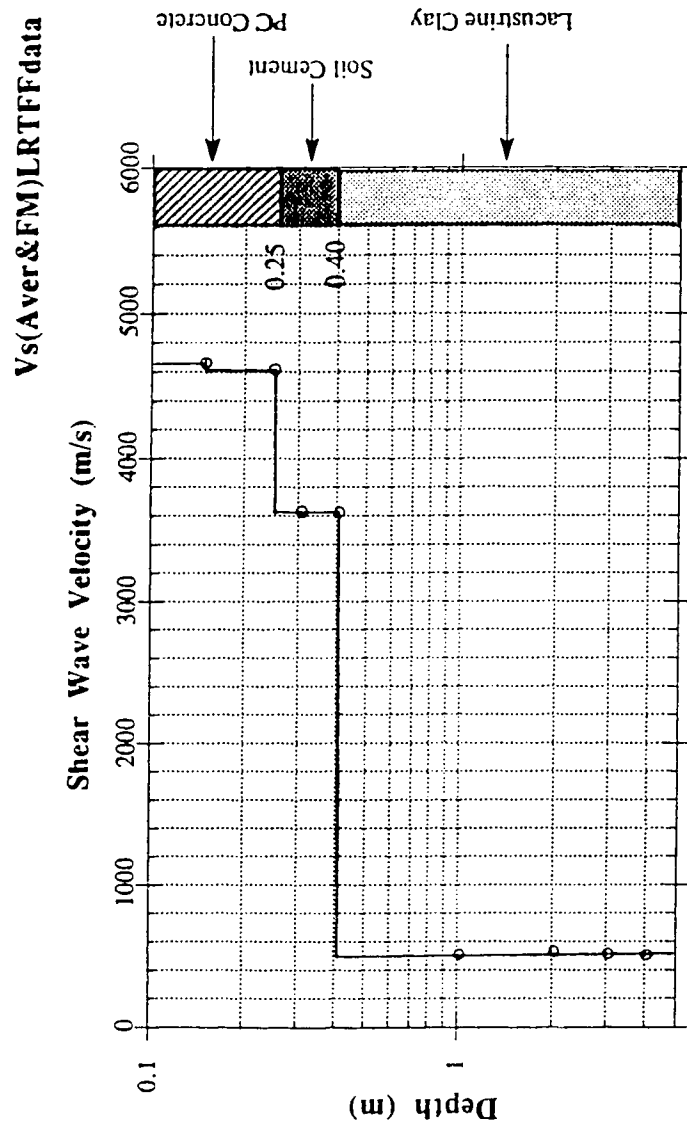


Figure A 11.8 Shear wave Velocity Profile (SASW-FM output), Pavement Section FF

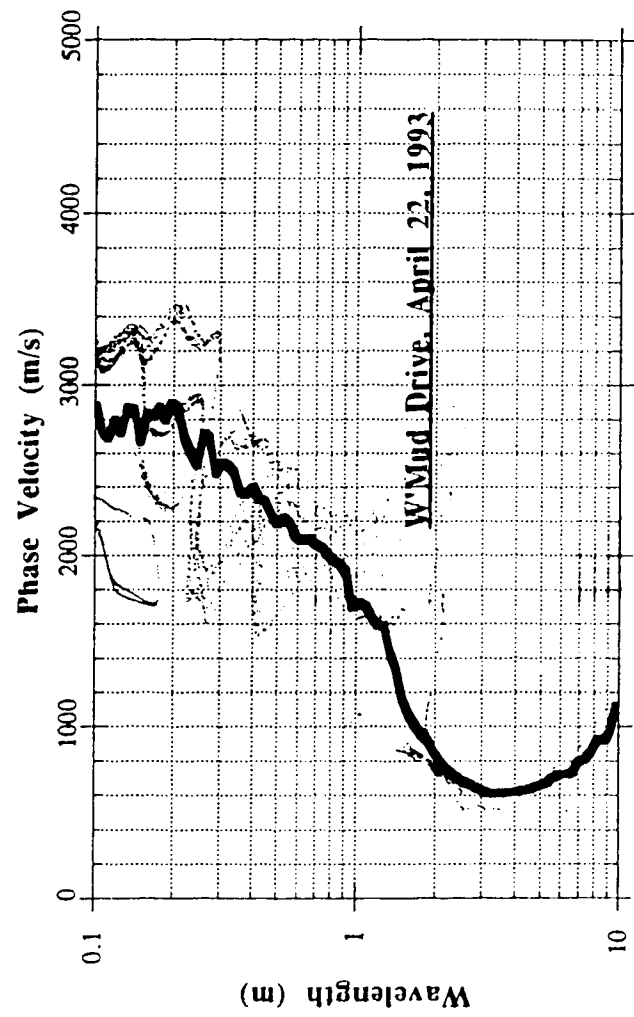


Figure A II.9 Dispersion curve from Whitemud Drive, April 22, 1993

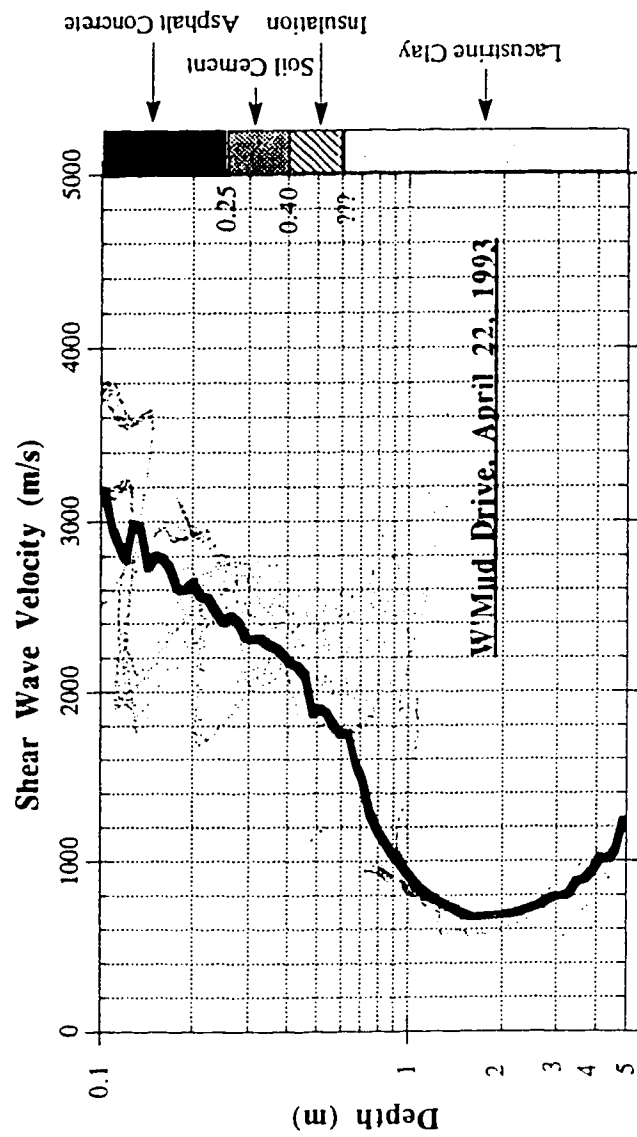


Figure A II.10 Shear wave velocity profile from Whitemud Drive, April 22, 1993

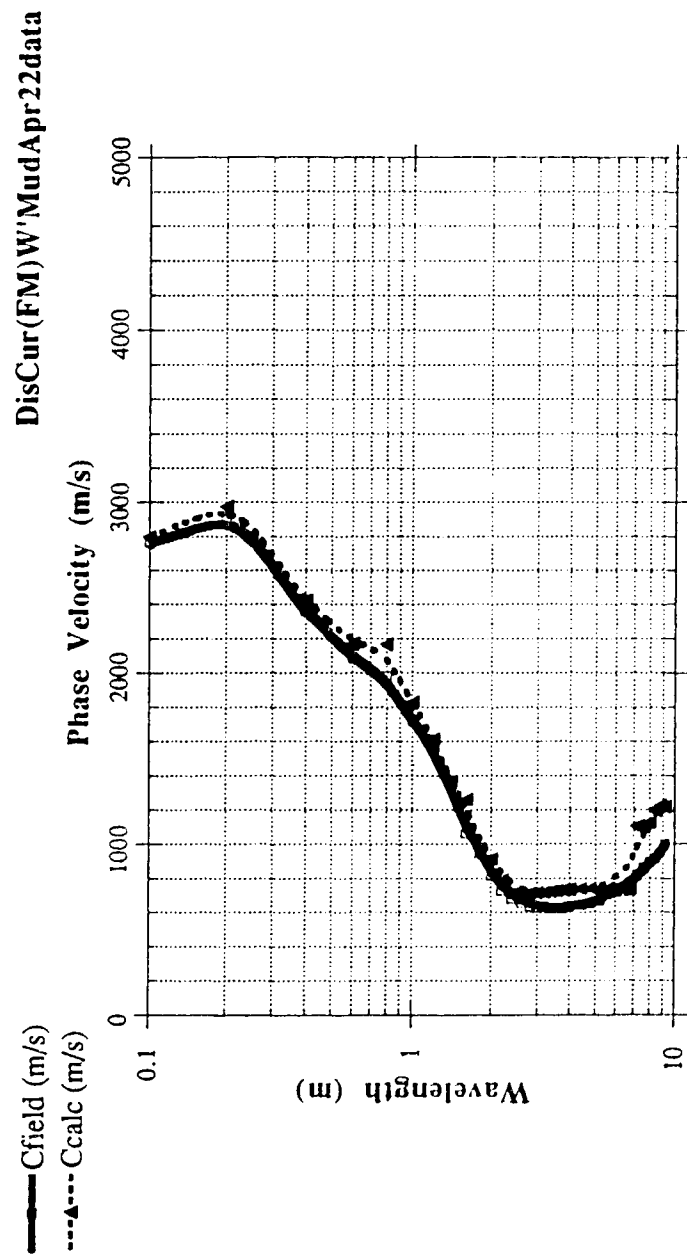


Figure A 11.11 Dispersion curves (SASW-FM) from Whitemud Drive, April 22, 1993

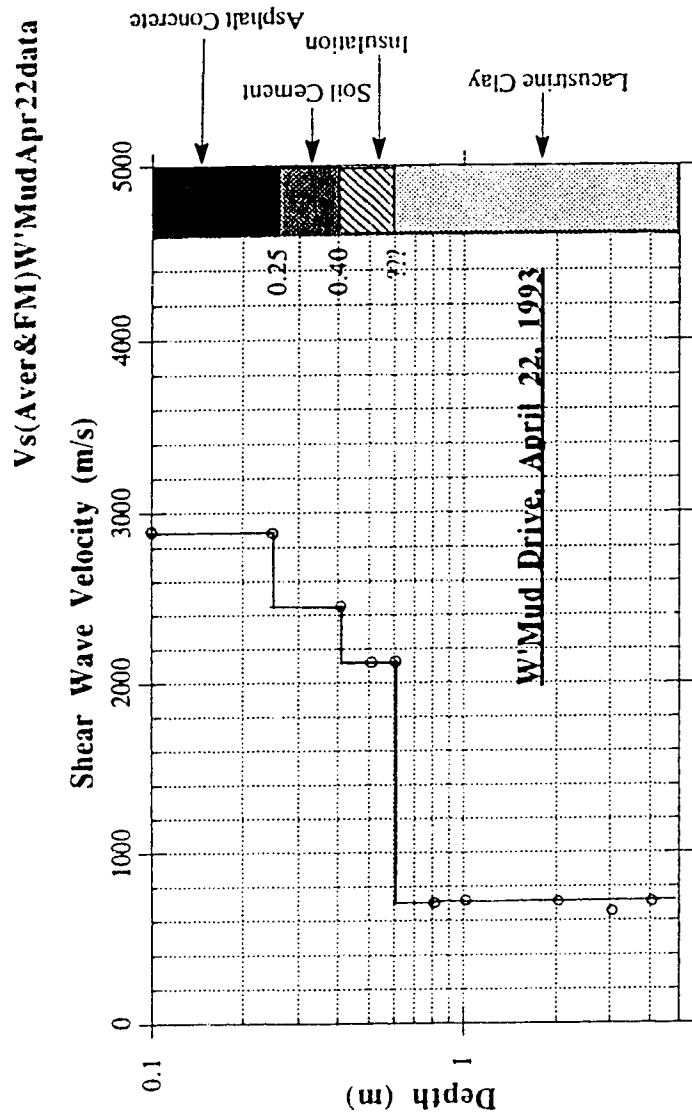


Figure A II.12 Shear Wave Velocity Profile (SASW-FM output), Whitemud Drive, April 22, 1993



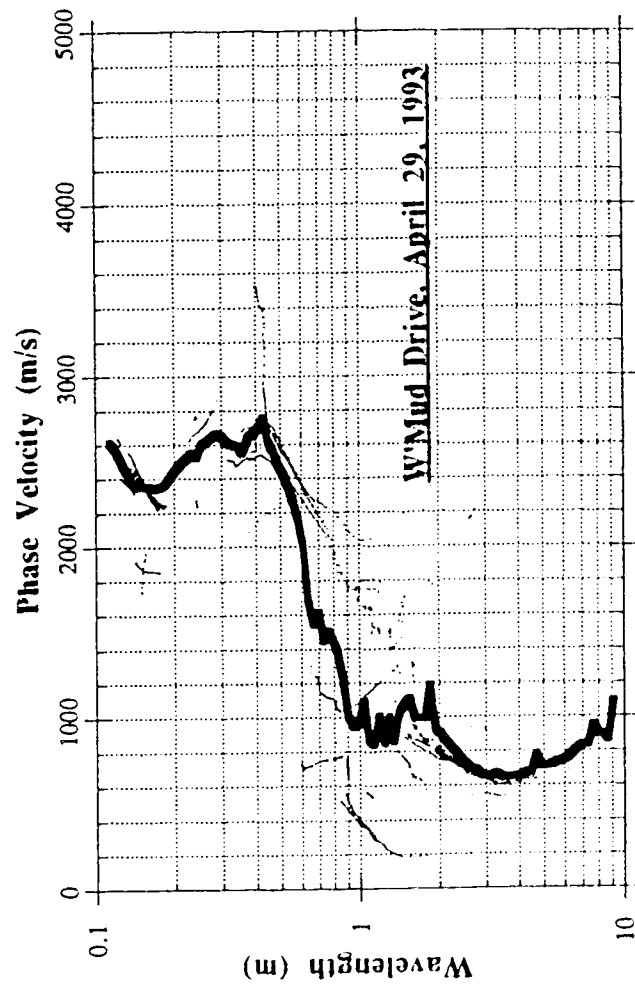


Figure A II.13 Dispersion Curve from Whitemud Drive, April 29, 1993

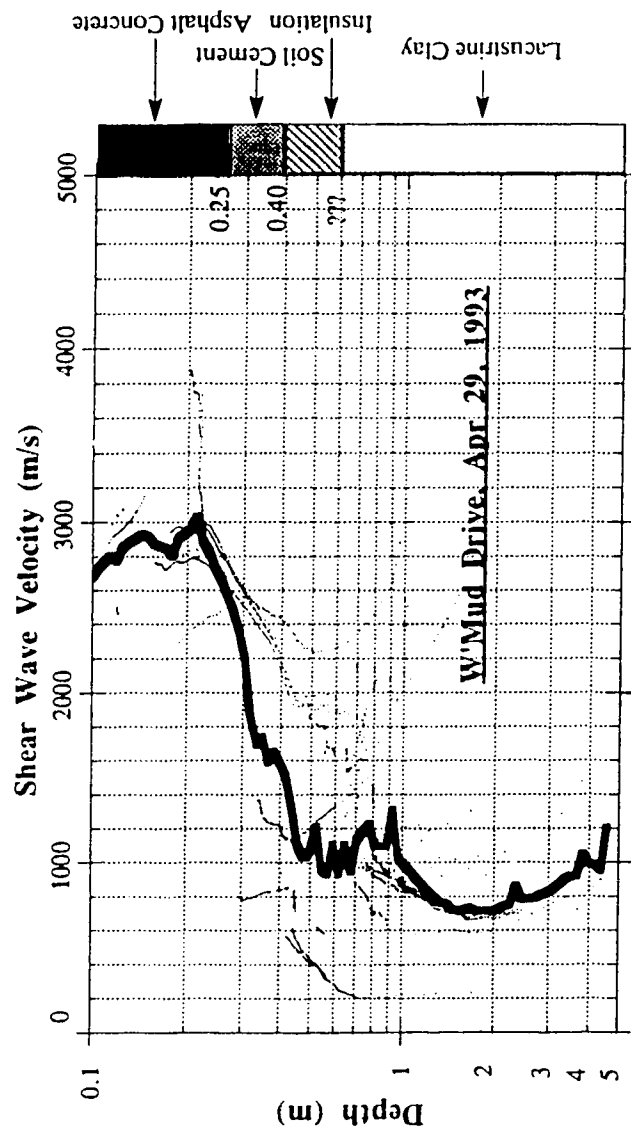


Figure A II.14 Shear wave velocity profile from Whitemud Drive, April 29, 1993

DisCur(FM)W\Mudapr29data

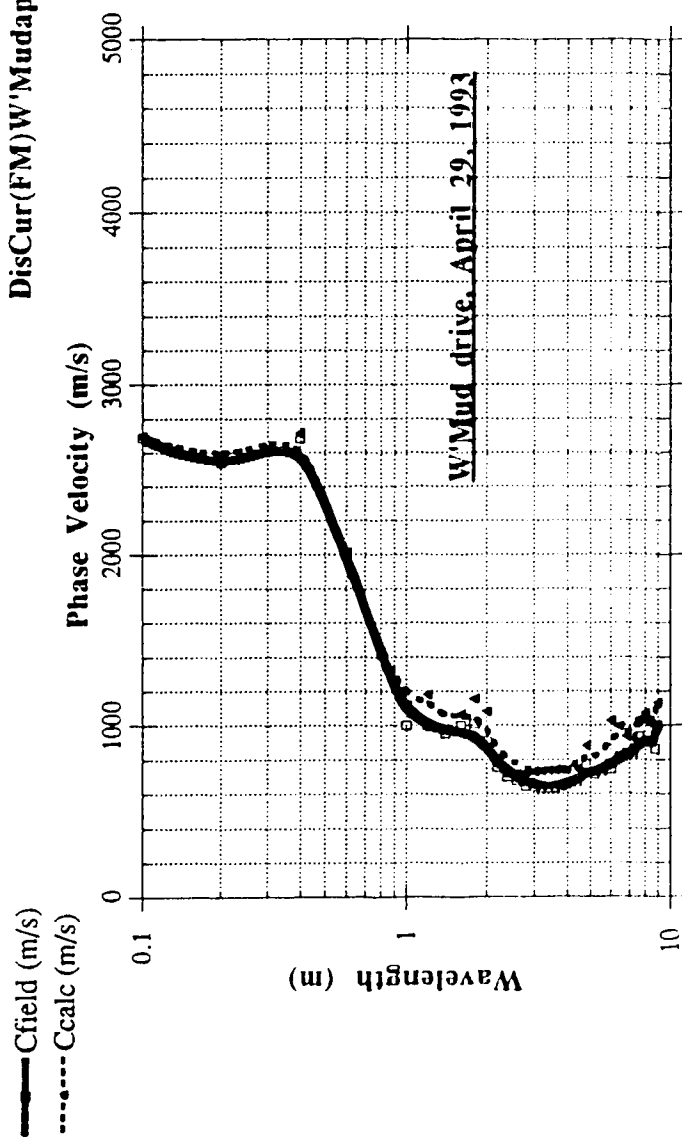


Figure A II.15 Dispersion curves (SASW-FM) From Whitemud Drive, April 29, 1993

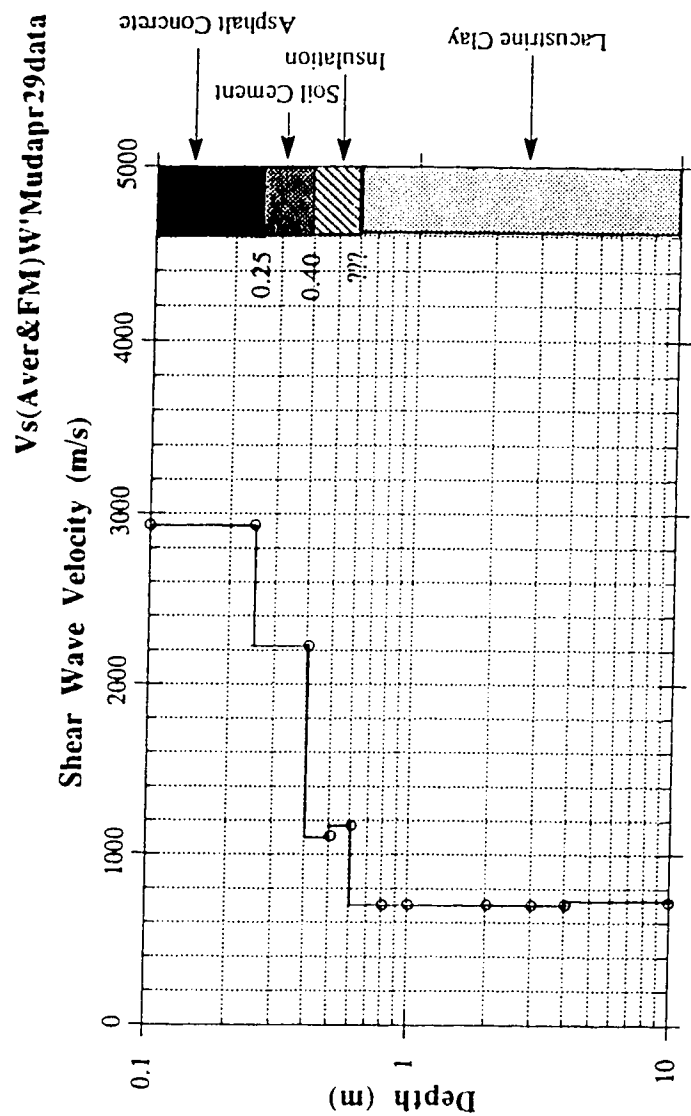


Figure A II.16 Shear Wave Velocity Profile (SASW-FM Output), Whitemud Drive, April 29, 1993

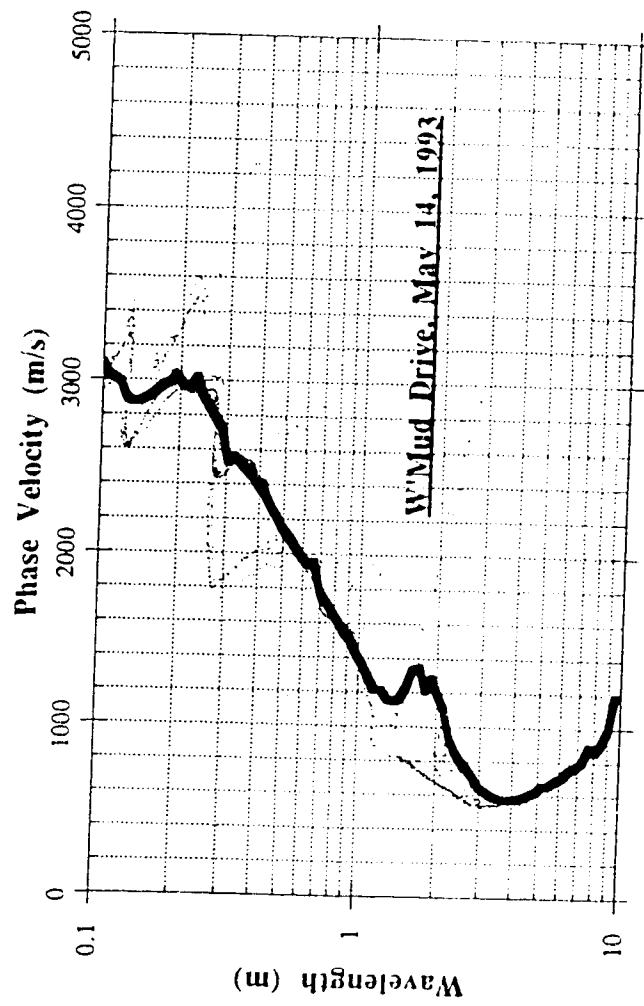


Figure A II.17 Dispersion curve from Whitemud Drive, May 14, 1993

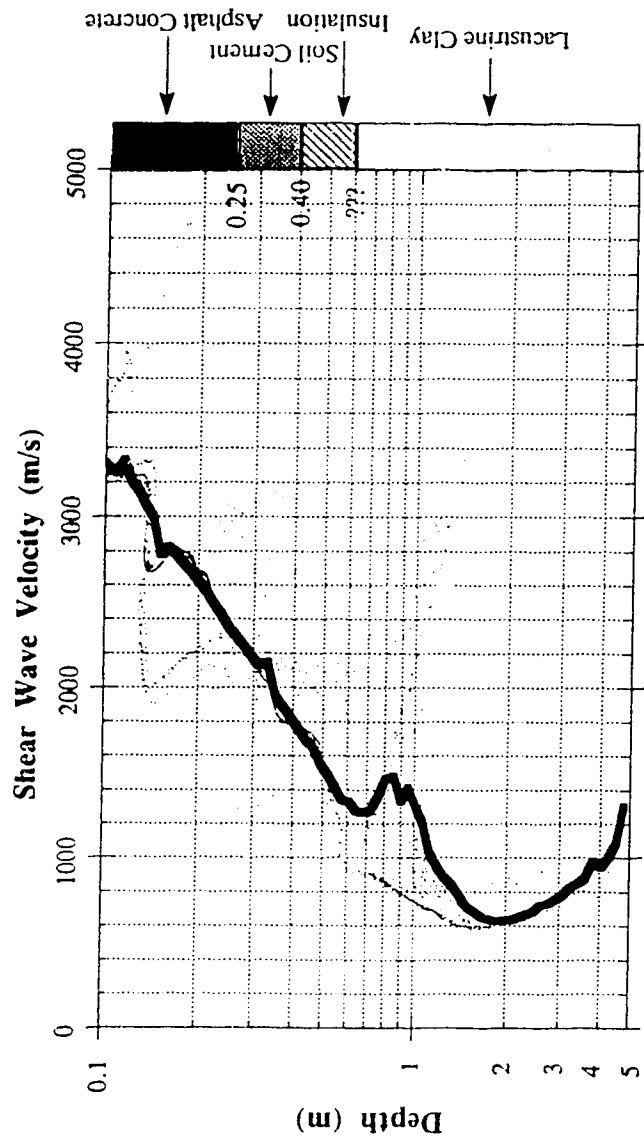


Figure A II.18 Shear wave velocity profile from Whitemud Drive, May 14, 1993

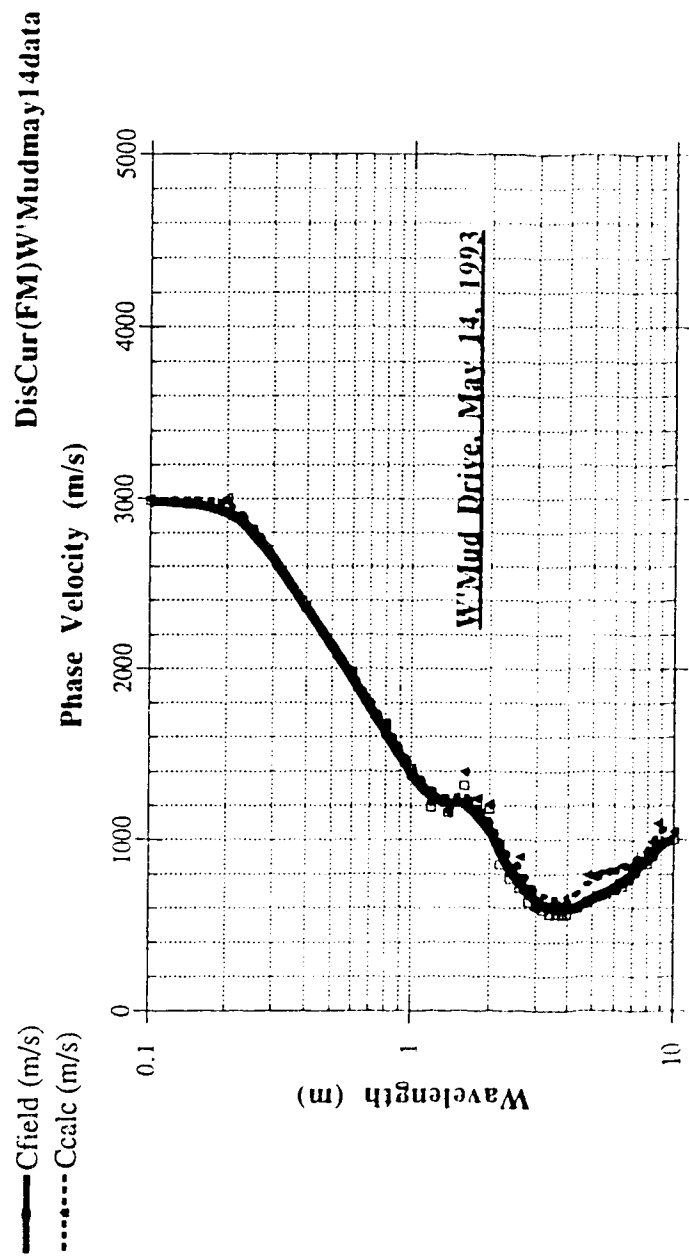


Figure A II.19 Dispersion curves (SASW-FM) from Whitemud Drive, May 14, 1993

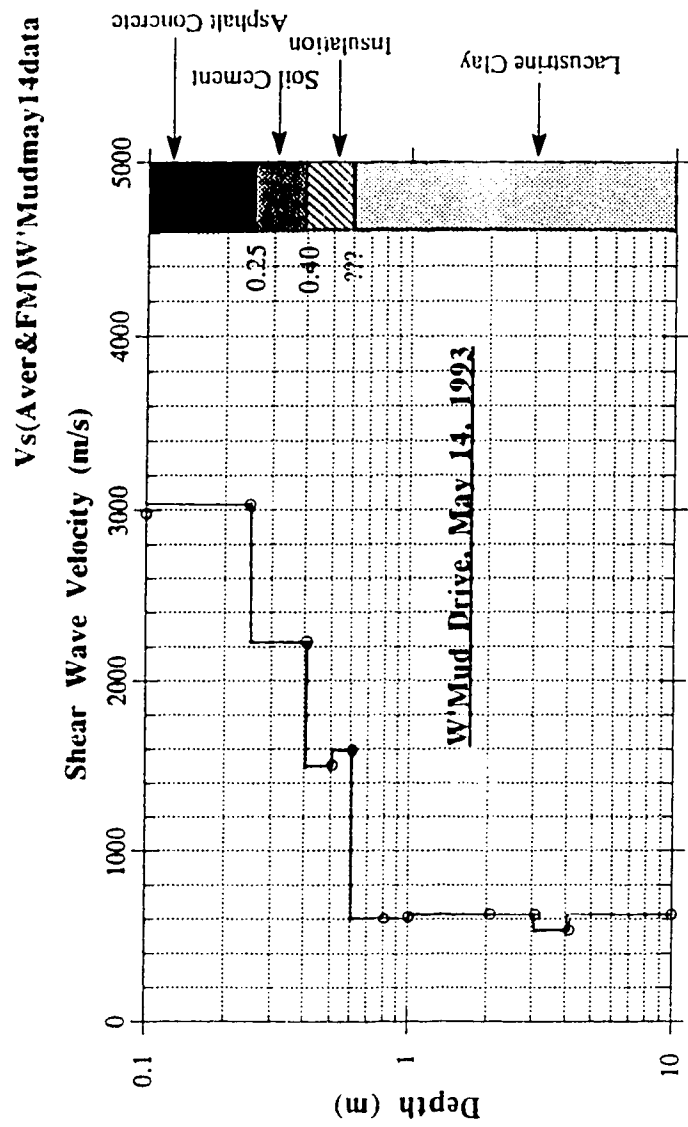


Fig. c A II.20 Shear Wave Velocity Profile (SASW-FM output), Whitemud Drive, May 14, 1993



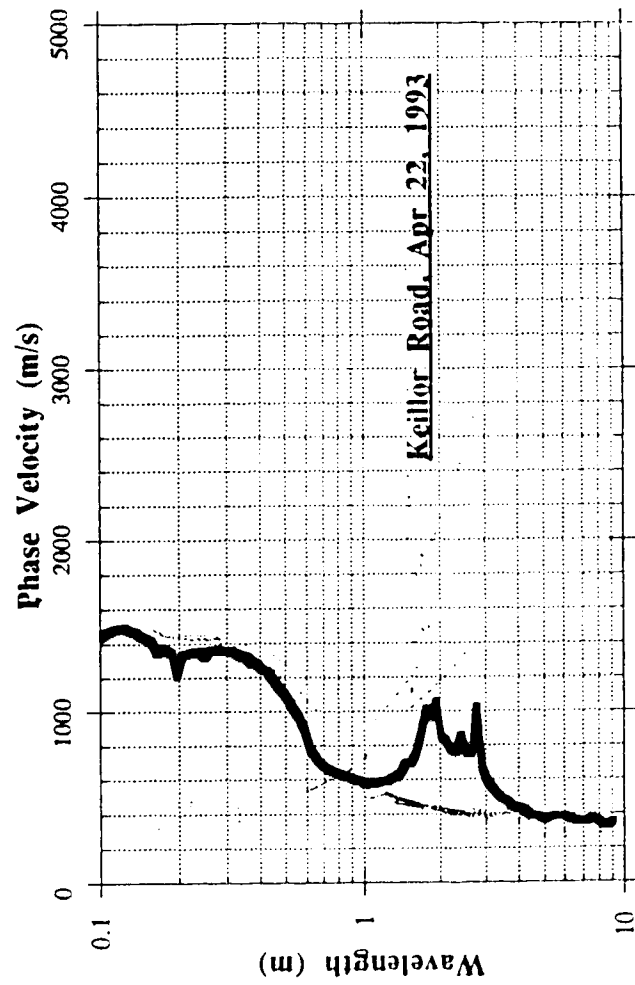


Figure A II.21 Dispersion Curve from Keillor Road, April 22, 1993

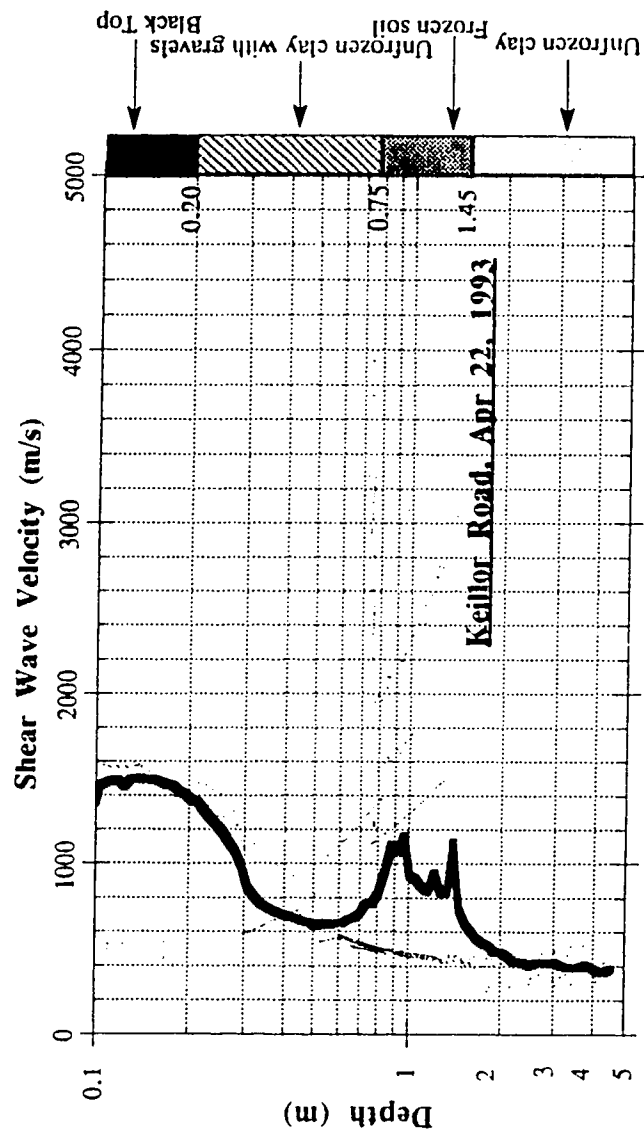


Figure A II.22 Shear wave velocity profile from Keillor Road, April 22, 1993

DisCur(FM)Keilrapr22data

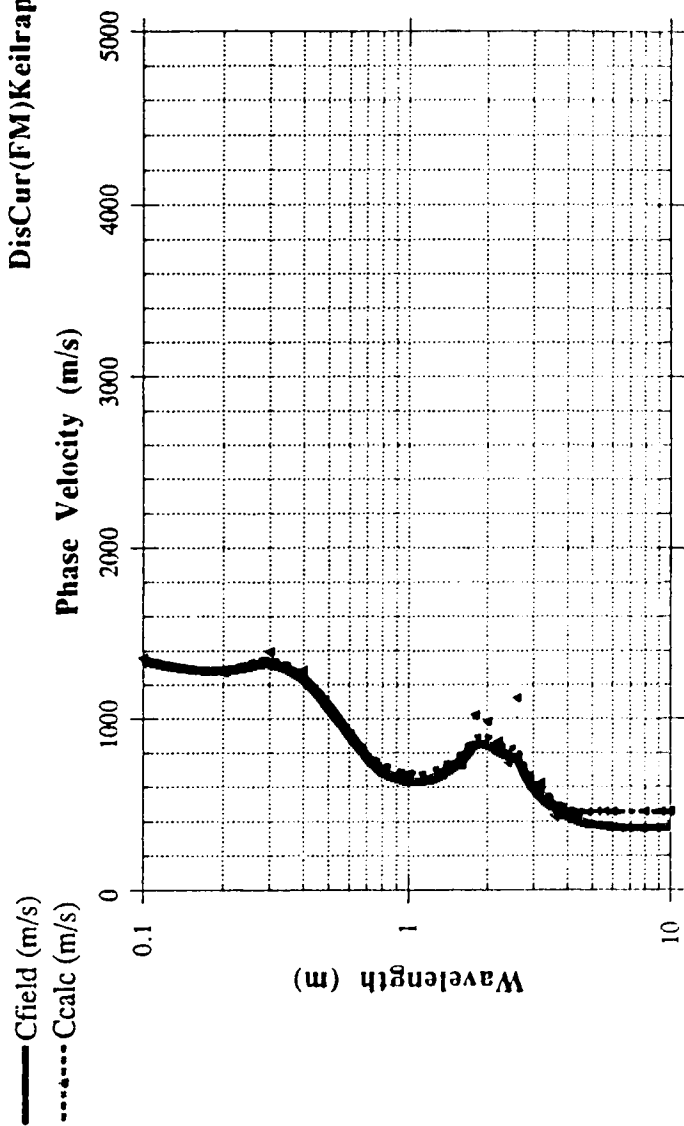


Figure A II.23 Dispersion curves (SASW-FM) from Keillor Road, April 22, 1993

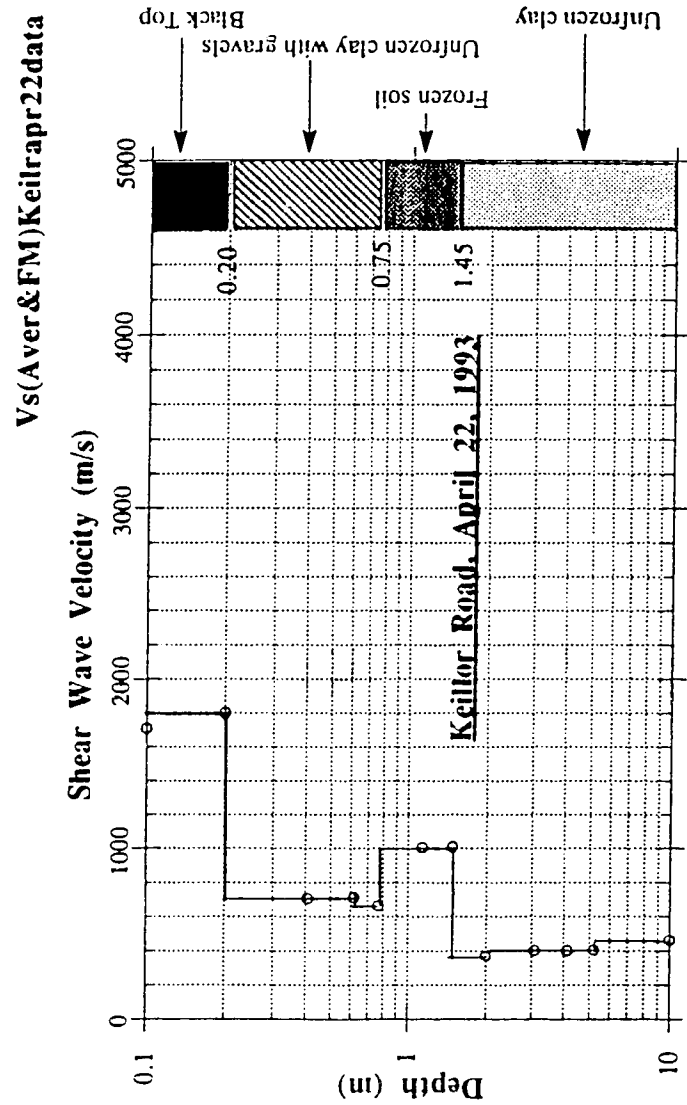


Figure A 11.24 Shear Wave Velocity Profile (SASW-FM output) from Keillor Road, April 22, 1993

**Fig7.59 & 60 & 62 & 63 data**

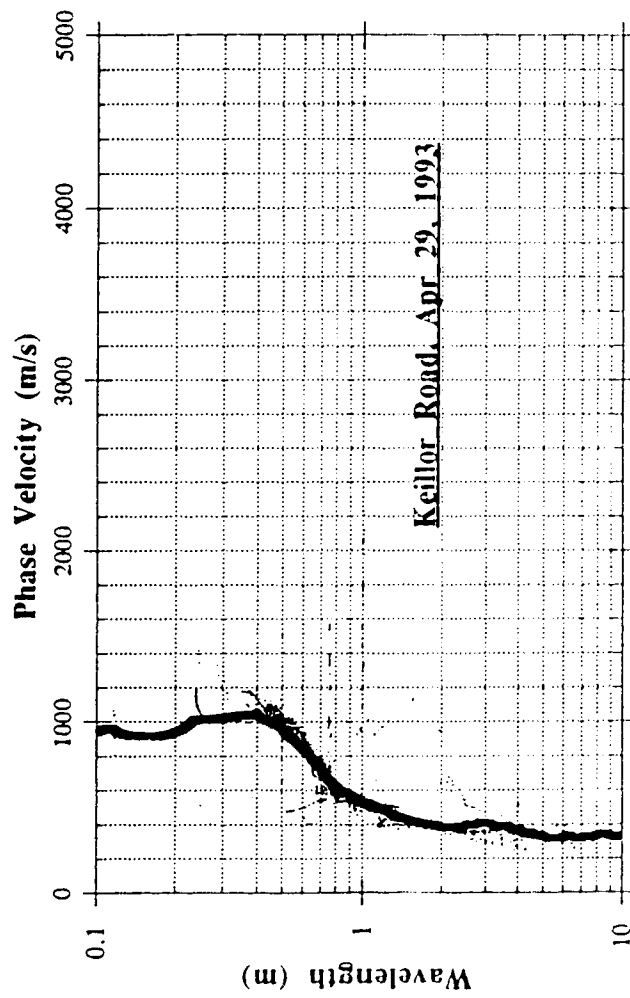


Figure A II.25 Dispersion Curve from Keillor Road, April 29, 1993

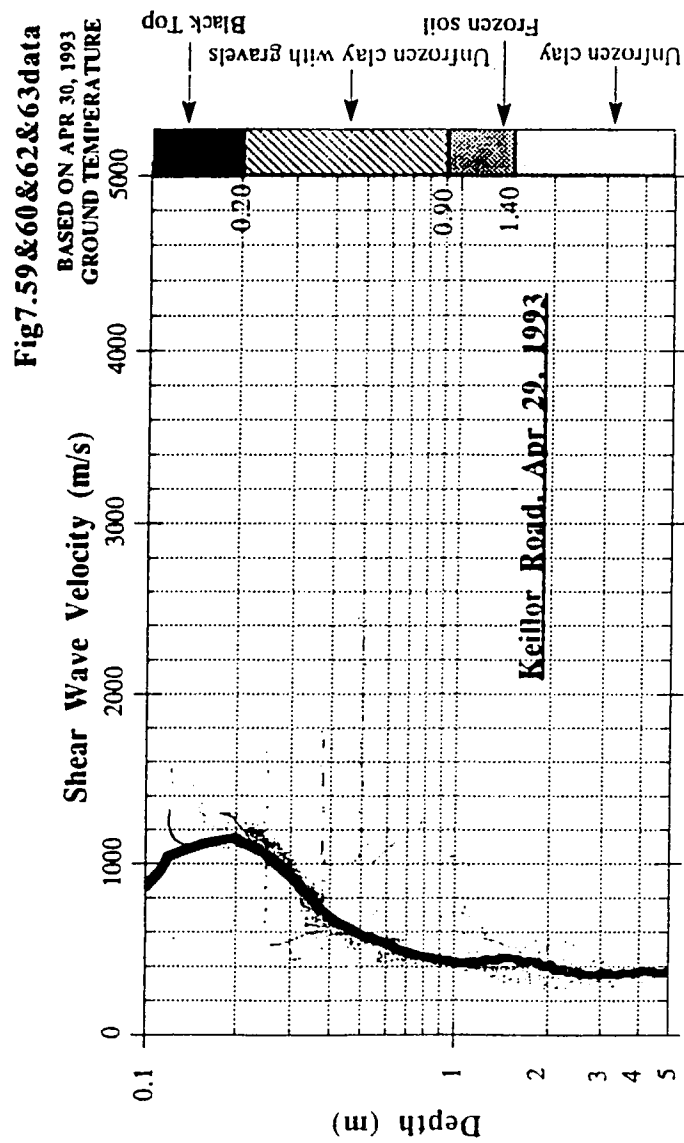


Figure A II.26 Shear wave velocity profile from Keillor Road, April 29, 1993

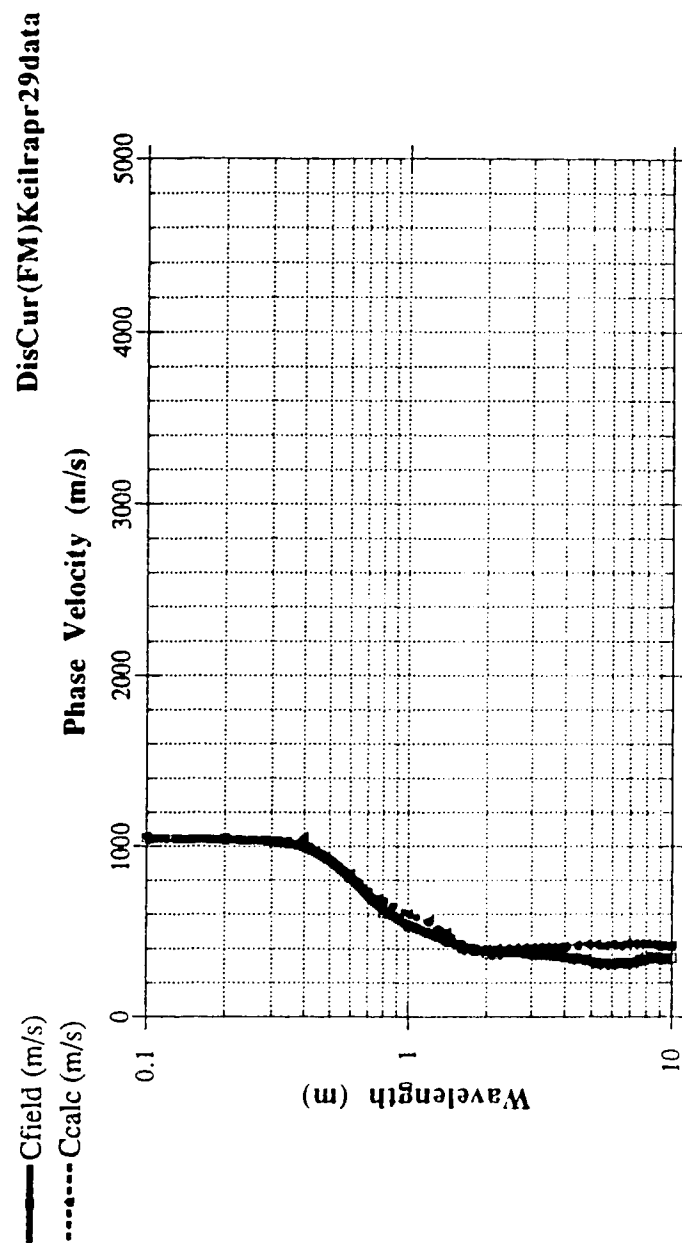


Figure A II.27 Dispersion curves (SASW-FM) from Keillor Road, April 29, 1993

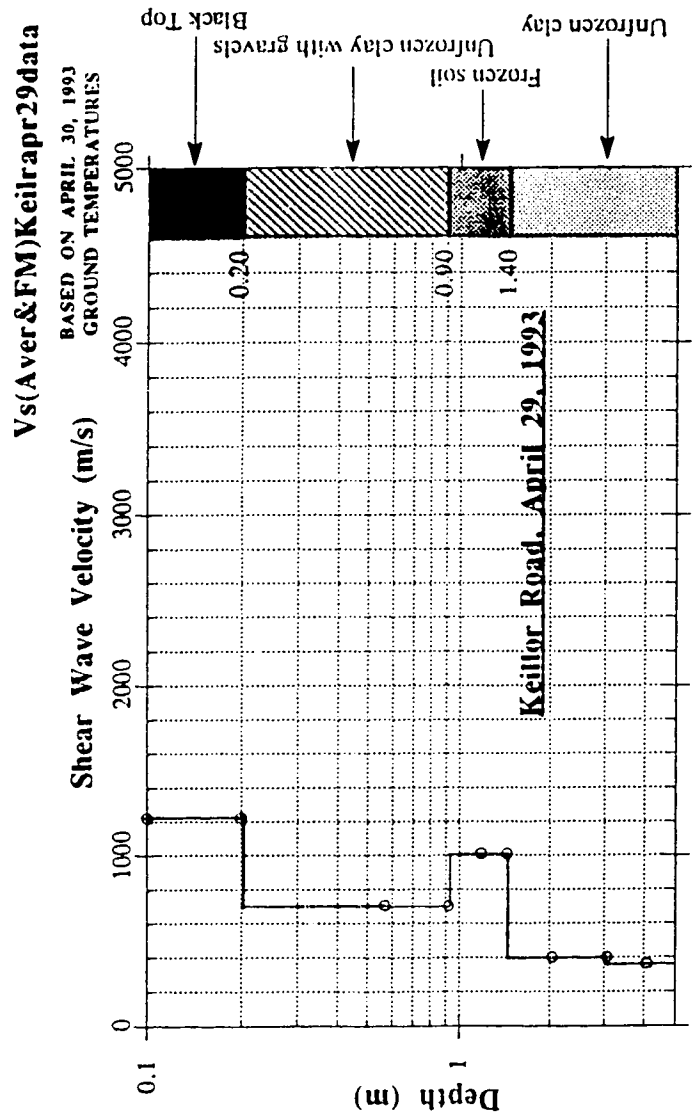


Figure A II.28 Shear Wave Velocity Profile (SASW-FM output) from Keillor Road, April 29, 1993



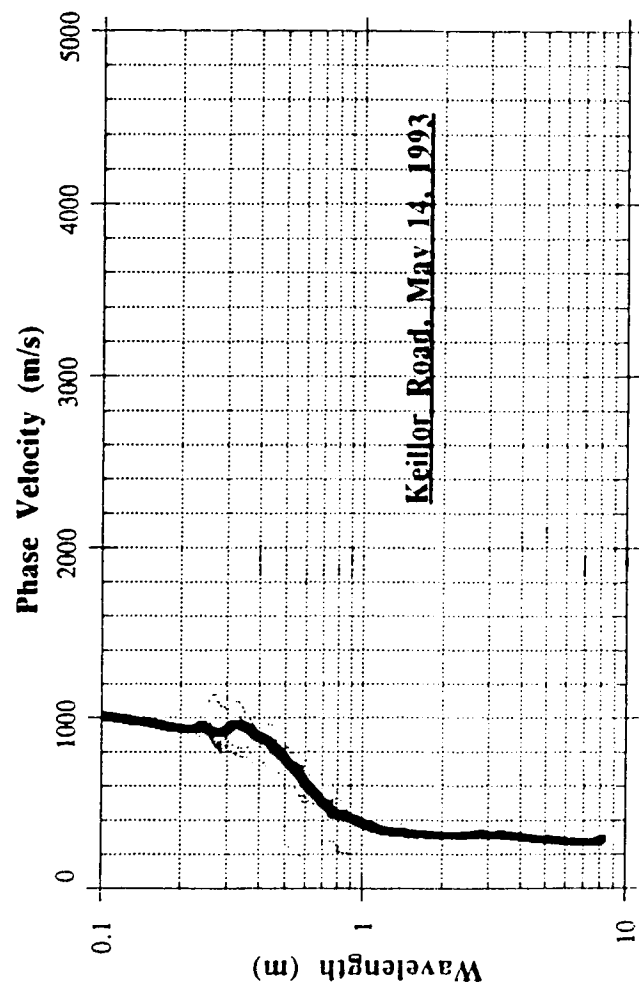


Figure A II.29 Dispersion Curve from Keillor Road, May 14, 1993

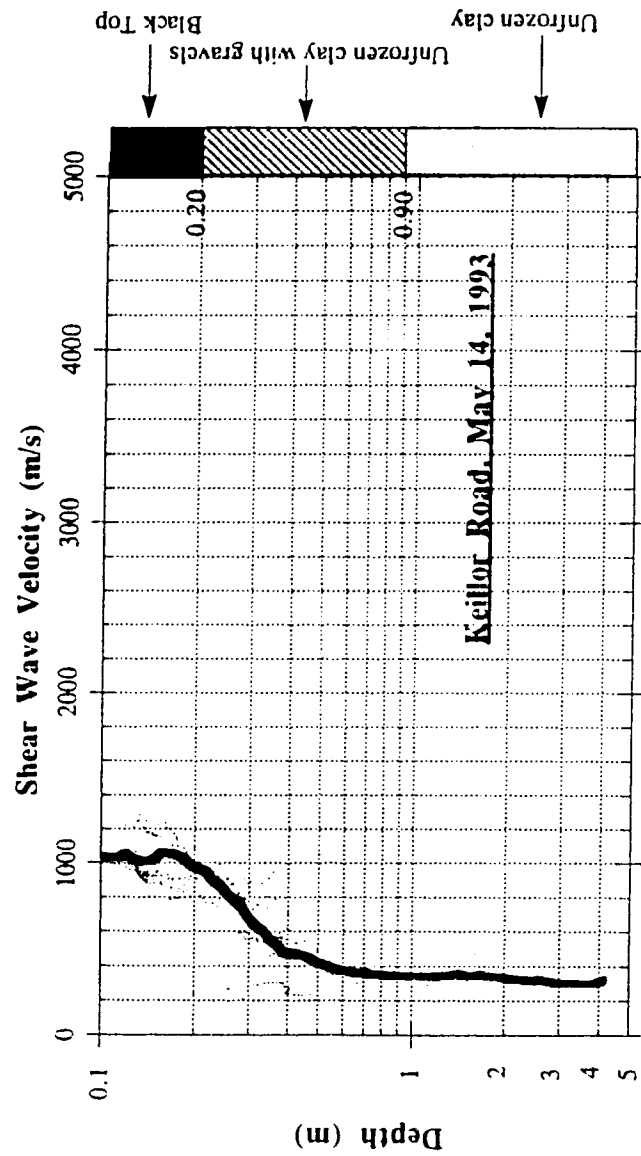


Figure A II.30 Shear wave velocity profile from Keillor Road, May 14, 1993

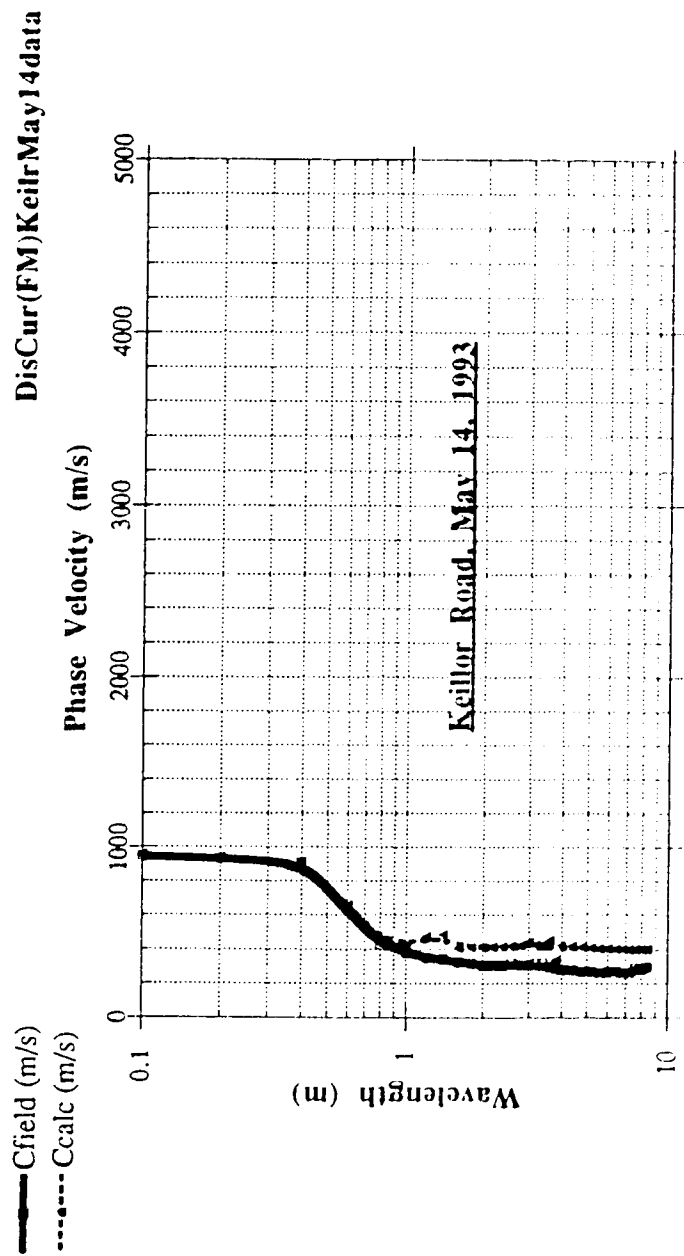


Figure A II.31 Dispersion curves (SASW-FM) from Keillor Road, May 14, 1993

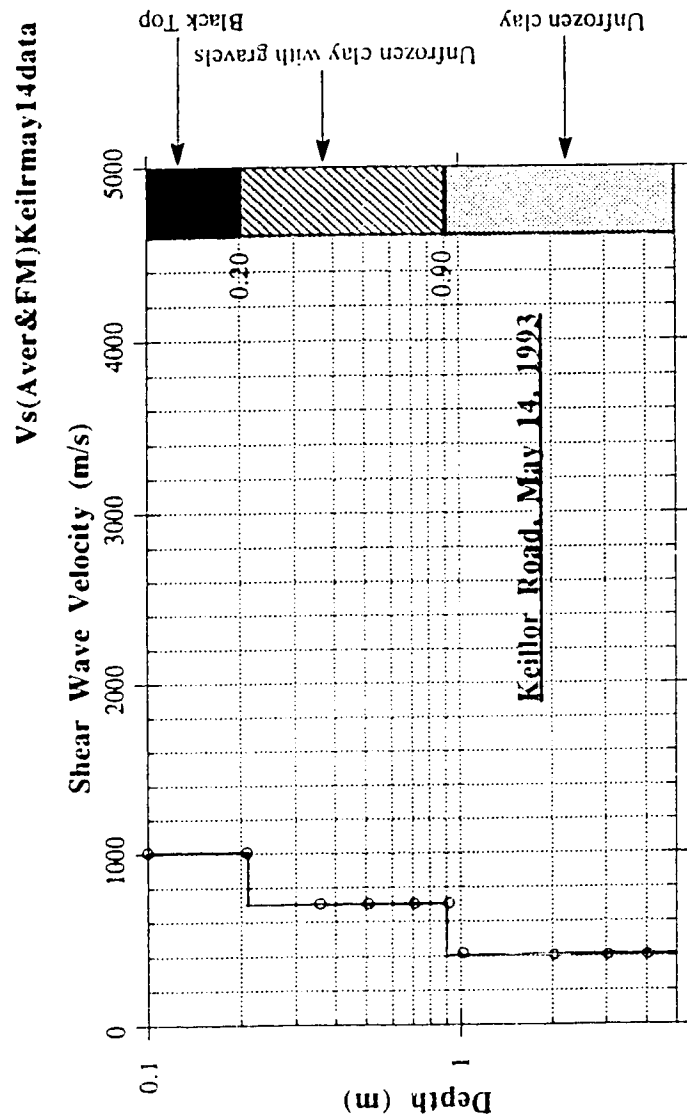


Figure A II.32 Shear Wave Velocity Profile (SASW-FM output) from Keillor Road, May 14, 1993

## **APPENDIX III**

### **Effect of SASW-FM Input Parameters on SASW Output Results**

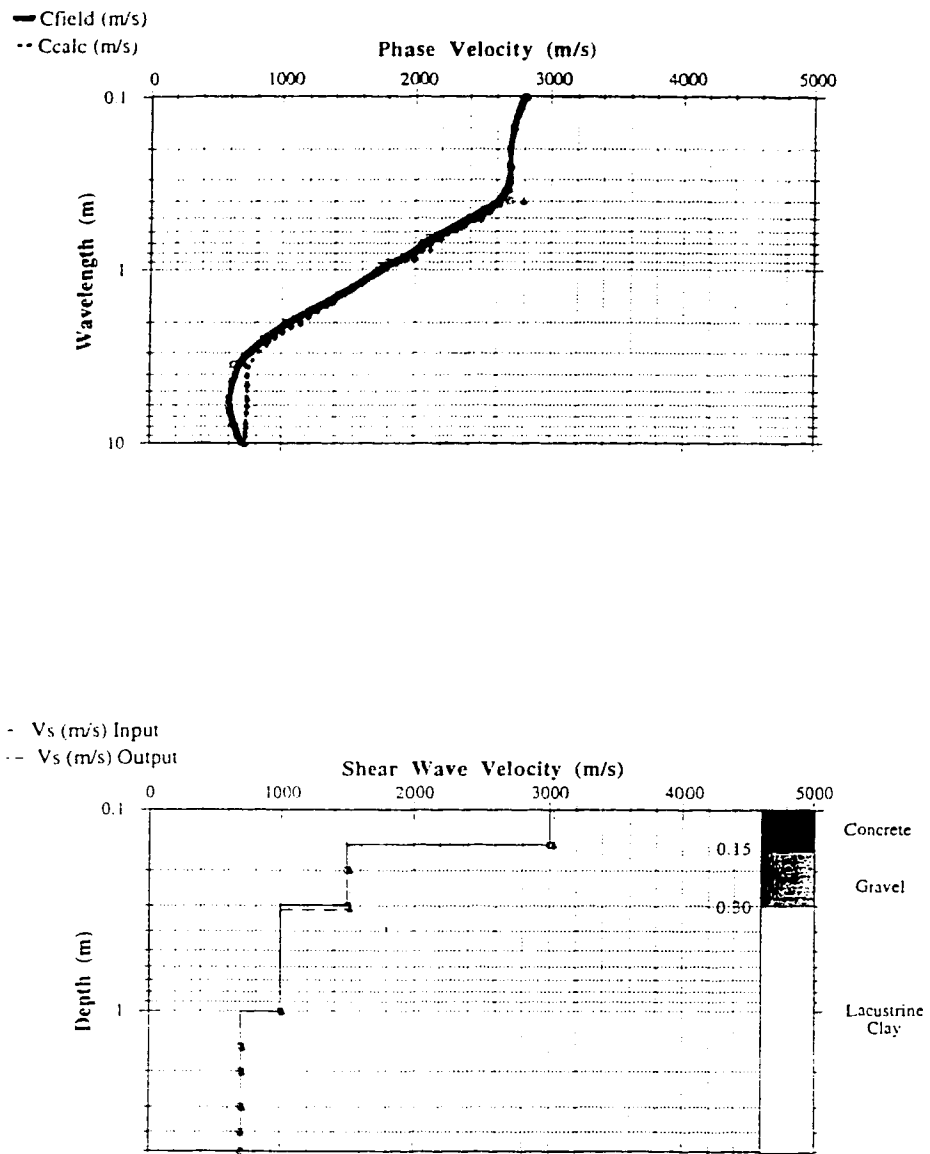


Figure A III.1 Effect of SASW-FM Input Parameters on SASW-FM Output Results  
(Set 1: Room CEB-B11, Basement Slab)

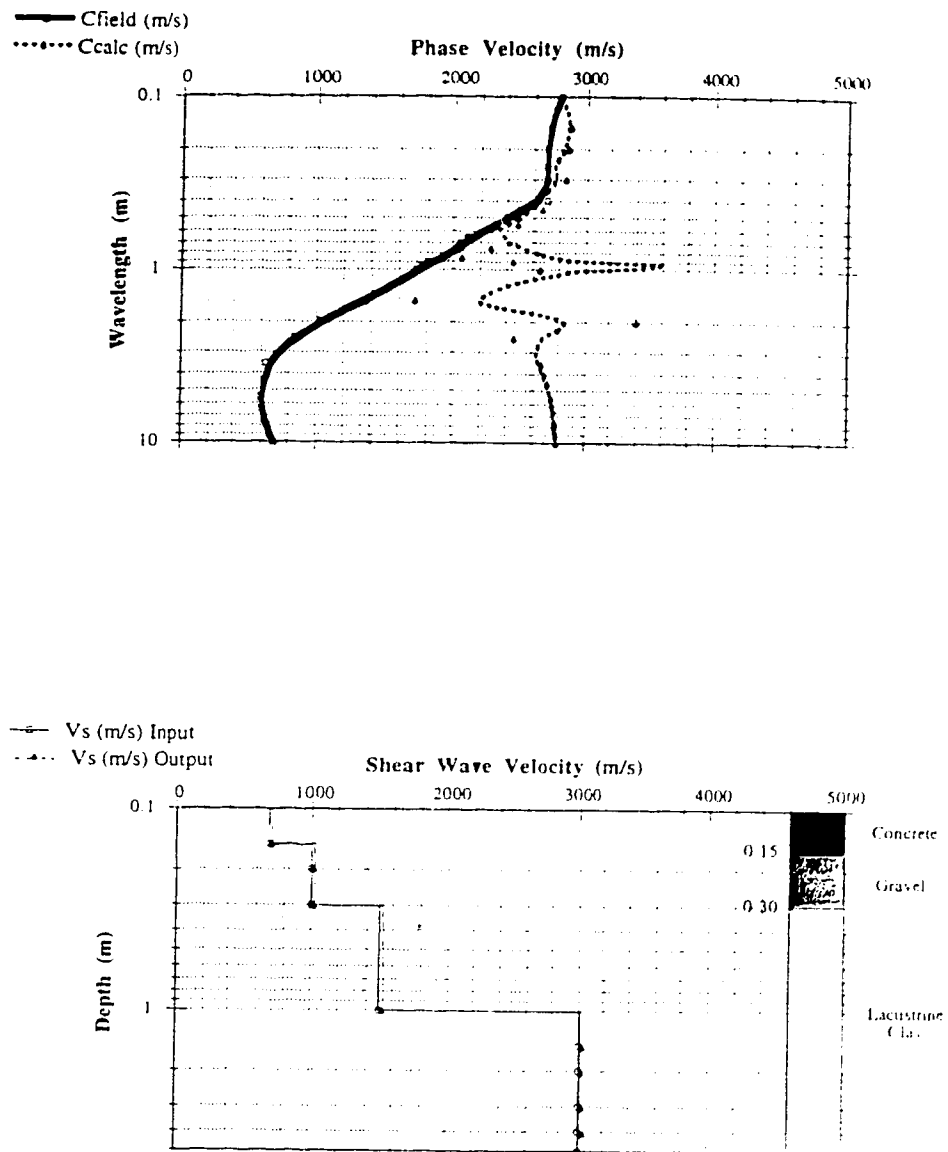


Figure A III.2 Effect of SASW-FM Input Parameters on SASW-FM Output Results  
(Set 2: Room CEB-B11, Basement Slab)

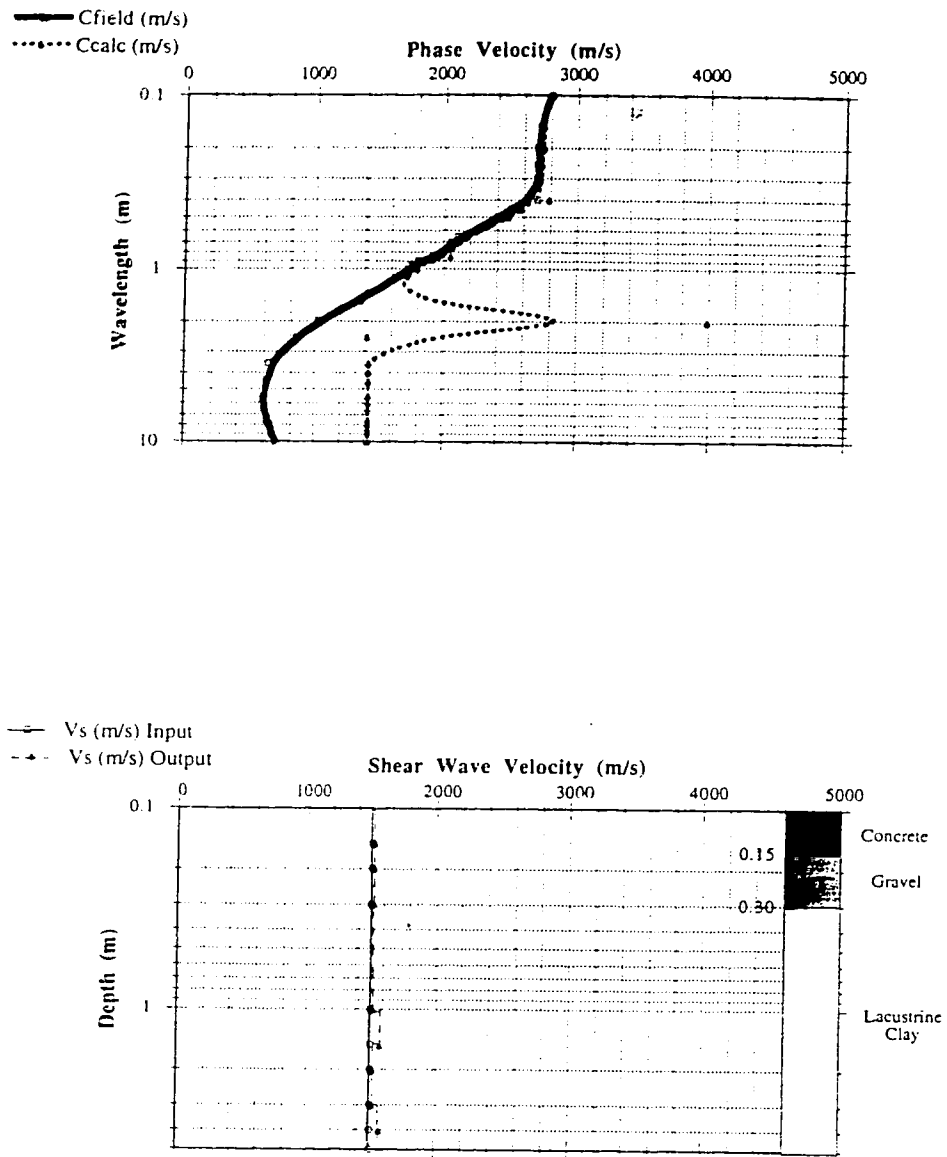


Figure A III.3 Effect of SASW-FM Input Parameters on SASW-FM Output Results  
(Set 3: Room CEB-B11, Basement Slab)



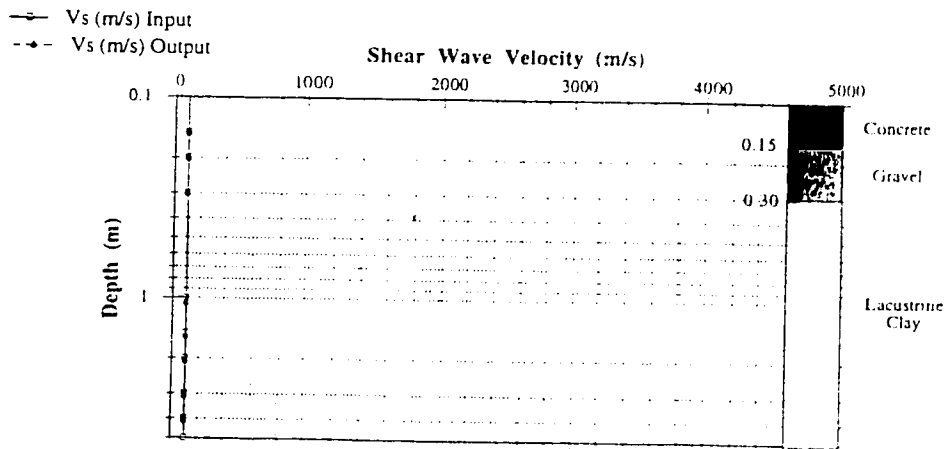
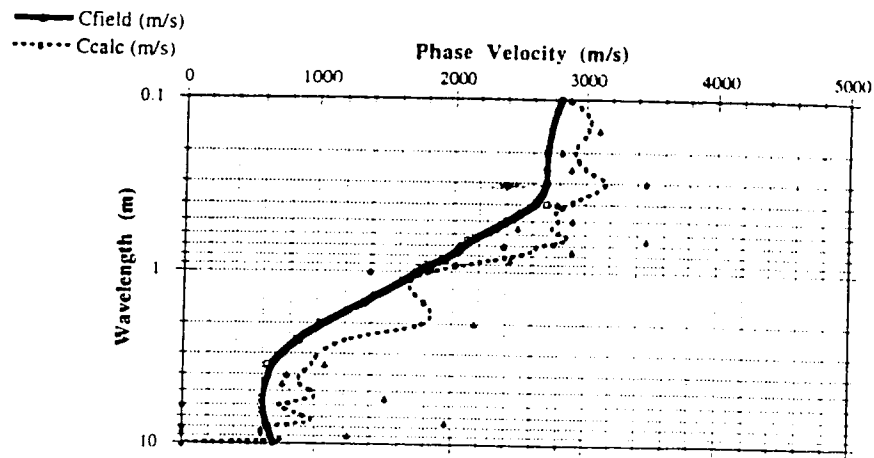


Figure A III.4 Effect of SASW-FM Input Parameters on SASW-FM Output Results  
(Set 4: Room CEB-B11, Basement Slab)

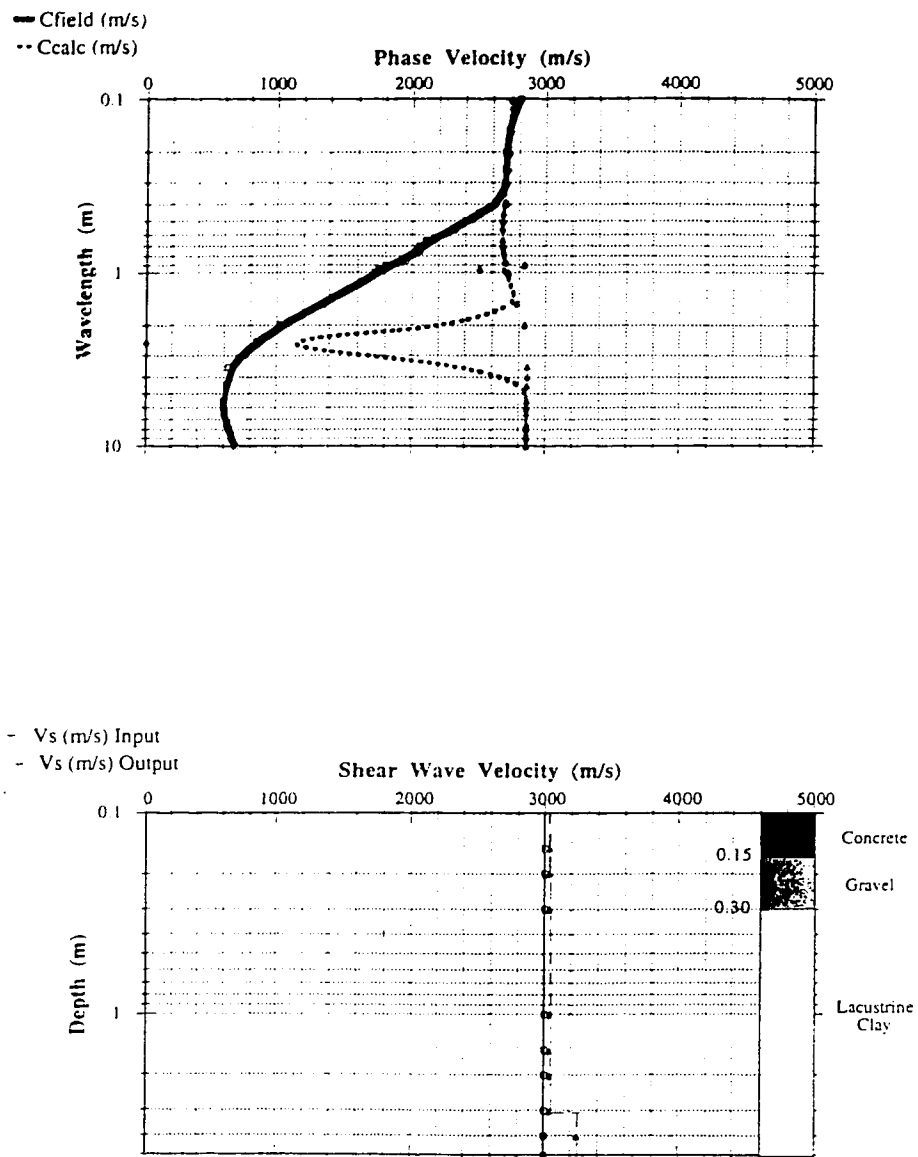


Figure A III.5 Effect of SASW-FM Input Parameters on SASW-FM Output Results  
(Set 5: Room CEB-B11, Basement Slab)

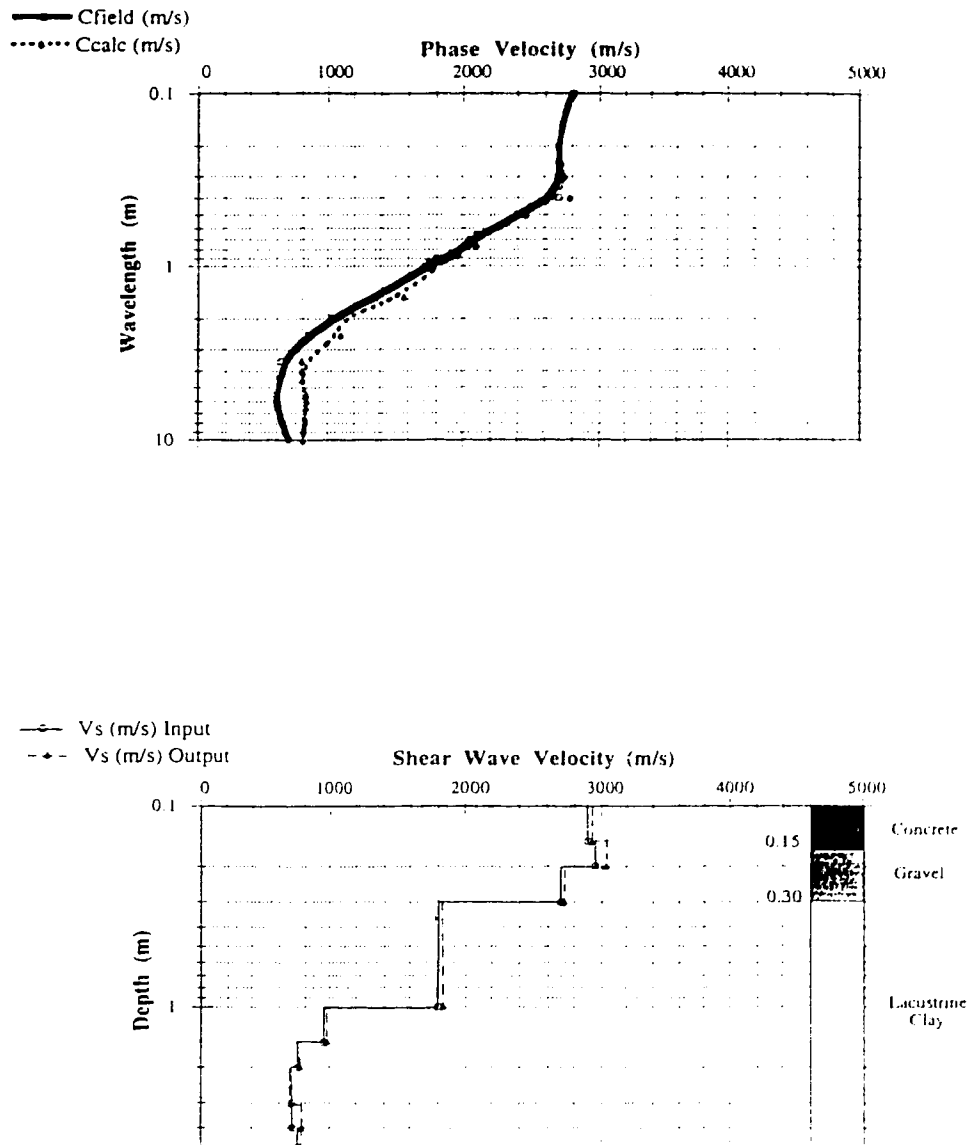


Figure A III.6 Effect of SASW-FM Input Parameters on SASW-FM Output Results  
(Set 6: Room CEB-B11, Basement Slab)

# **APPENDIX IV**

## **Modulus Profiles**

**b11nov92 MODULUS data**

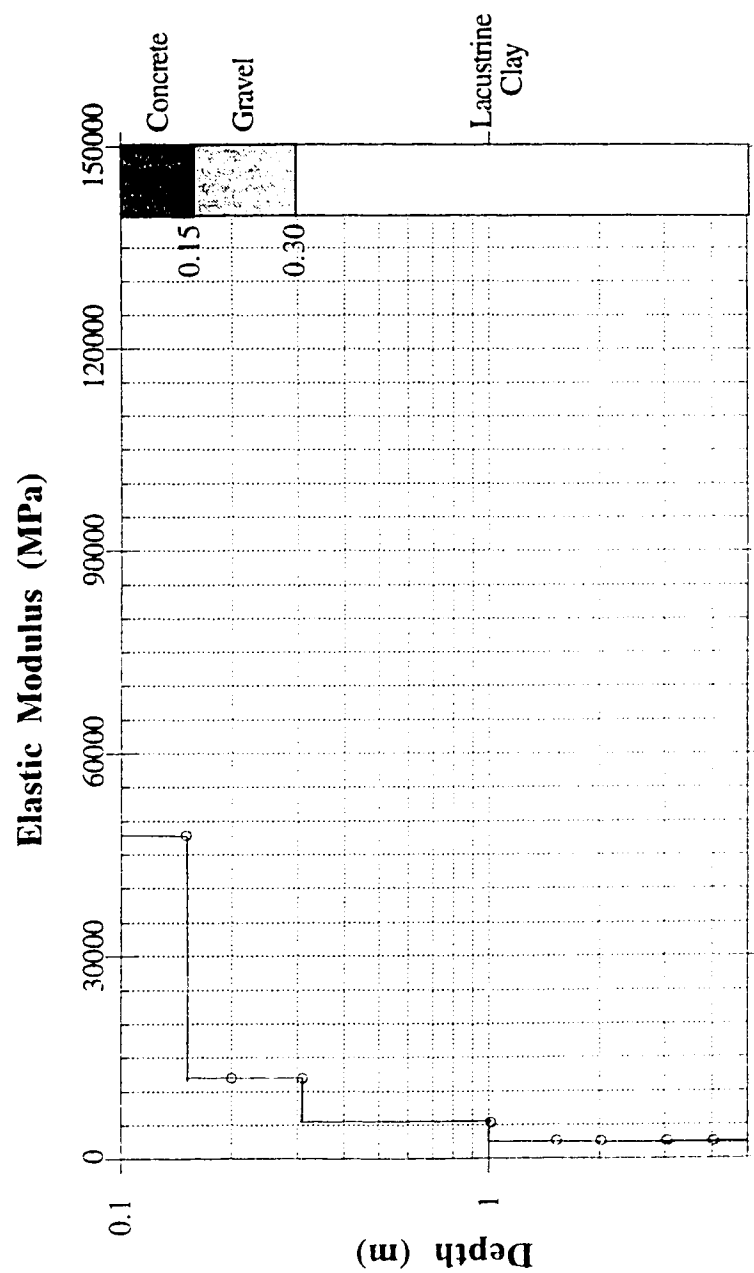


Figure A IV.1 Modulus Profile, Room CEB-B11, November 1992

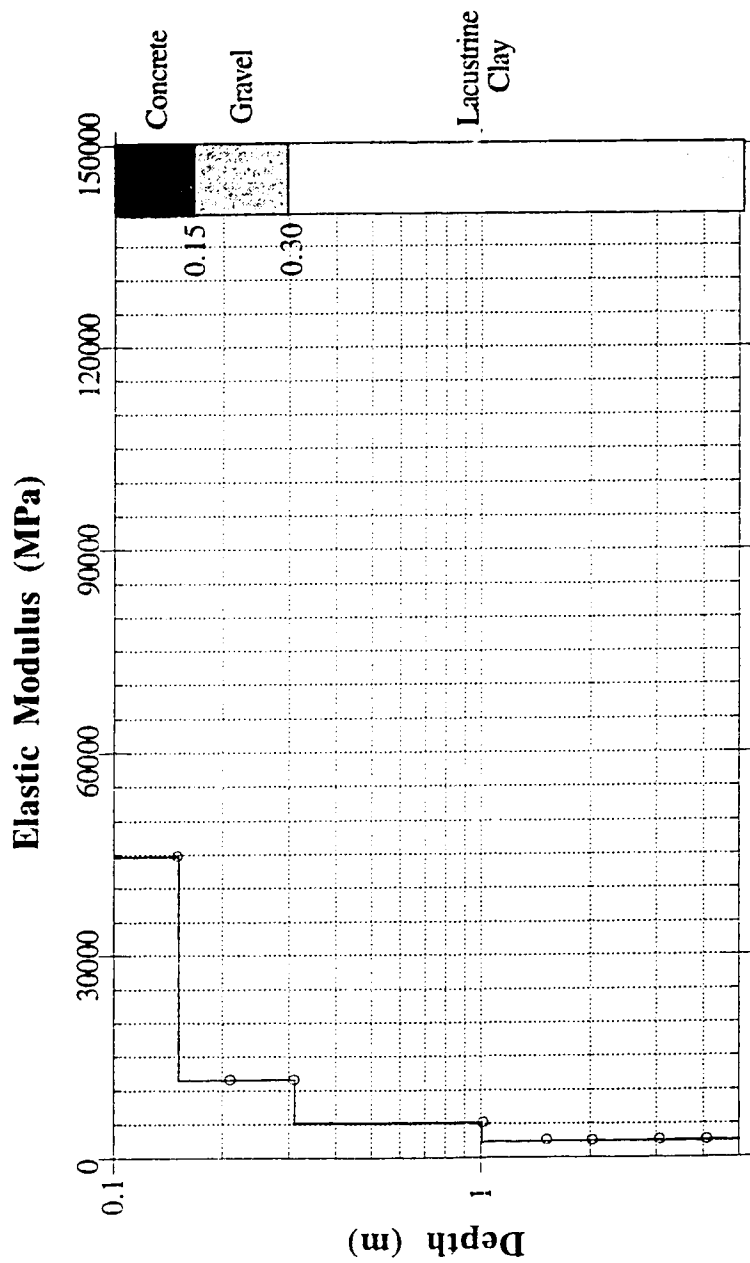


Figure A IV.2 Modulus Profile, Room CEB-B11, May 1993

# LRTCC MODULUS data

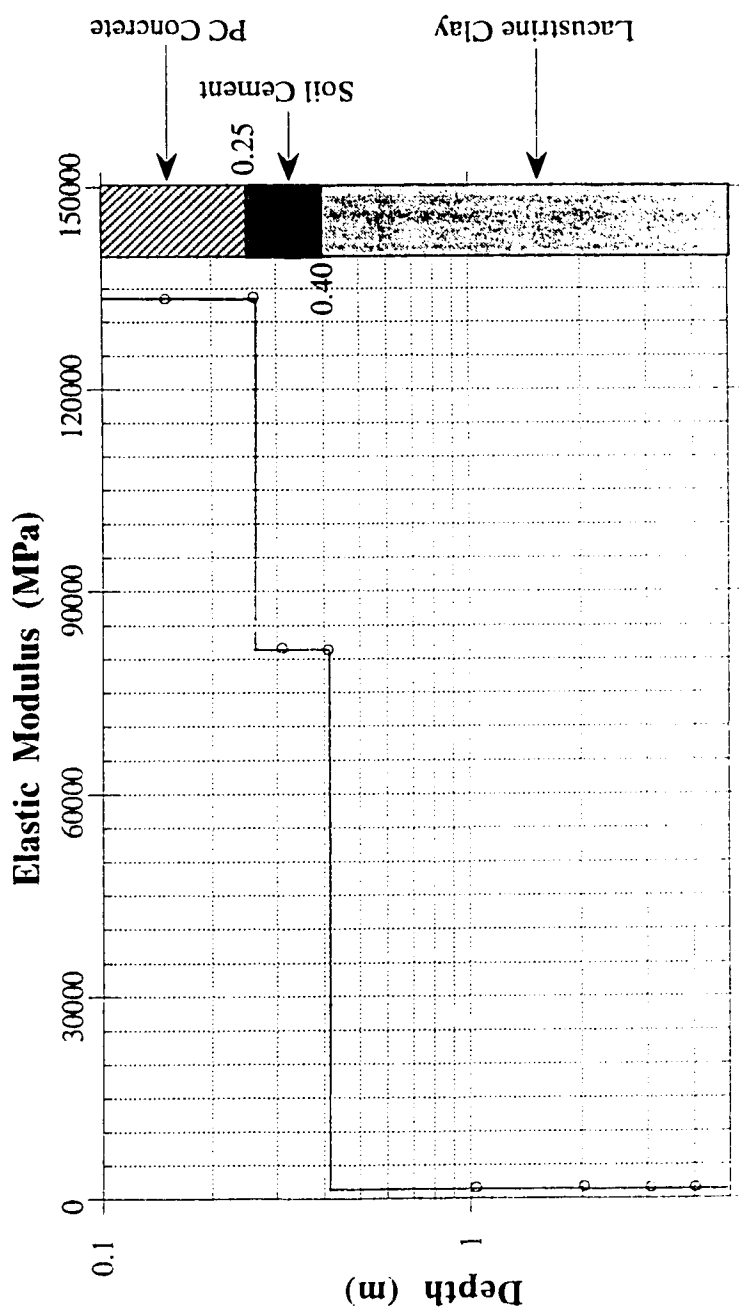


Figure A IV.3 Modulus Profile, Pavement Section CC

# LRTEE MODULUS data

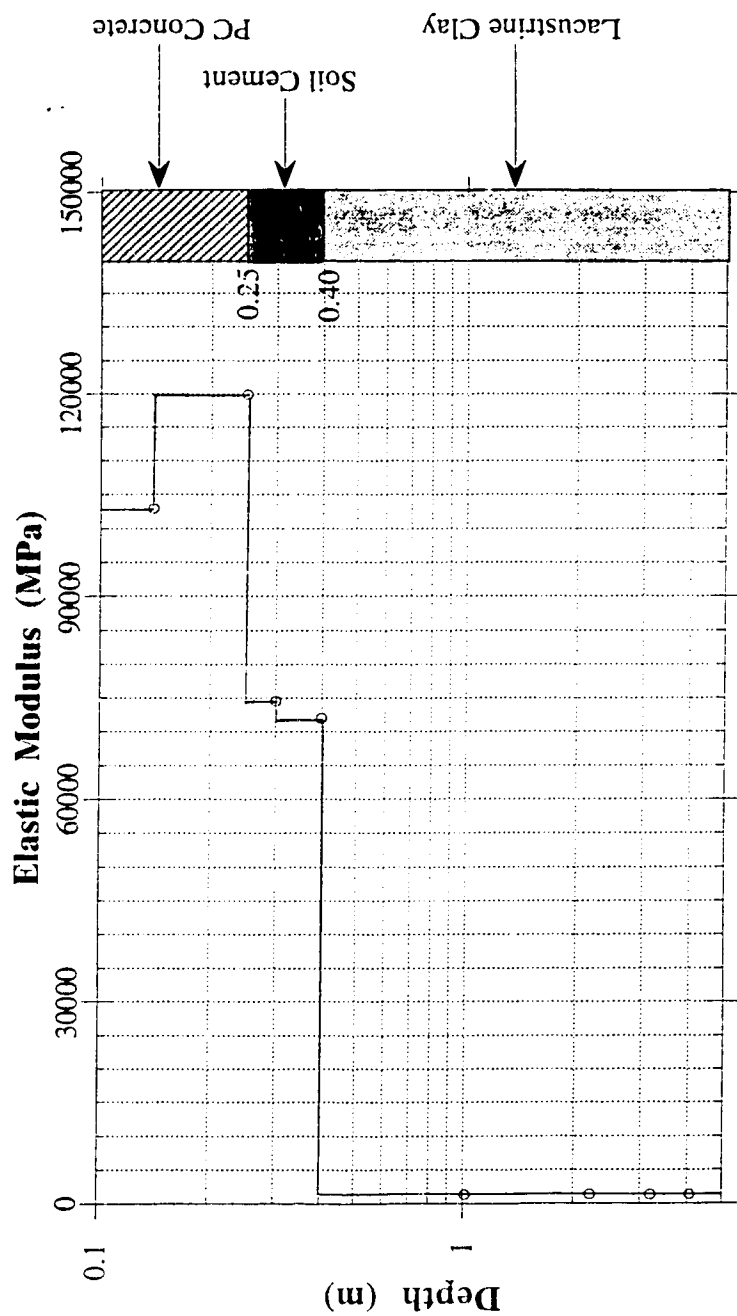


Figure A IV.4 Modulus Profile, Pavement Section EE



# **LRTFF MODULUS data**

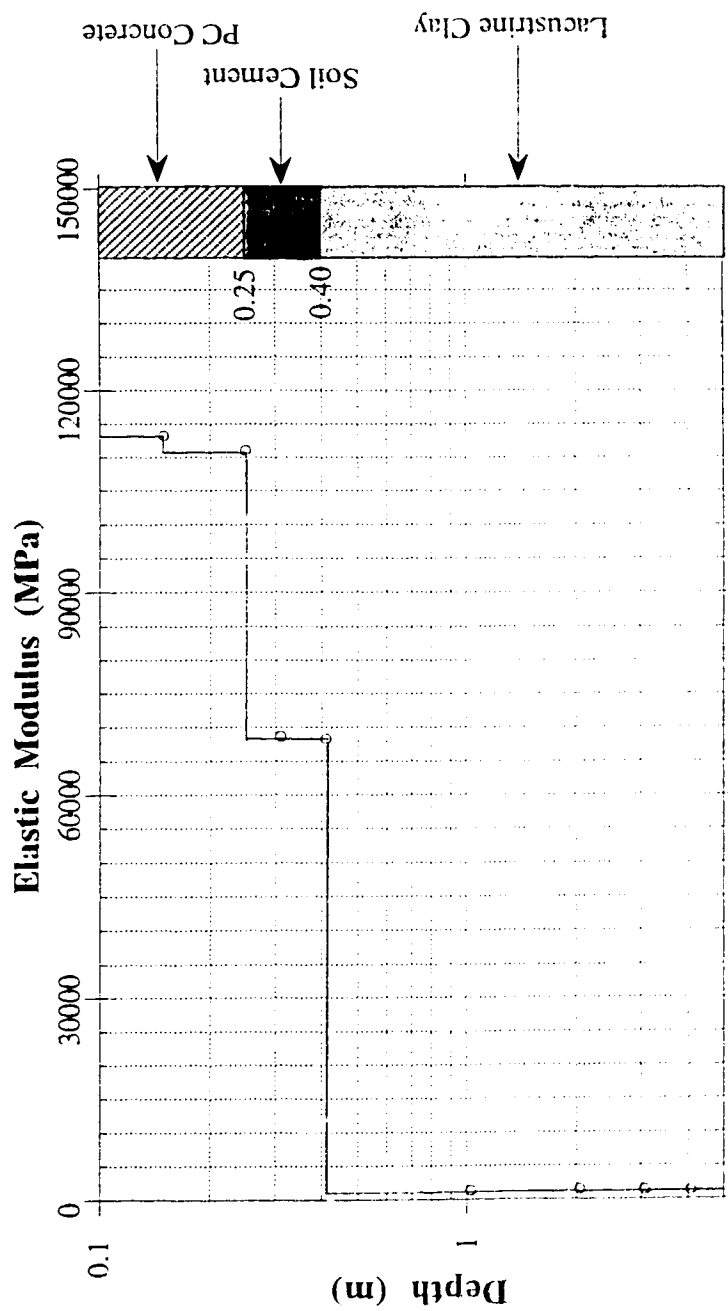


Figure A IV.5 Modulus Profile, Pavement Section FF

# W'MudApr9 MODULUS data

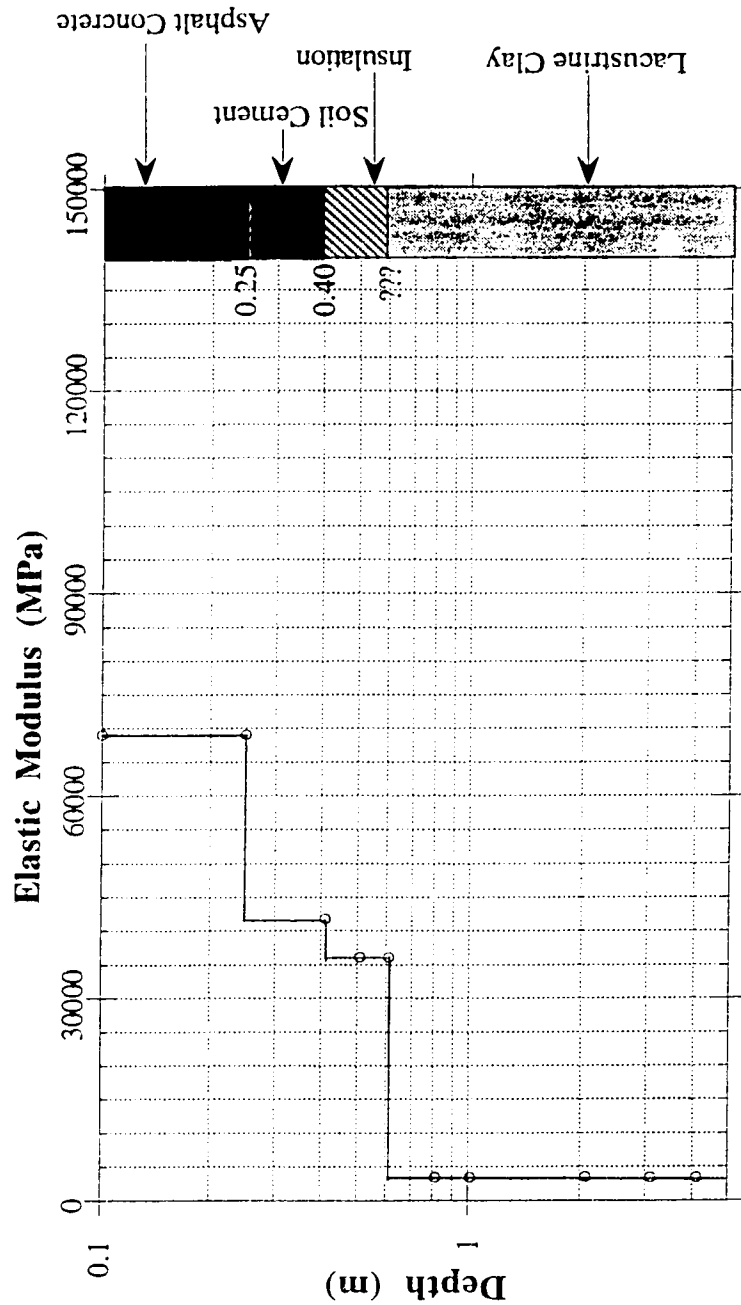


Figure A IV.6 Modulus Profile, Whitemud Drive, April 9, 1993

# W'MudApr22 MODULUS data

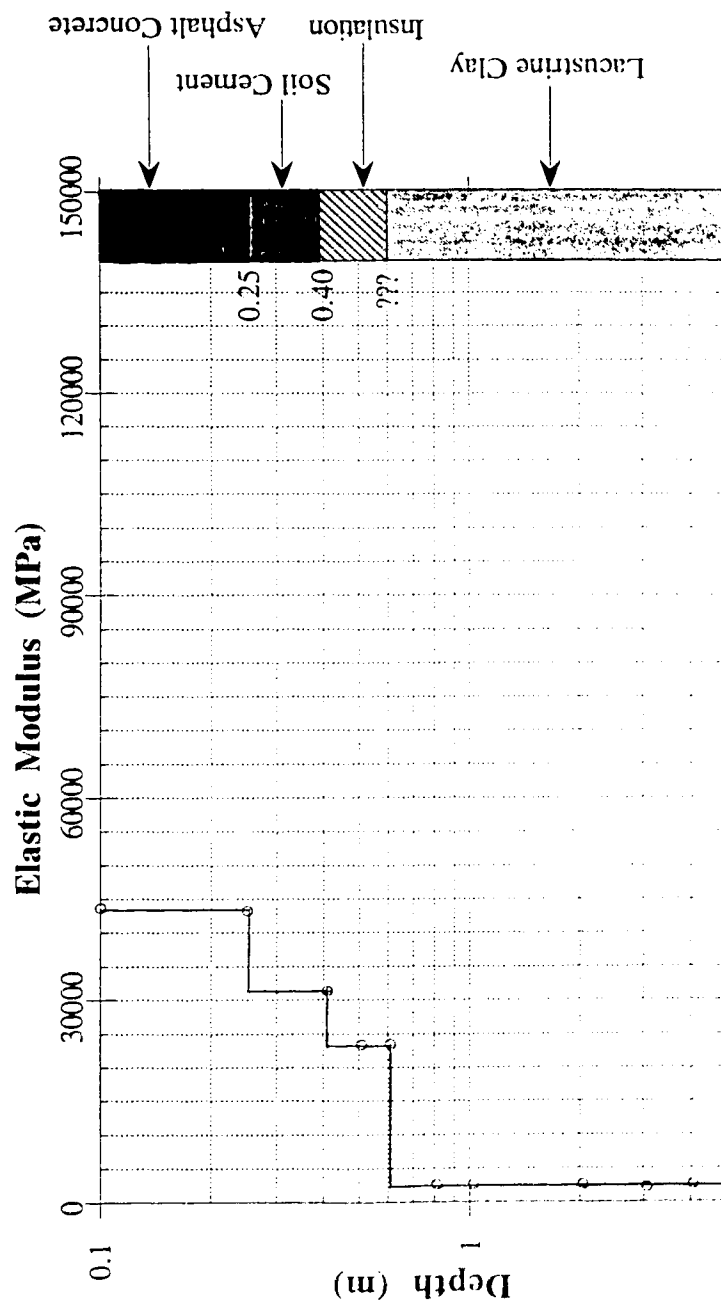


Figure A IV.7 Modulus Profile, Whitemud Drive, April 22, 1993

# W'Mudapr29 MODULUS data

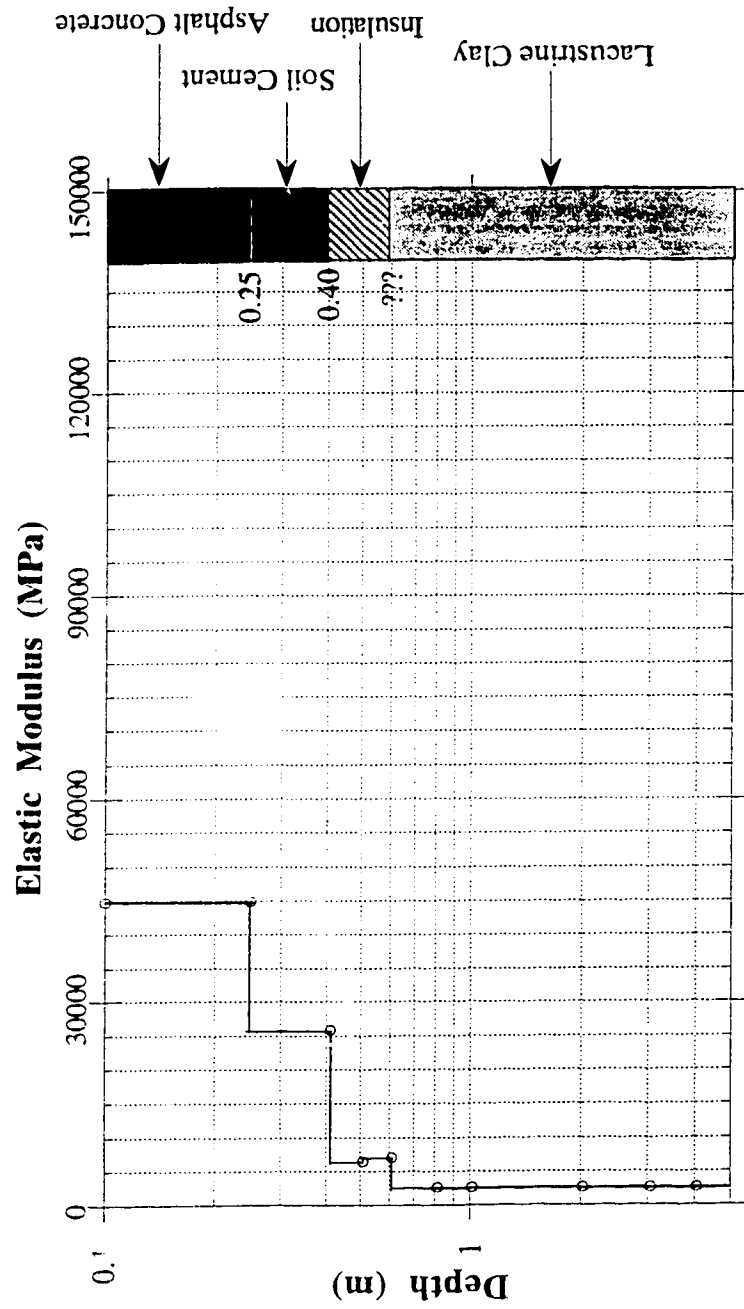


Figure A IV.8 Modulus Profile, Whitemud Drive, April 29, 1993

# W'Mudmay14 MODULUS data

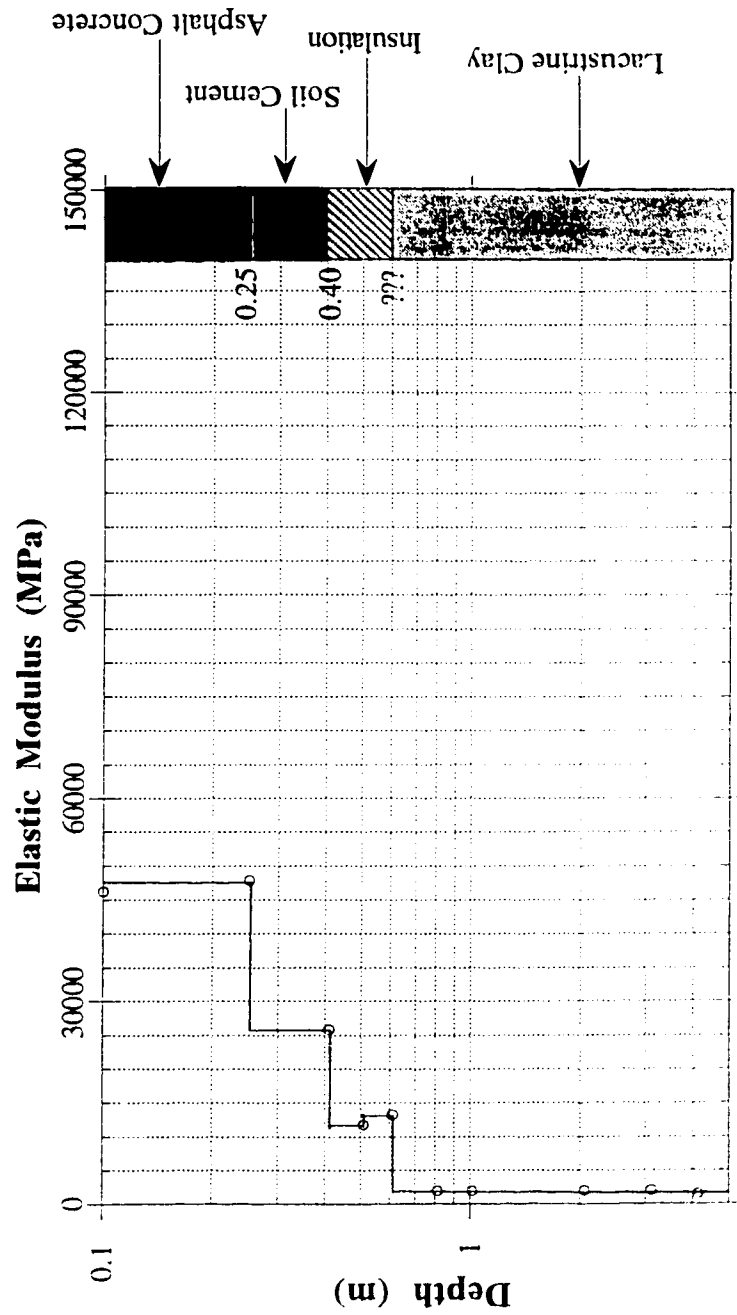


Figure A IV.9 Modulus Profile, Whitemud Drive, May 14, 1993

# **Keilrapr14 MODULUS data**

BASED ON APRIL 22/93  
GROUND TEMPERATURES

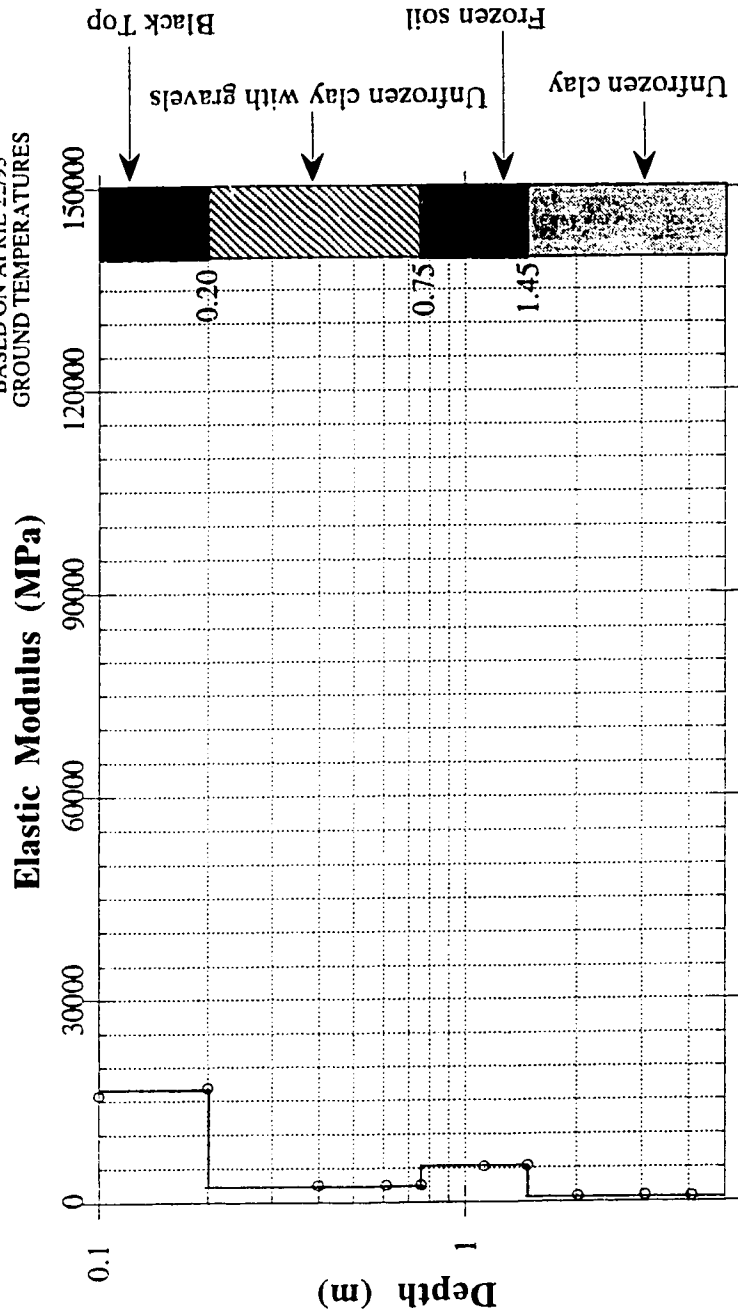


Figure A IV.10 Modulus Profile, Keillor Road, April 14, 1993

# Keilrapr22 MODULUS data

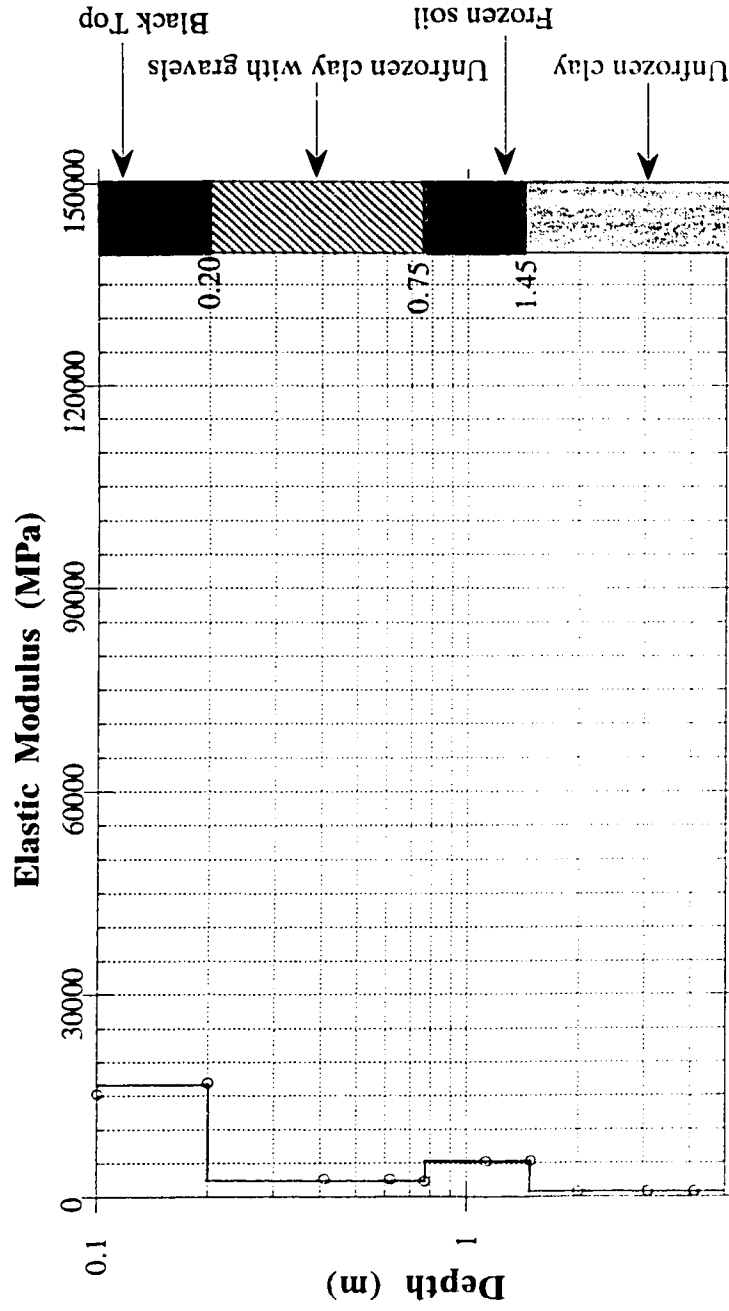


Figure A IV.11 Modulus Profile, Keillor Road, April 22, 1993

# Keilrapr29 MODULUS data

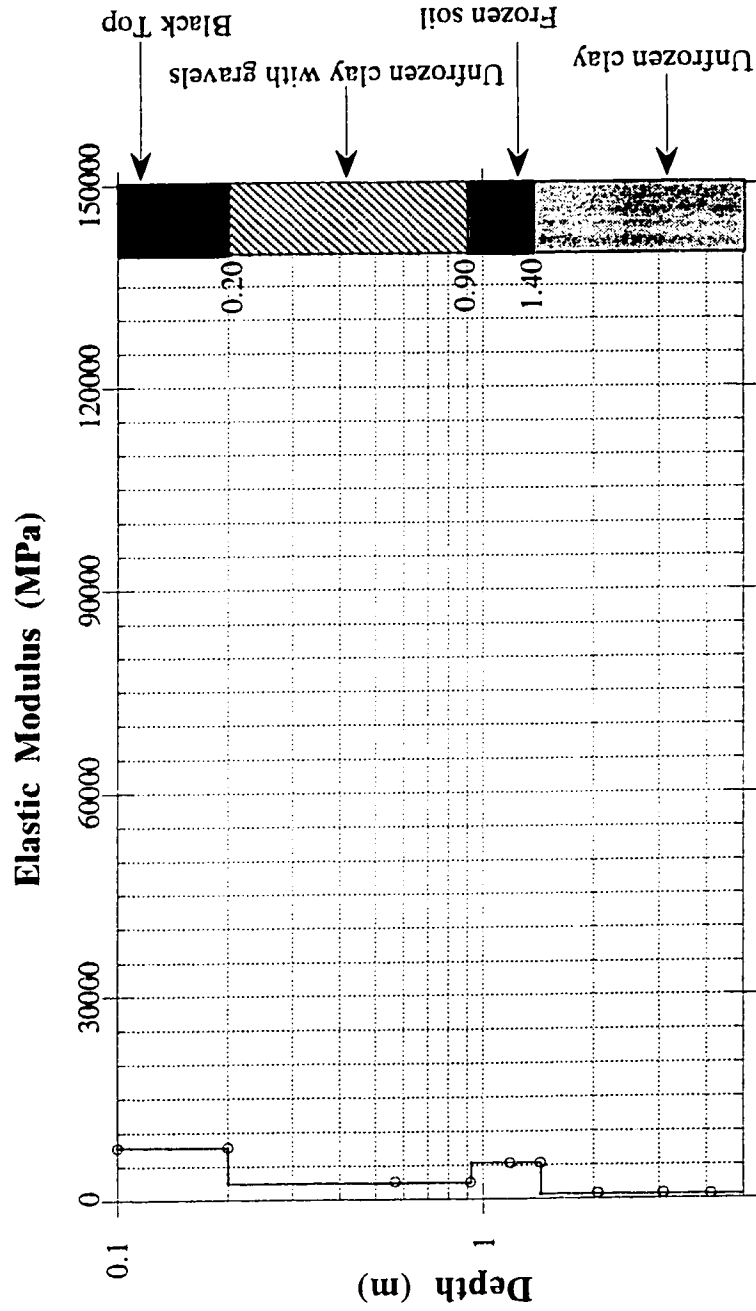


Figure A IV.12 Modulus Profile, Keillor Road, April 29, 1993



# Keilrmay14 MODULUS data

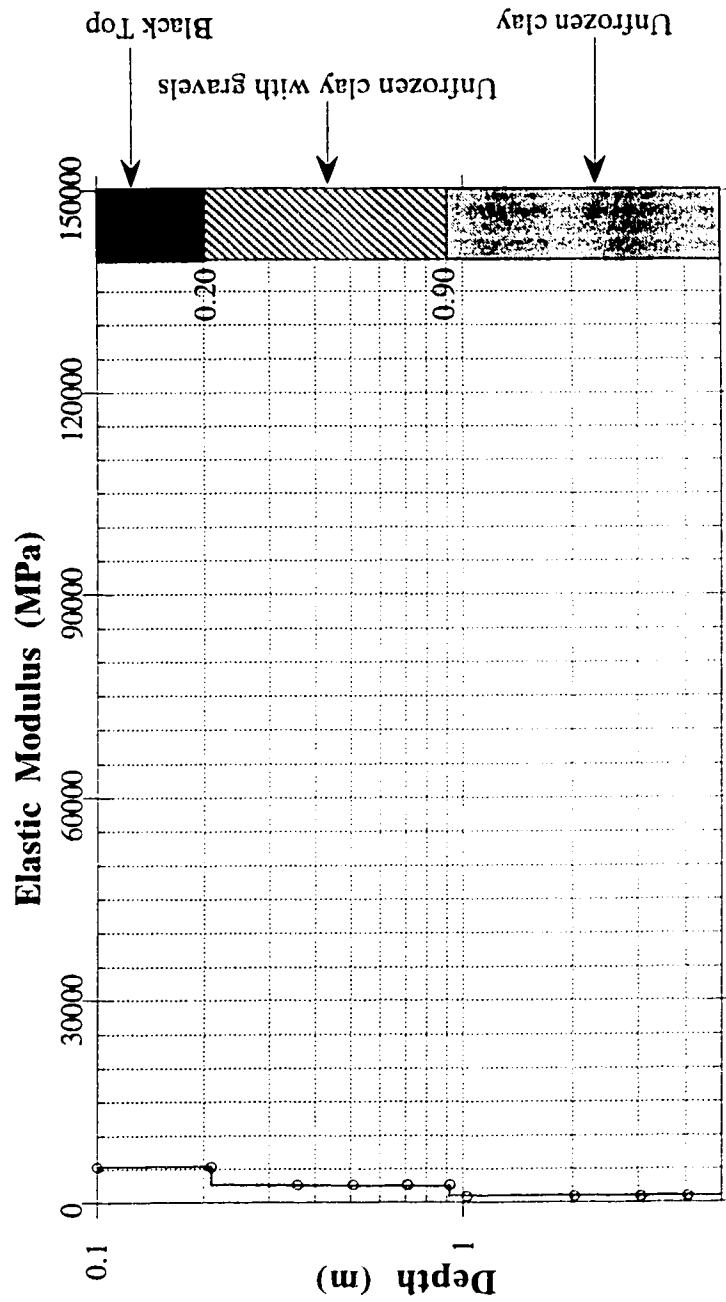


Figure A IV.13 Modulus Profile, Keillor Road, May 14, 1993

# **APPENDIX V**

## **Calculation of Frost Thaw (Keillor Road)**

### CALCULATION OF FROST THAW (Keillor Road)

The performance of pavements in frost-affected regions depends to a large degree on the depth of frost penetration. Prediction of the maximum depth of frost can be accomplished in several ways, including correlation of field penetration data with temperature data and theoretical formulas and charts.

Depth of frost penetration [Yoder, (1975)],  $z = \lambda \sqrt{\frac{48kF}{L}}$  in feet

where:  $\lambda$  = dimensionless factor  
 $k$  = thermal conductivity (BTU's per square foot per degree Fahrenheit, per foot, per hour)  
 $F$  = surface freezing index, degree (F) days  
 $L = 1.434 * \omega * \gamma_d$  = volumetric heat of latent fusion (BTU's per cubic foot)

For the samples obtained from this site:

Dry density ( $\gamma_d$ ) = 100.0 pcf  
 Moisture content ( $\omega$ ) = 22 %  
 Duration of freezing in the winter of 1992-93 = 158 days  
 Freezing Index = 1226.3 degree (C) days = 7231.34 degree (F) days  
 Mean annual air temperature for 1992 = 4.7 deg C = 40.46 deg F  
 Mean annual air temperature for 1993 = 4.4 deg C = 39.92 deg F

Heat capacity in unfrozen state,

$$C_u = 100 * (0.17 + 0.22) = 39.0 \text{ BTU per cu ft per deg F}$$

Heat capacity in frozen state,

$$C_f = 100 * (0.17 + 0.5 * 0.22) = 28.0 \text{ BTU per cu ft per deg F}$$

Volumetric heat of latent fusion,

$$L = 1.43 * 22 * 100 = 3146 \text{ BTU per cu ft}$$

Thermal conductivity of soil in unfrozen state,

$$k_u = \frac{10}{12} = 0.833 \text{ BTU per hour per ft per deg F}$$

Thermal conductivity of soil in frozen state,

$$k_f = \frac{13.5}{12} = 1.125 \text{ BTU per hour per ft per deg F}$$

Thermal ratio,

$$\alpha = \frac{v_o}{v_s} = \frac{v_o * t}{F} = \frac{8.19 * 158}{7231.34} = 0.179$$

where  $v_o$  = temperature by which mean annual temperature exceeds freezing point of soil moisture, deg F

$v_s$  = temperature by which effective surface temperature is less than freezing point of soil moisture during freezing period (F/t) in deg F

t = duration of freezing period, days

Fusion parameter,

$$\mu = \frac{C}{L} * v_s = \frac{C * F}{L * t} = \frac{33.5 * 7231.34}{3146 * 158} = 0.487$$

where C = volumetric heat, in BTU per cu ft deg F

Therefore the correction coefficient ( $\lambda$ ) from Aldrich, (1956) is,

$$\lambda = 0.88$$

Therefore , depth of frost penetration,

$$z = \lambda \sqrt{\frac{48 * k * F}{L}} = 0.88 * \sqrt{\frac{48 * 0.979 * 7231.34}{3146}} = 9.15 \text{ ft} = 2.79 \text{ m}$$

